

REPORT NO.
UCB/EERC-79/12
MAY 1979

EARTHQUAKE ENGINEERING RESEARCH CENTER

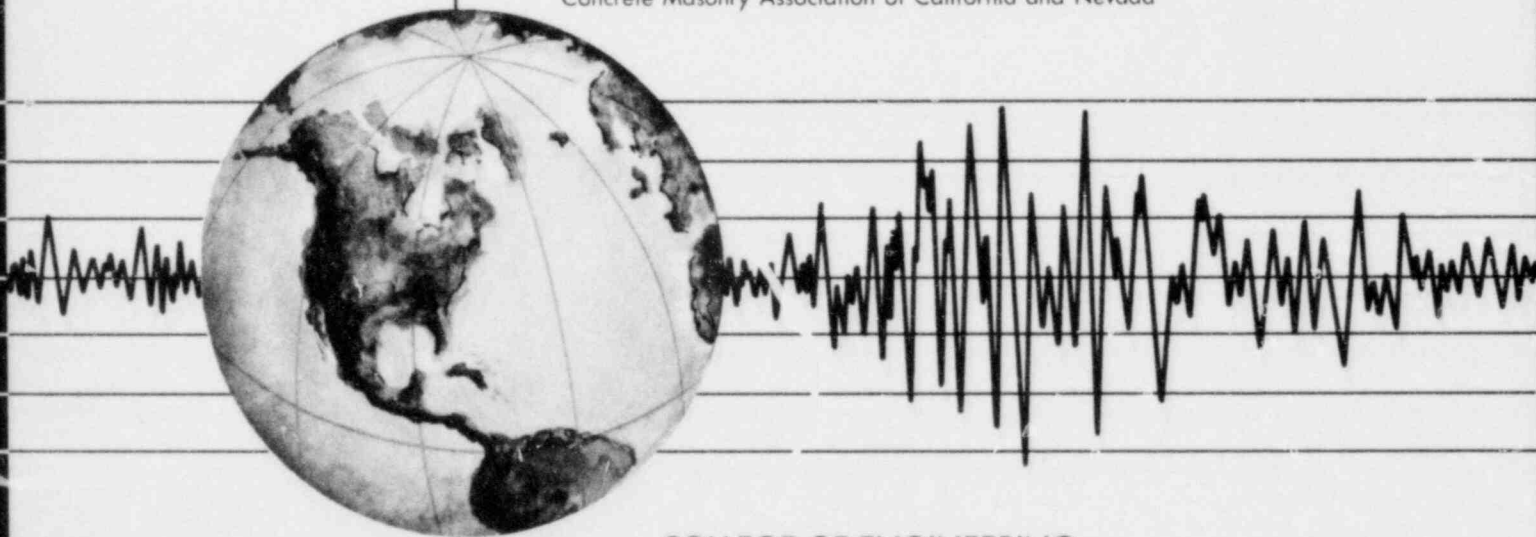
CYCLIC LOADING TESTS OF MASONRY SINGLE PIERS VOLUME 3 - HEIGHT TO WIDTH RATIO OF 0.5

by

PEDRO A. HIDALGO
RONALD L. MAYES
HUGH D. McNIVEN
and
RAY W. CLOUGH

Report to:

National Science Foundation
Masonry Institute of America
Western States Clay Products Association
and the
Concrete Masonry Association of California and Nevada



COLLEGE OF ENGINEERING

UNIVERSITY OF CALIFORNIA · Berkeley, California

8107270174 810717
PDR ADDCK 05000266
G PDR

CYCLIC LOADING TESTS OF MASONRY SINGLE PIERS
VOLUME 3 - HEIGHT TO WIDTH RATIO OF 0.5

by

Pedro A. Hidalgo
Ronald L. Mayes
Hugh D. McNiven
and
Ray W. Clough

Report to

National Science Foundation
Masonry Institute of America
Western States Clay Products Association
Concrete Masonry Association of California and Nevada

Report No. UCB/EERC-79/12

Earthquake Engineering Research Center
College of Engineering
University of California
Berkeley, California

May 1979

ABSTRACT

This report presents the results of eighteen cyclic, in-plane shear tests on fixed ended masonry piers having a height to width ratio of 0.5. These eighteen tests form part of a test program consisting of eighty single pier tests. Previous reports have presented the results of forty-five piers having height to width ratios of 2 and 1 and a subsequent report will present the test results of the remaining seventeen piers.

The test setup was designed to simulate, insofar as possible, the boundary conditions the piers would experience in a perforated shear wall of a complete building. Each test specimen was a full scale pier 40 inches high and 80 inches wide. Three types of masonry construction were used; a hollow concrete block and a hollow clay brick type that used an 8 inch wide unit, and a double wythe grouted core clay brick, 10 inch thick wall, that consisted of two wythes 3 1/2 inches thick and a 3 inch grouted core. The variable included in the investigation was the quantity of horizontal reinforcement. All of the piers were fully grouted.

The results are presented in the form of hysteresis envelopes, graphs of stiffness degradation, energy dissipation and shear distortion, and tabulated data on the ultimate strength and hysteresis indicators. A discussion of these test results is presented but no definitive conclusions are offered. These will be included in a final report at the completion of the eighty tests.

ACKNOWLEDGEMENTS

This investigation was jointly sponsored by the National Science Foundation under Grant ENV76-04265, the Masonry Institute of America, the Western States Clay Products Association and the Concrete Masonry Association of California and Nevada. The authors wish to express their appreciation for technical advice and encouragement received from Mr. Walter Dickey, Mr. John Tawresey, Mr. Donald Wakefield, Mr. Dick Wasson, Mr. James Amrhein, Mr. Stuart Beavers and Mr. Don Prebble. D.A. Sullivan and Co. constructed all the test specimens. Many thanks also are due to Messrs. David Steere, Ivo Van Asten, Robert Robinson, Derald Clearwater, John McNab and Steve Miller of the Earthquake Engineering Research Center for their electronic and machine shop work. The authors also wish to thank students Bjorn Sveinsson and John Baniesrael for their help in performing the tests and reducing the test data, and Dr. B. Bolt for reviewing the manuscript. The computing facilities to reduce the data were provided by the Computer Center at the University of California, Berkeley.

The typing was done by Ms. Shirley Edwards and the drafting by Ms. Gail Feazell.

TABLE OF CONTENTS

	<u>Page</u>
ABSTRACT	i
ACKNOWLEDGEMENTS	ii
TABLE OF CONTENTS	iii
LIST OF TABLES	v
LIST OF FIGURES	vi
1. INTRODUCTION	1
1.1 The Multistory Building Research Program	1
1.2 Objectives and Scope of the Single Pier Test Program	2
2. TEST SPECIMENS	9
2.1 Design and Construction of Specimens	9
2.2 Material Properties	10
3. TEST EQUIPMENT AND PROCEDURE	23
3.1 Test Equipment	23
3.2 Loading Sequence	24
3.3 Instrumentation	25
3.4 Data Acquisition and Data Processing	26
4. TEST RESULTS	33
4.1 Introduction	33
4.2 Modes of Failure	33
4.3 Load-Displacement Characteristics	37
5. DISCUSSION OF TEST RESULTS	49
5.1 Introduction	49
5.2 Modes of Failure	49

	<u>Page</u>
5.3 Lateral Load Strength	51
5.4 Inelastic Behavior	53
5.5 Stiffness Degradation	54
5.6 Energy Dissipation	56
5.7 Effect of Compressive Load on Inelastic Behavior . . .	57
5.8 Correlator Between Square Panel and Pier Critical Tensile Strengths	57
5.9 Other Test Results	59
REFERENCES	77
APPENDIX A. CATALOG OF TEST RESULTS	79

LIST OF TABLES

<u>Table</u>		<u>Page</u>
1.1	Single Pier Test Program	5
2.1	Test Program	12
2.2	Material Properties	13
3.1	Loading Sequence	27
4.1	Pier Characteristics and Test Results	42
5.1	Comparison of Shear Crack Strength and Ultimate Strength	61
5.2	Effect of Shear Stress and Steel Reinforcement on Stiffness Degradation	62
5.3	Correlation Between Square Panel and Pier Critical Tensile Strength	63

LIST OF FIGURES

<u>Figure</u>		<u>Page</u>
1.1	Typical Shear Walls	6
1.2	Double Pier Test Setup	7
1.3	Single Pier Test Setup	8
2.1	Pier Dimensions	14
2.2	Construction of Test Specimens	15
2.3(a)	Specimens to Determine Material Properties (HCBL) . . .	16
2.3(b)	Specimens to Determine Material Properties (HCBR) . . .	17
2.3(c)	Specimens to Determine Material Properties (CBRC) . . .	18
2.4(a)	Reinforcing Steel Arrangements for Hollow Concrete Block Piers (HCBL)	19
2.4(b)	Reinforcing Steel Arrangements for Hollow Clay Brick and Grouted Core Clay Brick Piers (HCBR and CBRC)	20
2.5	Prism Test	21
2.6	Square Panel Test	22
3.1	Schematic Illustration of Single Pier Test	28
3.2	Overview of Single Pier Test	29
3.3	Pier Instrumentation	30
3.4	Measurement of Average Shear Distortion	31
3.5	Test Control Consoles and Data Acquisition System . . .	32
4.1(a)	Shear Mode of Failure	43
4.1(b)	Combined Shear and Sliding Mode of Failure	44
4.1(c)	Combined Flexural and Sliding Mode of Failure	45
4.2	Forces Acting on the Pier	46
4.3	Definition of Hysteresis Indicators and Computation of Initial Stiffness.	47

<u>Figure</u>		<u>Page</u>
4.4	Definitions of Energy Dissipation Ratio and Pier Stiffness	48
5.1	Hysteresis Envelopes for Hollow Concrete Block Piers	64
5.2	Hysteresis Envelopes for Hollow Clay Brick Piers	65
5.3	Hysteresis Envelopes for Grouted Core Clay Brick Piers	66
5.4(a)	Sliding Strength HCBR Piers Combined Flexural and Sliding Mode of Failure	67
5.4(b)	Sliding Strength CBRC Piers Combined Flexural and Sliding Mode of Failure	68
5.5(a)	Sliding Strength HCBL Piers Combined Shear and Sliding Mode of Failure	69
5.5(b)	Sliding Strength CBRC Piers Combined Shear and Sliding Mode of Failure	70
5.6	Stiffness Degradation for Hollow Concrete Block Piers	71
5.7	Stiffness Degradation for Hollow Clay Brick Piers	72
5.8	Stiffness Degradation for Grouted Core Clay Brick Piers	73
5.9	Energy Dissipation for Hollow Concrete Block Piers	74
5.10	Energy Dissipation for Hollow Clay Brick Piers	75
5.11	Energy Dissipation for Grouted Core Clay Brick Piers	76

1. INTRODUCTION

1.1 The Multistory Masonry Building Research Program

A multistory masonry building research program was initiated at the Earthquake Engineering Research Center in September 1972, and has continued for the past six years. After an extensive review of the literature [5,6]* dealing with resistance of masonry to earthquakes, it was concluded that shear walls perforated by numerous window openings (Fig. 1.1) were the components of multistory masonry buildings most frequently damaged in past earthquakes, and it was decided that an experimental study of the seismic behavior of such components was necessary.

Two types of structural components can be identified in the shear wall of Fig. 1.1, the piers and the spandrel beams. In order to study the pier behavior, a test fixture was designed to subject typical full-scale double pier specimens to combined static vertical (gravity) and cyclic lateral (seismic) loads (Fig. 1.2). The results obtained from seventeen such specimens have been reported by Mayes et al [8,9]. These results show significant variations in the pier behavior with the various test parameters including the type of grouting, types of reinforcement and the rate of loading. The results were not conclusive and demonstrated the need for more extensive tests to establish definitive parametric relationships.

The cost of the double pier tests, both in money and time, precluded carrying out extensive parametric variations with the double pier test setup and, consequently, a single pier test system was designed

* References are arranged in alphabetical order of the authors' names, and are listed at the end of the text.

which greatly simplified the investigation (Fig. 1.3). A series of eighty single pier tests was planned, which included the following test parameters: type of masonry construction, height to width ratio of the piers, type of grouting, and amount and distribution of both vertical and horizontal steel reinforcement. The present report deals with the experimental results of specimens with a height to width ratio of 0.5.

1.2 Objectives and Scope of the Single Pier Test Program

In determining the strength of masonry piers and panels, the first step is to evaluate the mode of failure. Because most failures in past earthquakes have been characterized by diagonal cracks, many research programs have concentrated on this type of failure mechanism. Test techniques used by Blume^[1], Greenley and Cattaneo^[3] and others induce the diagonal tension or shear mode of failure. Scrivener^[15], Meli^[11], Williams^[16] and Priestley and Bridgeman^[13], however, recognized that there are two possible modes of failure for cantilever piers. In addition to the shear or diagonal tension mode they recognized that, for certain piers, a flexural failure could occur. This mechanism is characterized by yielding of the tension steel of the wall, followed by a secondary failure at the compressive toe, with associated buckling of the reinforcement once confinement is lost. Meli^[11] described the flexural failure as similar to that of an under-reinforced concrete beam; i.e., extensive flexural cracking and strength limited by yielding of the reinforcement, with failure finally due either to crushing of the compressive corner or to rupture of the extreme bars.

Because the double pier tests were the first fixed ended piers to be tested cyclically, the objective of those tests was to determine the effect of various parameters and compare the results with those already

known for cantilever piers. Both the shear and flexural modes of failure were included in that investigation.

One of the main objectives of the single pier test program was to investigate thoroughly the effects of different parameters on the behavior shown in the shear mode of failure. It was evident from the double pier test program that the flexural mode of failure of a fixed ended pier has desirable inelastic characteristics, although these are not as desirable as those obtained by Priestley^[14] for cantilever piers. Furthermore, it was recognized that for fixed ended piers, with height to width ratios commonly found in multistory buildings, the amount of horizontal reinforcement required to induce a flexural mode of failure is substantially greater than that required by current codes. Therefore, it was decided to investigate the effects of lesser amounts of horizontal reinforcement on the shear mode of failure to determine if desirable inelastic behavior could be obtained.

The eighteen tests reported herein are a part of a total program of eighty single pier tests; a matrix characterizing the first sixty-three tests is shown in Table 1.1. The parameters for the remaining seventeen tests will be selected after an evaluation of these sixty-three. The test parameters, other than the type of construction and height to width ratio, include the amount of reinforcement and the effect of partial grouting. Hollow concrete block piers having height to width ratio of 2 were not included in the single pier test program because such piers were investigated in the original double pier tests.

This report presents the results for piers with a height to width ratio of 0.5, of which six tests were performed on hollow concrete block specimens (HCBL), six on hollow clay brick specimens (HCBR) and six on double wythe grouted core clay brick specimens (CBRC). Previous

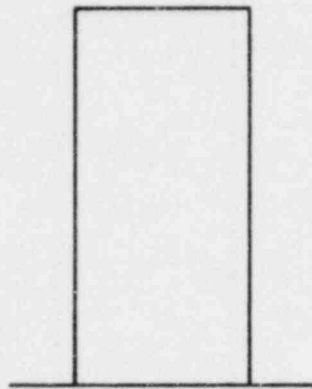
reports^[4,2] presented the results obtained from piers with height to width ratios of 2 and 1. The results from the series of seventeen specimens which will complete the proposed research program will also be presented in a separate report. The organization of the present volume is similar to the two previous ones^[4,2]. The general background of the single pier test program has been included in this report in order to make it as self-contained as possible.

TABLE 1.1

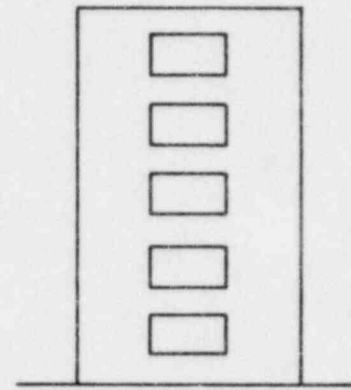
SINGLE PIER TEST PROGRAM*
(Number of test specimens)

HEIGHT TO WIDTH RATIO	TYPE OF MASONRY	HOLLOW CLAY BRICK (HCBR)	DOUBLE WYTHE GROUTED CORE CLAY BRICK (CBRC)	HOLLOW CONCRETE BLOCK (HCBL)	TOTAL NUMBER
2 : 1		9	5	0	14
1 : 1		13	7	11	31
1 : 2		6	6	6	18

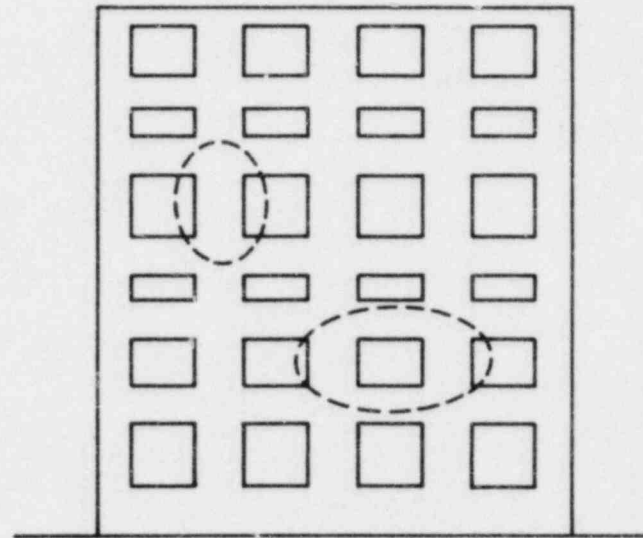
* Last 17 tests to be decided after this phase is completed



VERTICAL
CANTILEVER
SHEAR WALL



COUPLED
SHEAR WALL



PERFORATED SHEAR WALL

FIG. 1.1 TYPICAL SHEAR WALLS

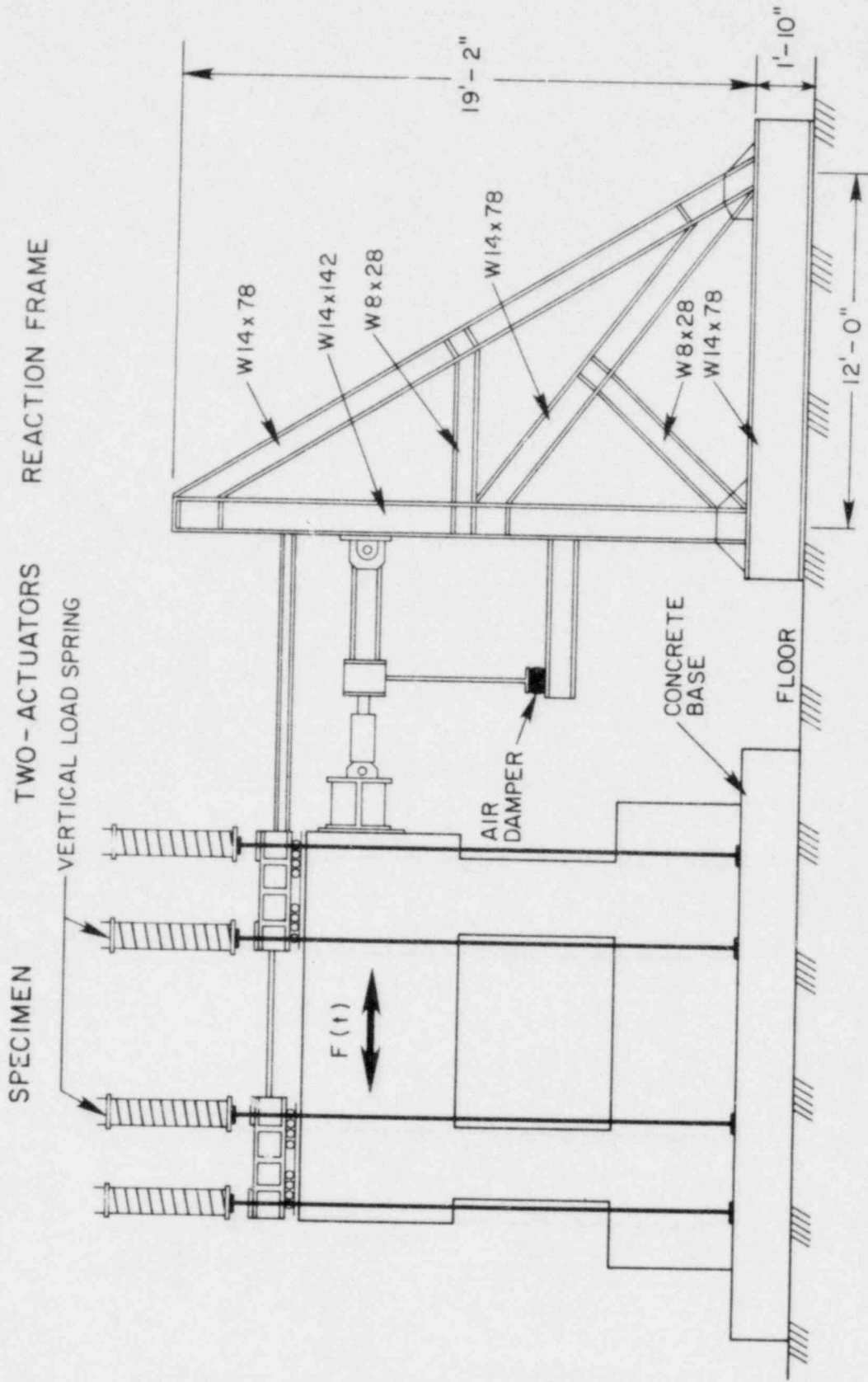


FIG. 1.2 DOUBLE PIER TEST SETUP

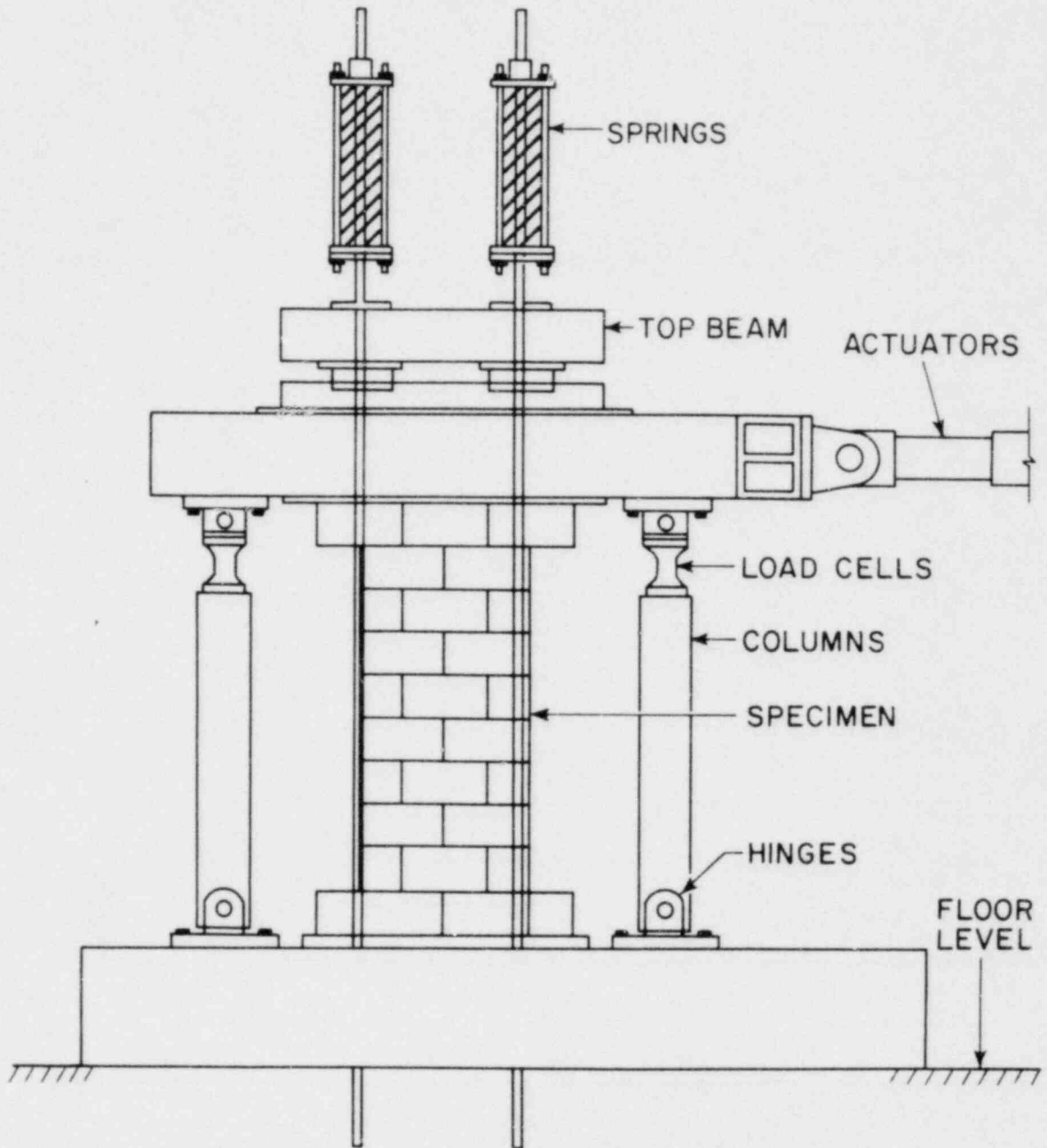


FIG. 1.3 SINGLE PIER TEST SETUP

2. TEST SPECIMENS

2.1 Design and Construction of Specimens

The overall dimensions of the test specimens discussed here are shown in Fig. 2.1. The height of all eighteen piers was 40 inches. The width was 80 inches for the hollow concrete block piers (HCBL) and 78 inches for the hollow clay brick (HCBR) and double wythe grouted clay brick (CBRC) piers. The thickness was $7\frac{5}{8}$ inches for the HCBL piers, $7\frac{3}{8}$ inches for the HCBR piers and 10 inches for the CBRC piers.

The HCBL panels were constructed from standard two-core hollow concrete blocks, nominally 8 inches wide x 8 inches high x 16 inches long, as shown in Fig. 2.3(a). The cored area of each block is approximately 50.6 square inches and the ratio of net to gross area is 58%.

The HCBR piers were constructed from standard two-core hollow clay bricks, nominally 8 inches wide x 4 inches high x 12 inches long as shown in Fig. 2.3(b). The cored area of each brick is approximately 57.4 square inches and the ratio of net to gross area is 67%.

The CBRC piers were constructed from two wythes of "solid" clay bricks nominally 4 inches wide x 4 inches high x 12 inches long as shown in Fig. 2.3(c). The grouted space between the wythes was 3 inches wide and was filled after the steel reinforcement had been placed in position. The bricks have a core (hollow) area slightly less than 25% of the gross area. The Uniform Building Code definition of a "solid brick" is one with 25% or less coring.

The piers were constructed on 0.75 inch thick steel plates as shown in Fig. 2.2. A similar plate was added on top of the pier after the grout was poured. Both plates had holes to permit anchorage of the vertical steel reinforcement and keys to provide an adequate shear

transfer between the masonry pier and the steel plate. The plates also had welded bolts and holes to anchor the pier to the test rig.

All the eighteen piers were fully grouted. The series of tests was planned to determine the effect of the quantity of horizontal steel reinforcement on the strength and deformation properties of the piers, as shown in the test program (Table 2.1). Details of the reinforcing bar arrangements are shown in Fig. 2.4(a) for the HCBL piers and in Fig. 2.4(b) for the HCBR piers and the CBRC piers. The actual position of the vertical reinforcement is indicated in Fig. 2.1. When horizontal reinforcement was used, the bars were evenly distributed over the height of the pier.

2.2 Material Properties

Table 2.2 shows the mechanical properties of the materials used in the construction of the test specimens. The specimens used to determine the material properties are shown in Fig. 2.3(a), (b) and (c).

The tests of the single masonry units followed the ASTM C67-73 Specification^[10] and were based on three samples for each test.

The joint mortar was specified as standard ASTM type M (i.e., 1 Cement: 1/4 Lime: 2 1/4-3 Sand, by volume), with a minimum compressive strength of 2500 psi at 28 days. The grout was specified as 1 Cement: 3 Sand: 2 G, where G refers to 10 mm maximum size local gravel. Because the specimens were not constructed or grouted at the same time, the mortar and grout strength varied according to normal workmanship. A minimum of three samples of both mortar and grout was taken from each batch used during construction.

ASTM A615 Grade 60 steel was specified for both the vertical and horizontal steel reinforcement. Three samples of each bar size were tested to determine the properties listed in Table 2.2.

Six prisms for uniaxial compression tests and three square panels for diagonal tension tests were constructed from the same mortar and grout used in each set of wall panels. Three of the six prisms had a height to thickness ratio of 5 and the other three had a height to thickness ratio of 2. All prism tests were performed at a loading rate of 100,000 lb/min. (Fig. 2.5). The compressive strengths are shown in Table 2.2.

The square panels were tested as shown in Fig. 2.6 at a loading rate of 20,000 lb/min. The ultimate load for the square panel tests is also shown in Table 2.2. The square panels corresponding to the HCBR piers do not appear in Table 2.2 and Fig. 2.3(b) because they were accidentally broken before the test.

The mortar, grout, prism and square panel samples were cured under the same normal atmospheric conditions as the piers; also the prism and square panel tests were performed during the tests of the corresponding piers.

TABLE 2.1

TEST PROGRAM

Pier General Characteristics	Specimen Designation	Test Frequency (cps)	Grouting Full (F) Solid(S)	Reinforcing Steel	
				Vertical	Horizontal
Masonry type: Hollow Concrete Block	HCBL-12-1	0.02	F	3#7	No
Pier height: H = 40 in	-2	0.02	F	3#7	1#5
Pier width: D = 80 in	-3	0.02	F	3#7	2#5
Pier thickness: 7.625 in	-4	0.02	F	3#7	3#5
Gross section area: 610 in ²	-5	0.02	F	3#7	4#5
Bearing load: 32 kip	-6	0.02	F	3#7	4#6
Bearing stress: 52 psi					
Masonry type: Hollow Clay Brick	HCBR-12-1	0.02	F	3#7	No
Pier height: H = 40 in	-2	0.02	F	3#7	1#6
Pier width: D = 78 in	-3	0.02	F	3#7	2#6
Pier thickness: 7.375 in	-4	0.02	F	3#7	3#6
Gross section area: 575.25 in ²	-5	0.02	F	3#7	4#6
Bearing load: 32 kip	-6	0.02	F	3#7	5#7
Bearing stress: 56 psi					
Masonry type: Double Wythe Grouted Core Clay Brick	CBRC-12-1	0.02	S	3#7	No
Pier height: H = 40 in	-2	0.02	S	3#7	1#6
Pier width: D = 78 in	-3	0.02	S	3#7	2#6
Pier thickness: 10 in	-4	0.02	S	3#7	3#6
Gross section area: 780 in ²	-5	0.02	S	3#7	4#6
Bearing load: 39 kip	-6	0.02	S	3#7	5#7
Bearing stress: 50 psi					

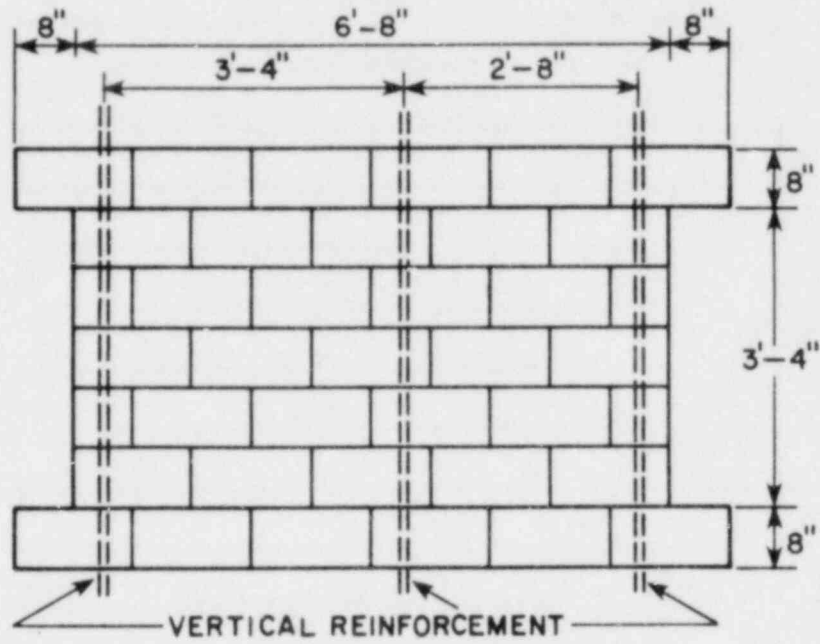
TABLE 2.2

MATERIAL PROPERTIES

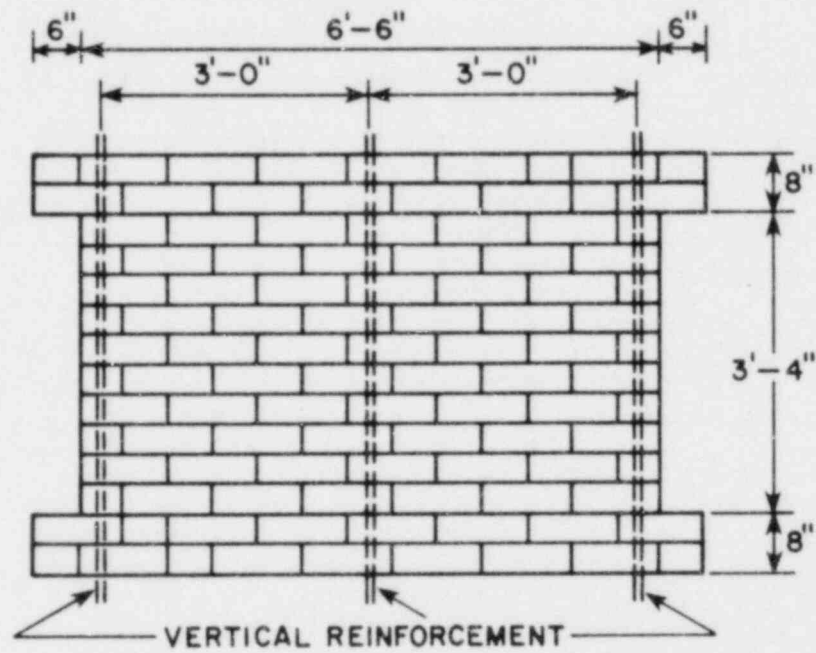
(Average values. Number in parenthesis indicates the standard deviation as percent of average value)

MASONRY	HCBL-12	HCBR-12	CBRC-12
Masonry unit gross compressive strength (psi)	1878 (5%)	5816 (6%)	9422 (4%)
Masonry unit net tensile strength (psi)	221 (14%)	466 (19%)	303 (24%)
Mortar compressive strength (psi)	5530 (26%)	3460 (24%)	4903 (29%)
Grout compressive strength (psi)	3890 (3%)	3890 (3%)	3785 (4%)
Prism (2:1) compressive strength (psi)	3604 (9%)	3589 (7%)	2948 (11%)
Prism (5:1) compressive strength (psi)	2988 (13%)	2838 (15%)	2876 (3%)
Ultimate load of square panel (kip)	155.0 (4%)	—	186.3 (11%)

STEEL REINFORCEMENT	No. 5 bar	No. 6 bar	No. 7 bar
Yield strength (ksi)	69.6 (4%)	67.3 (1%)	80.3 (11%)
Ultimate strength (ksi)	109.8 (4%)	108.6 (1%)	125.4 (9%)
Modulus of elasticity (ksi)	28700	28800	28800
Yield strain (in/in)	0.00243	0.00234	0.00279



HOLLOW CONCRETE BLOCK PIERS



HOLLOW CLAY BRICK AND GROUTED
CORE BRICK PIERS

FIG. 2.1 PIER DIMENSIONS

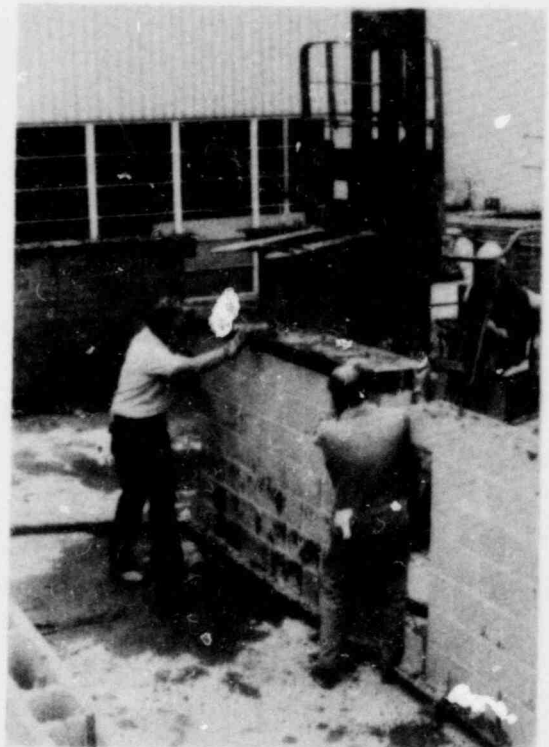
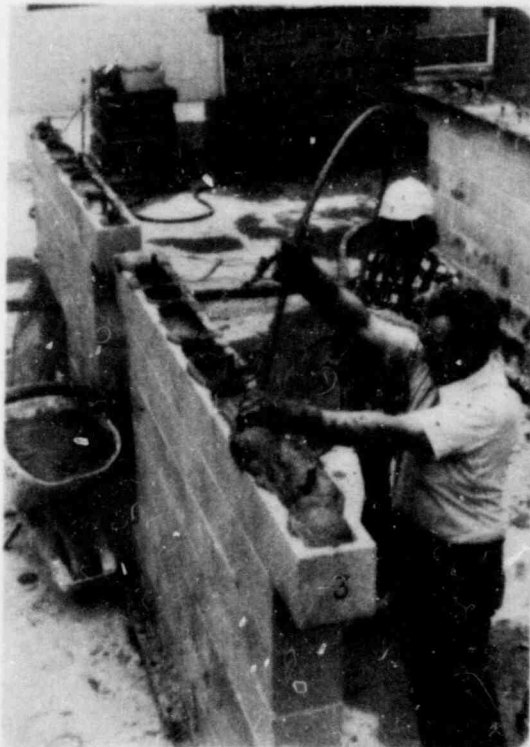
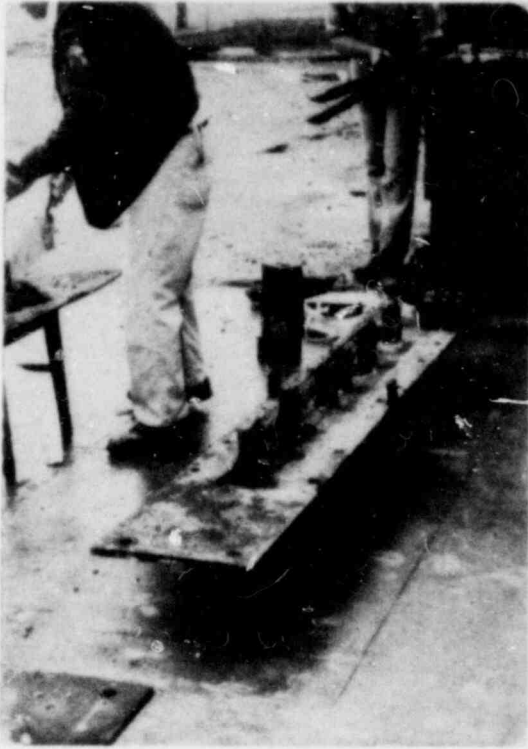
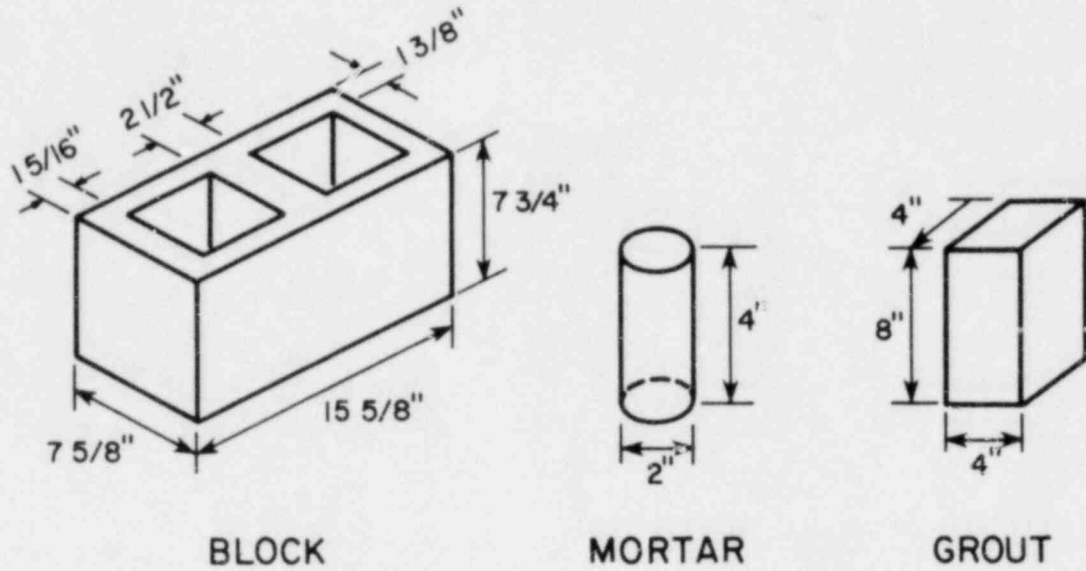


FIG. 2.2 CONSTRUCTION OF TEST SPECIMENS

BASIC MATERIALS



MASONRY SUBASSEMBLAGES

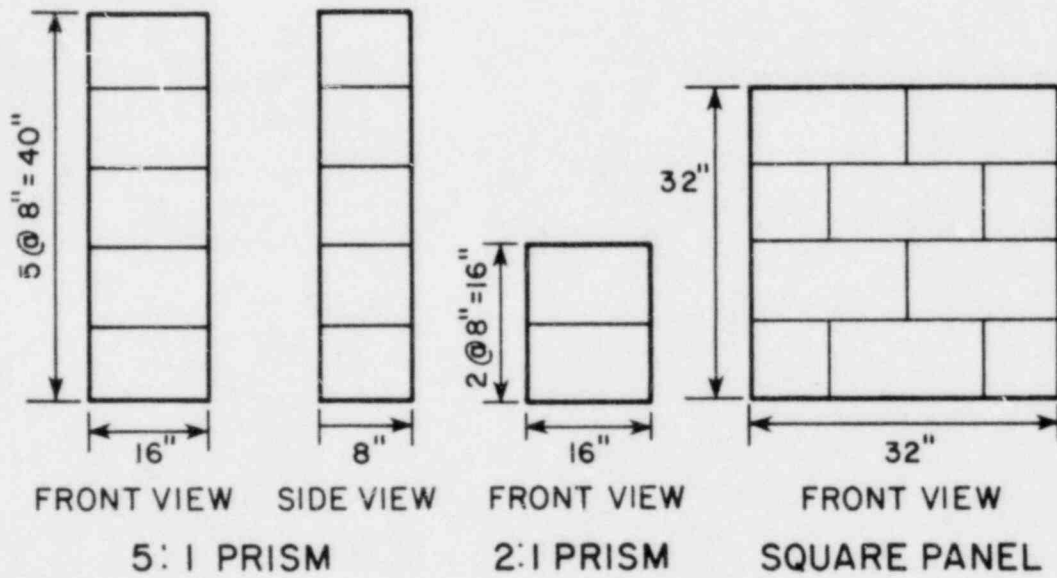
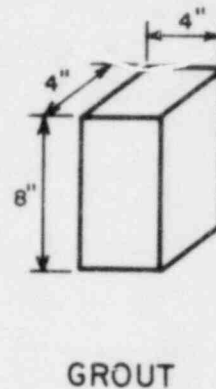
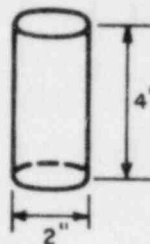
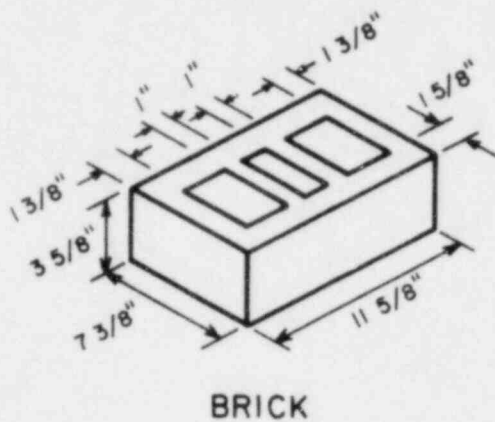


FIG. 2.3(a) SPECIMENS TO DETERMINE MATERIAL PROPERTIES (HCBL)

BASIC MATERIALS



MASONRY SUBASSEMBLAGES

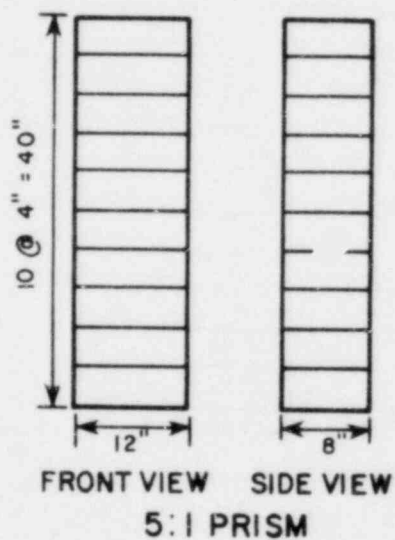
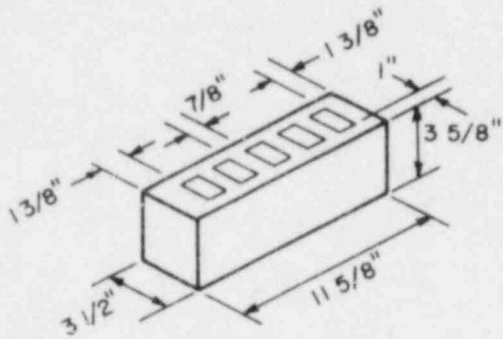


FIG. 2.3(b) SPECIMENS TO DETERMINE MATERIAL PROPERTIES (HCBR)

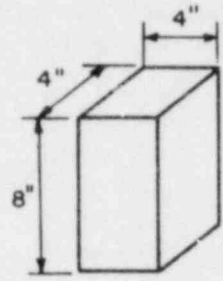
BASIC MATERIALS



BRICK

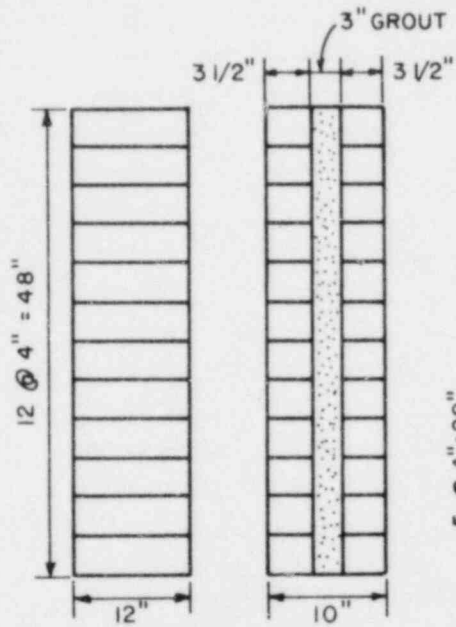


MORTAR

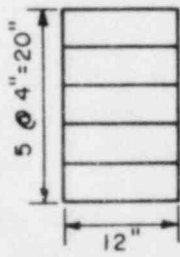


GROUT

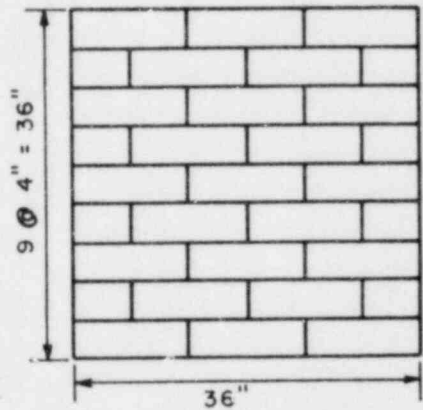
MASONRY SUBASSEMBLAGES



FRONT VIEW SIDE VIEW
5:1 PRISM

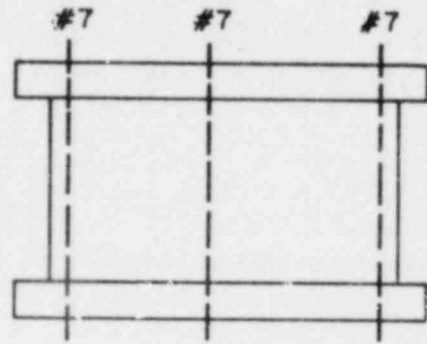


FRONT VIEW
2:1 PRISM



FRONT VIEW
SQUARE PANEL

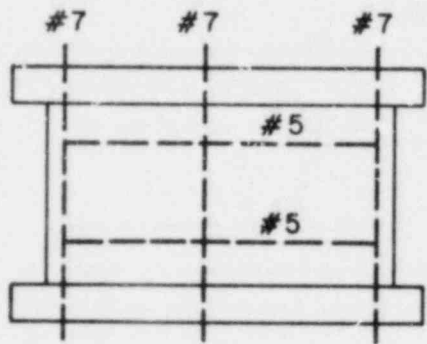
FIG. 2.3(c) SPECIMENS TO DETERMINE MATERIAL PROPERTIES (CBRC)



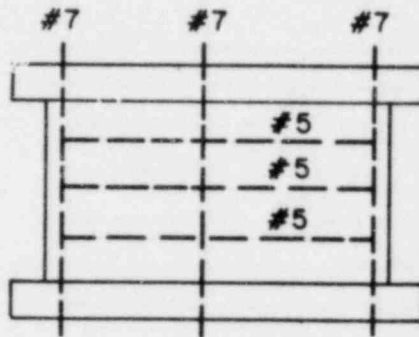
HCBL-12-1 FULL GROUTING



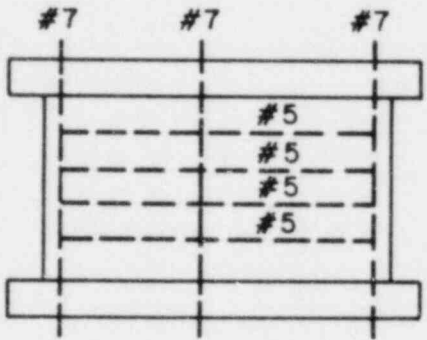
HCBL-12-2 FULL GROUTING



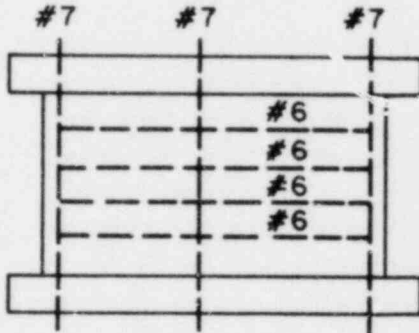
HCBL-12-3 FULL GROUTING



HCBL-12-4 FULL GROUTING



HCBL-12-5 FULL GROUTING



HCBL-12-6 FULL GROUTING

FIG. 2.4(a) REINFORCING STEEL ARRANGEMENTS FOR HOLLOW CONCRETE BLOCK PIERS (HCBL)

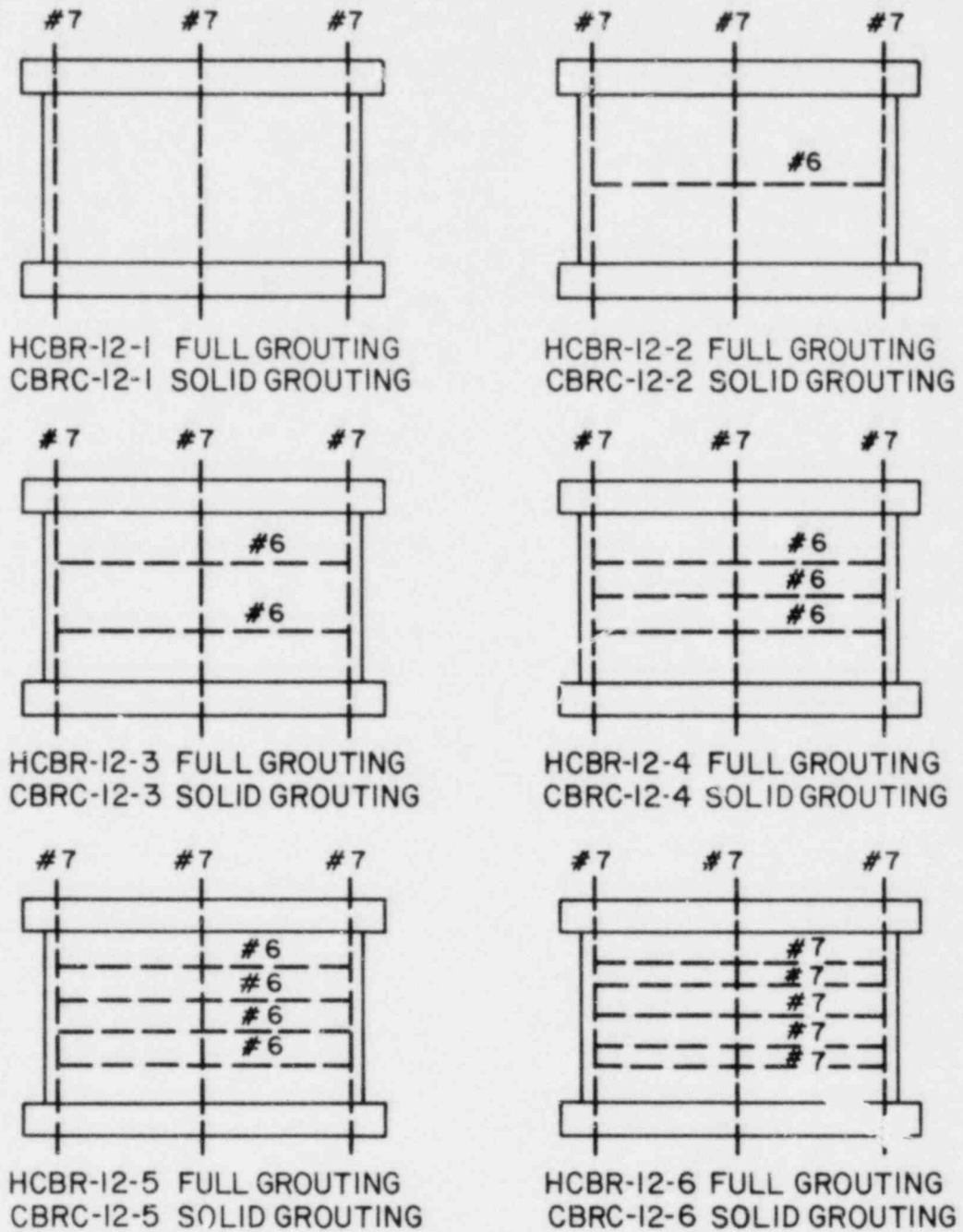


FIG. 2.4(b) REINFORCING STEEL ARRANGEMENTS FOR HOLLOW CLAY BRICK AND GROUTED CORE CLAY BRICK PIERS (HCBR AND CBRC)

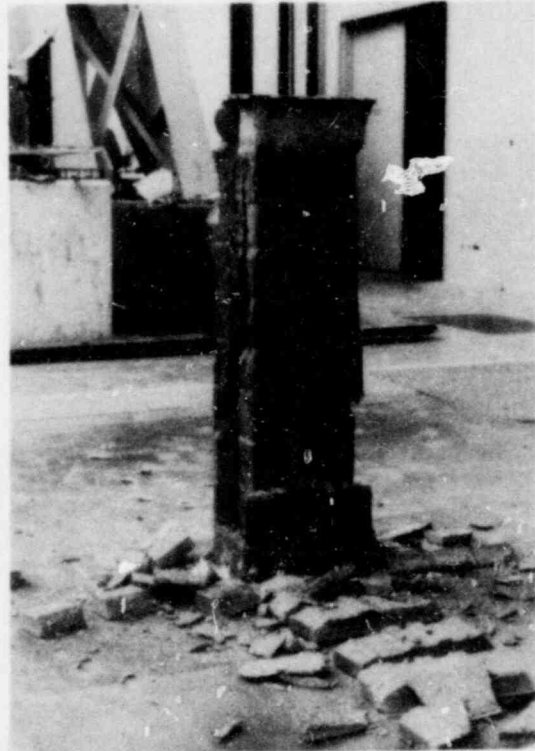
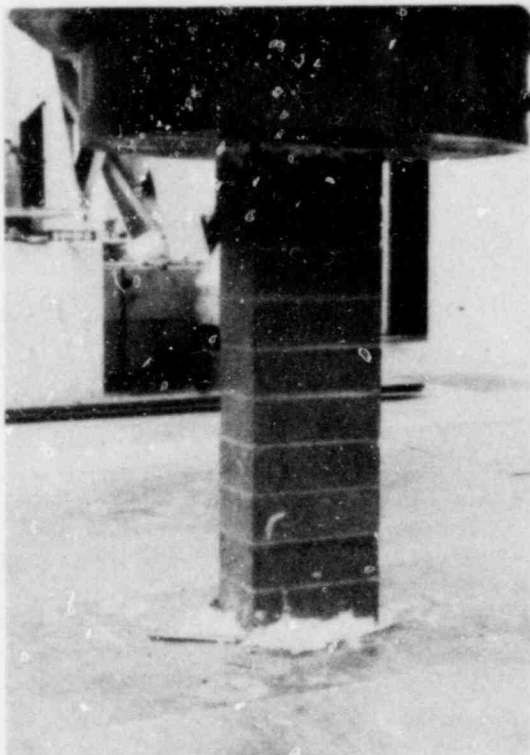
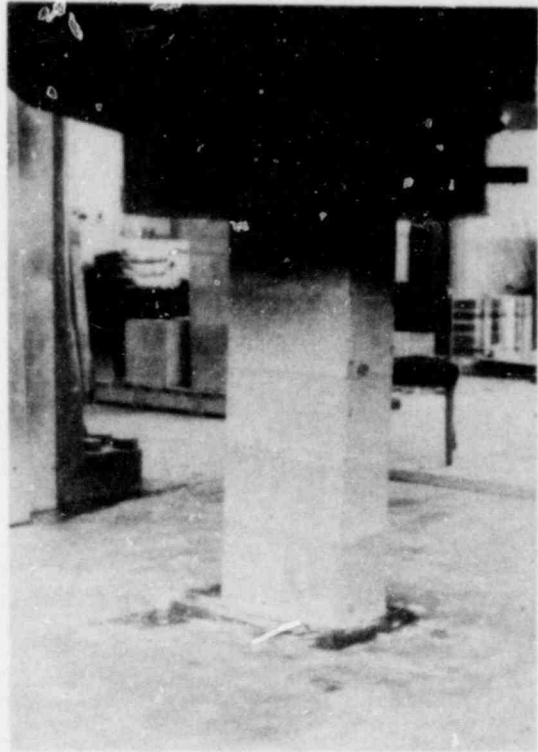


FIG. 2.5 PRISM TEST

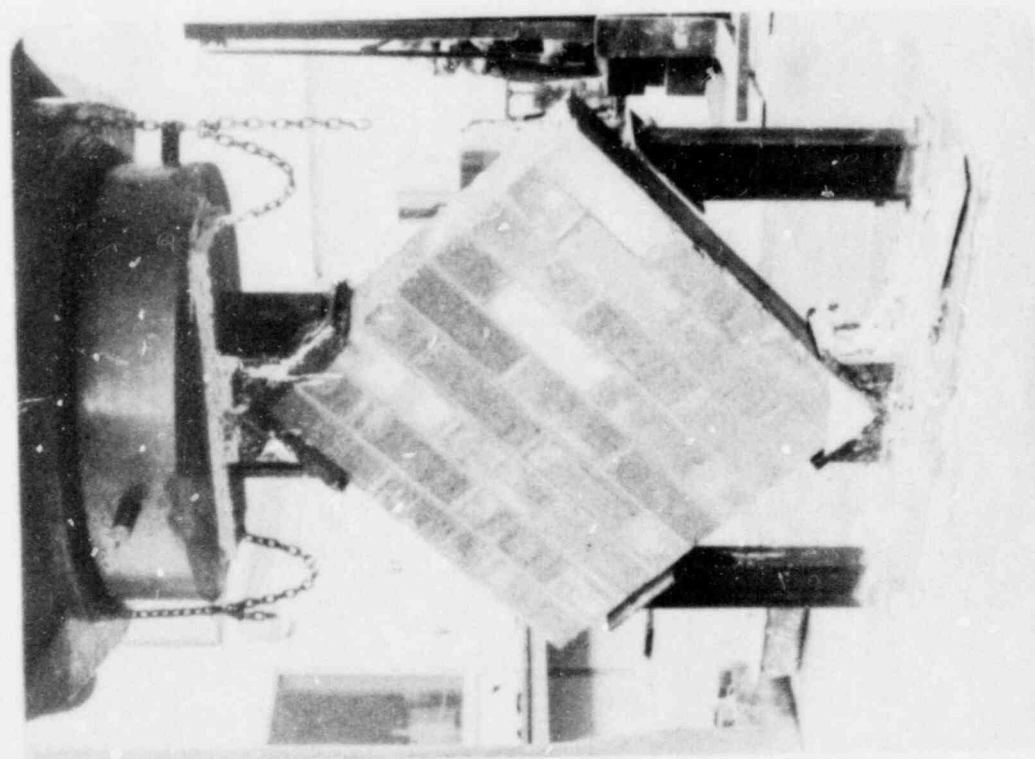
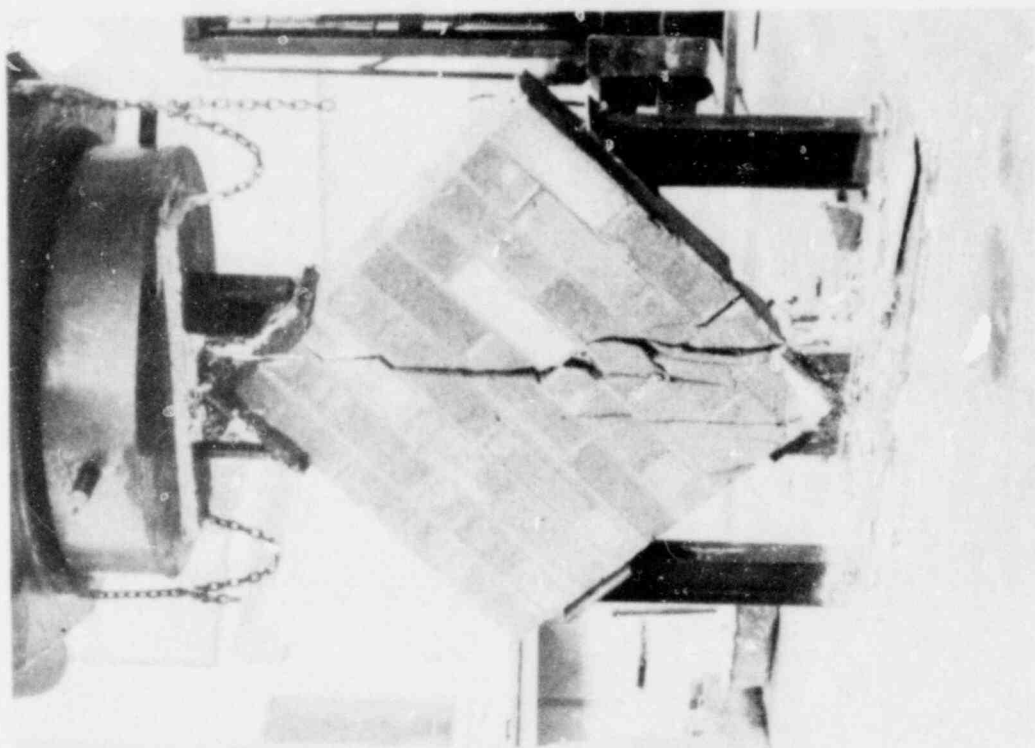


FIG. 2.6 SQUARE PANEL TEST

3. TEST EQUIPMENT AND PROCEDURE

3.1 Test Equipment

The test equipment shown in Figs. 3.1 and 3.2 permits lateral loads to be applied in the plane of the piers in a manner similar to which a floor diaphragm would load the piers during earthquake excitation. It consists of two 20 feet high, heavily-braced reaction frames supporting a horizontally acting hydraulic actuator; a mechanism capable of applying vertical bearing loads similar to the gravity loads experienced by the piers in an actual structure; a bottom beam composed of a concrete base and a wide flange steel beam which provides anchorage to the test floor and suitable connection holes to the bottom plate of the specimen; and a top beam fabricated from two wide flange, steel beams as shown in Fig. 3.2. The top and bottom beams simulate the action of the spandrel beams in actual masonry construction; they are connected by two steel columns located 10 feet 7 inches apart, which prevent rotation of the top beam and thus provide approximate fixed-fixed end conditions during the test.

The maximum load which may be developed by the horizontal actuator is 450 kips, using a hydraulic pressure of 3000 psi. Either displacement or load can be controlled with this actuator.

A vertical load up to 160 kips can be applied to the pier through the springs and rollers shown in Fig. 3.2. The Thomson Dual Roundway Bearings connecting the springs to the top of the panel allow the panel to move freely with minimal friction force. The coefficient of friction of bearings is purported to be 0.17.

An additional vertical, compressive load results from the characteristics of this test setup. As significant lateral displacements

are imposed on the top beam by the hydraulic actuator, the constraint provided by the side columns forces the top beam to move in a circular arc. The vertical component of this motion is opposed by the axial stiffness of the pier, resulting in a compressive load being applied to the pier. The significance of this additional, cyclic varying compressive load on the test results is discussed in Chapter 5.

Each pier was constructed on a 0.75 inch thick steel plate and had a similar plate on top, as discussed in Section 2.1. This allowed the piers to be moved into place before each test and bolted to the bottom and top steel beams. Prior to the bolting process, hydrostone was placed between the surfaces of the plates and beam flanges as well as between the top plate and the top brick course of the pier.

3.2 Loading Sequence

Each pier was subjected to a series of displacement controlled, in-plane shear loads. The full sequence of loading consisted of sets of three sinusoidal cycles of loading at a specified actuator displacement amplitude. The specified amplitude was gradually increased; the full loading sequence is given in Table 3.1. After each stage, (one set of three sinusoidal displacements at the same amplitude), the walls were visually inspected and the crack pattern identified and photographed. The sinusoidal cycles were applied at a frequency of 0.02 cycles per second throughout the test program.

The test of each pier had a duration of 2-1/2 to 3 hours. The test was usually terminated when the shear strength of the pier had dropped below one third of the maximum shear strength. All of the tests were carried out under a constant primary bearing stress between 50 and 56 psi. Additional cyclic vertical compressive loads were developed

during the test, as described in Section 3.1, and discussed further in the following chapters. All the piers tested were subjected to a maximum input displacement amplitude ranging from 0.50 inch to 0.80 inch.

Because of the flexibility of the reaction frame and other load transferring devices, the lateral displacement actually experienced by the pier was always less than the actuator input displacement, this difference being smaller towards the end of the test when the pier stiffness had attained its lowest values. There was also a slight difference between the maximum loads developed during the push and pull half cycles due to the different types of stress placed on the bolting system and to the different pier stiffnesses associated with non-symmetric crack patterns.

3.3 Instrumentation

The total horizontal load applied by the hydraulic actuator, as well as the vertical forces developed by the side columns, were measured using pre-calibrated load cells. Each pier was instrumented as indicated in Fig. 3.3.

DCDT's (direct current differential transformers) H_1 , H_2 and H_3 were attached to an external reference frame in order to measure the lateral deformation of the pier during each sequence of loading. The difference between H_1 and H_3 was used to indicate the relative lateral deflection of each pier. DCDT's D_1 , D_2 , D_3 , and D_4 measured the changes in distance between points along the diagonals of the pier and were used to indicate the shear distortion of the pier as defined in Fig. 3.4. DCDT's V_1 and V_2 were also attached to the external reference frame and measured the rotation at the top steel beam. This provided

a measurement of how well the side columns prevented the rotation of the top section of the pier.

Finally, strain gages were attached by epoxy glue to the vertical reinforcing bars at the bottom section of the pier, in order to measure the steel strain at the sections that were expected to crack first during a test.

3.4 Data Acquisition and Data Processing

Two different data acquisition systems were used during the test program. The main one consisted of a high speed scanner able to handle up to 25 channels of information, and the corresponding tape recording system (Fig. 3.5). All the data were acquired and stored on tape after being scanned at a rate of 1 point per second per channel. (No higher rate was necessary because of the low frequency used to run the test). Three computer programs were used to read the original tape data, to input the calibration values and geometrical data of each pier and to reduce the response data to their final presentation in computer plots.

The second data acquisition system was used to monitor the progress of the test and to act as a back-up system in case of any failure in the main system. It consisted of a direct writing oscillograph (visicorder) and was used only to record the most important data; namely, forces at the actuator and side columns, actuator stroke and lateral displacement of the pier. This second data acquisition system proved to be extremely useful in detecting occasional malfunctions of the actuator or the instruments attached to the piers and provided excellent visualization of the behavior of the piers as the test progressed.

TABLE 3.1

LOADING SEQUENCE

STAGE*	INPUT DISPLACEMENT AMPLITUDE (in)	STAGE*	INPUT DISPLACEMENT AMPLITUDE (in)
1	0.005	12	0.22
2	0.010	13	0.26
3	0.015	14	0.30
4	0.020	15	0.35
5	0.03	16	0.40
6	0.04	17	0.45
7	0.06	18	0.50
8	0.08	19	0.55
9	0.10	20	0.60
10	0.14	21	0.70
11	0.18	22	0.80
		23	0.90

* Each stage consists of three sinusoidal cycles at the amplitude shown

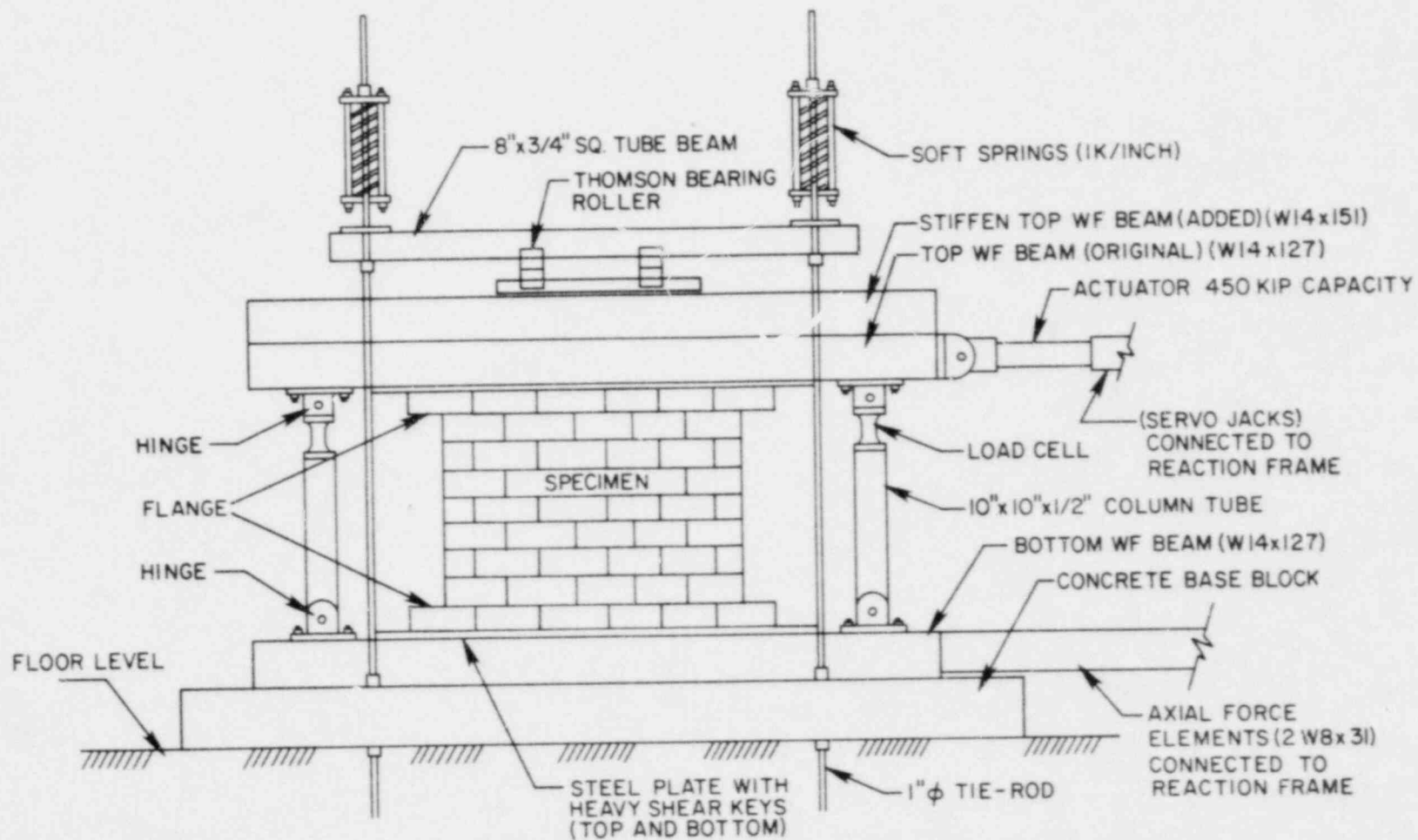


FIG. 3.1 SCHEMATIC ILLUSTRATION OF SINGLE PIER TEST

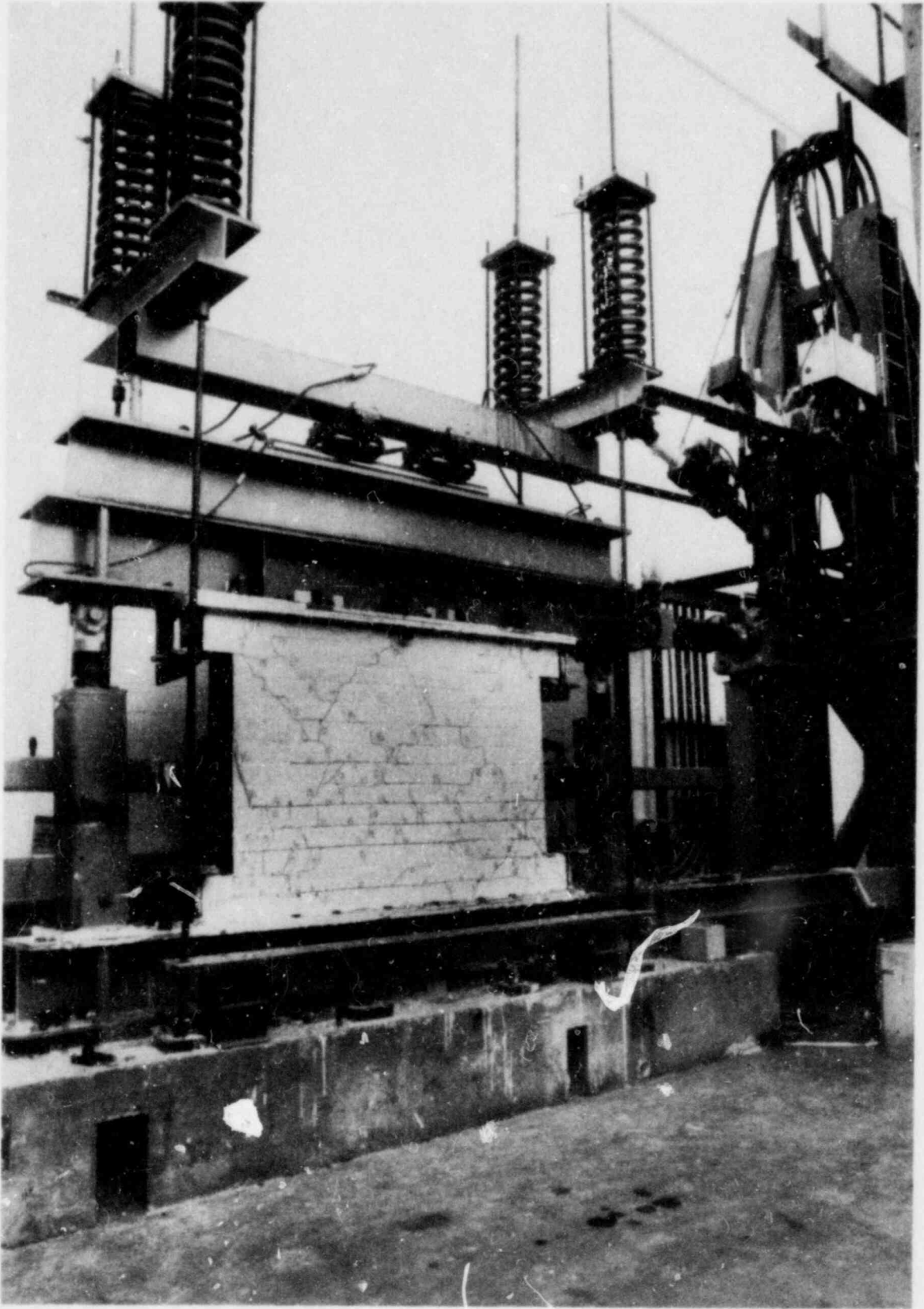


FIG. 3.2 OVERVIEW OF SINGLE PIER TEST

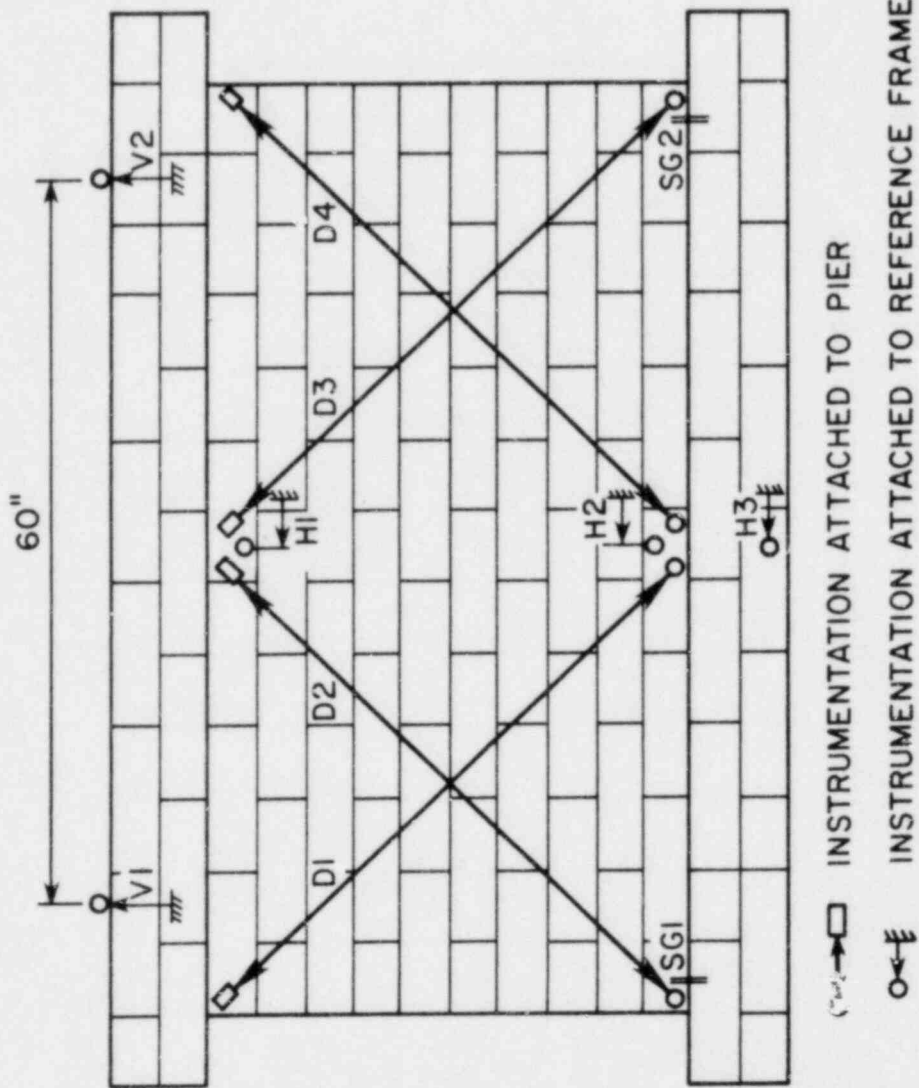
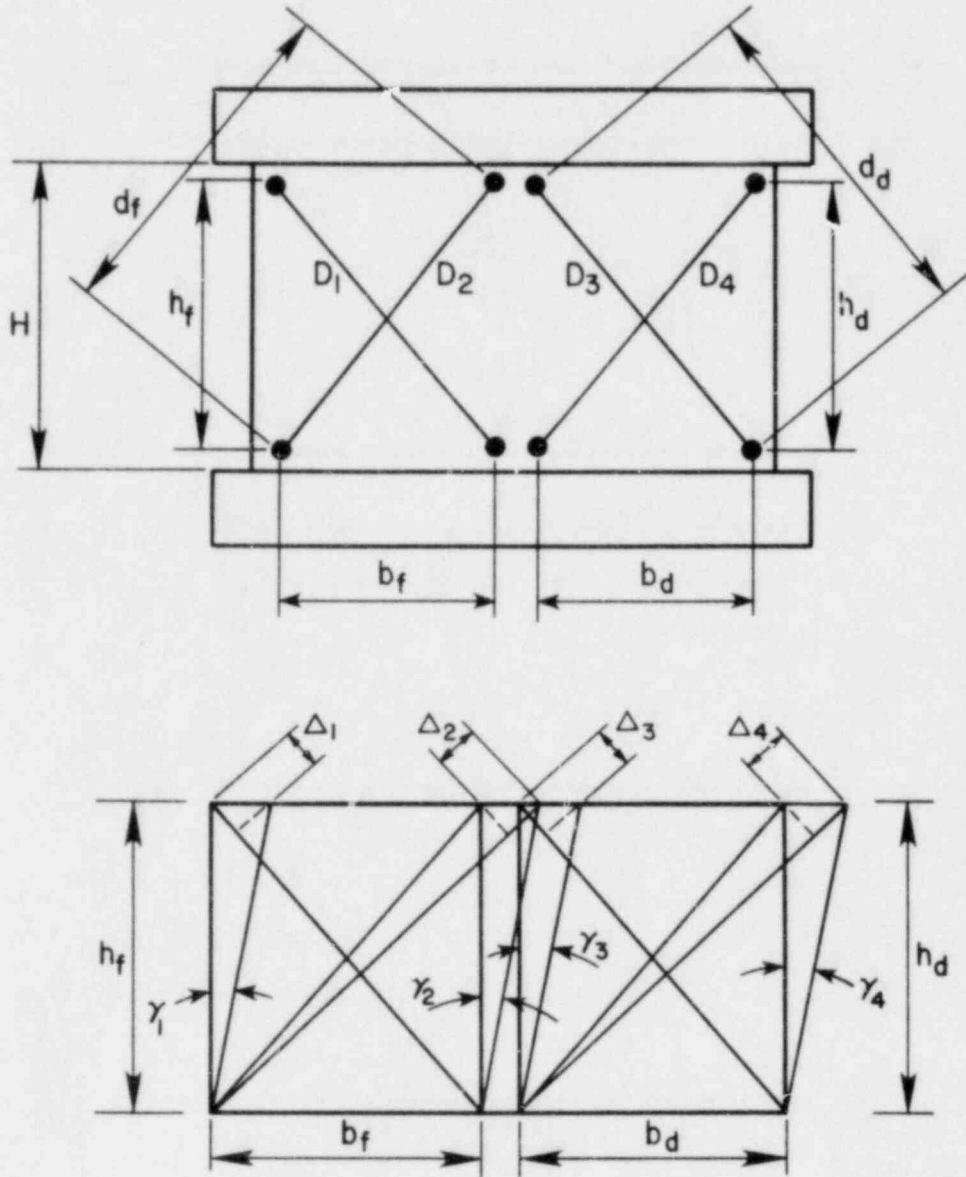


FIG. 3.3 PIER INSTRUMENTATION



d_f, b_f, h_f = AVERAGE DIMENSIONS, FRAME SIDE

d_d, b_d, h_d = AVERAGE DIMENSIONS, DOOR SIDE

Δ_i = LENGTH CHANGE IN DIAGONAL D_i

γ_i = SHEAR ROTATION

$\gamma_{AVG.}$ = AVERAGE SHEAR ROTATION

δ_S = AVERAGE SHEAR DISTORTION

$$\gamma_i = |\Delta_i| \frac{d_f}{b_f \cdot h_f} \quad i = 1, 2$$

$$\gamma_j = |\Delta_j| \frac{d_d}{b_d \cdot h_d} \quad j = 3, 4$$

$$\gamma_{AVG.} = \frac{1}{4} \sum_{i=1}^4 \gamma_i$$

$$\delta_S = \gamma_{AVG.} \cdot H$$

FIG. 3.4 MEASUREMENT OF AVERAGE SHEAR DISTORTION

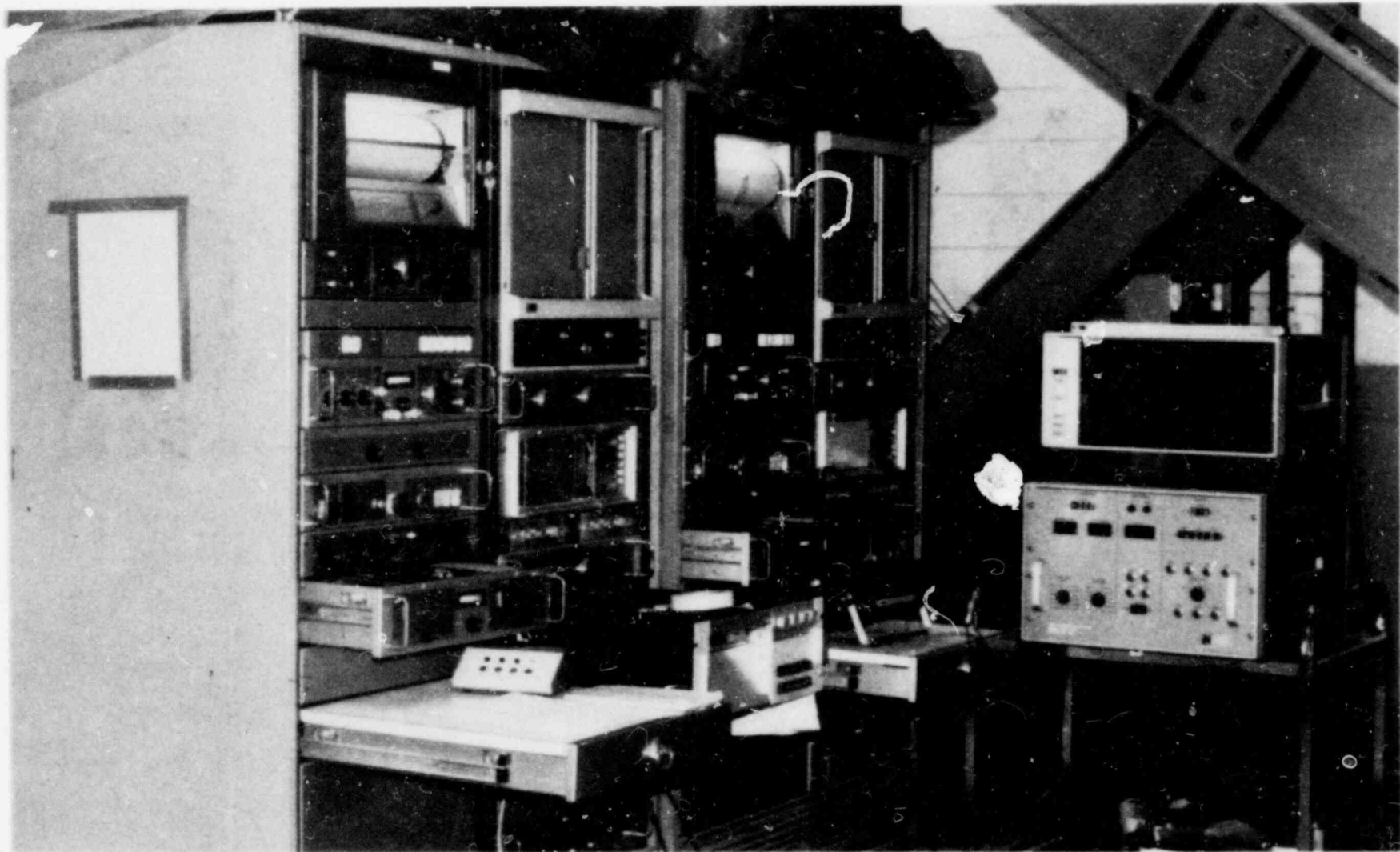


FIG. 3.5 TEST CONTROL CONSOLES AND DATA ACQUISITION SYSTEM

4. TEST RESULTS

4.1 Introduction

The experimental results for the eighteen piers having a height to width ratio of 0.5 are presented in the form of hysteresis loops, hysteresis envelopes, stiffness degradation properties, energy dissipation characteristics, and relative shear distortion. In addition, a sequence of photographs of the successive crack patterns is given for each test. An explanation of how each of the graphs was obtained and the meaning of the terms used above is included in Section 4.3. The complete presentation of the figures and photographs has been arranged by test numbers and is included in Appendix A. In order to show the relation between the sequence of the crack pattern photographs and the diagrams showing the results, a black dot has been drawn on each of the graphs and next to the corresponding picture of the crack pattern. The loading stage individualized by the black dot generally corresponds to the stage at which the first major diagonal crack occurred.

In addition, data on the ultimate strength and hysteresis indicators for each test are listed in Table 4.1. A discussion of the modes of failure observed follows in Section 4.2 and a discussion of the test results is presented in Chapter 5.

4.2 Modes of Failure

Three modes of failure were observed during this series of tests: a shear mode, a combined shear and sliding mode and a combined flexural and sliding mode. The initial crack pattern was similar in all cases: early horizontal (flexural) cracks at the bottom corners of the piers, which later either became diagonal (inclined) cracks (HCBL piers) or

continued horizontally through the bottom courses of the specimens (HCBR and CBRC piers).

The shear mode of failure occurred in tests HCBL-12-1, 2, 3, 6, HCBR-12-2, 3, 4 and CBRC-12-6, and is illustrated in Fig. 4.1(a). This mode of failure is characterized by major diagonal cracks in both directions that finally destroy the moment resisting mechanism when the diagonal crack runs through the compression toe of the pier. Strength degradation occurs because of crushing and grinding along the diagonal cracks.

The characteristics of the shear mode of failure depended on the type of masonry construction. In the case of the HCBL piers, a family of diagonal cracks developed in both directions with none of these cracks involving by itself the whole width of the pier. After the first major diagonal crack occurred, the lateral load strength of the pier appeared to be carried by diagonal compression struts bounded by the diagonal cracks. This shear resistance mechanism has also been observed by Park and Paulay^[12] in squat reinforced concrete shear walls. In all the HCBL piers that had a shear mode of failure, the final failure was prompted by the buckling of these compression struts which led to the formation of a diagonal crack that completely separated the top from the bottom of the pier (Fig. 4.1a). In some of the cases (particularly HCBL-12-6) this final failure was quite explosive and accompanied by a sharp strength degradation. In the case of the HCBR piers, the diagonal cracks usually involved the whole width of the pier with a horizontal segment above the midheight section (Fig. 4.1a). The final failure occurred when the diagonal crack destroyed the compression toe of the pier. In some cases (HCBR-12-3, Fig. 4.1a) the failure crack included both diagonal and horizontal branches.

The combined shear and sliding mode of failure occurred in tests HCBL-12-4, 5 and CBRC-12-1, 2 and 3 and is illustrated in Fig. 4.1(b). In this case the diagonal cracks developed in a pattern similar to that of the shear mode of failure specimens. However, the final failure mechanism was due to sliding through a bell-shaped path determined by two side, diagonal cracks and an horizontal branch at the top course of the pier. Even though there was crushing and grinding along the side diagonal cracks, typical of a shear failure, the sliding of the top of the pier relative to the bottom part was the feature that controlled the response of these piers, as will be explained in Chapter 5.

The combined flexural and sliding mode of failure was present in tests HCBR-12-1, 5, 6 and CBRC-12-4 and 5. In all of these cases the horizontal (flexural) cracks run continuously through the bottom courses of the piers and the final failure occurred when a sliding motion developed along this horizontal crack. A number of diagonal cracks (HCBR-12-6) or none of them (HCBR-12-1) had developed by the time the sliding failure occurred (Fig. 4.1c). In particular, the failure observed in specimen HCBR-12-6 was of the same type as that reported by Priestley^[14] in his cantilever tests. It must be noted that none of the HCBL piers developed a continuous horizontal crack through the bottom course and therefore, none of them presented this type of failure.

From a comparative point of view, the crack patterns presented in Appendix A show that the HCBL piers were the specimens that developed the largest number of diagonal cracks and the least number of horizontal cracks; the HCBR piers developed peculiar corner diagonal cracks that did not participate in the final failure mechanism; and the CBRC piers developed the largest number of horizontal cracks,

sometimes through the bottom three or four courses of the piers, and exhibited the least number of major diagonal cracks.

The readings obtained from the strain gages placed at the bottom sections of the side vertical reinforcing bars (Fig. 3.3) indicate that the tensile stresses in these bars increased with increasing values of the lateral load, until the ultimate load was attained. In some of the tests these side vertical bars showed yielding strains for a few stages around the ultimate load, while in the rest of the tests they never attained the yield condition. This strain pattern appears to be independent of the mode of failure exhibited by the pier.

Knowing the tensile strain, and therefore the tensile stress, in the extreme vertical bar, it is possible to find the stress in the central reinforcing bar, by considering the distribution of forces indicated in Fig. 4.2. If a section along the bottom cross section of the pier is considered, the moment equation about O will permit finding the stress at the bottom section of the central bar, provided both the moment of the resultant of the compressive forces in the masonry and the moment of the force at the reinforcing bar closest to O are neglected. The results of such analyses show that the central vertical bar at the bottom section of the pier was usually in compression, sometimes with values very close to the yield stress. Even though the assumptions used to compute this stress lead to overestimation of the compressive stresses in the central bar, it is clear that the design objective of avoiding tension yielding in the central reinforcing bar was accomplished.

The same moment equation about the corner point O may be used to locate the actual position of the resultant of the compressive forces

along the bottom section of the pier, when the forces developed by both the central bar and the side bar closest to 0 are included in that resultant. This analysis indicates that the resultant was usually located in the pier, within 5 to 10 inches from point 0, at the time the maximum lateral load developed. This result verifies the observation that the compressive toe in squat piers is wide enough to carry a significant shear, thus requiring an ultimate lateral load larger than that required to produce the first major diagonal crack.

4.3 Load-Displacement Characteristics

As mentioned above, Table 4.1 summarizes the strength and hysteresis characteristics of the piers and Appendix A presents the test results for each of the specimens. The correspondence between the photographs of the crack patterns and the diagrams showing the results is indicated by a black dot drawn on each of the graphs and next to the corresponding crack pattern.

The details of the derivation of each of the figures in Appendix A are discussed in the following sections.

a) Hysteresis Loops. (Shear Stress vs. Lateral Deflection Diagram).

This graph was obtained by plotting the gross shear stress against the relative lateral displacement of the pier for the duration of the test. (Since all the piers were fully grouted, the gross shear stress is equal to the net shear stress.) The gross shear stress was computed by dividing the measured horizontal force by the gross (or net) cross section area of the pier (the thickness multiplied by the width), as indicated in Table 2.1 (610 in^2 for the HCBL piers, 575 in^2 for the HCB piers and 780 in^2 for the CBRC piers). The relative lateral displacement was computed from the

difference between the lateral deflections at the top and bottom of the pier ($H_1 - H_3$ as defined in Fig. 3.3). In the case of the piers that failed in a combined shear and sliding mode of failure, (HCBL-12-4, 5 and CBRC-12-1, 2 and 3), the DCDT at the top of the pier (H_1) did not record the horizontal motion of the top portion because the bell-shape crack always developed above H_1 . Therefore, this reading was obtained from the actuator stroke by using the following procedure. First, the flexibility of the reaction frame at the level where the actuator reacts was measured; a linear, elastic behavior of the reaction frame was detected at all load levels, with a flexibility coefficient of 0.0003007 in/kip. Then, the horizontal displacement at the top of the pier was obtained by subtracting the lateral displacement of the reaction frame from the actuator stroke, and the resulting value was plotted against H_1 for the seven tests which did not exhibit combined shear and sliding failure. This plot showed a consistent linear relation between the measured H_1 and the value calculated from the actuator stroke, the actuator load and the reaction frame flexibility, for the whole range of displacements, (the measured H_1 was always 95% of the calculated value). The plot was then used to obtain H_1 for the failure stages of the tests that displayed a combined shear and sliding failure, using the readings from the actuator stroke and the actuator load.

b) Hysteresis Envelopes

The hysteresis envelope was determined from the hysteresis loops by averaging the absolute values of the three extreme positive and the three extreme negative forces (or gross shear stresses) and the

corresponding absolute values of the relative lateral displacement, for each stage of the test at a given input displacement. One point on the hysteresis envelope was obtained for each stage of 3 cycles of loading. The average lateral displacement given by the hysteresis envelope is always less than the input displacement, as explained in Section 3.2.

The black dot indicated on this graph generally corresponds to the stage at which the first major diagonal crack occurred, as observed in the corresponding photographs. This shear crack usually developed during the first of the three cycles that comprised each stage of loading.

The maximum strength obtained from the hysteresis envelope is indicated in Table 4.1 under "average ultimate shear force or stress". The "peak ultimate shear force or stress" values that appear in Table 4.1 were obtained from the average maximum force (stress) developed in any one cycle of loading. The average value is always less than the peak value, varying from 94% to 97% of the peak value. The compressive load at ultimate indicated in Table 4.1 corresponds to the maximum axial compressive load developed during each of the tests. This maximum value always occurred at the same time as the peak ultimate shear force, and was computed from the readings of the load cells located in the vertical columns plus the bearing load applied prior to each test (Table 2.1).

The last two columns of Table 4.1 correspond to hysteresis indicators obtained from the hysteresis envelopes and defined in Fig. 4.3. The level of $0.70 P_u$ used to define these indicators, where P_u is the maximum strength indicated by the hysteresis envelope, was arbitrarily chosen. Indicator h_1 tells how much the

pier deviated from its initial, theoretical stiffness, and indicator d_2 gives an indication of the deformation capability of the pier. The initial theoretical stiffness of the pier was computed assuming that the piers were fixed against rotation at both the top and bottom. The moment of inertia was calculated using the gross, uncracked section, neglecting the effect of steel reinforcement; the modulus of elasticity was taken from the measured values (Fig. 2.6, reference [2], for the HCBL piers, Tables 2.3a and 2.3b, reference [4], for the HCBR and CBRC piers, respectively), and Poisson's ratio was assumed to be 0.15. Further discussion on the correlation of the theoretical stiffness and the measured stiffness is presented in Chapter 5.

c) Stiffness Degradation

A cyclic definition of the stiffness, as indicated in Fig. 4.4, was used to measure the stiffness of the piers throughout each test. The three cyclic stiffness values obtained from each stage of loading were averaged and plotted against the average gross shear stress and the relative lateral displacement, as defined for the hysteresis envelope plot.

d) Energy Dissipation

The energy dissipated per cycle of loading was expressed in terms of a dimensionless ratio EDT. EDT is defined as the ratio of the energy dissipated to the total stored strain energy per cycle and is diagrammatically shown in Fig. 4.4. The three EDT values obtained for each stage of loading were averaged and plotted against the average relative lateral displacement.

e) Shear Distortion

The values of the shear distortion δ_s were calculated as indicated in Fig. 3.4. The absolute values of δ_s corresponding to the three extreme positive and three extreme negative forces were averaged for each stage of the test, and plotted against the respective average relative lateral displacements (total deformation of the pier), as given by H_1-H_2 (Fig. 3.3). The plot shows how much of the total deformation of the pier is due to shear distortion as defined in Fig. 3.4. Since the instruments used to measure the diagonal deformations were usually removed two or three stages before the end of the test, the number of stages used to plot this graph is usually smaller than the number used for the previous graphs.

TABLE 4.1

PIER CHARACTERISTICS AND TEST RESULTS

(Gross cross section of wall: HCBL piers = 610 in²; HCBR piers = 575 in²; CBRC piers = 780 in²)

Specimen	Test Frequency (cps)	Grouting Full (F) Partial (P) Solid (S)	Vert. reinf. steel		Horizontal reinforcing steel				Ratio of Total Area of Steel to Gross Area of Wall $P_v + P_h$	Average Ultimate Shear Force (kip)	Average Ultimate Shear Stress (psi)	Peak Ultimate Shear Force ⁽¹⁾ (kip)	Peak Ultimate Shear Stress (psi)	Compressive Load at Ultimate ⁽²⁾ (kip)	Bearing Stress at Ultimate (psi)	Hysteresis Indicators	
			No. of Bars	$P_v = \frac{A_{vs}}{A_g}$	No. of Bars	Yield Strength (ksi)	$P_h = \frac{A_{hs}}{A_g}$	$A_{hs} t_{hy}$ (kip)								h_1 (in)	d_2 (in)
HCBL-12-1	0.02	F	3#7	0.0030	No	—	—	—	0.0030	189.1	310	200.3	328	118.5	194	4.0	0.35
-2	0.02	F	3#7	0.0030	1#5	69.6	0.0005	21.6	0.0035	201.5	330	211.7	347	122.0	200	2.9	0.35
-3	0.02	F	3#7	0.0030	2#5	69.6	0.0010	43.2	0.0040	242.5	398	251.4	412	148.5	243	3.8	0.39
-4	0.02	F	3#7	0.0030	3#5	69.6	0.0015	64.7	0.0045	209.9	344	218.6	358	129.4	212	2.6	0.45 (3)
-5	0.02	F	3#7	0.0030	4#5	69.6	0.0020	86.3	0.005	220.2	361	228.0	374	130.9	215	3.6	0.49 (3)
-6	0.02	F	3#7	0.0030	4#6	67.3	0.0029	118.4	0.0058	252.0	413	261.7	429	143.0	234	3.5	0.37
HCBR-12-1	0.02	F	3#7	0.0031	No	—	—	—	0.0031	202.7	363	220.8	384	101.2	176	4.6	0.46 (4)
-2	0.02	F	3#7	0.0031	1#6	67.3	0.0008	29.6	0.0039	182.7	318	191.0	332	86.0	149	4.0	0.34
-3	0.02	F	3#7	0.0031	2#6	67.3	0.0015	59.2	0.0047	211.8	368	220.8	384	114.1	198	4.5	0.45
-4	0.02	F	3#7	0.0031	3#6	67.3	0.0023	88.8	0.0054	245.8	427	255.3	444	142.4	248	4.5	0.42
-5	0.02	F	3#7	0.0031	4#6	67.3	0.0031	118.4	0.0062	223.8	389	232.7	404	100.7	175	3.5	0.30 (4)
-6	0.02	F	3#7	0.0031	5#7	80.3	0.0052	240.9	0.0083	251.4	437	259.0	450	128.0	223	5.3	0.47 (4)
CBRC-12-1	0.02	S	3#7	0.0023	No	—	—	—	0.0023	190.4	244	197.2	253	83.9	108	3.6	0.30 (3)
-2	0.02	S	3#7	0.0023	1#6	67.3	0.0006	29.6	0.0025	186.3	239	194.8	250	98.9	127	3.6	0.38 (3)
-3	0.02	S	3#7	0.0023	2#6	67.3	0.0011	59.2	0.0034	207.9	267	217.3	279	117.1	150	3.5	0.48 (3)
-4	0.02	S	3#7	0.0023	3#6	67.3	0.0017	88.8	0.0040	227.1	291	235.0	301	96.1	123	3.3	0.24 (4)
-5	0.02	S	3#7	0.0023	4#6	67.3	0.0023	118.4	0.0046	183.0	235	192.3	247	109.8	141	4.5	0.31 (4)
-6	0.02	S	3#7	0.0023	5#7	80.3	0.0038	240.9	0.0062	207.3	266	216.1	277	110.7	142	3.6	0.28

(1) Peak value among averages of extreme values developed during any one cycle

(2) Average of values at extreme shear forces that produced the peak ultimate shear force

(3) Piers with a combined shear and sliding failure

(4) Piers with a combined flexural and sliding failure

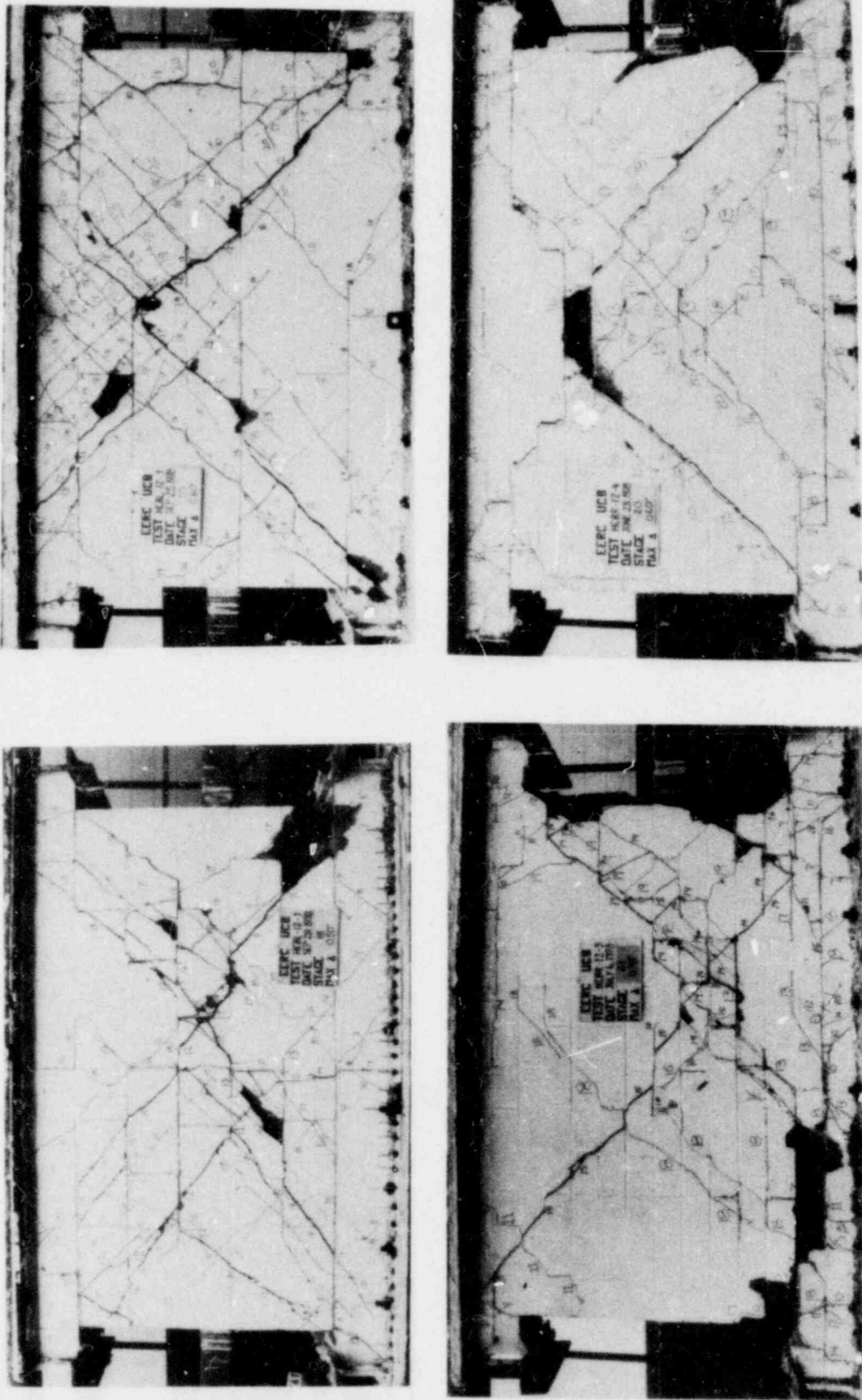


FIG. 4.1(a) SHEAR MODE OF FAILURE

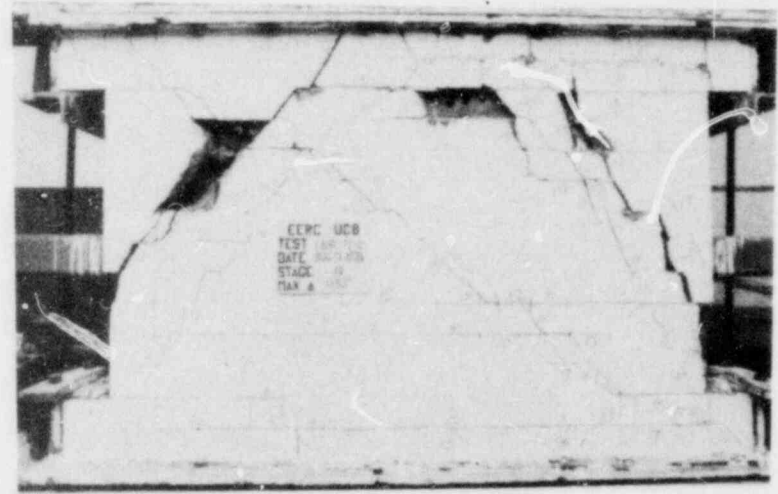
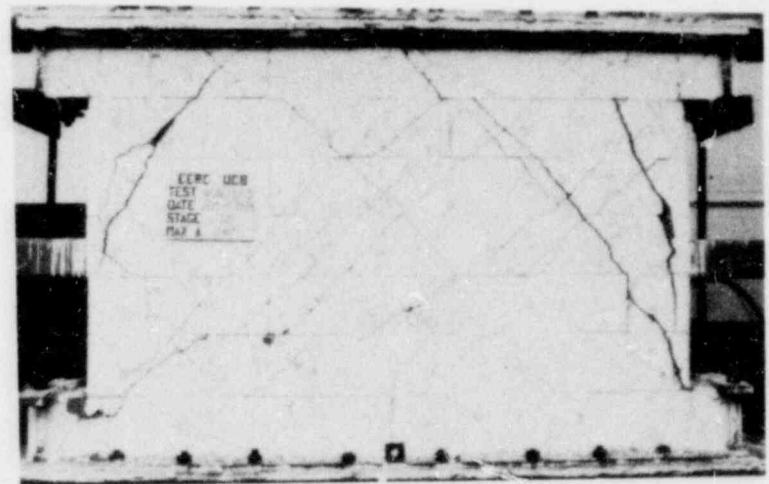
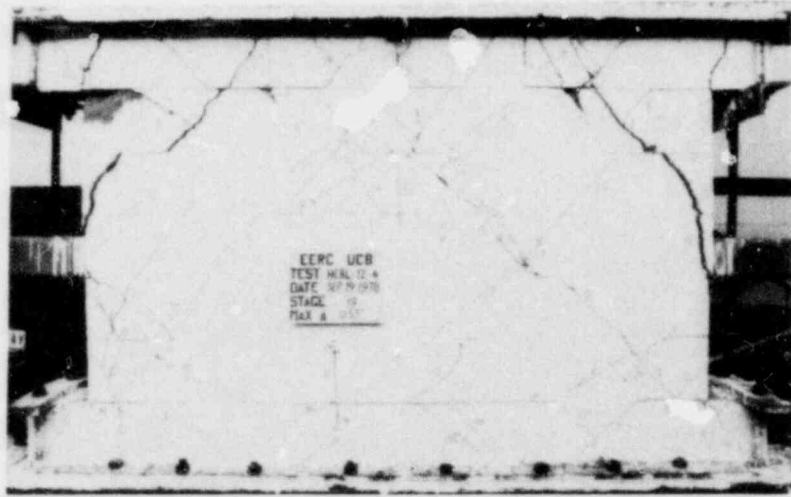


FIG. 4.1(b) COMBINED SHEAR AND SLIDING MODE OF FAILURE

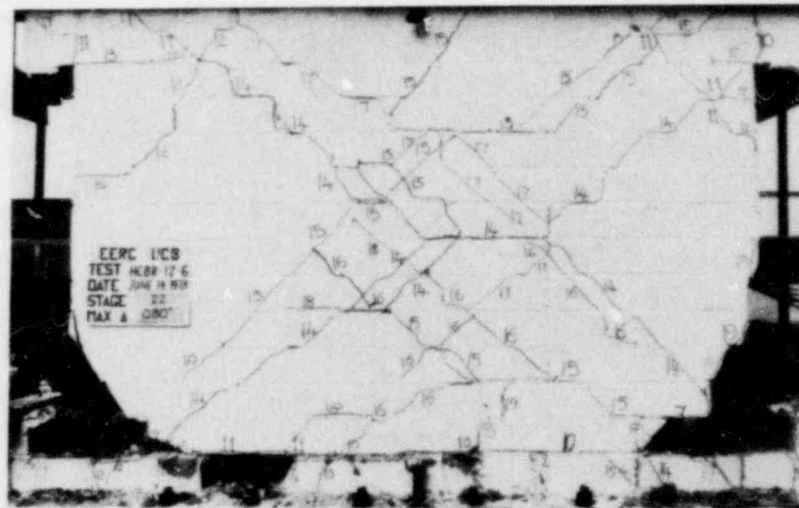


FIG. 4.1(c) COMBINED FLEXURAL AND SLIDING MODE OF FAILURE

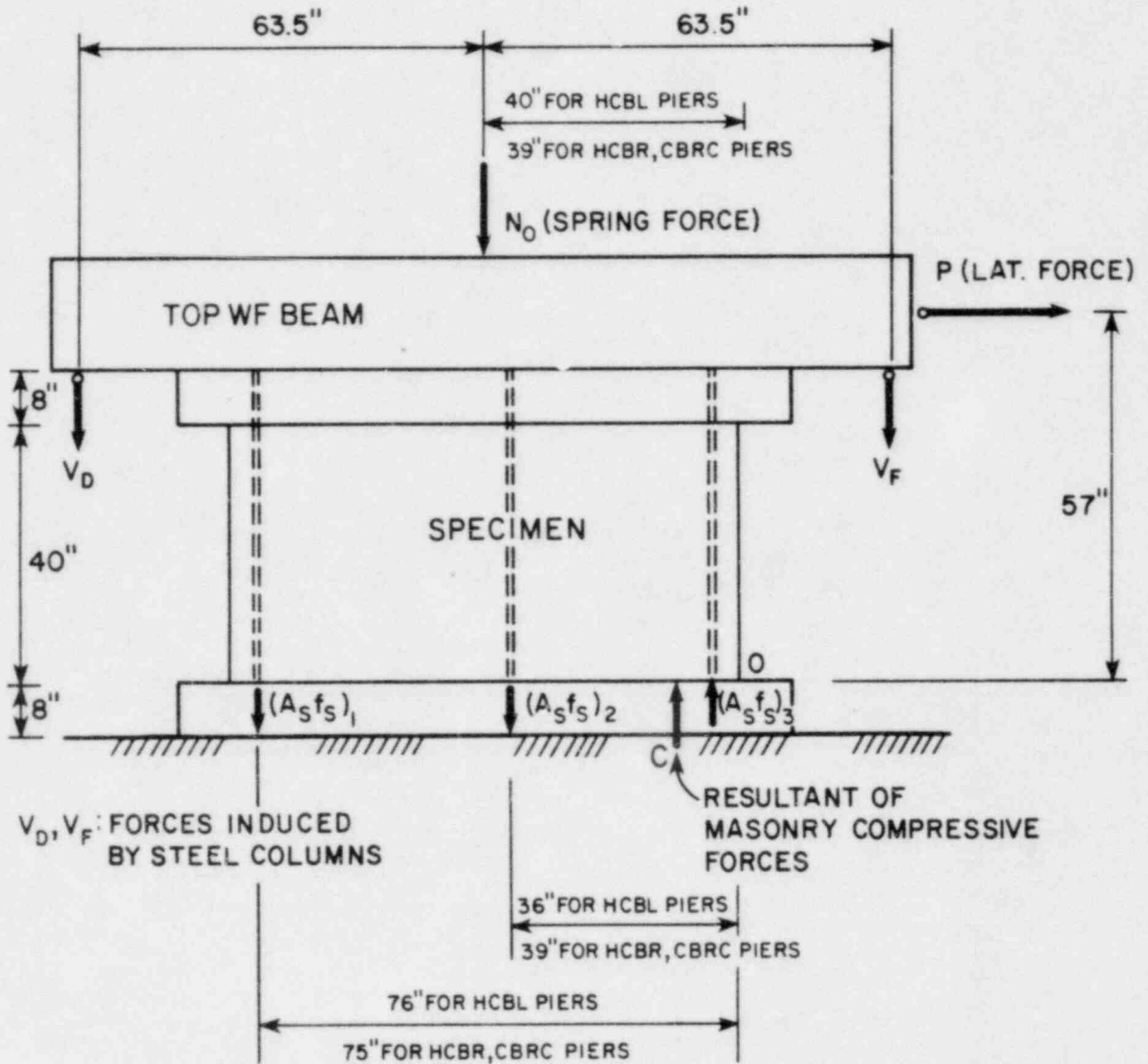
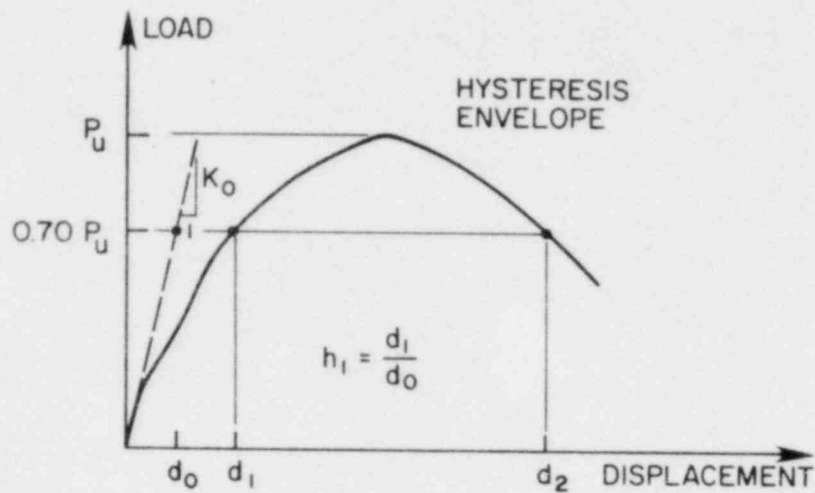


FIG. 4.2 FORCES ACTING ON THE PIER



DEFINITION OF HYSTERESIS INDICATORS h_1 AND d_2

COMPUTATION OF INITIAL STIFFNESS K_0

$$K_0^{-1} = \frac{L^3}{12EI} + 1.2 \frac{L}{AG}$$

L = height of pier

E = modulus of elasticity

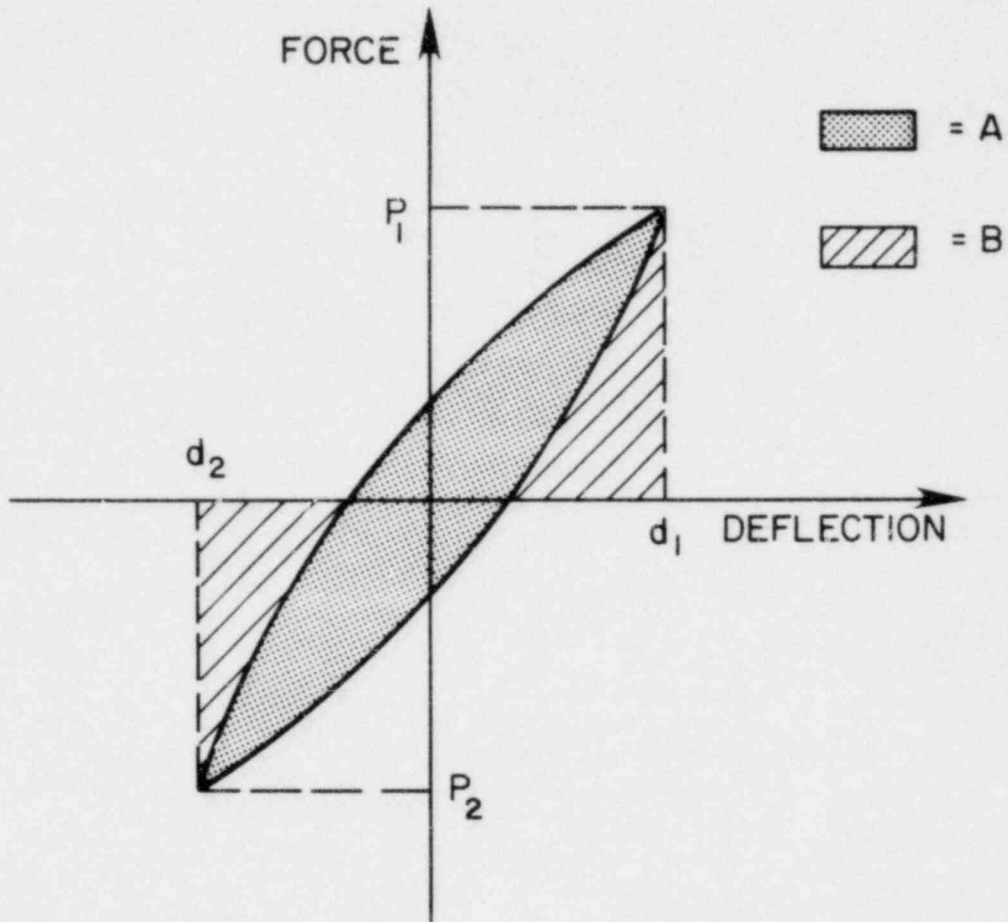
$G = \frac{E}{2(1+\nu)}$ shear modulus

D = width of pier

t = thickness of pier

SPECIMEN	L (in)	D (in)	t (in)	I (in ⁴)	A (in ²)	E (ksi)	ν	K_0 (kip/in)
HCBL-12	40	80	7.625	325,333	610.00	1140	0.15	5,776
HCBR-12	40	78	7.375	291,652	575.25	2450	0.15	11,655
CBRC-12	40	78	10.00	395,460	780.00	1720	0.15	11,095

FIG. 4.3 DEFINITION OF HYSTERESIS INDICATORS AND COMPUTATION OF INITIAL STIFFNESS



ENERGY DISSIPATION RATIO :

$$EDT = \frac{\text{DISSIPATED ENERGY}}{\text{TOTAL STORED ENERGY}} = \frac{A}{A+B}$$

PIER STIFFNESS :

$$K = \frac{|P_1 - P_2|}{|d_1 - d_2|} \quad P_1, P_2, d_1, d_2 \text{ MUST BE TAKEN WITH THEIR OWN SIGN}$$

FIG. 4.4 DEFINITIONS OF ENERGY DISSIPATION RATIO AND PIER STIFFNESS

5. DISCUSSION OF TEST RESULTS

5.1 Introduction

The test results presented in Appendix A and Table 4.1 are discussed in this chapter with reference to the two parameters that were varied during these eighteen tests, namely, the type of masonry construction and the amount of horizontal reinforcement. Other parameters, such as the initial bearing stress, the cyclic frequency, the amount of vertical reinforcement and the type of grouting, which were varied in previous pier tests [8,4,2], were held constant during these eighteen tests. Nevertheless, it must be noted that the test results were also influenced by the modes of failure exhibited by the piers, as described in Section 4.2, and this variable will be considered in the following discussion.

It is also important to note that the results presented herein were obtained from a particular loading sequence. The choice of this loading sequence has been discussed previously [8]. Other types of load sequences will be used in some of the additional seventeen tests that complete the single pier test program.

When considering the results of these eighteen tests on 1:2 piers it is important to realize that conclusions which appear valid for these tests may not hold for tests on piers with other height to width ratios. The complexity of the problem requires the completion of the test program (eighty tests) before valid conclusions concerning an adequate design of masonry structural elements can be made.

5.2 Modes of Failure

Once the modes of failure exhibited by these squat piers have been identified, it is interesting to speculate about the reasons behind

the development of each of these modes. One conclusion that is apparent from the test results is that the amount of horizontal reinforcement does not appear to have any influence on the mode of failure obtained. The type of masonry construction and the cracking pattern developed prior to failure are the variables that seem to dictate the final type of failure.

None of the HCIL piers developed a continuous horizontal crack along the bottom courses of the pier and consequently, none of them displayed a combined flexural and sliding mode of failure. There is no apparent reason to explain why two of the piers displayed combined shear and sliding failures and four of them showed typical shear failures. The crack patterns were similar in all of the cases and the mode of failure became evident only at the end of the test.

The HCBR piers did not develop any wide, diagonal cracks; therefore, they did not exhibit the combined shear and sliding type of failure obtained with the HCBL and CBRC piers. Three of the HCBR piers had a shear failure and the other three a combined flexural and sliding; these last three piers developed different numbers of shear cracks before the sliding failure through the bottom course of the pier: HCBR-12-6 had many diagonal cracks, HCBR-12-5 had only one and HCBR-12-1 had no diagonal cracks at the time of the sliding failure.

The CBRC piers developed the three modes of failure; however, unlike the other piers, they clearly showed a preference for horizontal cracks. Also fewer diagonal cracks developed during the tests.

The ultimate strength associated with the three modes of failure proved to be about the same; this can be seen from the hysteresis envelopes shown in Figs. 5.1, 5.2 and 5.3. Since the mode of failure

with the lowest ultimate strength will determine the mode of failure of a particular pier, there is no clear way to predict the modes of failure experienced by these squat piers. Section 5.3 presents the experimental sliding failure strengths of the piers as a function of the axial compressive stress. The ultimate shear strength is also discussed in Section 5.3.

Finally, it is important to recognize that in the case of an actual multistory masonry structure, for a pier to have a sliding type of failure it is necessary that all the lateral load resisting elements located at the same story level experience a sliding failure. From the results obtained for these squat piers it is clear that this type of failure is less likely to occur than a shear type of failure.

5.3 Lateral Load Strength

The lateral load strength of the piers is discussed at two levels: the strength developed by the piers at the time the first major diagonal crack occurs, which has been labeled shear crack strength; and the maximum or ultimate strength developed by the piers during the tests. It must be noted that in the tests of the piers with height to width ratios of 1 or 2 the shear crack strength always coincided with the ultimate strength and no reserve of strength was available after the first major diagonal crack occurred.

5.3.1 Shear Crack Strength

The shear crack strength of the piers (average of extreme values for the cycle where the first major diagonal crack occurred), is indicated in Table 5.1 and has been identified by a black dot on the hysteresis envelopes shown in Figs. 5.1, 5.2 and 5.3. The average shear crack strength is 225 psi for the HCBL piers, 362 psi for the HCBR piers

and 250 psi for the CBRC piers. When comparing the previous values for the different types of masonry, it should be noted that the average compressive stresses at the shear crack strength values were 98 psi, 145 psi and 117 psi for the HCBL, HCBR and CBRC piers, respectively.

The results of Table 5.1 also show an increase in shear crack strength with increasing amounts of horizontal reinforcement in the case of the HCBL and HCBR piers, although there exists some inconsistency (HCBL-12-4) in the trend observed. In the case of the double wythe grouted core clay brick piers (CBRC) there is no relation between the shear crack strength and the amount of horizontal reinforcement.

5.3.2 Ultimate Strength

The average ultimate strength is shown in Table 4.1 and Figs. 5.1, 5.2 and 5.3. The average values for each series of six piers are 359 psi, 384 psi and 257 psi for the HCBL, HCBR and CBRC piers, respectively. Consideration of the bearing stresses concurrent with these values is required if a meaningful comparison is desired. As in the case of the shear crack strength, there seems to be a positive correlation between amount of horizontal reinforcement and ultimate strength. However, this correlation is less consistent than before because of the different modes of failure experienced by the piers.

Table 5.1 presents a comparison between the peak ultimate shear strength (peak value among averages of extreme values developed during any one cycle) and the shear crack strength. The last column of Table 5.1 indicates that the reserve strength that was available after the first major diagonal crack occurred was larger for the HCBL than for the HCBR piers, (this reserve was almost negligible for the CBRC piers).

However, it must be noted that the shear crack strength of the HCBL piers was significantly less than that of the HCBR piers.

The experimental sliding strength of the piers, as a function of the axial compressive stress, is presented in Figs 5.4 and 5.5, which show the complete cyclic response of the piers after the sliding failure began to develop. If the loading portions of the curves are considered, the average ratios between the shear stress and the bearing stress are 2.64 (HCBR) and 2.54 (CBRC) for the piers exhibiting a combined flexural and sliding failure (Fig. 5.4). The same ratios for the piers that had a combined shear and sliding failure (Fig. 5.5) are 1.85 (HCBL piers) and 2.29 (CBRC piers).

5.4 Inelastic Behavior

The hysteresis envelopes (average maximum force-deflection curves) are used as a frame of reference to discuss the inelastic behavior of the piers. The question of what can be considered a desirable hysteresis envelope has been discussed in reference [8], pp. 68-70, in qualitative terms. It is appropriate to recall that the usefulness of the hysteresis envelopes is that they provide visual comparisons of ductility and ultimate strength; however, they give no indication of the energy dissipated per cycle, and consideration of this parameter in conjunction with the ultimate strength, the deformation capacity and a comparison of crack patterns at equal displacements is necessary to evaluate completely the inelastic characteristics of the pier behavior.

Figures 5.1, 5.2 and 5.3 show the changes in the hysteresis envelopes as the amount of horizontal reinforcement varies. At the same time, these figures also show how the inelastic behavior is affected by the mode of failure experienced by the piers.

As the amount of horizontal reinforcement increases, the piers show a trend towards a higher ultimate strength and higher ultimate deformation capacity, although this trend is nonuniform since some piers show less desirable inelastic behavior than a similar pier with significantly less horizontal reinforcement. The influence of the horizontal reinforcement is also obscured by the mode of failure of the piers. Piers displaying a combined shear and sliding mode of failure show a larger deformation capacity than piers exhibiting a shear or a combined flexural and sliding type of failure, since the bell-shaped sliding crack, typical of the combined shear and sliding failure, leaves a healthy bottom portion of the pier, which continues to take load when the sliding crack closes. This effect leads to an elasto-plastic hysteresis envelope before the load finally drops off because of a transfer of load deterioration along the bell-shaped crack.

The discussion presented above is quantitatively expressed by the hysteresis indicators shown in the last two columns of Table 4.1. While hysteresis indicator h_1 shows a nearly constant value (3.4 for the HCBL piers, 4.4 for the HCBR piers and 3.7 for the CBRC piers), hysteresis indicator d_2 shows significant increases for the piers that exhibited a combined shear and sliding mode of failure (from 0.37 inch to 0.47 inch in the case of the HCBL piers, and from 0.28 inch to 0.39 inch in the case of the CBRC piers). It is also interesting to note that the hysteresis indicator d_2 shows a general increase from the CBRC type piers, to the HCBL, and finally to the HCBR type piers.

5.5 Stiffness Degradation

All the piers suffered substantial stiffness degradation when subjected to gradually increasing lateral displacements. Table 5.2

summarizes this effect and shows two types of results. The first is a comparison between the theoretical initial stiffness and the maximum stiffness measured during the early stages of the test. The theoretical initial stiffness has been computed in Fig. 4.3 and the assumptions used are indicated in Section 4.3(b). The measured value is always smaller than the theoretical value and it ranges from 75% to 99% of the theoretical value for the HCBL piers, from 49% to 94% for the HCBR piers and from 55% to 94% for the CBRC piers. The differences between theoretical and measured initial values are significantly smaller than those obtained for single piers with height to width ratios of 1 and 2 [2,4]. This fact supports the hypothesis that these differences are due to the flexibility of the boundary conditions at small lateral displacements, because the width of these piers is almost twice that of the previous single piers, and the same horizontal displacement at the top is related to a smaller rotation and a better reproduction of a fixed rotation condition at the top of the pier. An excessively large value was measured for the initial stiffness of specimen HCBL-12-6, probably caused by an improper measurement of the lateral displacement of this particular pier, and it has not been included in Table 5.2. Even though the hysteresis envelope of HCBL-12-6 looks normal (Fig. 5.1), any small error in the measurement of very small displacements may have led to an erroneous stiffness measurement.

The second set of results presented in Table 5.2 is a comparison of the measured stiffnesses of all piers at applied shear stresses of 50 psi, 75 psi, 100 psi, and 150 psi, and the percentage decreases in stiffness at these stress levels with respect to the maximum initial measured value. If specimen HCBL-12-6 is not considered, the average percentage decreases at 50 psi were 5%, 11% and 22% for the HCBL, HCBR

and CBRC piers, respectively. The same average percentage decreases at 100 psi were 20%, 28% and 39%. It should be noted that the first visible cracks appeared at stress levels of 66 psi, 100 psi and 62 psi for the HCBL, HCBR and CBRC piers, respectively, (average values for each series of six specimens).

All the stiffness degradation results were obtained with displacement increments that gradually increase. Later tests will determine if the type of degradation observed is similar under a more random type of loading sequence.

Figures 5.6, 5.7 and 5.8 present the stiffness degradation curves for different amounts of horizontal reinforcement for HCBL, HCBR and CBRC piers, respectively. It is difficult to visualize any relation between the amount of vertical or horizontal reinforcement and the rate at which the stiffness degrades.

5.6 Energy Dissipation

The effects of horizontal reinforcement and mode of failure on the EDT ratio are shown in Fig. 5.9 for the HCBL piers, Fig. 5.10 for the HCBR piers and Fig. 5.11 for the CBRC piers. It can be concluded from these graphs that the energy dissipation capacity of the piers seems to be independent of the amount of horizontal reinforcement. Likewise, the mode of failure of the piers seems to have little influence on the EDT ratio, except that the piers exhibiting the combined shear and sliding mode of failure show a smaller energy dissipation rate when compared with piers that had the shear or the combined flexural and sliding mode of failure.

As with stiffness degradation, investigation of the energy dissipation characteristics of the piers under a more random load sequence is important before analytical models based on the results are formulated.

5.7 Effect of Compressive Load on Inelastic Behavior

The additional compressive load imposed by the side columns during the tests has been mentioned in Section 3.1 and has been discussed and analyzed in detail in Section 5.6 of reference [4].

There is no indication at all, that the present piers changed their mode of failure because of the additional compressive load developed by the test setup, although this was the case for some of the piers with height to width ratio of 2 or 1. The maximum bearing stress developed by the piers reached values varying from 150 psi (CBRC piers), to 250 psi (HCBL and HCBR piers), which were significantly smaller than the maximum bearing stresses obtained with the more slender pier tests. Nevertheless, it is expected that the additional bearing stress, (in excess of the initial bearing stress of 50 psi), contributed to an increase of the ultimate strength of the piers exhibiting either a shear or a sliding mode of failure.

Since these squat piers never experienced the beginning of a flexural mode of failure, (Section 4.2), it is not possible to repeat the analysis performed for the piers with other height to width ratios^[4,2] to obtain the amount of the horizontal load that can be associated with the additional compressive load developed by the test setup.

5.8 Correlation Between Square Panel and Pier Critical Tensile Strengths

This analysis is presented in Table 5.3; it is discussed in more detail in reference[9]. The purpose of this investigation is to evaluate an alternative and more appropriate test procedure for determining the code allowable shear strength of masonry walls.

Currently, the code allowable shear strength is based on the compressive strength of a masonry prism.

The square panel critical tensile strength has been determined from a study made by Blume^[1], who proposed the expression shown in Table 5.3. The ultimate load P was taken as the average value obtained from three square panel tests for each type of pier, as indicated in Table 2.2. The square panel test results for the HCBR piers were not available, as explained in Section 2.2. Therefore, the correlation is presented for the HCBL and CBRC piers only.

The critical tensile strength of the piers has been computed at the neutral axis of the pier sections, following the simple beam theory for a section under combined flexure, shear and axial force. A parabolic distribution of shear stresses over the cross section has been assumed. The piers developed their first major diagonal shear crack before the ultimate strength was attained, as mentioned in Section 5.3. The shear crack strength (lateral load required to develop the first major diagonal crack), and its corresponding compressive load (Table 5.1) have been used to evaluate the pier critical tensile strength.

In spite of the squatness of the piers, the results shown in the last column of Table 5.3 indicate that the pier critical tensile strength has been accurately estimated. In fact, the correlation obtained is better than that obtained for piers with larger height to width ratios (Tables 5.2 and 5.3 in references [2] and [4], respectively). A comparison between the square panel test and the prism compressive test to predict the shear strength of masonry walls will be presented in a future report containing the overall results of the single pier test program.

5.9 Other Test Results

The last graph in the test results (Appendix A) is a comparison between the relative lateral displacement of the piers, as measured by H_1-H_2 (Fig. 3.3) and the percentage of this displacement that can be attributed to shear distortion as defined in Fig. 3.4. These results reflect the amount of diagonal cracking present at each stage of the test, and corroborate the observation presented in Section 4.2 that the number of diagonal cracks developed during the tests increased from the CBRC piers, to the HCBR piers, to the HCBL piers.

It is also interesting to comment on the shear distortion presented by the specimens HCBR-12-1, CBRC-12-4 and CBRC-12-5 toward the end of the tests. These piers had a combined flexural and sliding failure. When sliding began to occur through the bottom course of the specimens, most of the lateral displacement took place at the bottom course of the piers and H_1-H_2 began to decrease compared with previous stages. Nevertheless, the percentage of shear distortion continued to increase.

For these squat piers, the flexural and shear components of the deformation used to compute the initial stiffness (Fig. 4.3) are in the ratio of 1:11. The greater importance of the shear deformation of these piers in comparison with the importance of the shear deformation of piers with larger height to width ratio^[2,4] is reflected in the larger amount of shear distortion exhibited by the squat piers.

Finally, it is appropriate to report on how well the test rig reproduced the fixed end condition at the top of the pier. There are two measures of the rotation of the top section; one is an absolute measure obtained with the instruments placed at the top of the pier, (DCDT'S V_1 and V_2 in Fig. 3.3), and the other is the computation of the

location of the inflection point from the forces acting on the pier. The results of these measurements during the early stages of the tests show that the absolute rotation of the top spandrel was confined to values smaller than 0.008° ; however, these rotations are very small compared to the precision of the instruments and no valid conclusions can be drawn from them. On the other hand, the position of the inflection point throughout the tests never rose more than 12 inches (30% of the pier height) from the mid-height section of the pier.

TABLE 5.1

COMPARISON OF SHEAR CRACK STRENGTH AND ULTIMATE STRENGTH
(Average of extreme values during any one cycle considered)

Specimen	Grouting Full(F) Solid(S)	Initial Bearing Stress (psi)	Vertical Reinforcement No. Bars	Horizontal Reinforcement		Shear Crack Strength		Compressive Stress at Shear Crack (psi)	Peak Ultimate Shear		Compressive Stress at Ultimate (psi)	Peak Ult. Shear Shear Cr. Strength
				No. Bars	$A_{hs} f_y$ (kip)	Force (kip)	Stress (psi)		Force (kip)	Stress (psi)		
HCBL-12-1	F	52	3#7	—	—	121.7	200	85	200.3	328	194	1.65
-2	F	52	3#7	1#5	21.6	125.4	206	86	211.7	347	200	1.69
-3	F	52	3#7	2#5	43.2	130.9	215	83	251.4	412	243	1.92
-4	F	52	3#7	3#5	64.7	159.1	261	127	218.6	358	212	1.37 *
-5	F	52	3#7	4#5	86.3	137.9	226	106	228.0	374	215	1.65 *
-6	F	52	3#7	4#6	118.4	148.9	244	102	261.7	429	234	1.76
HCBR-12-1	F	56	3#7	—	—	Did not have a shear crack			220.8	384	176	— **
-2	F	56	3#7	1#6	29.6	183.6	319	125	191.0	332	149	1.04
-3	F	56	3#7	2#6	59.2	202.1	351	150	220.8	384	198	1.09
-4	F	56	3#7	3#6	88.8	204.7	356	143	255.3	444	248	1.25
-	F	56	3#7	4#6	118.4	226.8	394	154	232.7	404	175	1.03 **
-6	F	56	3#7	5#7	240.9	225.7	392	153	259.0	450	223	1.15 **
CBRC-12-1	S	50	3#7	—	—	197.2	253	108	197.2	253	108	1.00 *
-2	S	50	3#7	1#6	29.6	194.8	250	127	194.8	250	127	1.00 *
-3	S	50	3#7	2#6	59.2	214.6	275	138	217.3	279	150	1.01 *
-4	S	50	3#7	3#6	88.8	Did not have a shear crack			235.0	301	123	— **
-5	S	50	3#7	4#6	118.4	179.8	231	116	192.3	247	141	1.07 **
-6	S	50	3#7	5#7	240.9	187.5	240	94	216.1	277	142	1.15

* Piers with a combined shear and sliding failure

** Piers with a combined flexural and sliding failure

TABLE 5.2

EFFECT OF SHEAR STRESS AND STEEL REINFORCEMENT ON STIFFNESS DEGRADATION

Specimen	Grouting Full (F) Solid (S)	Vertical Steel Reinforcement	Horizontal Steel Reinforcement	Theoretical Initial Stiffness (kip/in)	Measured Maximum Initial Stiffness (kip/in)	Stiffness at 50 psi		Stiffness at 75 psi		Stiffness at 100 psi		Stiffness at 150 psi	
						Measured (kip/in)	Percentage Decrease (%)	Measured (kip/in)	Percentage Decrease (%)	Measured (kip/in)	Percentage Decrease (%)	Measured (kip/in)	Percentage Decrease (%)
HCBL-12-1	F	3#7	No	5776	4353	*	*	4709	3	3549	18	2955	32
-2	F	3#7	1#5	5776	5096	4927	3	4504	12	3882	24	3286	36
-3	F	3#7	2#5	5776	5546	5423	2	4913	11	4780	14	3723	33
-4	F	3#7	3#5	5776	5693	5588	2	4855	15	4446	22	3450	39
-5	F	3#7	4#5	5776	5098	4471	12	4182	18	3976	22	3131	39
-6	F	3#7	4#6	5776	—	—	—	—	—	—	—	—	—
HCBR-12-1	F	3#7	No	11655	8874	7131	20	6169	30	5418	39	4450	50
-2	F	3#7	1#6	11655	7367	6951	6	6650	10	5848	21	4802	35
-3	F	3#7	2#6	11655	10902	9227	15	8107	26	6369	42	4501	59
-4	F	3#7	3#6	11655	8585	7978	7	7622	11	6659	22	5120	40
-5	F	3#7	4#6	11655	7957	7579	5	6662	16	6320	21	5191	35
-6	F	3#7	5#7	11655	5751	4937	14	4700	18	4408	23	3756	35
CBRC-12-1	S	3#7	No	11095	6971	6841	2	5719	18	5020	28	3839	45
-2	S	3#7	1#6	11095	9642	7061	27	5851	39	4716	51	3469	64
-3	S	3#7	2#6	11095	6152	6031	2	5670	8	4932	20	3985	35
-4	S	3#7	3#6	11095	9456	7163	24	6449	32	5423	43	4503	52
-5	S	3#7	4#6	11095	10443	6300	40	5253	50	3887	63	2762	74
-6	S	3#7	5#7	11095	6907	4533	34	5392	22	4819	30	3714	46

* Maximum initial stiffness obtained after 50 psi

TABLE 5.3

CORRELATION BETWEEN SQUARE PANEL AND PIER CRITICAL TENSILE STRENGTH
(Average of extreme values during any one cycle considered)

Specimen	SQUARE PANEL (1)				PIER (2)						$\frac{\sigma_{tcr}^o}{\sigma_{tcr}}$
	Ultimate Load P(kip)	Side Area A(in ²)	$\tau = \frac{P}{\sqrt{2A}}$ (psi)	Blume's Formula $\sigma_{tcr}^o = 0.734\tau$ (psi)	Shear Crack Force P(kip)	Compressive Load at Shear Crack N(kip)	Cross Section A(in ²)	Shear Crack Stress $\frac{P}{A}$ (psi)	Bearing Stress at Shear Crack $\frac{N}{A}$ (psi)	Critical Strength σ_{tcr} (psi)	
HCEL-12-1	155.0	244	449.2	329.7	121.7	51.8	610.0	199.5	84.9	259.8	1.27
-2	155.0	244	449.2	329.7	125.4	52.6		205.6	86.2	268.2	1.23
-3	155.0	244	449.2	329.7	130.9	50.6		214.6	83.0	283.1	1.16
-4	155.0	244	449.2	329.7	159.1	77.3		260.8	126.7	333.0	0.99
-5	155.0	244	449.2	329.7	137.9	64.8		226.1	106.2	290.1	1.14
-6	155.0	244	449.2	329.7	148.9	62.1		244.1	101.8	318.8	1.03
CBRC-12-1	186.3	360	365.9	268.6	197.2	83.9	780.0	252.8	107.6	329.2	0.82
-2	186.3	360	365.9	268.6	194.8	98.9		249.7	126.8	316.5	0.85
-3	186.3	360	365.9	268.6	214.6	107.9		275.1	138.3	349.3	0.77
-4	186.3	360	365.9	268.6	Did not have a shear crack			—	—	—	—
-5	186.3	360	365.9	268.6	179.8	90.5		230.5	116.0	292.6	0.92
-6	186.3	360	365.9	268.6	187.5	73.6		240.4	94.4	316.5	0.85

(1) Square Panel Critical Tensile Strength

$$\text{Blume's formula: } \sigma_{tcr}^o = -0.582 \frac{P}{A} - \frac{\sigma_c}{2} + \frac{1}{2} \sqrt{4.849 \left(\frac{P}{A}\right)^2 + \sigma_c^2}$$

$$\text{If edge pressure } \sigma_c = 0, \quad \sigma_{tcr}^o = 0.734 \frac{P}{\sqrt{2A}}$$

(2) Pier Critical Tensile Strength

Assuming a parabolic distribution of shear stresses

$$\sigma_{tcr}^o = -\frac{\sigma_c}{2} + \sqrt{(1.5\tau)^2 + \left(\frac{\sigma_c}{2}\right)^2}$$

 $\sigma_c = \frac{N}{A}$: applied compressive stress $\tau = \frac{P}{A}$: average shear stress

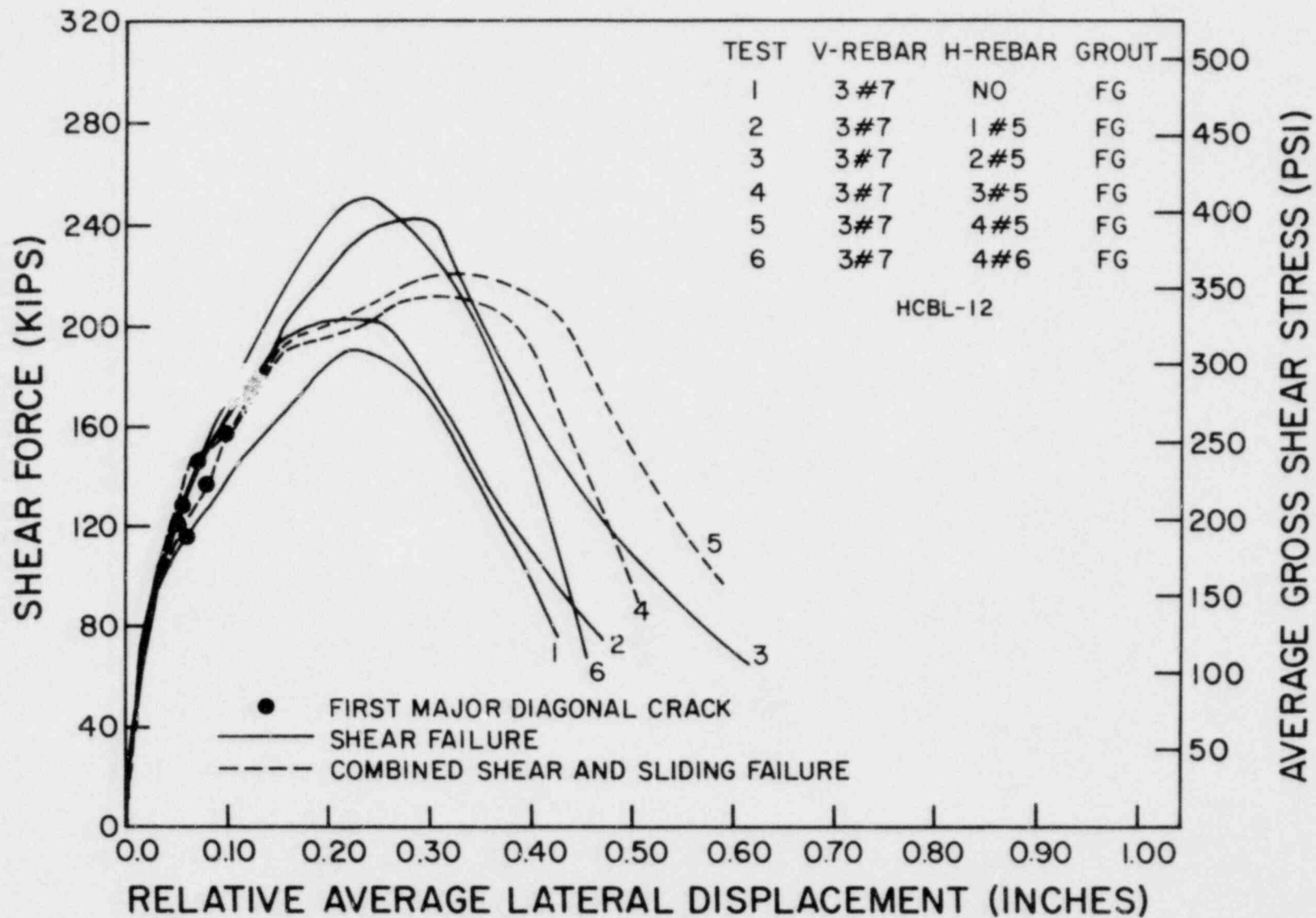


FIG. 5.1 HYSTERESIS ENVELOPES FOR HOLLOW CONCRETE BLOCK PIERS

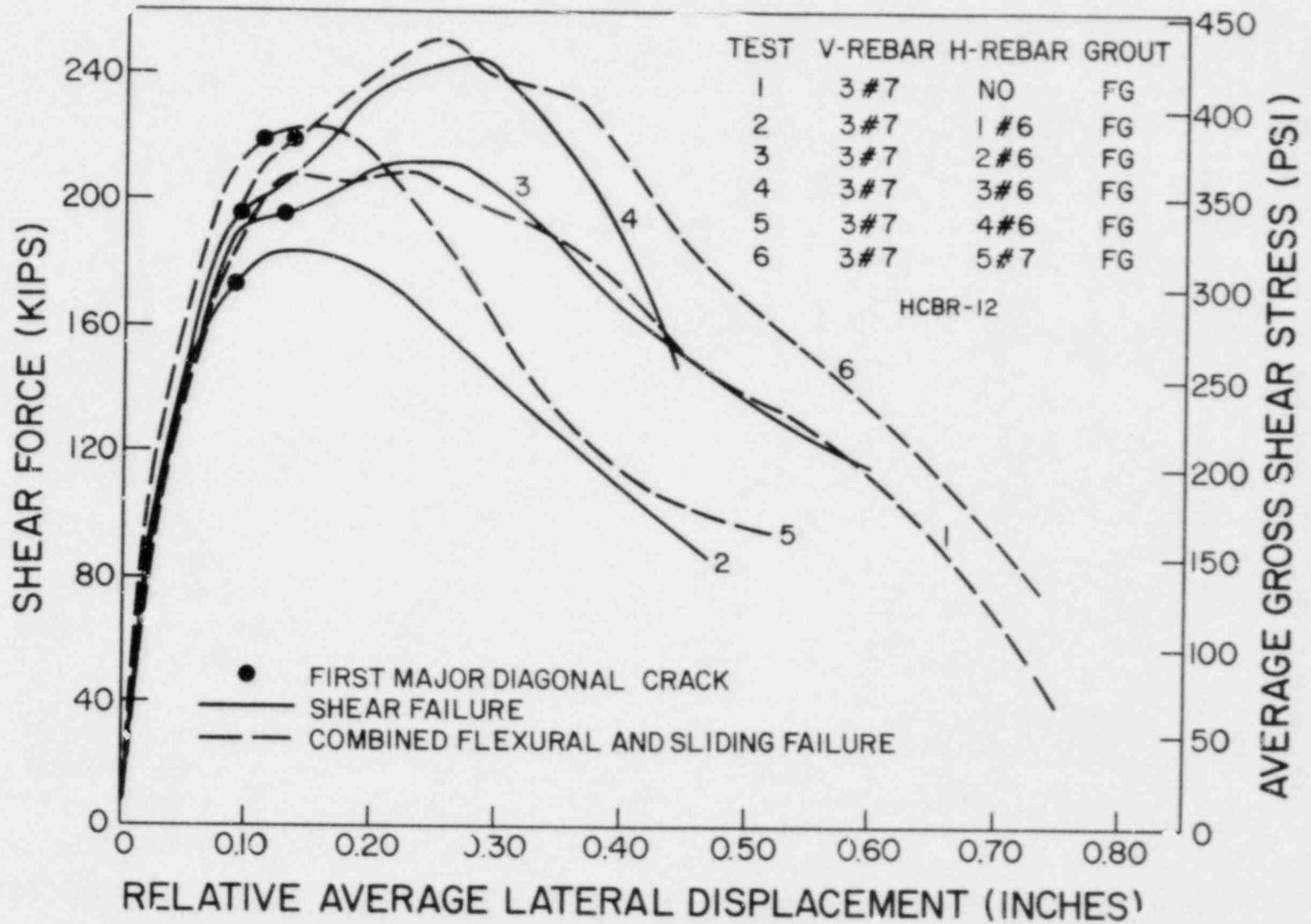


FIG. 5.2 HYSTERESIS ENVELOPES FOR HOLLOW CLAY BRICK PIERS

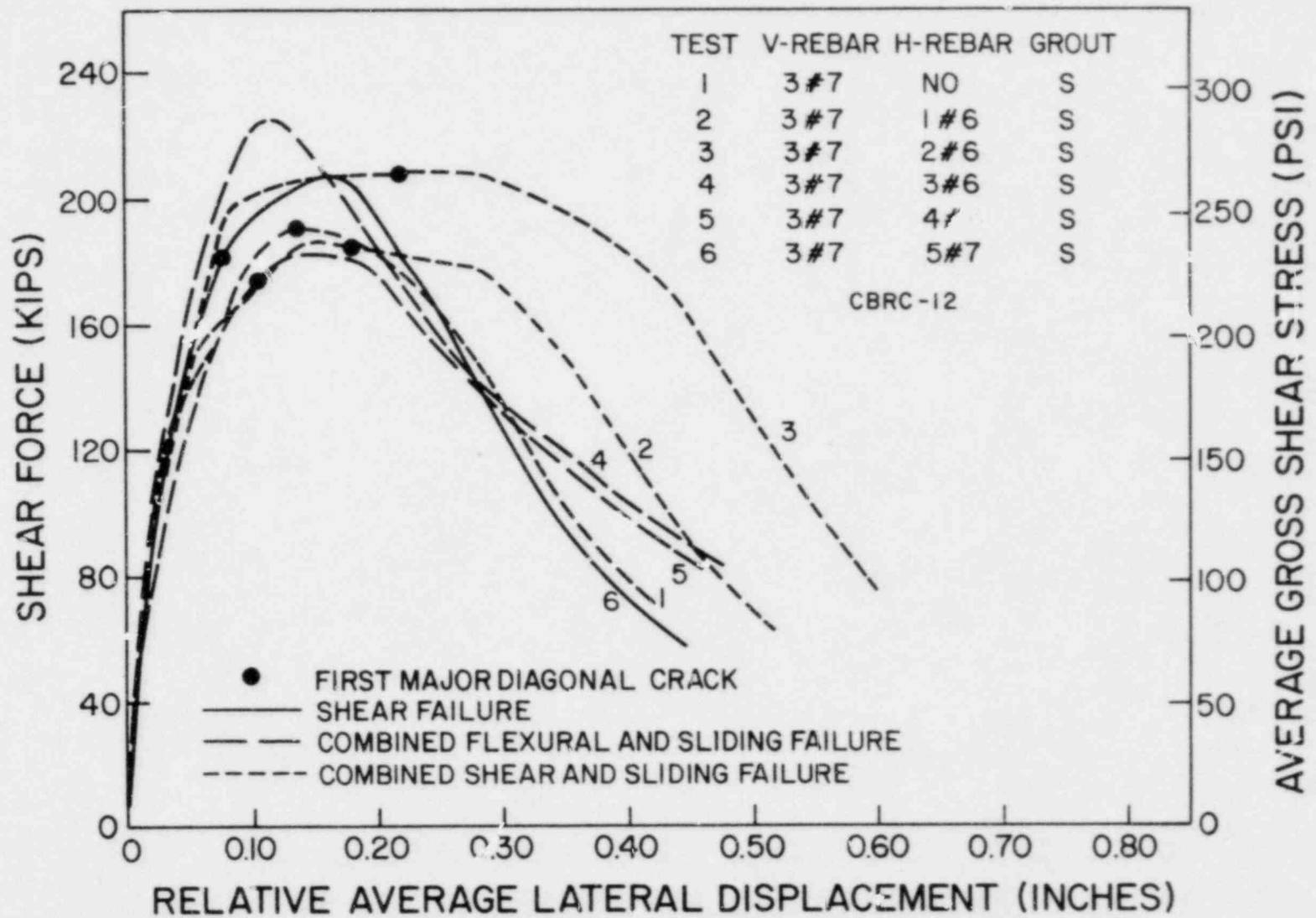


FIG. 5.3 HYSTERESIS ENVELOPES FOR GROUTED CORE CLAY BRICK PIERS

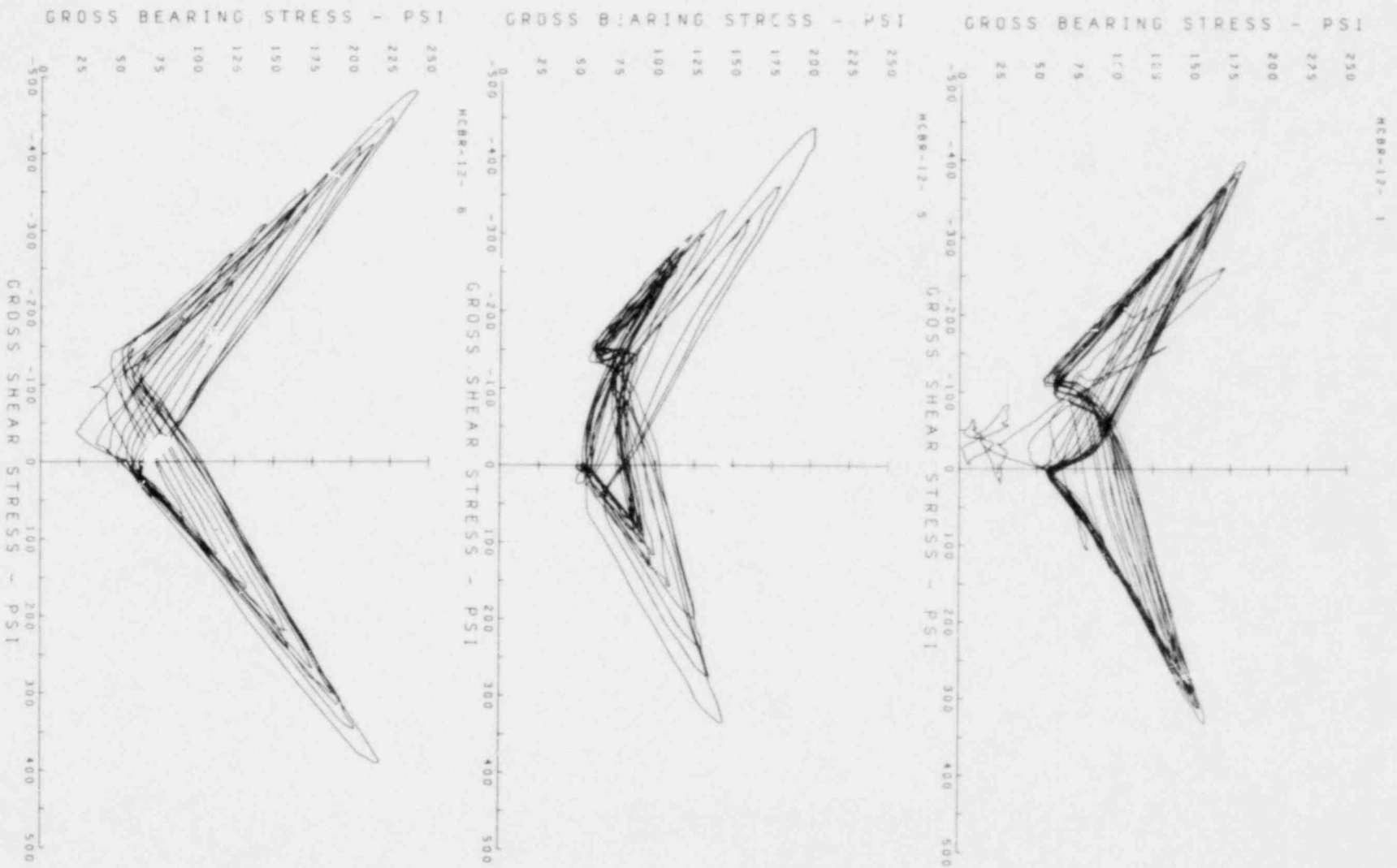


FIG. 5.4(a) SLIDING STRENGTH HCBR PIERS - COMBINED FLEXURAL AND SLIDING MODE OF FAILURE

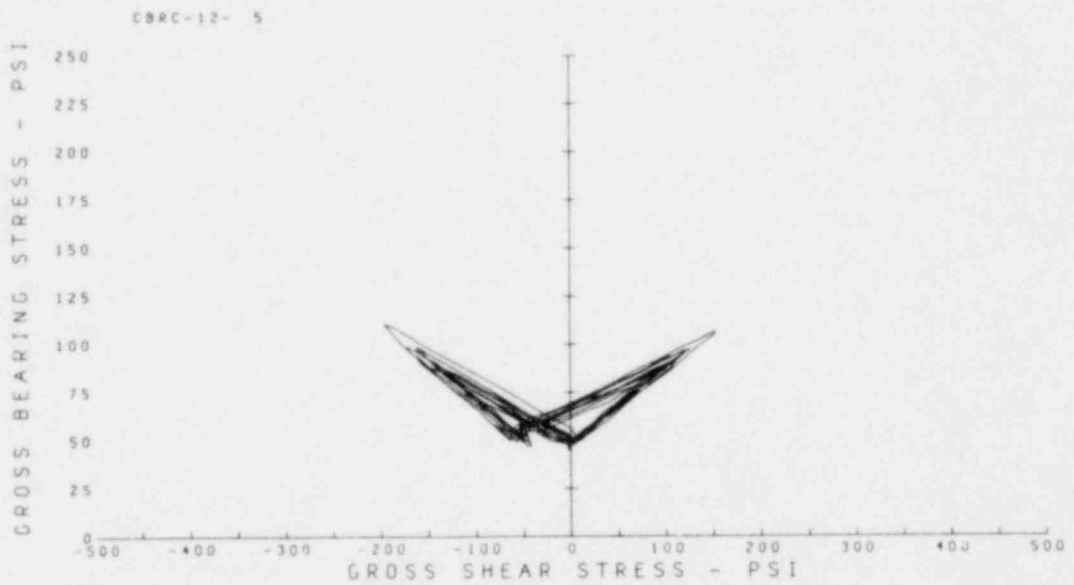
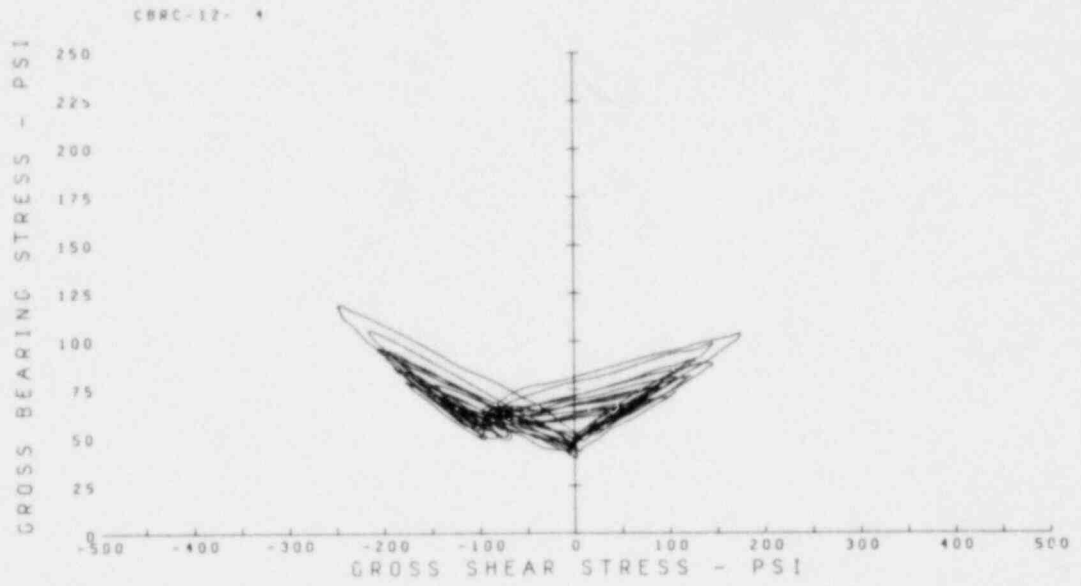


FIG. 5.4(b) SLIDING STRENGTH CBRC PIERS - COMBINED FLEXURAL AND SLIDING MODE OF FAILURE

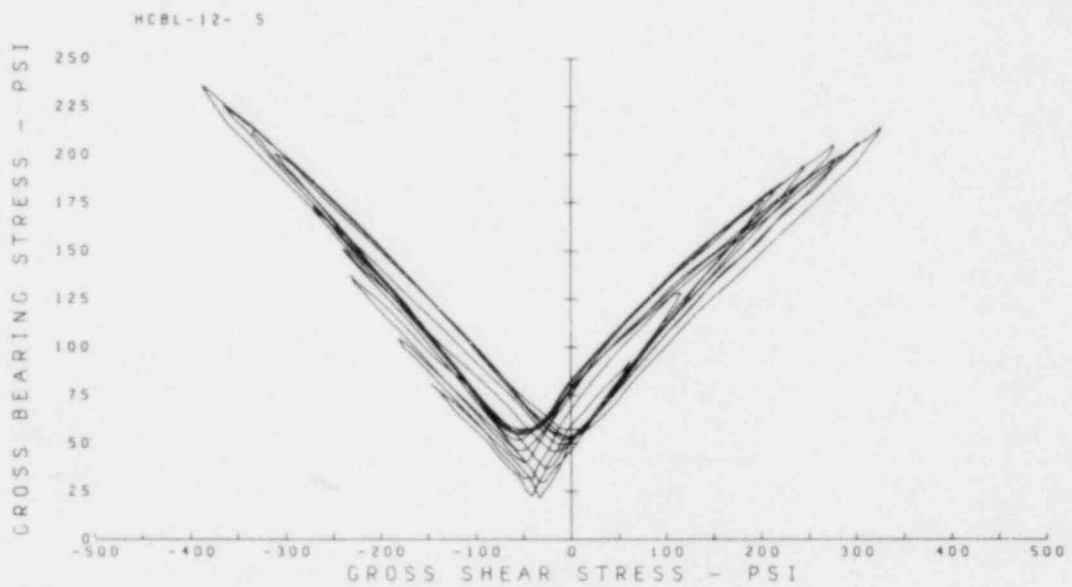
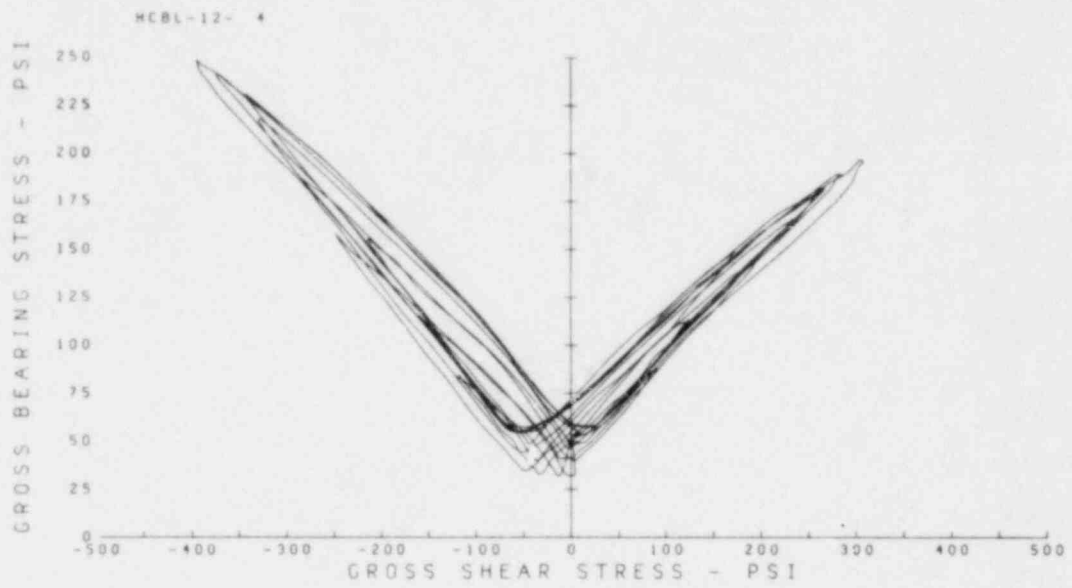


FIG. 5.5(a) SLIDING STRENGTH HCBL PIERS - COMBINED SHEAR AND SLIDING MODE OF FAILURE

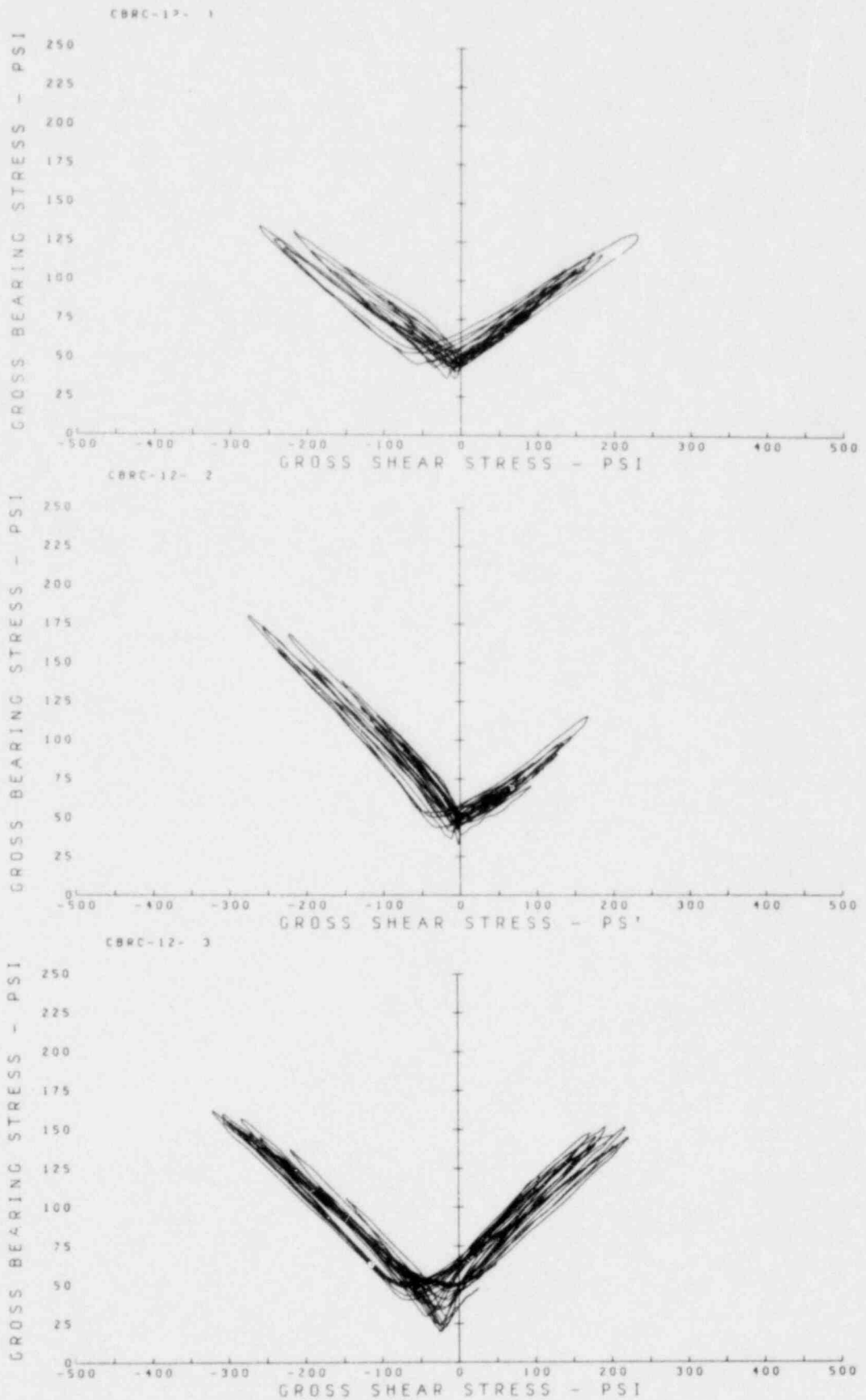


FIG. 5.5(b) SLIDING STRENGTH CBRC PIERS - COMBINED SHEAR AND SLIDING MODE OF FAILURE

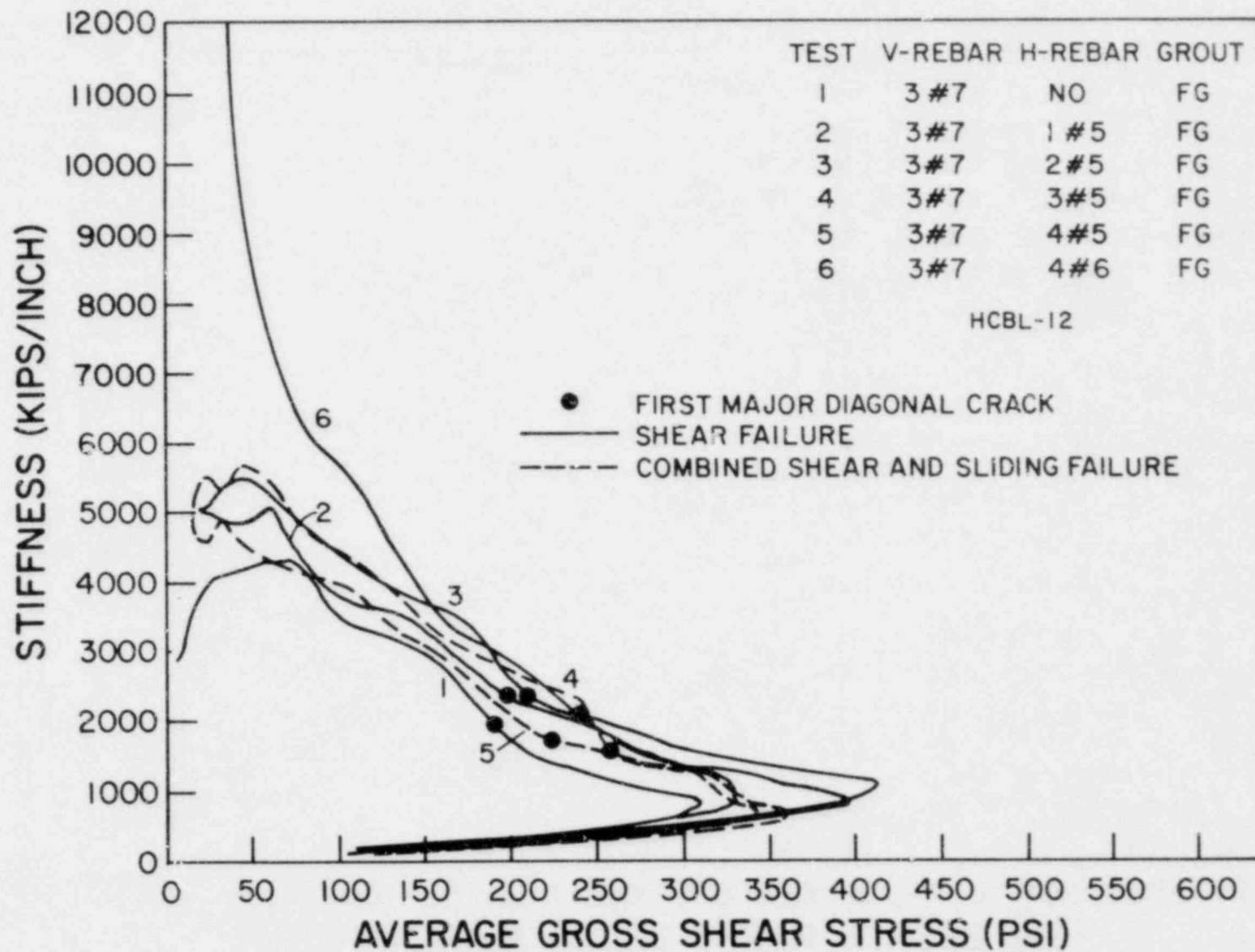


FIG. 5.6 STIFFNESS DEGRADATION FOR HOLLOW CONCRETE BLOCK PIERS

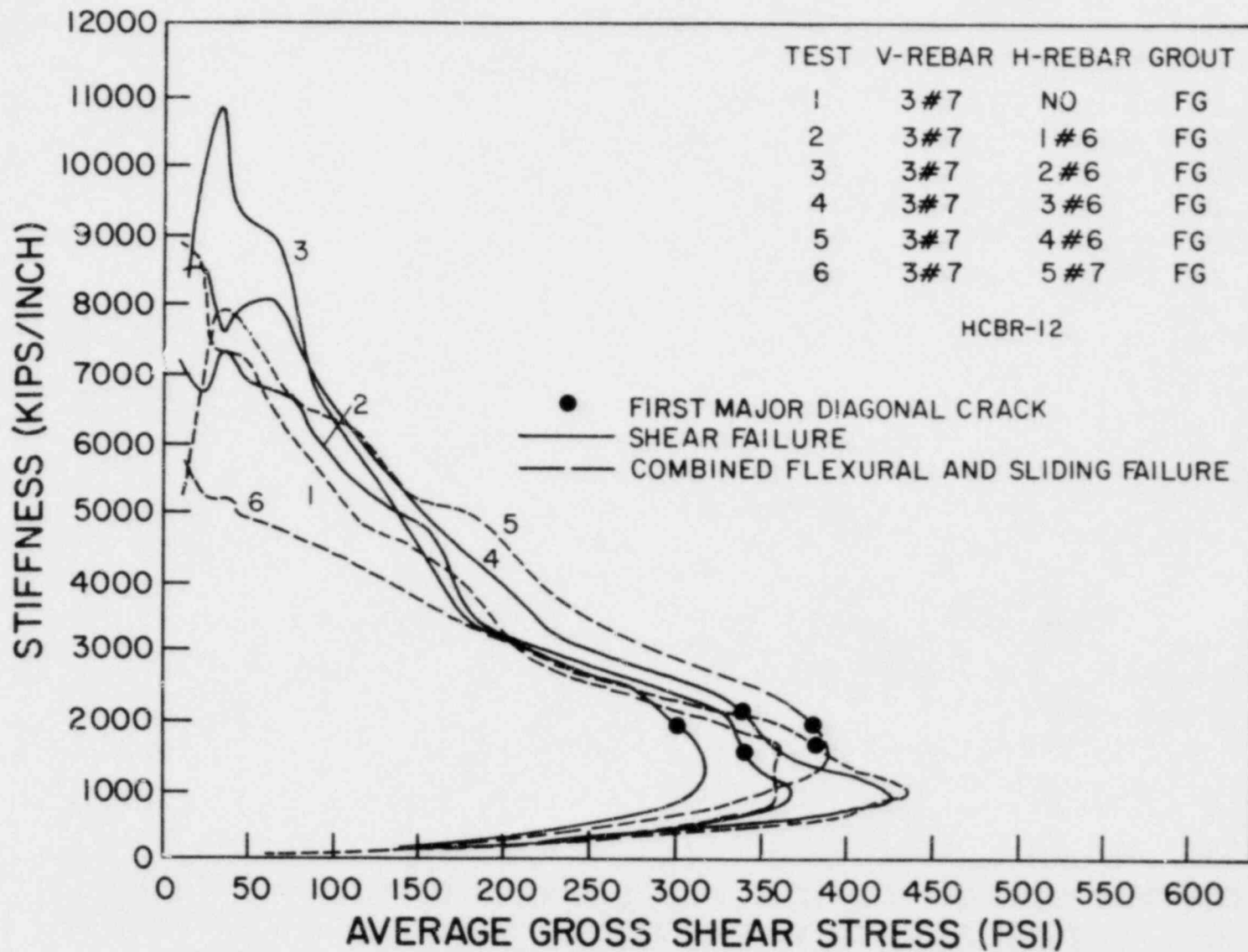


FIG. 5.7 STIFFNESS DEGRADATION FOR HOLLOW CLAY BRICK PIERS

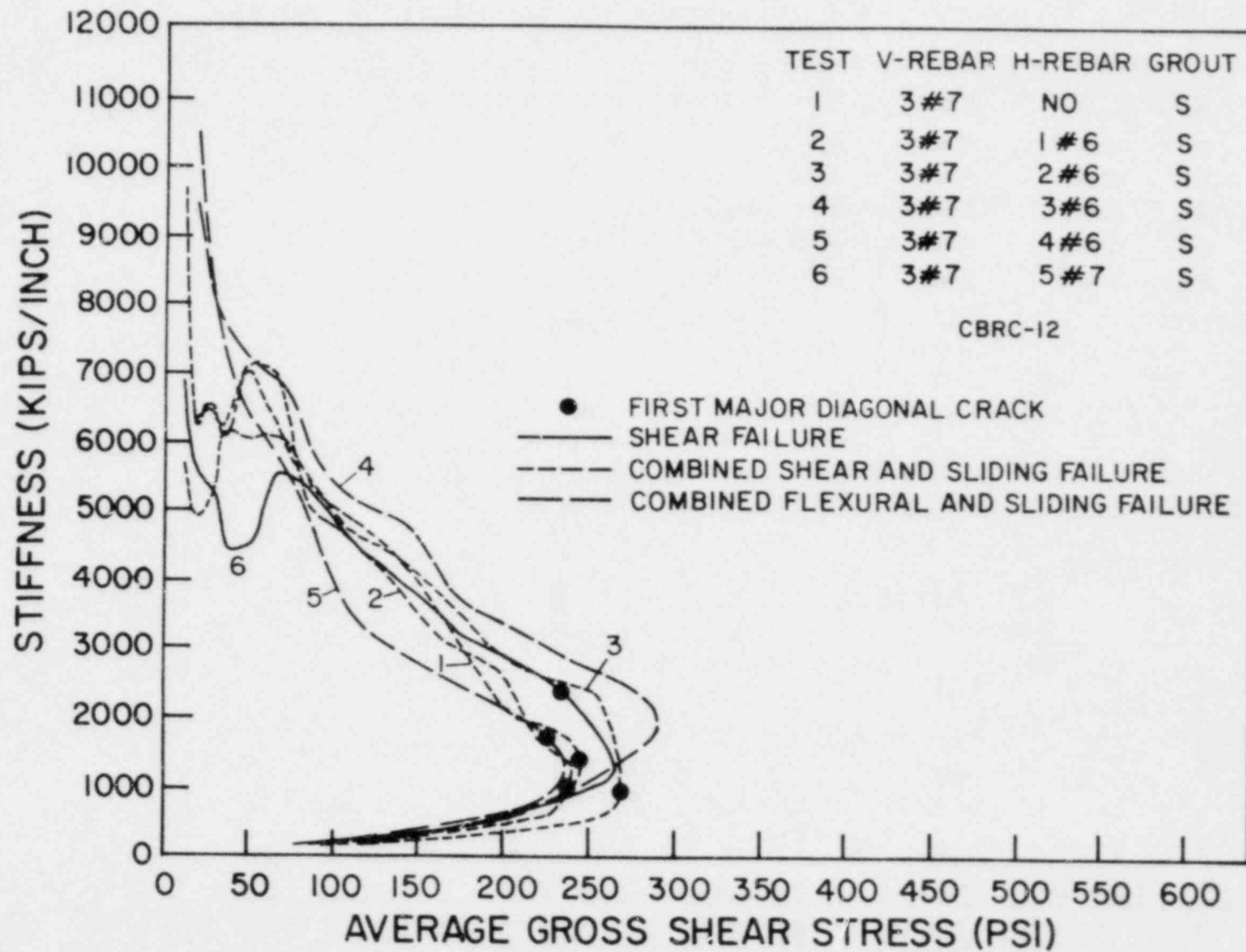


FIG. 5.8 STIFFNESS DEGRADATION FOR GROUTED CORE CLAY BRICK PIERS

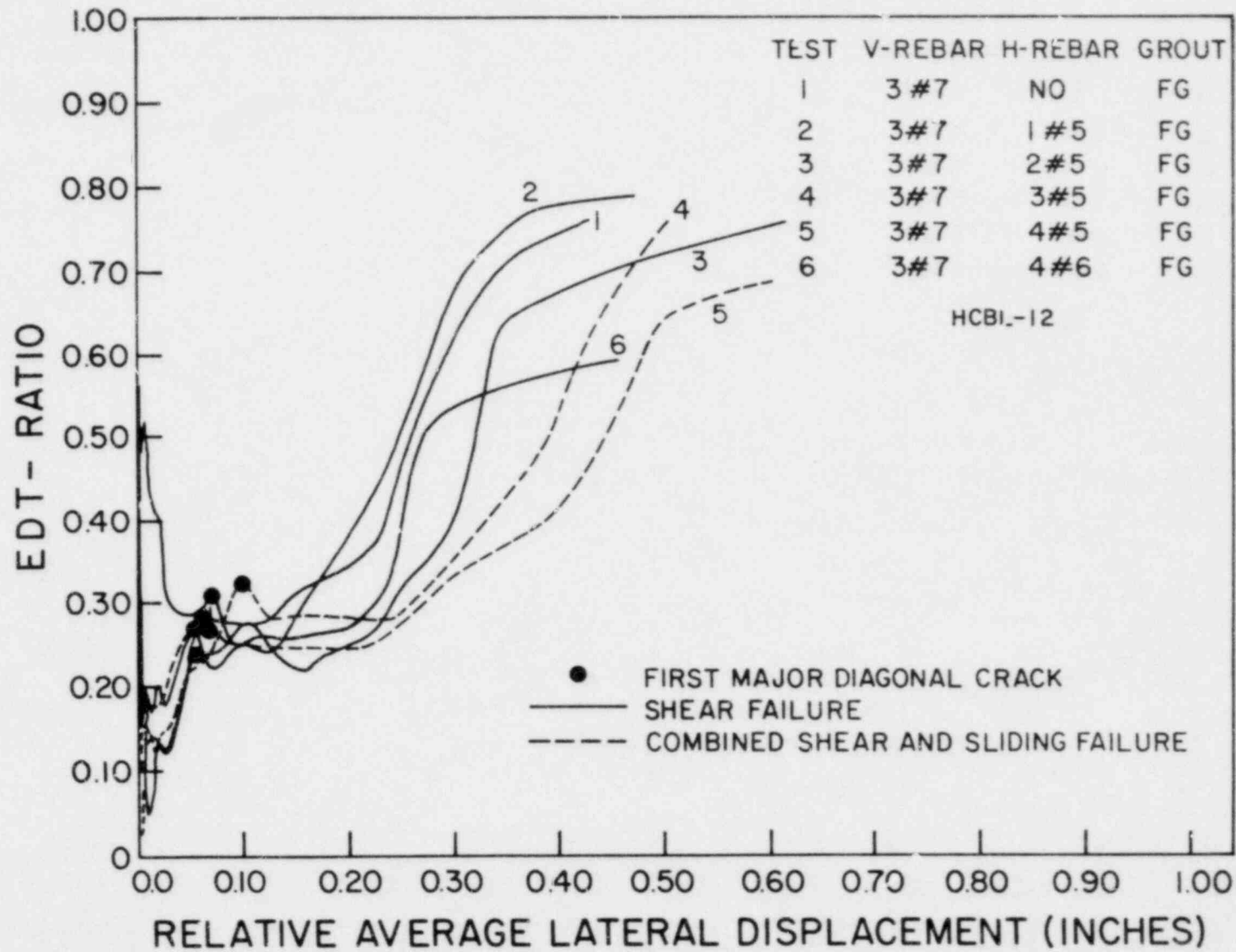


FIG. 5.9 ENERGY DISSIPATION FOR HOLLOW CONCRETE BLOCK PIERS

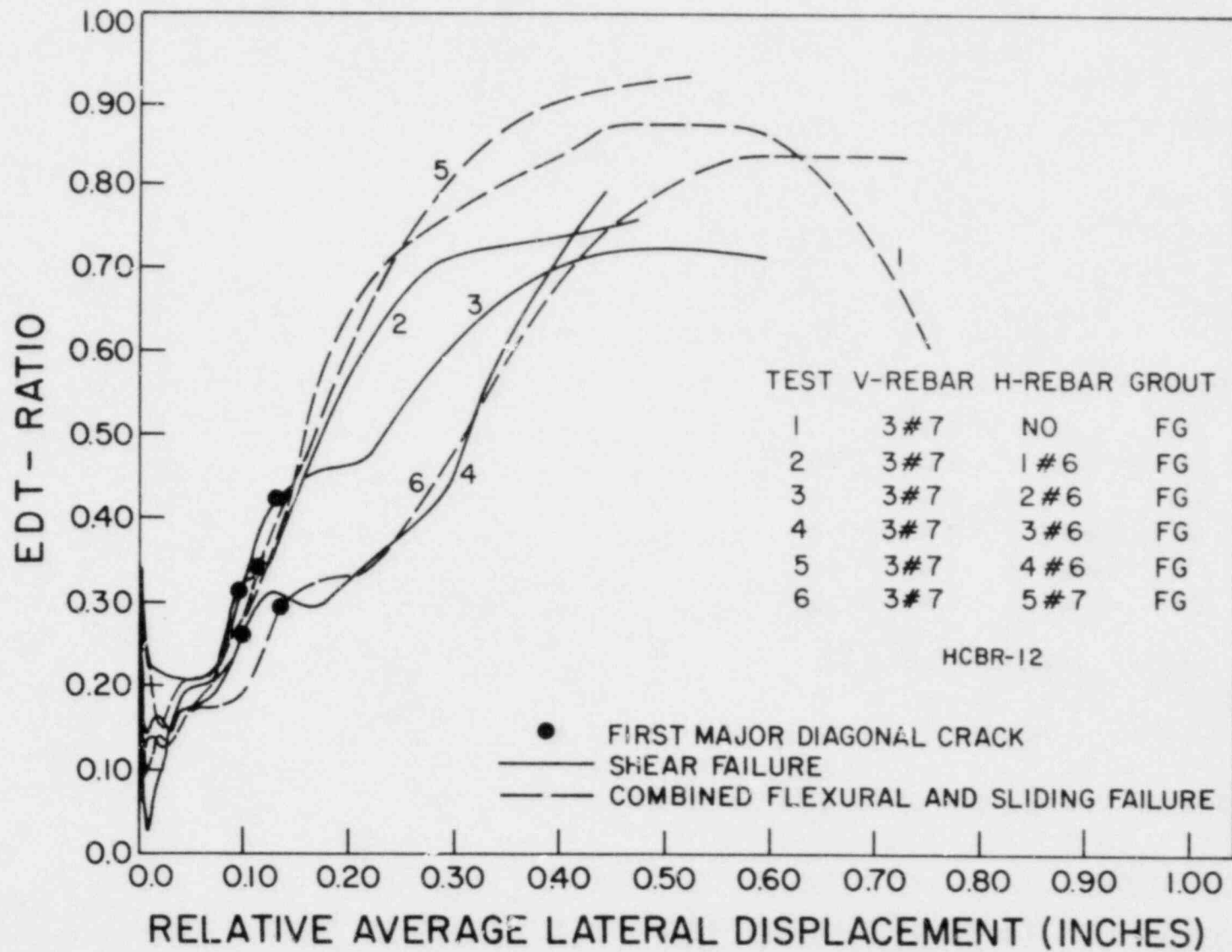


FIG. 5.10 ENERGY DISSIPATION FOR HOLLOW CLAY BRICK PIERS

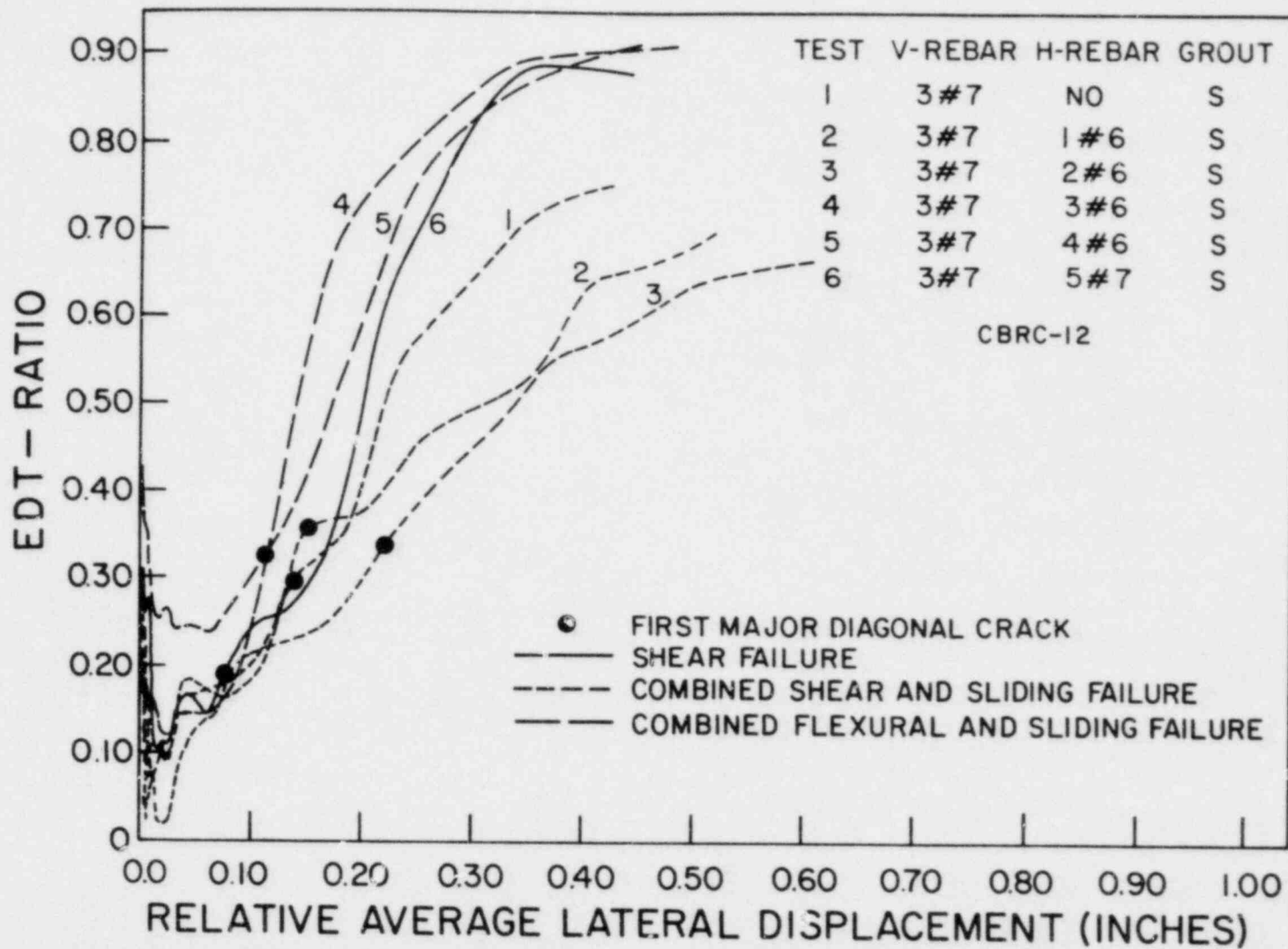


FIG. 5.11 ENERGY DISSIPATION FOR GROUTED CORE CLAY BRICK PIERS

REFERENCES

1. Blume, J.A. and Proulx, J., "Shear in Grouted Brick Masonry Wall Elements," Report to Western States Clay Products from J.A. Blume and Associates, 1968.
2. Chen, S-W.J., Hidalgo, P.A., Mayes, R.L., Clough, R.W., and McNiven, H.D., "Cyclic Loading Tests of Masonry Single Piers, Volume 2 - Height to Width Ratio of 1," EERC Report No. 78/28, University of California, Berkeley, 1978.
3. Greenley, D.G. and Cattaneo, L.E., "The Effect of Edge Load on the Racking Strength of Clay Masonry," Proceedings, Second International Brick Masonry Conference, Stoke-on-Trent, 1970.
4. Hidalgo, P.A., Mayes, R.L., McNiven, H.D. and Clough, R.W., "Cyclic Loading Tests of Masonry Single Piers, Volume 1 - Height to Width Ratio of 2," EERC Report No. 78/27, University of California, Berkeley, 1978.
5. Mayes, R.L., and Clough, R.W., "A Literature Survey - Compressive, Tensile, Bond and Shear Strength of Masonry," EERC Report No. 75-15, University of California, Berkeley, 1975.
6. Mayes, R.L., and Clough, R.W., "State-of-the-Art in Seismic Strength of Masonry - An Evaluation and Review," EERC Report No. 75-21, University of California, Berkeley, 1975.
7. Mayes, R.L., Omote, Y., Chen, S.W., and Clough, R.W., "Expected Performance of Uniform Building Code Designed Masonry Structures," EERC Report No. 76-7, University of California, Berkeley, 1976.
8. Mayes, R.L., Omote, Y., and Clough, R.W., "Cyclic Shear Tests of Masonry Piers, Volume 1 - Test Results," EERC Report No. 76-8, University of California, Berkeley, 1976.
9. Mayes, R.L., Omote, Y., and Clough, R.W., "Cyclic Shear Tests of Masonry Piers, Volume 2 - Analysis of Test Results," EERC Report No. 76-16, University of California, Berkeley, 1976.
10. 1977 Masonry Codes and Specifications, Published by the Masonry Industry Advancement Committee, California, 1977.
11. Meli, R., "Behavior of Masonry Walls under Lateral Loads," Proceedings of the Fifth World Conference on Earthquake Engineering, Rome, 1973.
12. Park, R., and Paulay, T., "Reinforced Concrete Structures", John Wiley and Sons, 1975.
13. Priestley, M.J.N., and Bridgeman, D.O., "Seismic Resistance of Brick Masonry Walls," Bulletin of the New Zealand National Society for Earthquake Engineering, Vol. 7, No. 4, 1974.

14. Priestley, M.J.N., "Seismic Resistance of Reinforced Concrete Masonry Shear Walls with High Steel Percentages," Bulletin of the New Zealand National Society for Earthquake Engineering, Vol. 10, No. 1, 1977.
15. Scrivener, J.C., "Concrete Masonry Wall Panel Tests with Predominant Flexural Effects," New Zealand Concrete Construction, 1966.
16. Williams, D.W., "Seismic Behaviour of Reinforced Masonry Shear Walls," Ph.D. Thesis, University of Canterbury, Christchurch, New Zealand, 1971.

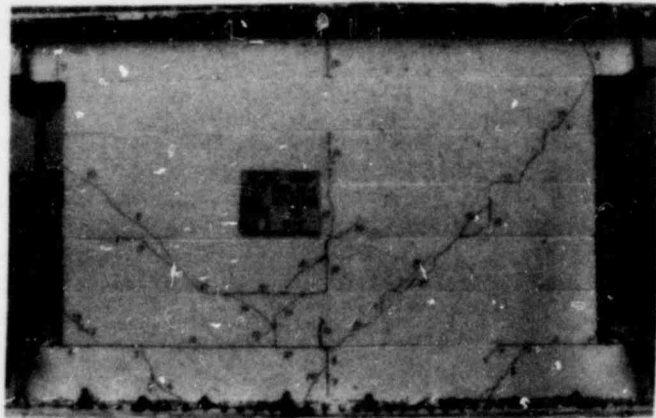
APPENDIX A

CATALOG OF TEST RESULTS

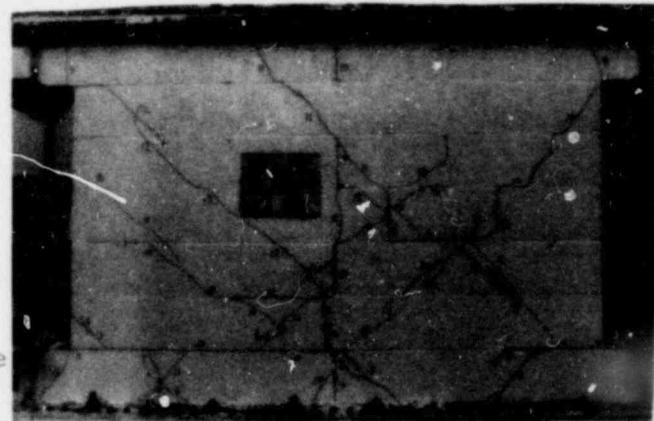
The experimental results for each test are arranged on three pages containing six photographs of the successive crack patterns and six graphs obtained from the data collected during the test. These graphs include the hysteresis loops, the hysteresis envelope, stiffness degradation, energy dissipation and amount of shear distortion as compared with total deformation.

In order to show the relation between the photographs of the crack patterns and the diagrams showing the results, a black dot has been drawn on each of the graphs and next to the corresponding picture of the crack pattern. The dot generally corresponds to the stage at which the first major diagonal crack occurred.

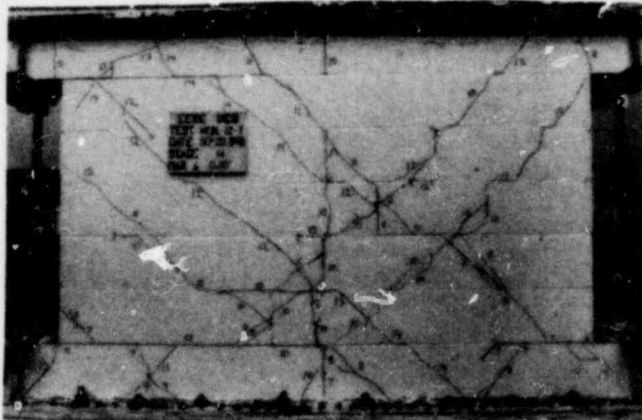
Details on how each of the diagrams was obtained are presented in Chapter 4.



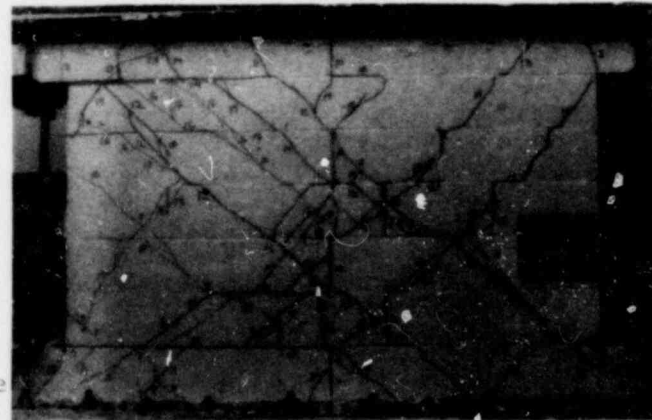
Stage
10



Stage
12

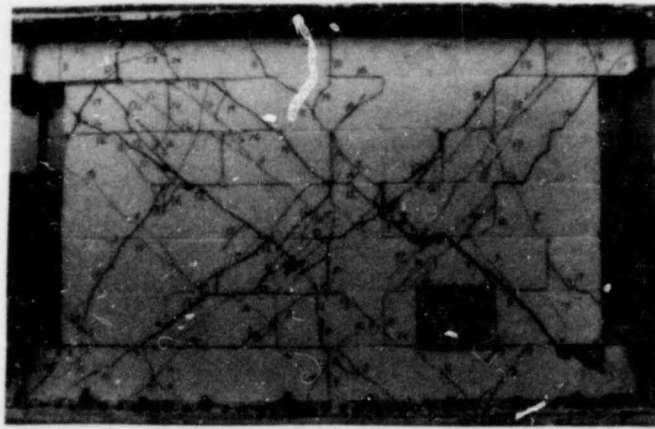


Stage
14

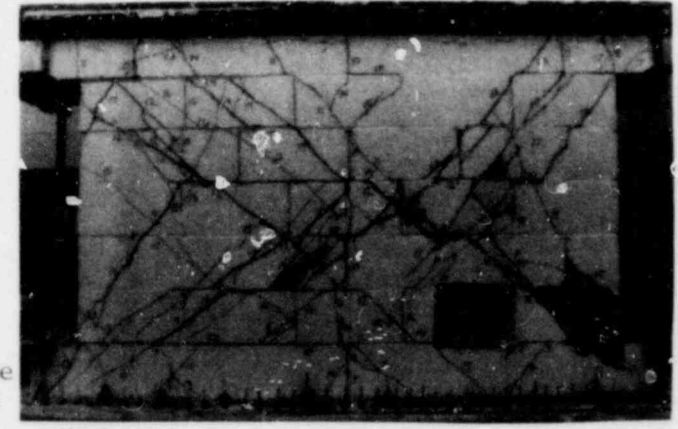


Stage
16

FIG. A.1 SUCCESSIVE CRACK FORMATION AND EXPERIMENTAL RESULTS TEST HCBL-12-1



Stage
17



Stage
18

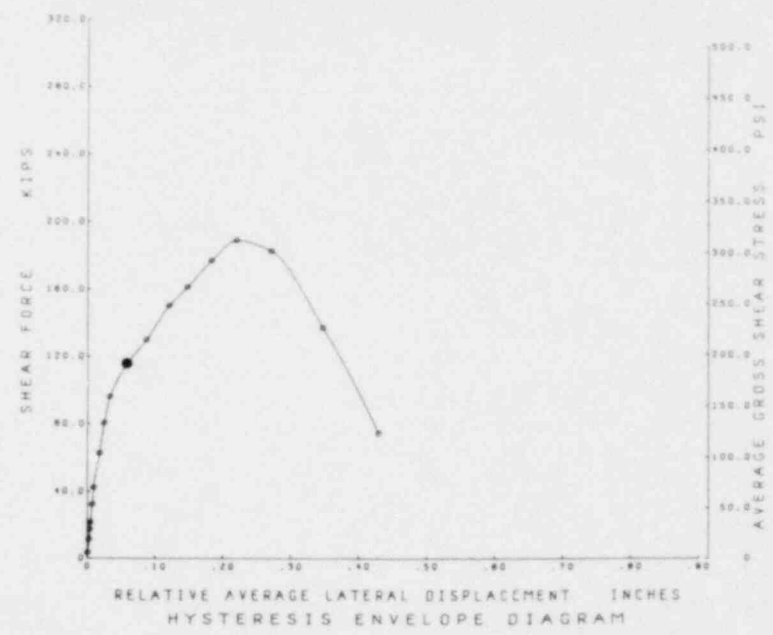
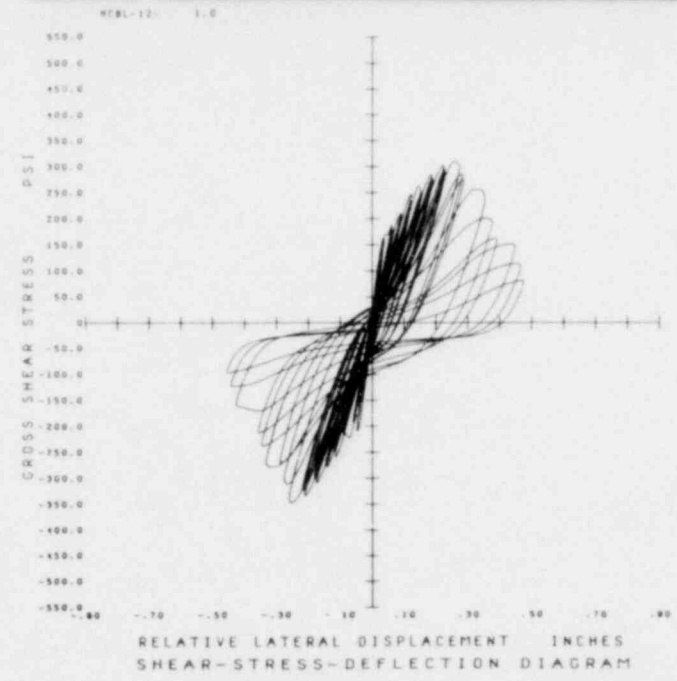


FIG. A.1 CONTINUED HCBL-12-1

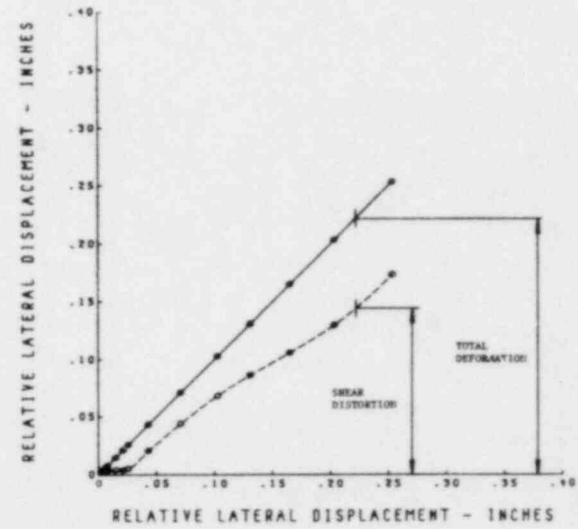
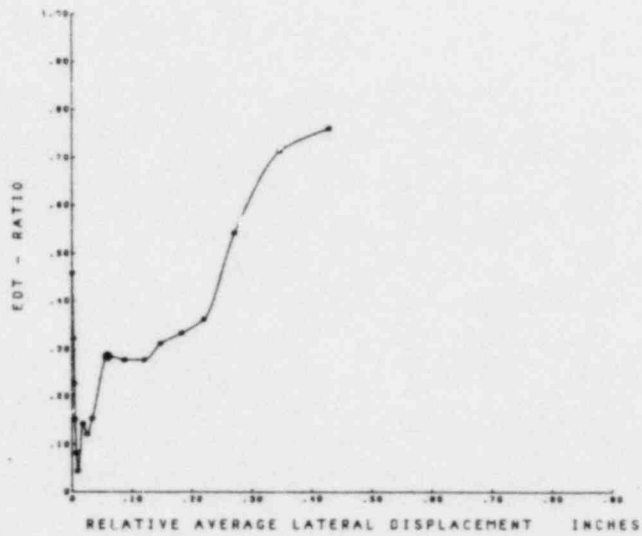
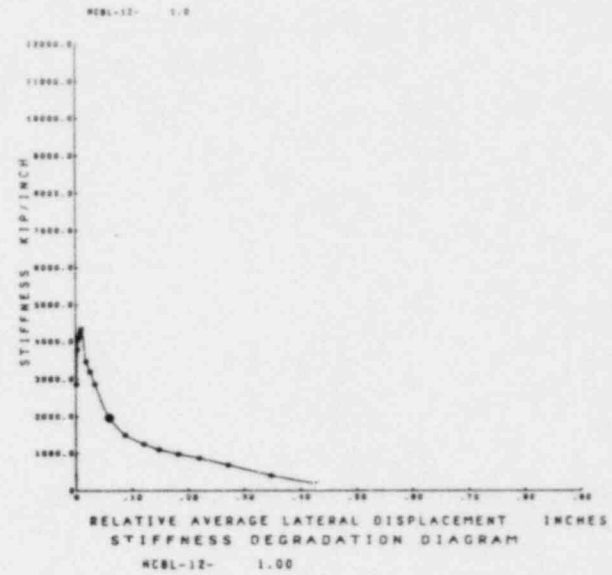
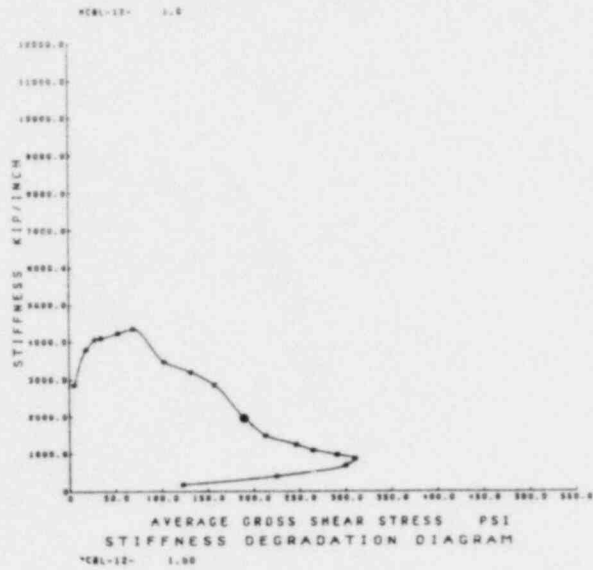
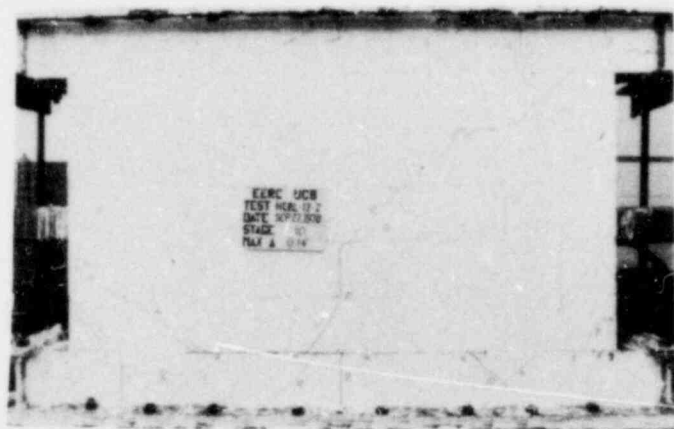
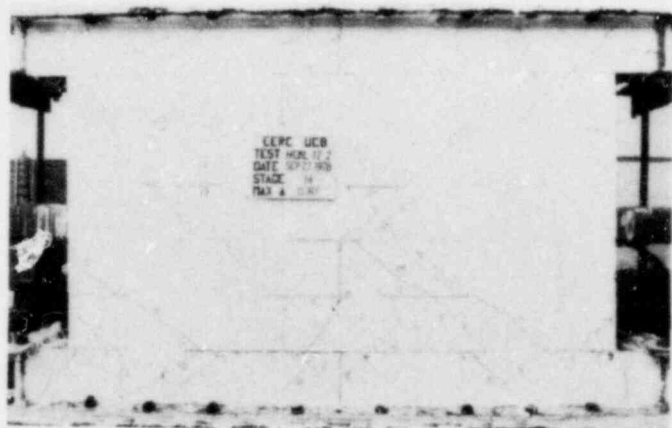
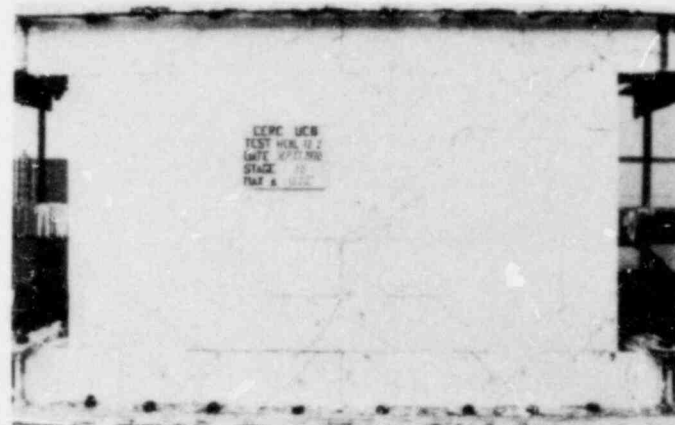


FIG. A.1 CONTINUED HCBL-12-1



●
Stage Stage
10 12



Stage Stage
14 16

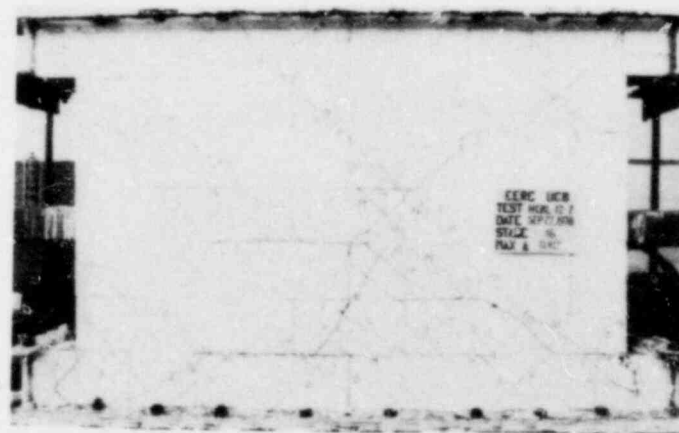
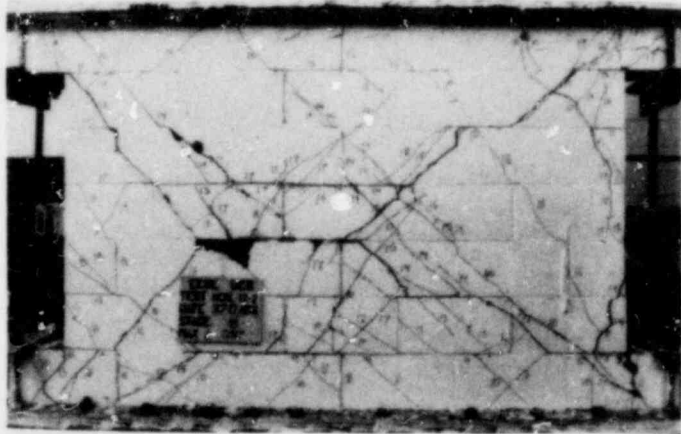


FIG. A.2 SUCCESSIVE CRACK FORMATION AND EXPERIMENTAL RESULTS TEST HCBL-12-2



Stage Stage
18 19

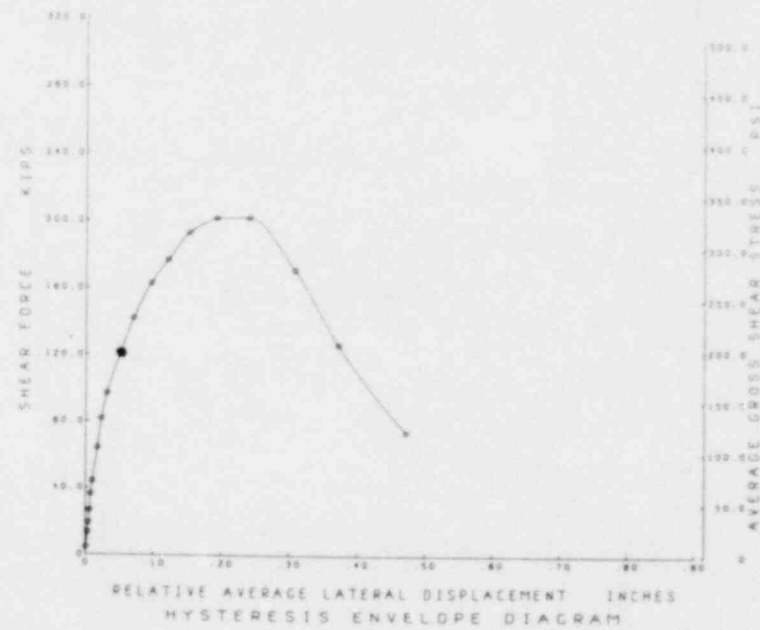
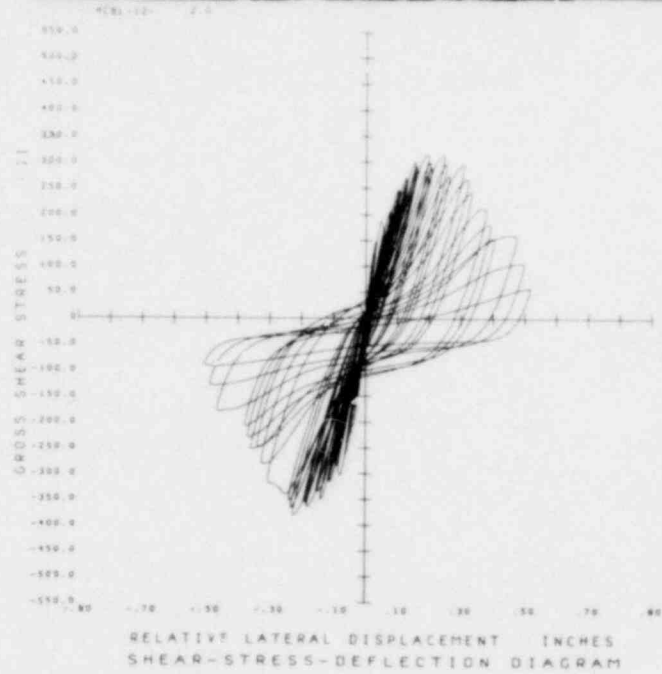


FIG. A.2 CONTINUED HCBL-12-2

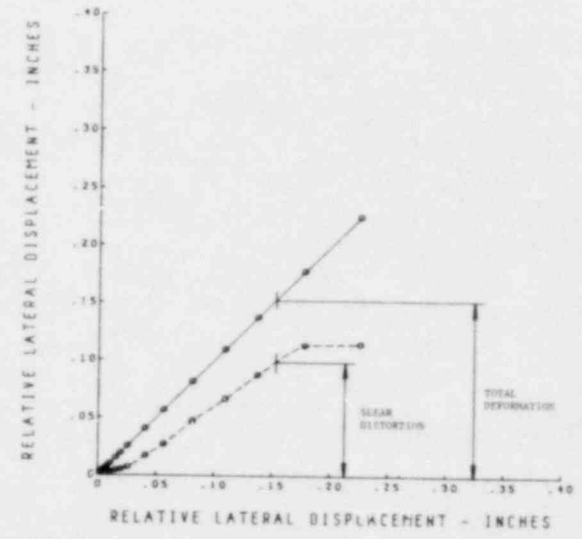
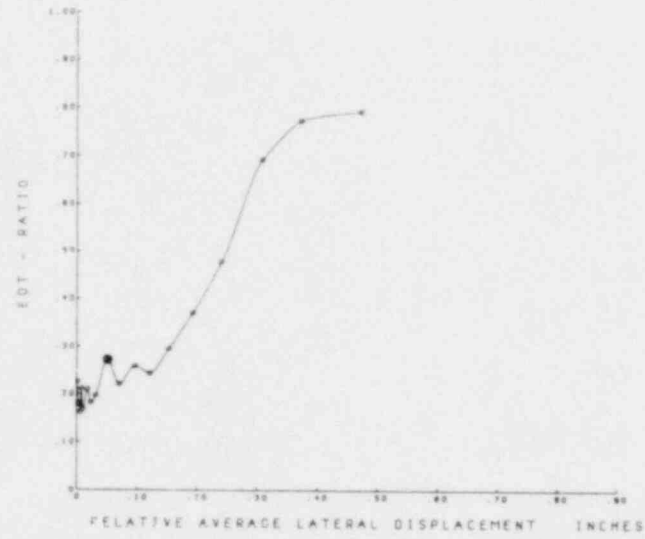
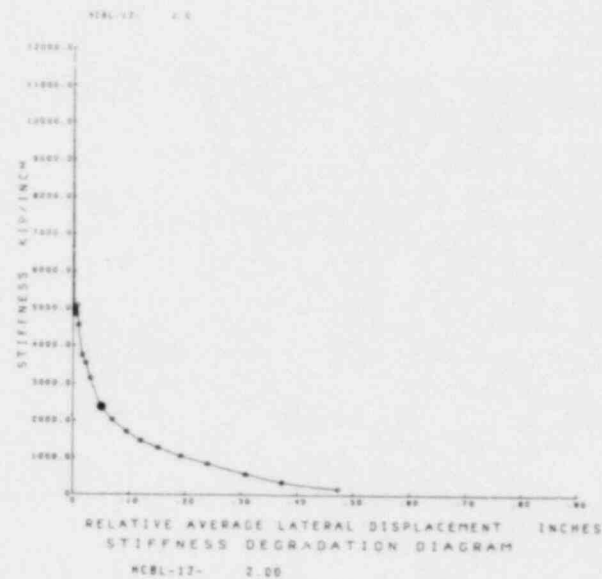
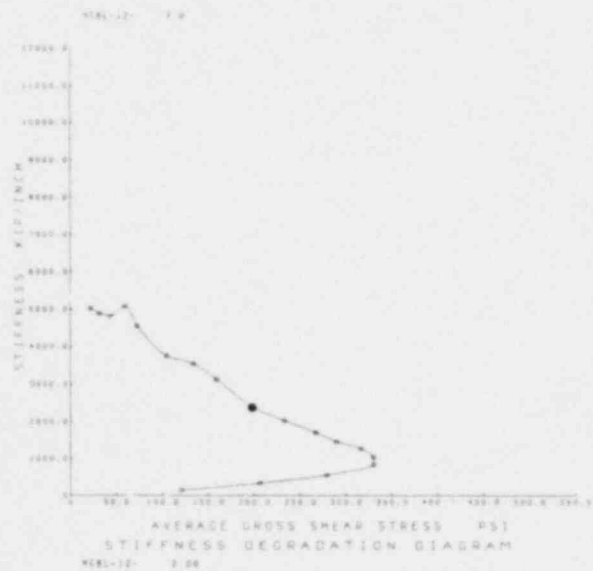
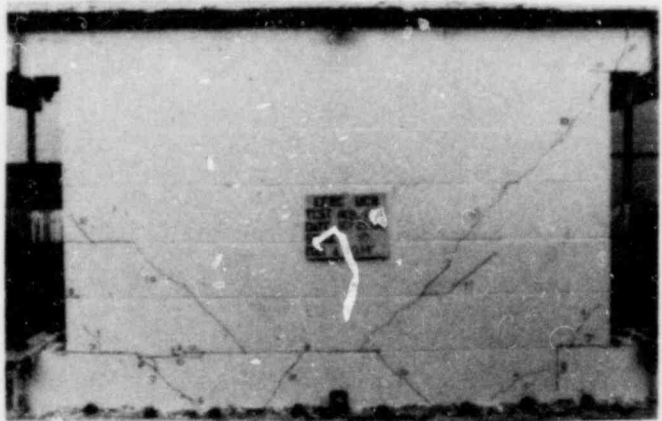
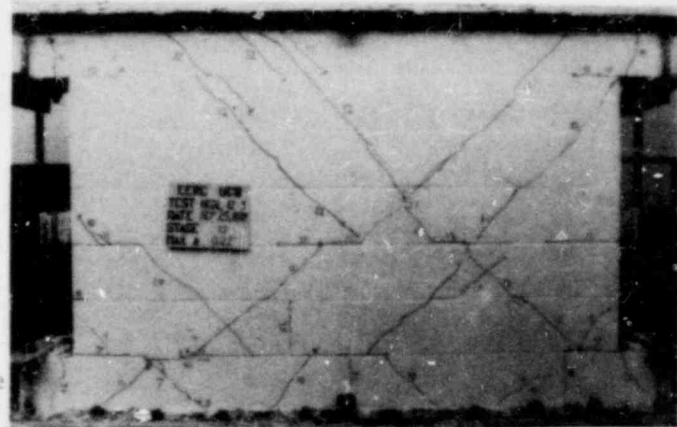


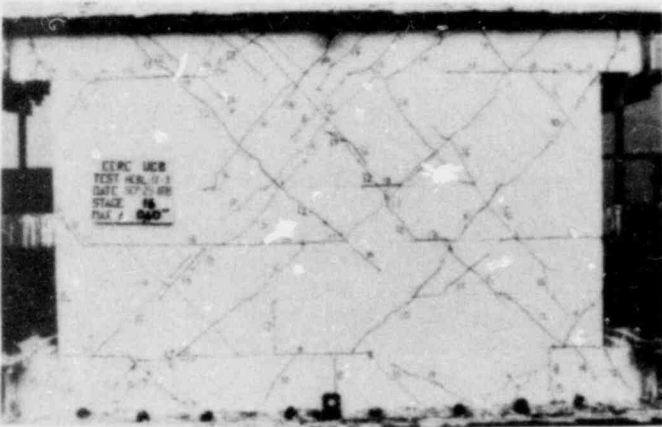
FIG. A.2 CONTINUED HCBL-12-2



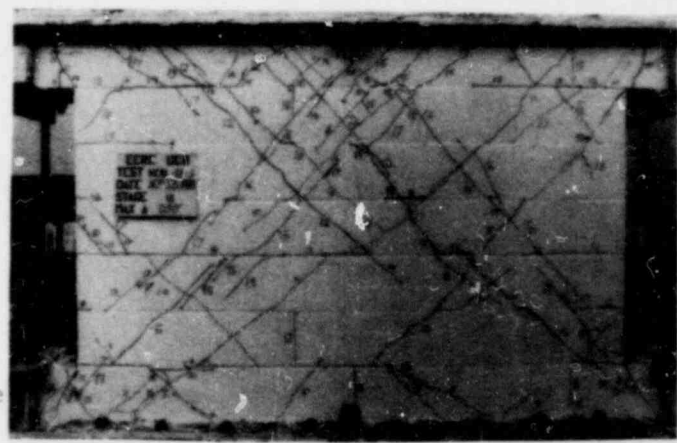
Stage 10



Stage 12

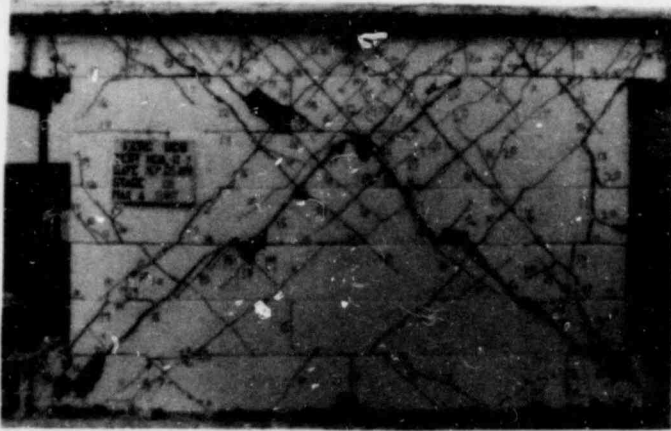


Stage 16



Stage 18

FIG. A.3 SUCCESSIVE CRACK FORMATION AND EXPERIMENTAL RESULTS TEST HCBL-12-3



Stage Stage
20 21

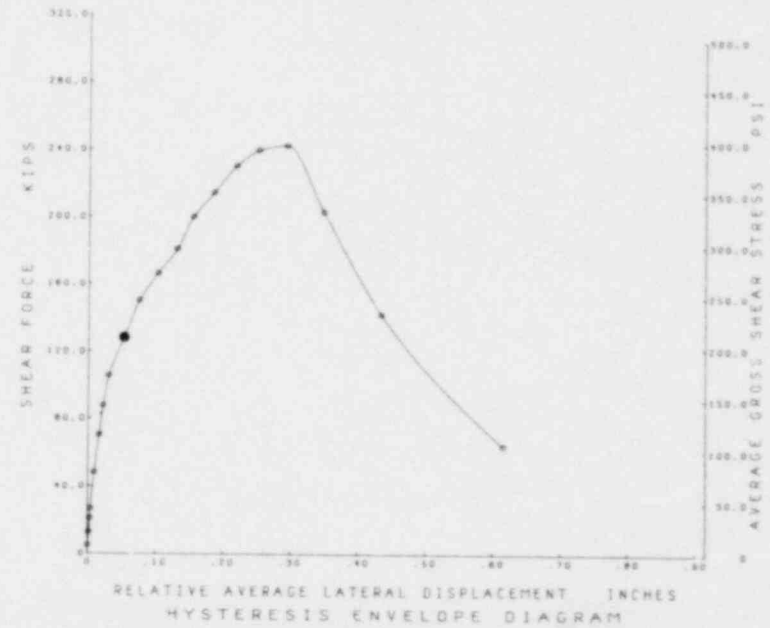
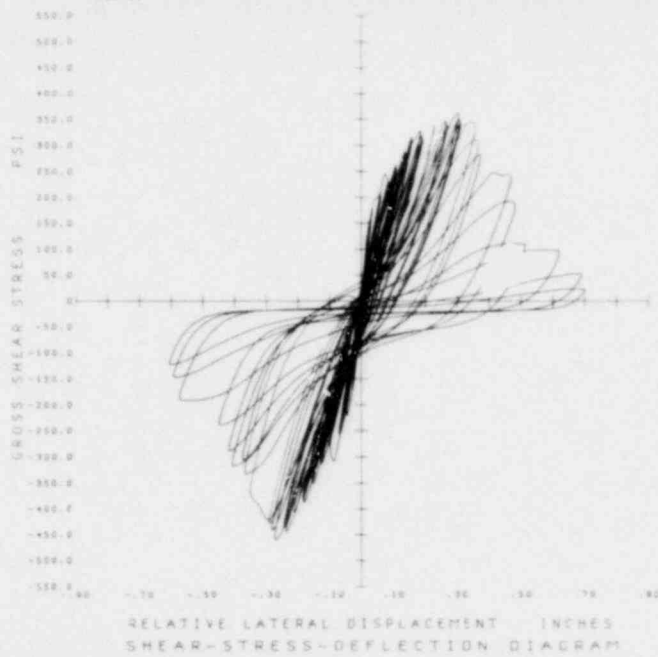
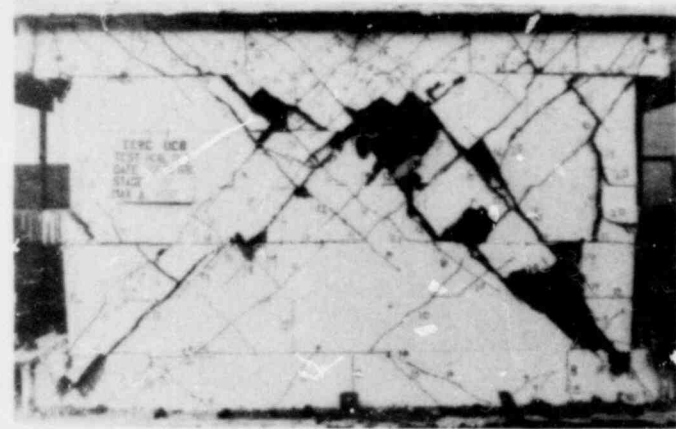


FIG. A.3 CONTINUED HCBL-12-3

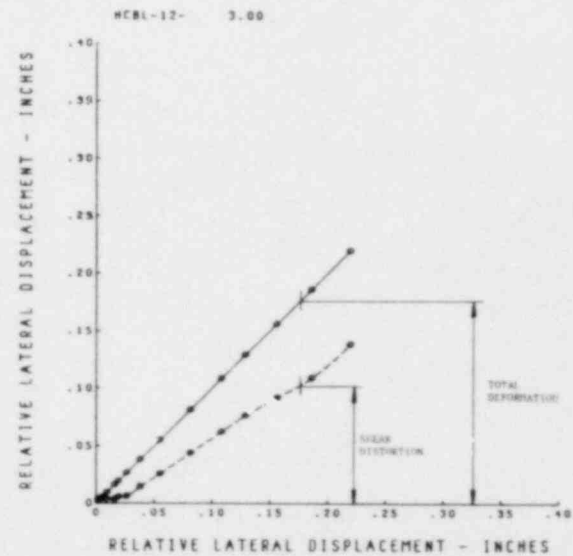
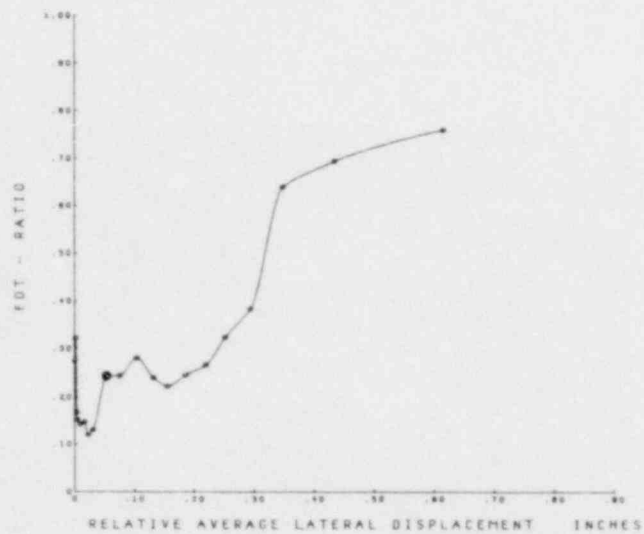
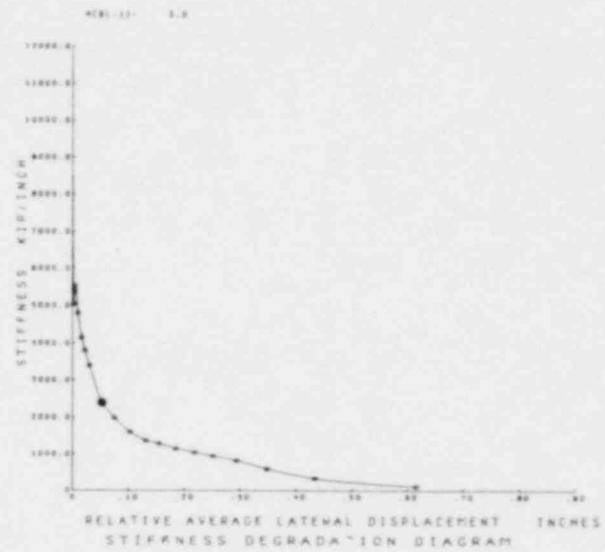
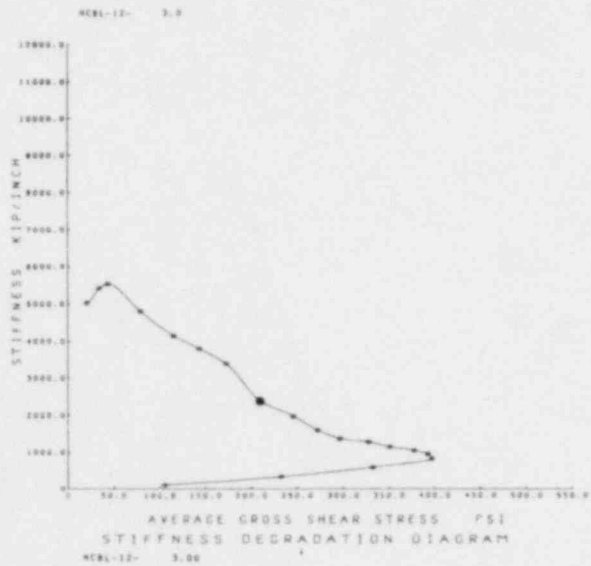
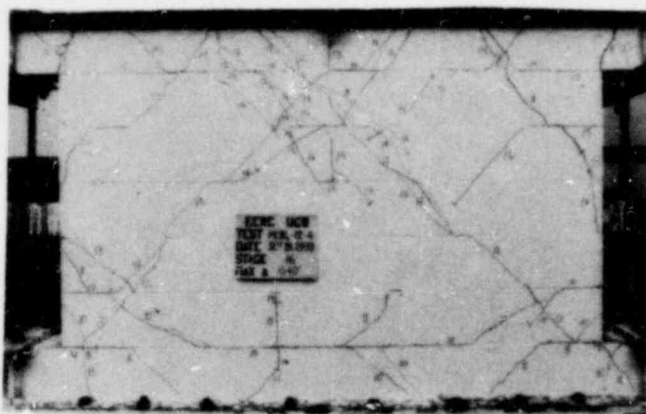
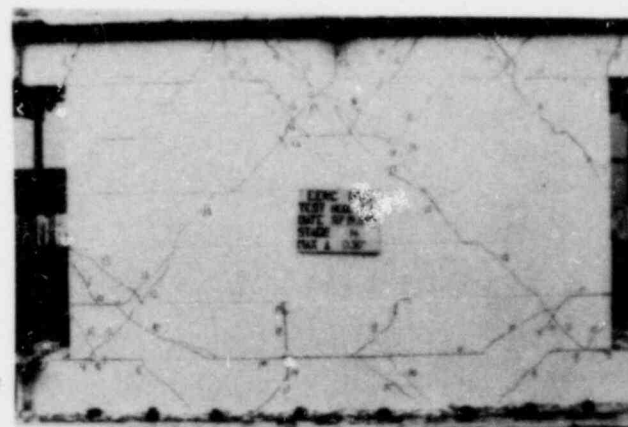


FIG. A.3 CONTINUED HCBL-12-3



●
Stage
12

Stage
14



Stage
16

Stage
17

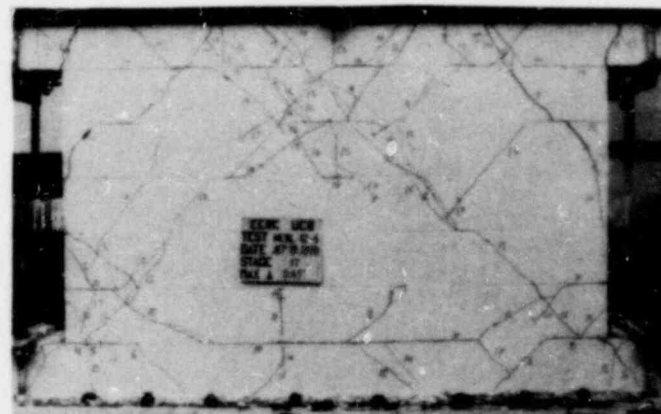
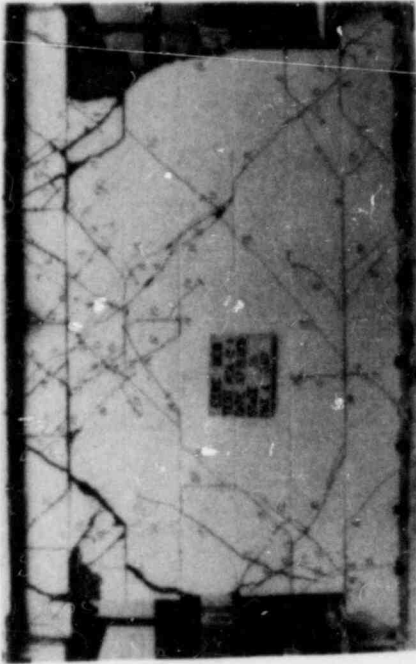
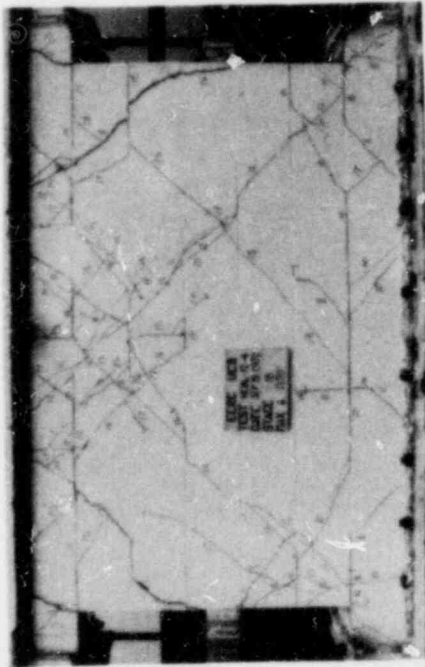


FIG. A.4 SUCCESSIVE CRACK FORMATION AND EXPERIMENTAL RESULTS TEST HCBL-12-4



Stage Stage
18 20



4.2

4.3

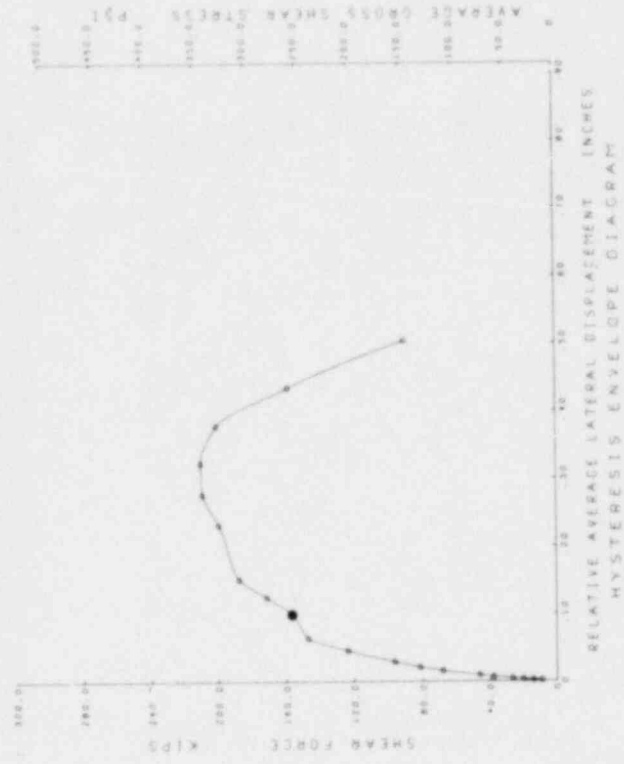
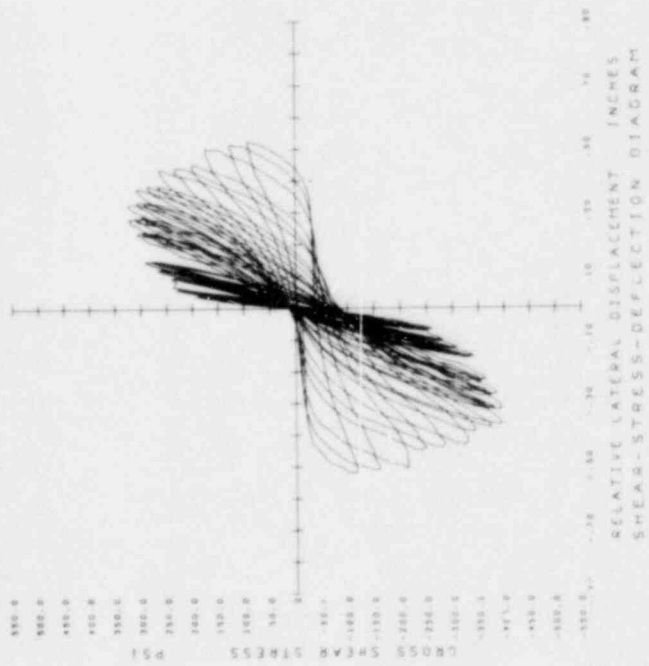
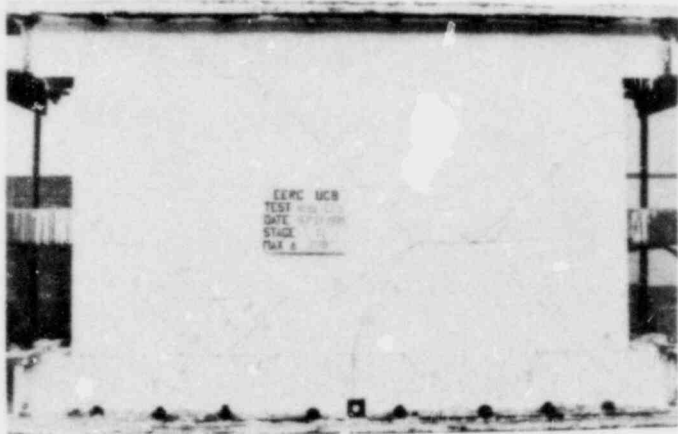
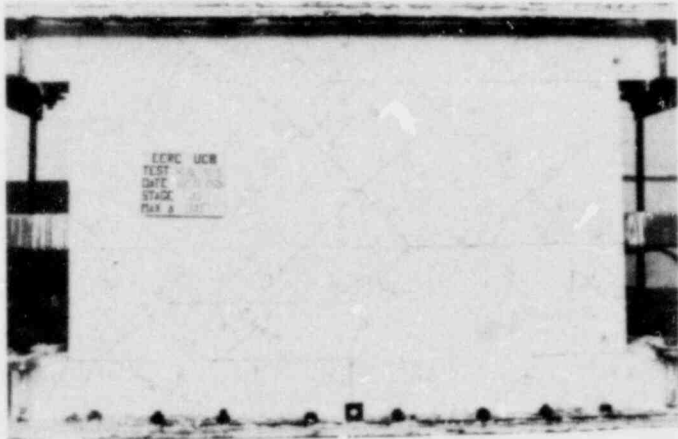
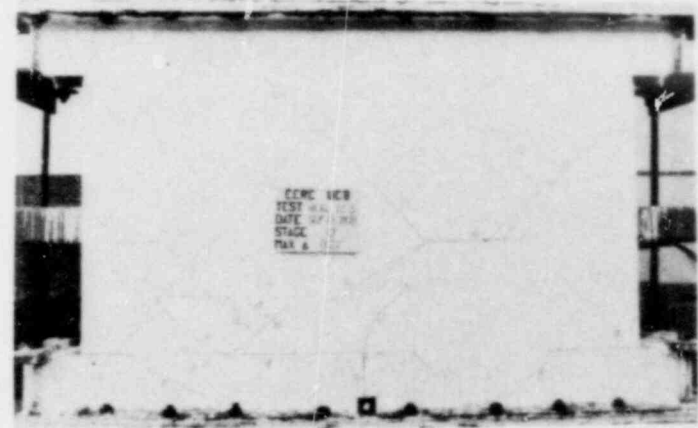


FIG. A.4 CONTINUED HCBI.-12-4



●
Stage Stage
11 12



Stage Stage
15 18



FIG. A.5 SUCCESSIVE CRACK FORMATION AND EXPERIMENTAL RESULTS TEST HCBL-12-5



HCBL-12- 7.0



HCBL-12- 5.0

Stage 20 Stage 21

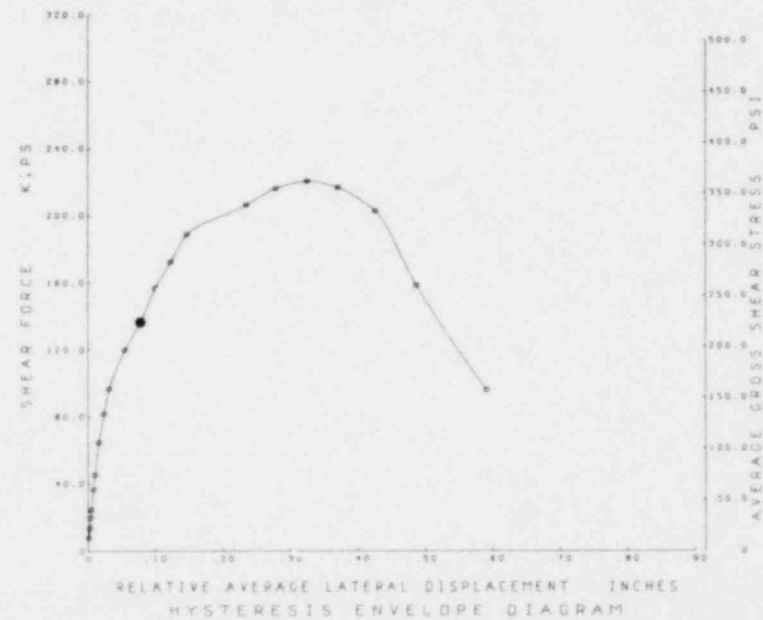
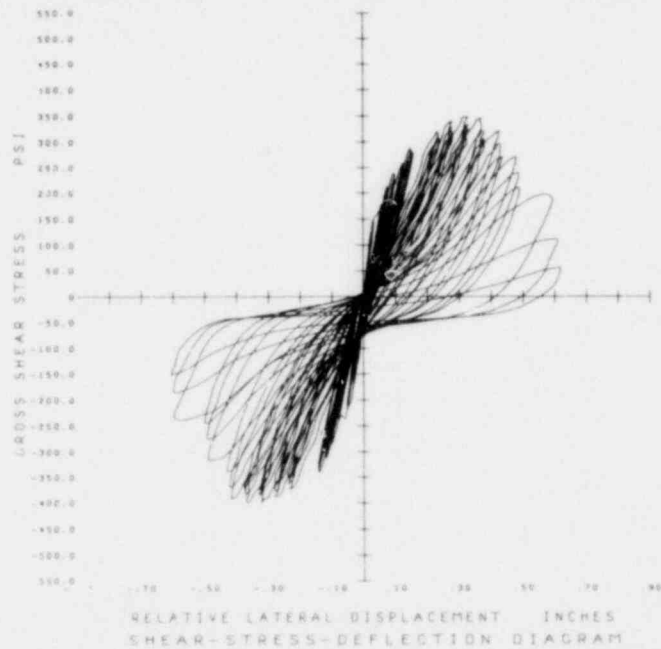


FIG. A.5 CONTINUED HCBL-12-5

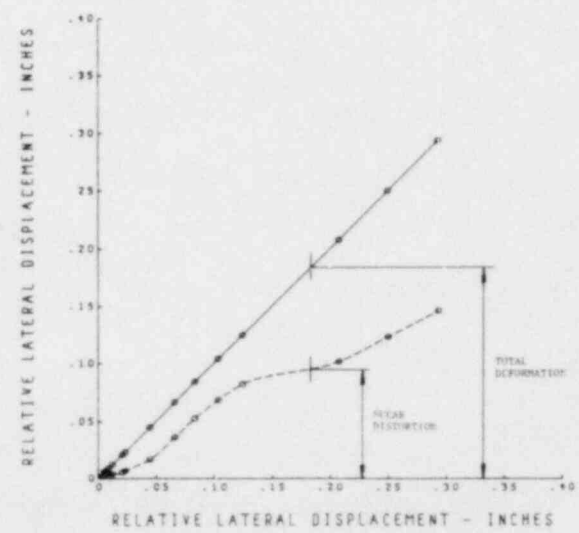
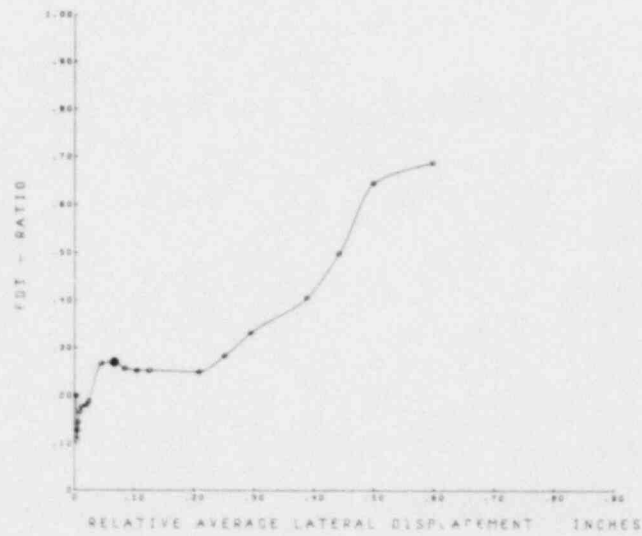
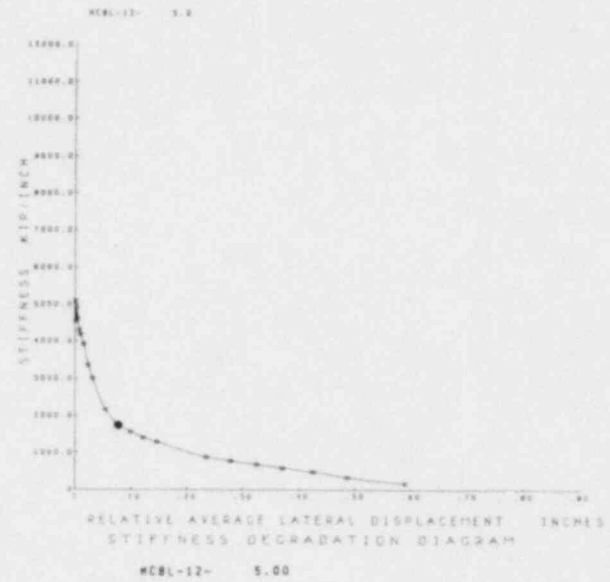
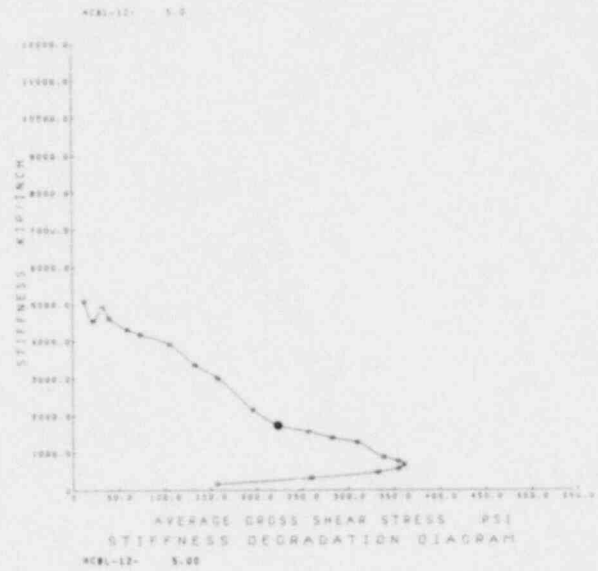
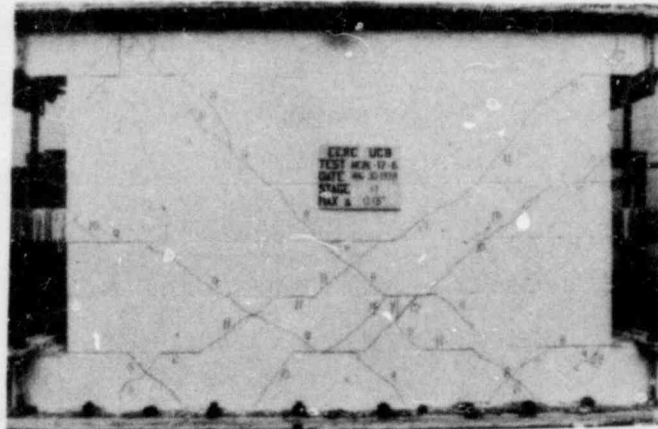
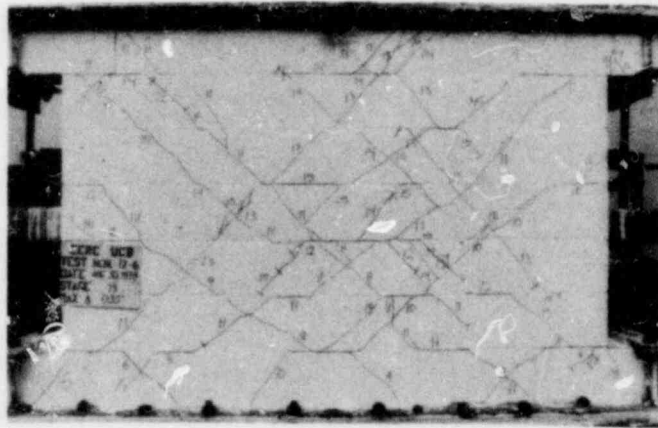
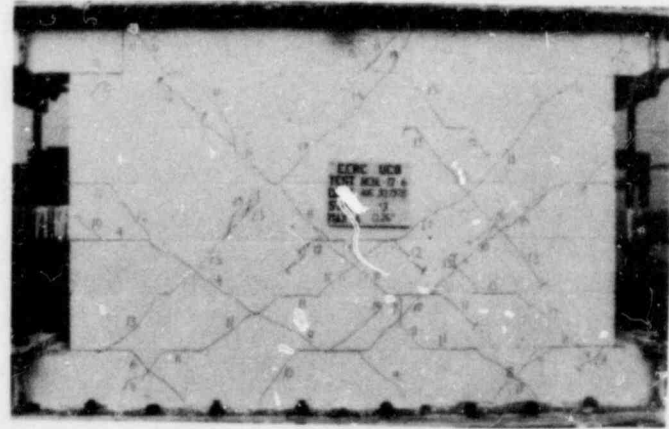


FIG. A.5 CONTINUED HCBL-12-5



●
Stage 11 Stage 13



Stage 15 Stage 17

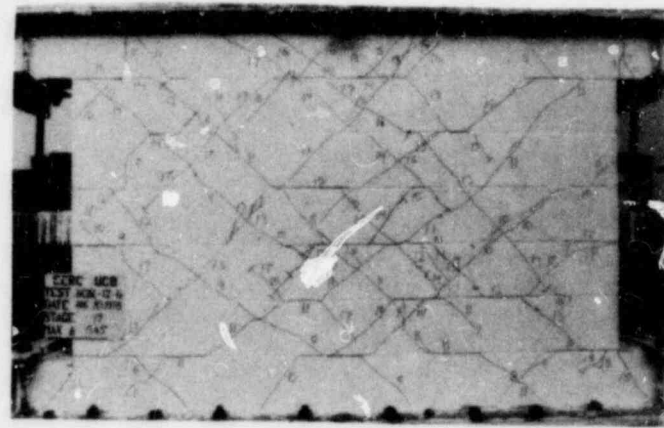


FIG. A.6 SUCCESSIVE CRACK FORMATION AND EXPERIMENTAL RESULTS TEST HCBL-12-6



HCBL-12-6



HCBL-12-6

Stage Stage
18 19

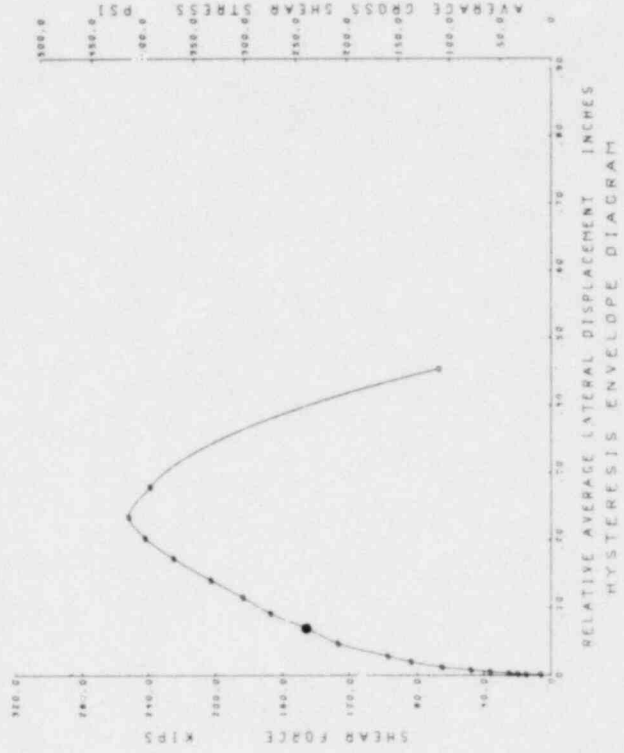
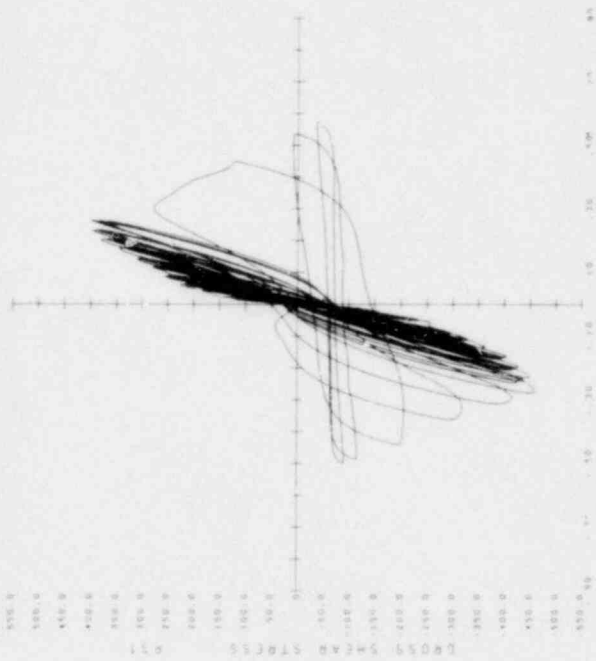


FIG. A.6 CONTINUED HCBL-12-6

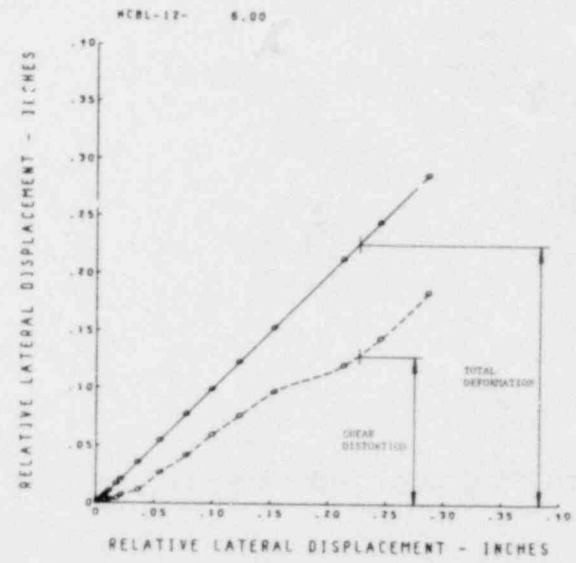
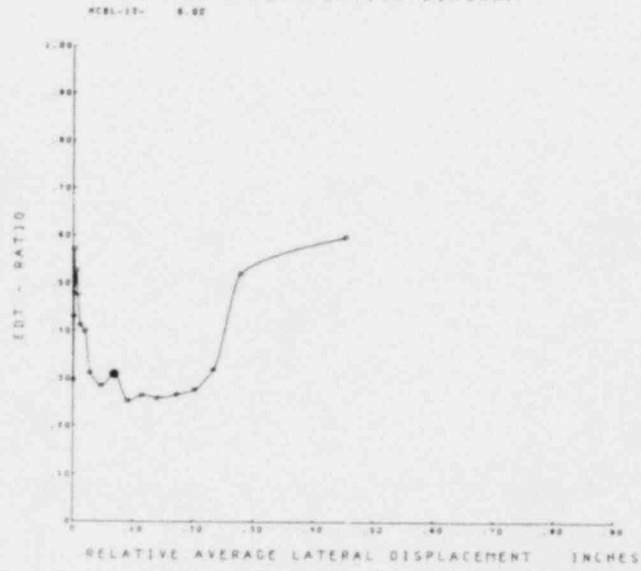
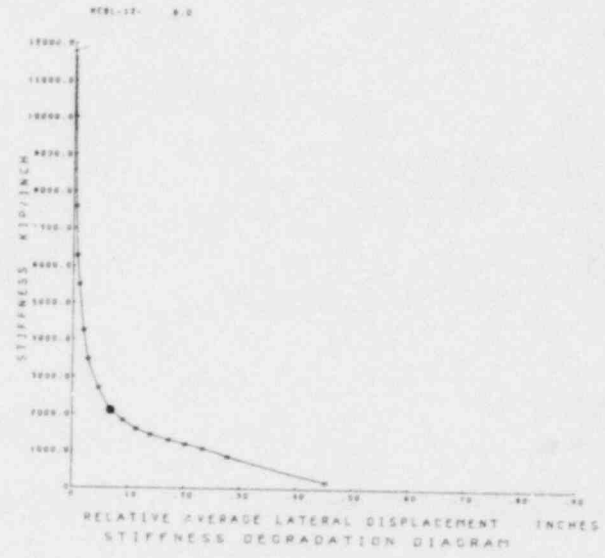
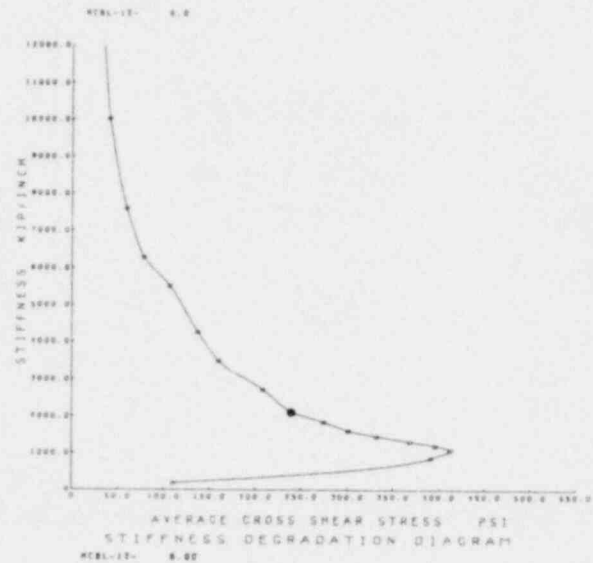
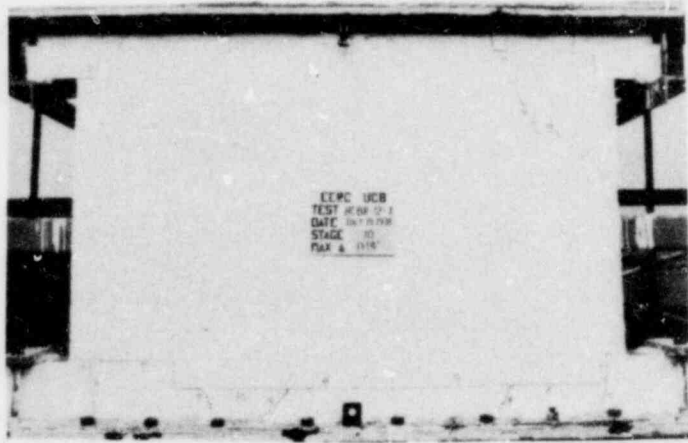
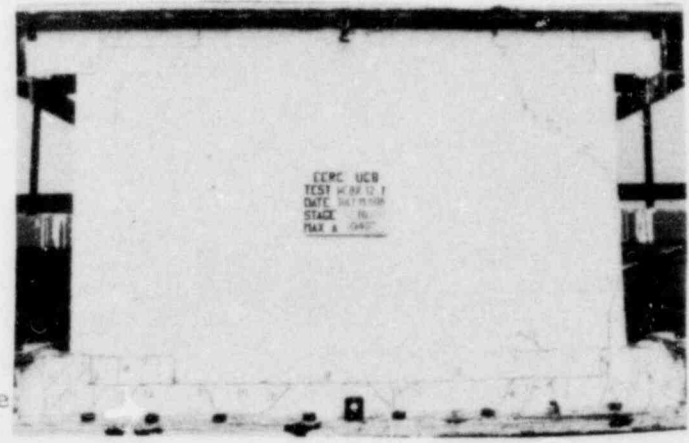


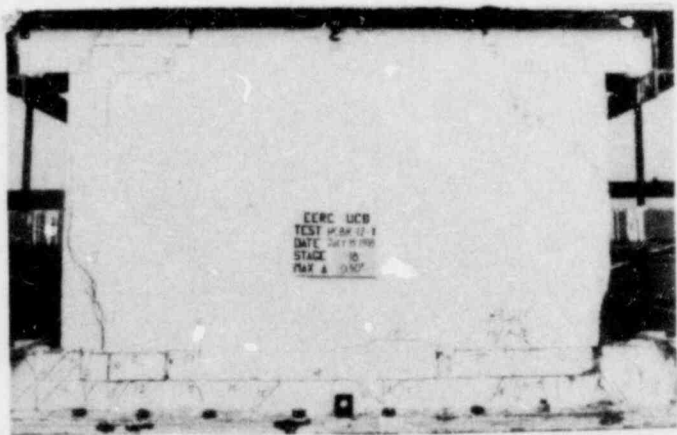
FIG. A.6 CONTINUED HCBL-12-6



Stage 10



Stage 16



Stage 18



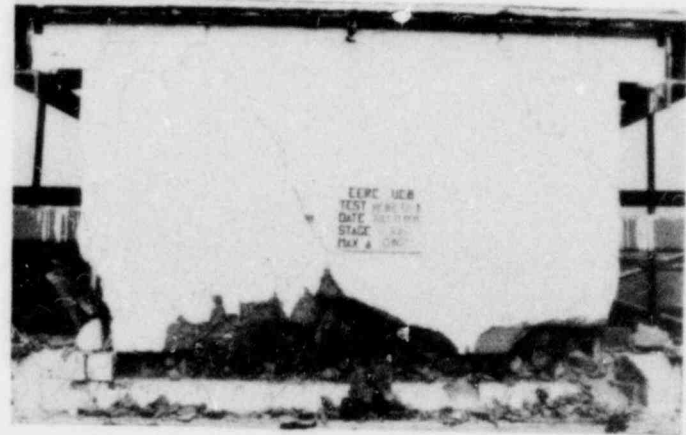
Stage 20

FIG. A.7 SUCCESSIVE CRACK FORMATION AND EXPERIMENTAL RESULTS TEST HCBR-12-1



HCBR-12-1 1.0

Stage 21 Stage 22



HCBR-12-1 1.0

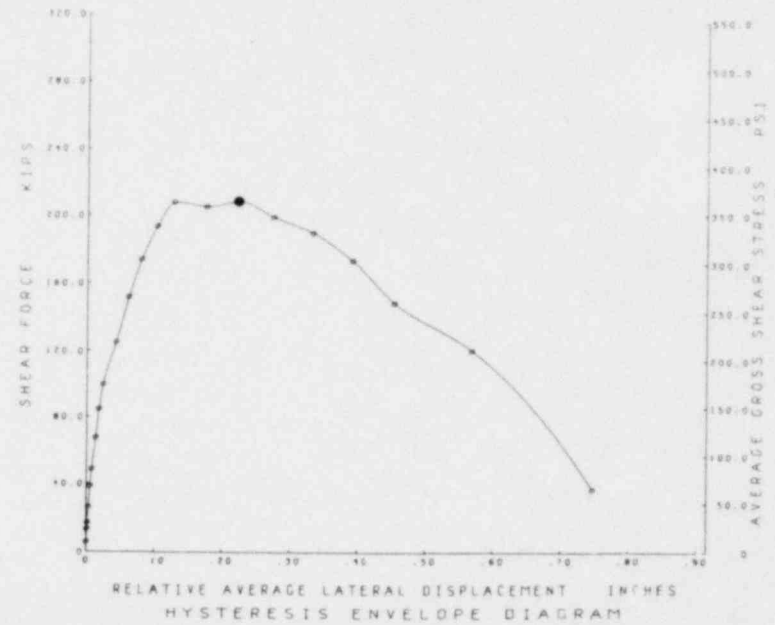
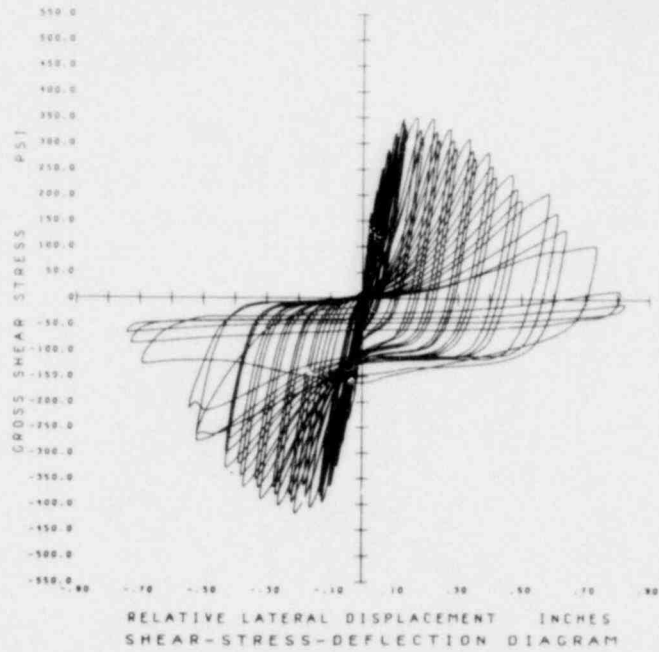


FIG. A.7 CONTINUED HCBR-12-1

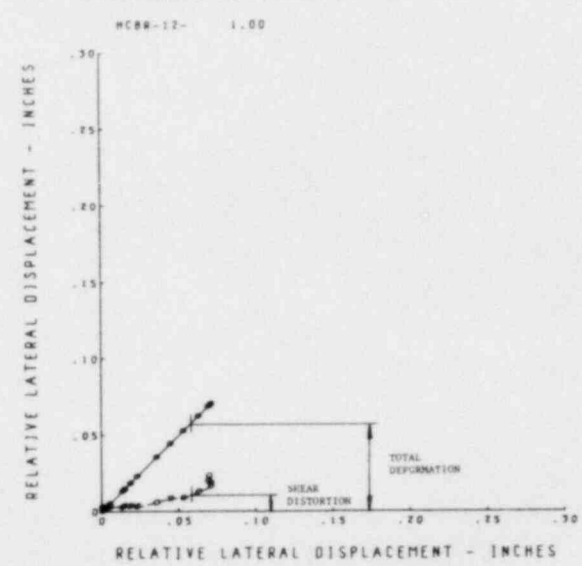
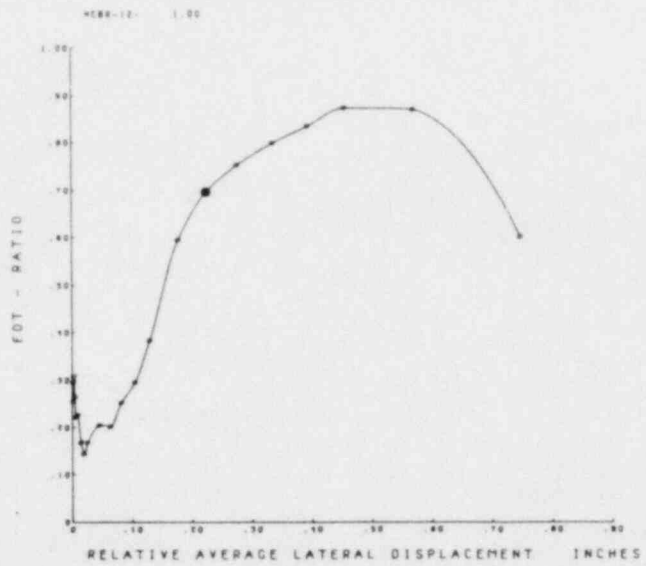
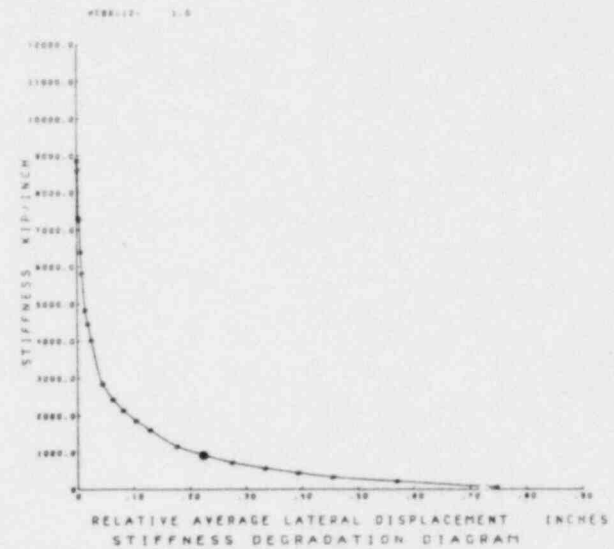
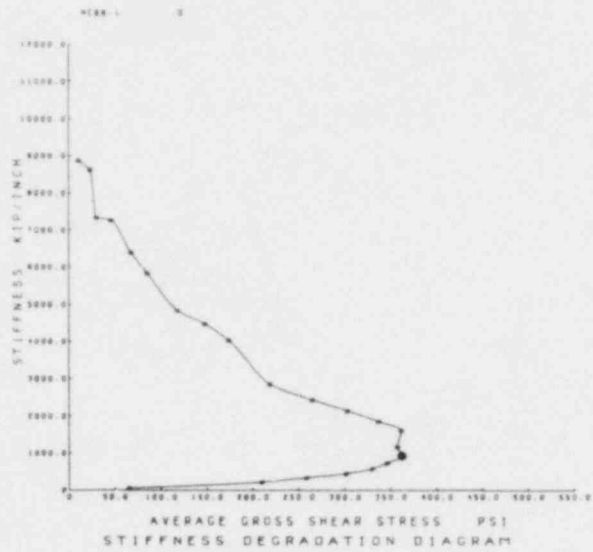
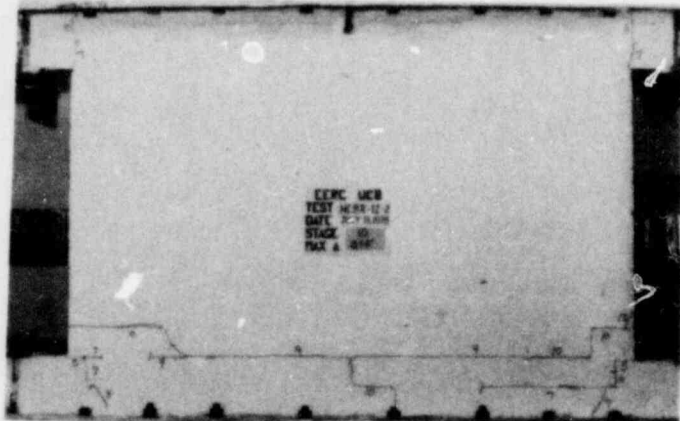
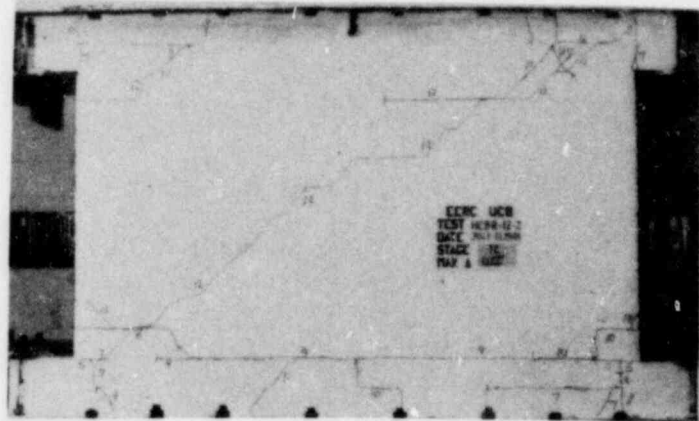


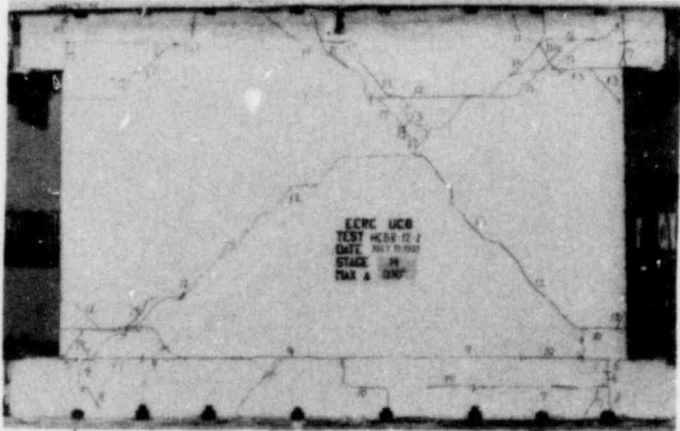
FIG. A.7 CONTINUED HCBR-12-1



Stage 10



Stage 12



Stage 14



Stage 15

FIG. A.8 SUCCESSIVE CRACK FORMATION AND EXPERIMENTAL RESULTS TEST NCBR-12-2



Stage 17 Stage 19

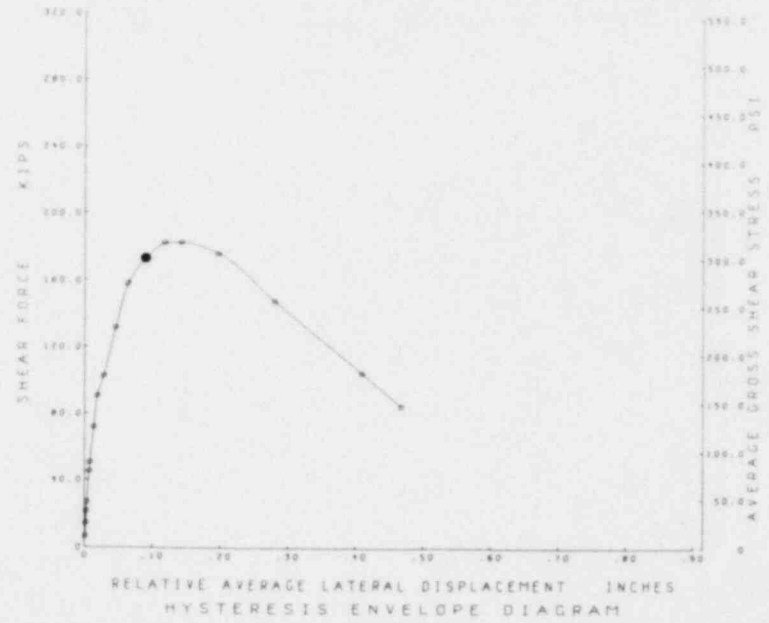
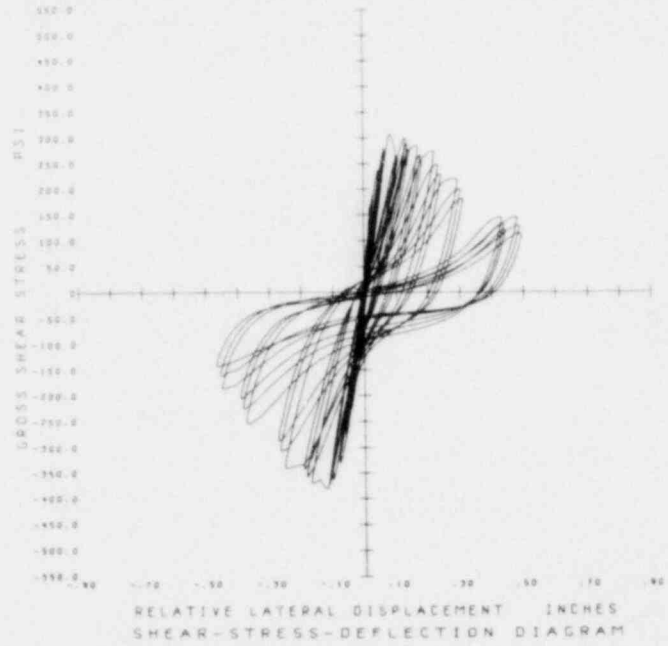


FIG. A.8 CONTINUED HCBR-12-2

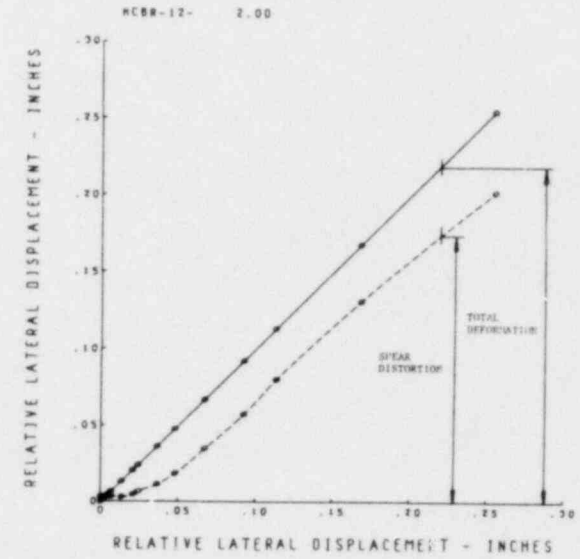
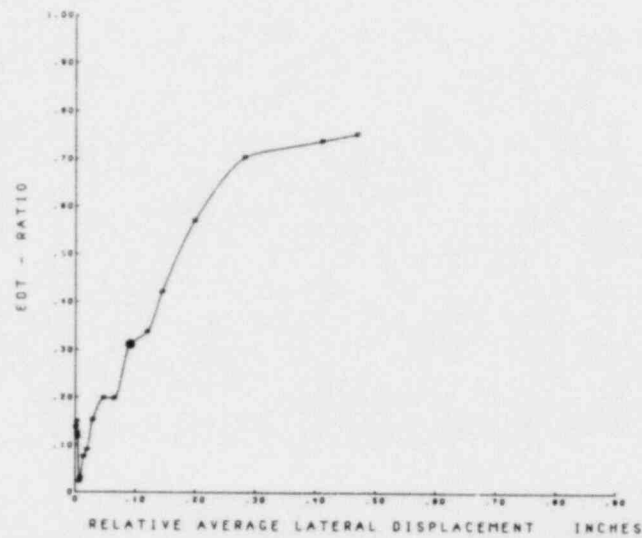
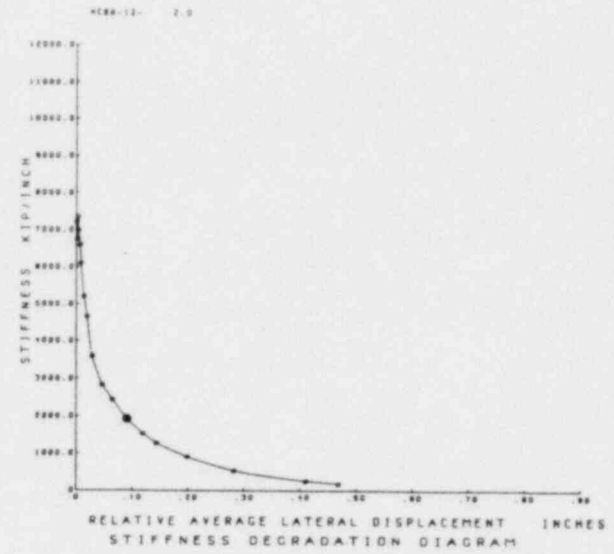
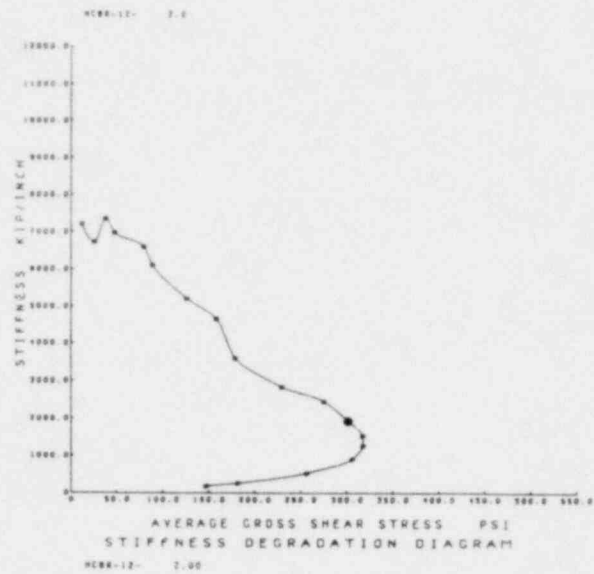
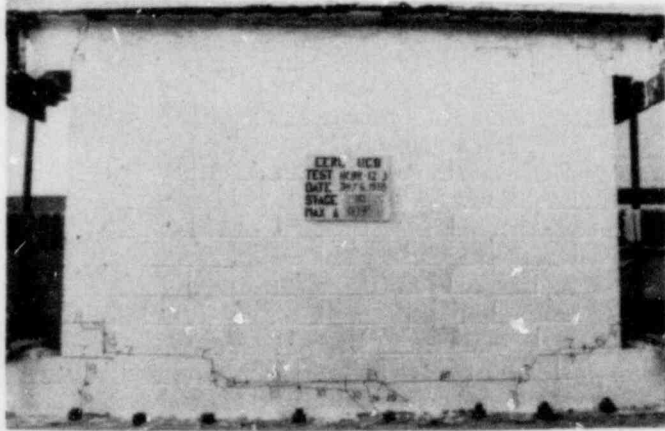
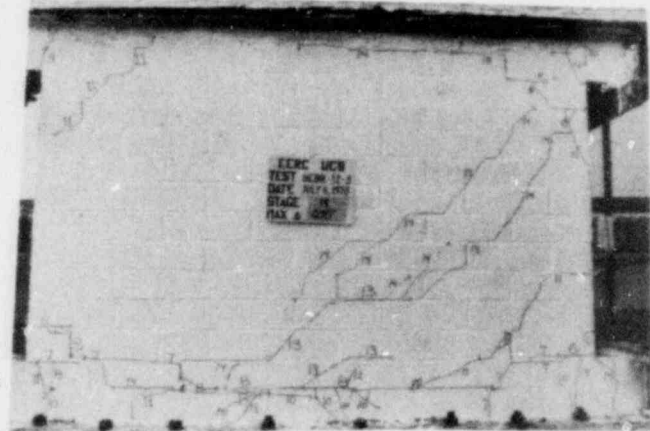


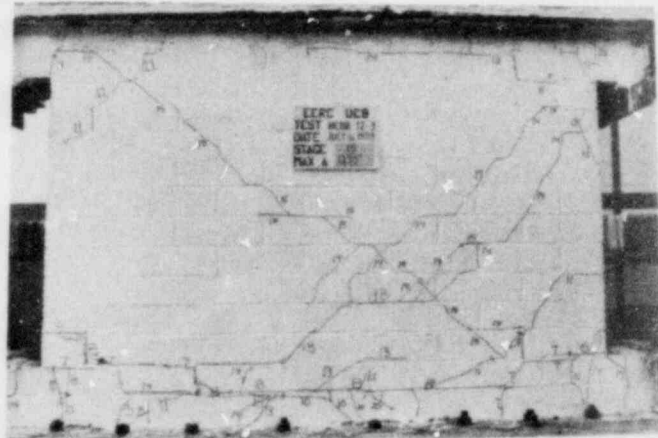
FIG. A.8 CONTINUED HCBR-12-2



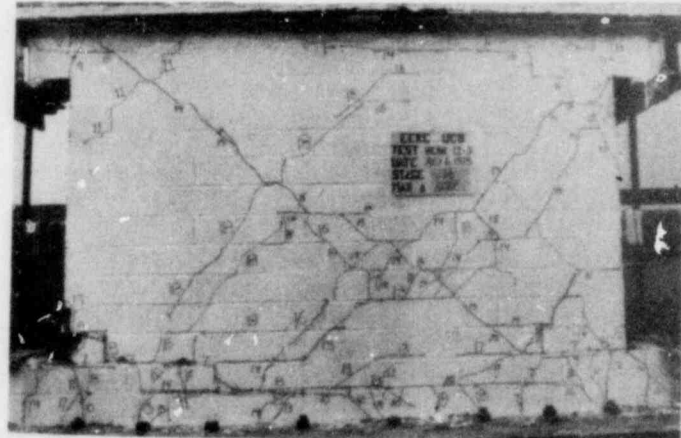
Stage 10



Stage 14

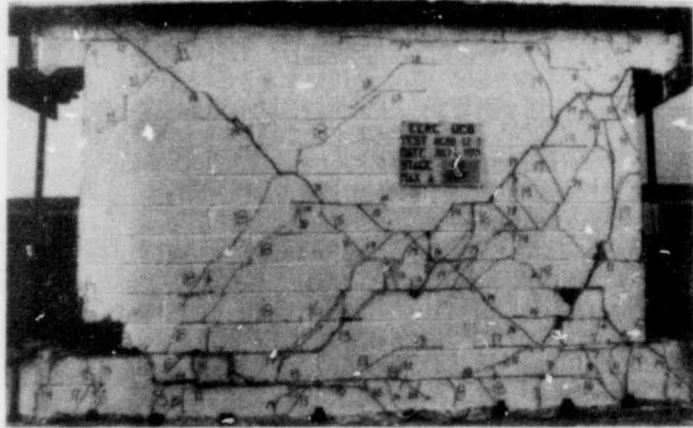


Stage 15



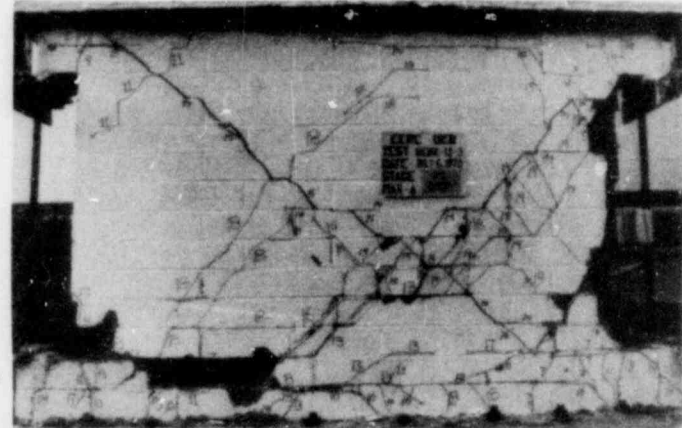
Stage 18

FIG. A.9 SUCCESSIVE CRACK FORMATION AND EXPERIMENTAL RESULTS TEST HCBR-12-3



HCBR-12-3 3.0

Stage 20 Stage 21



HCBR-12-3 3.0

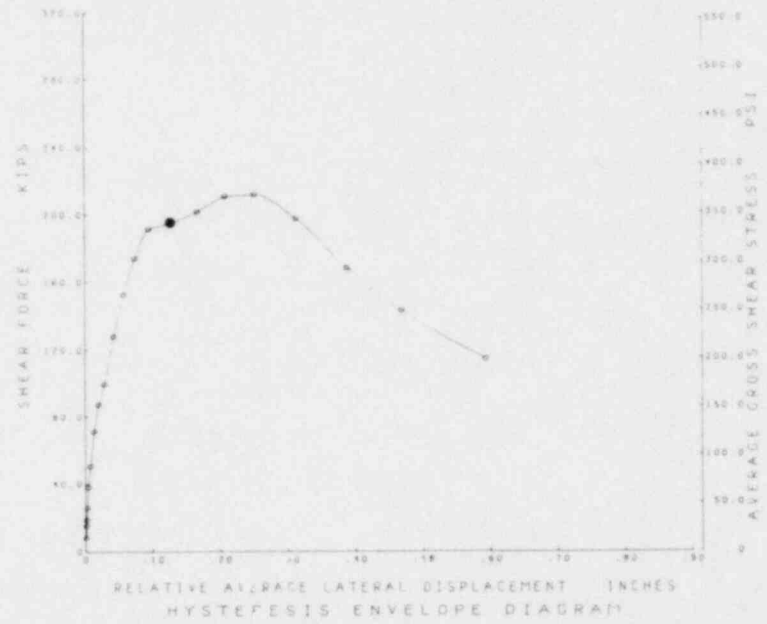
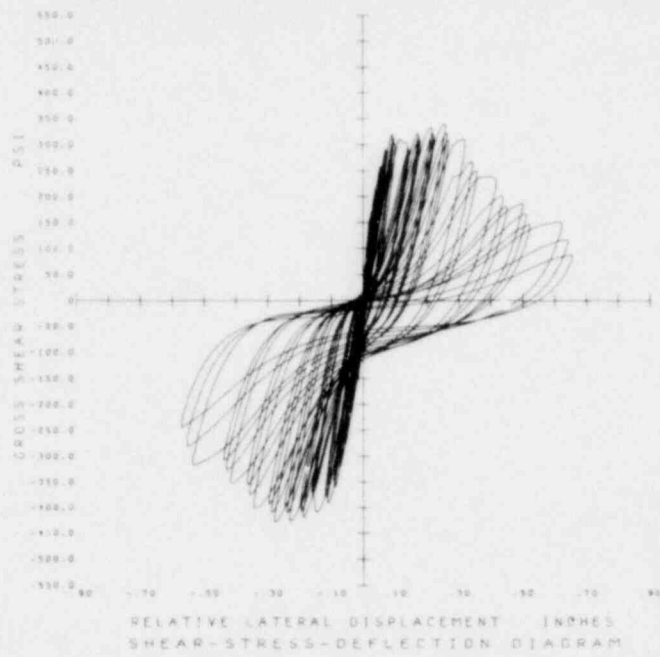


FIG. A.9 CONTINUED HCBR-12-3

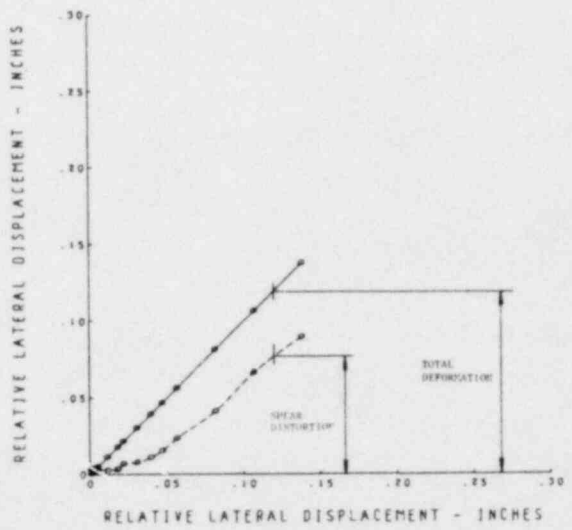
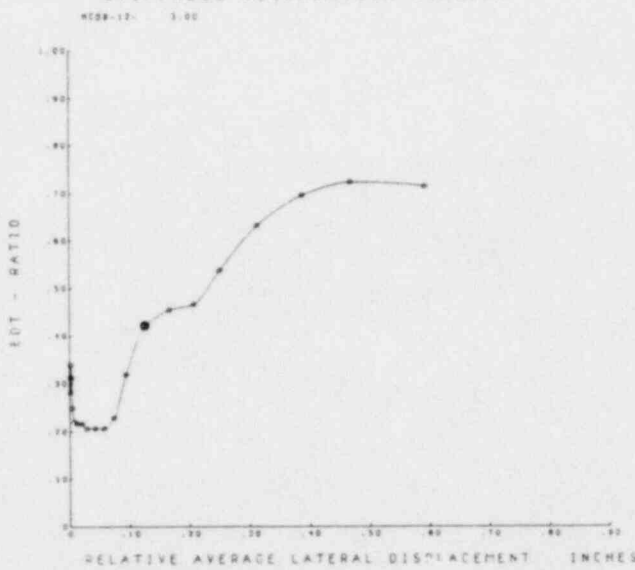
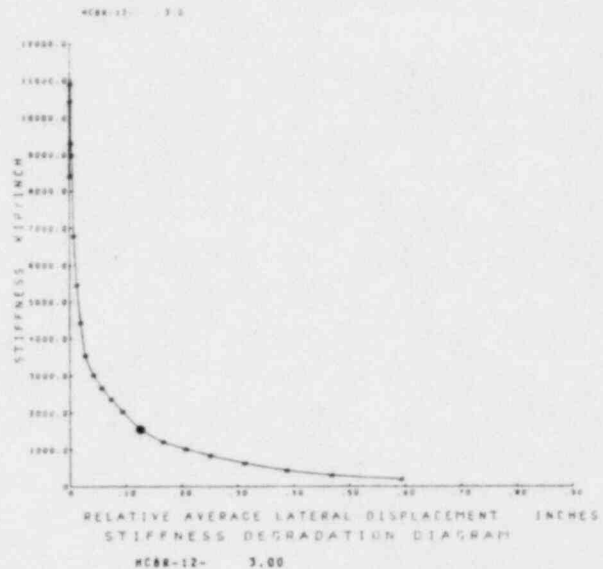
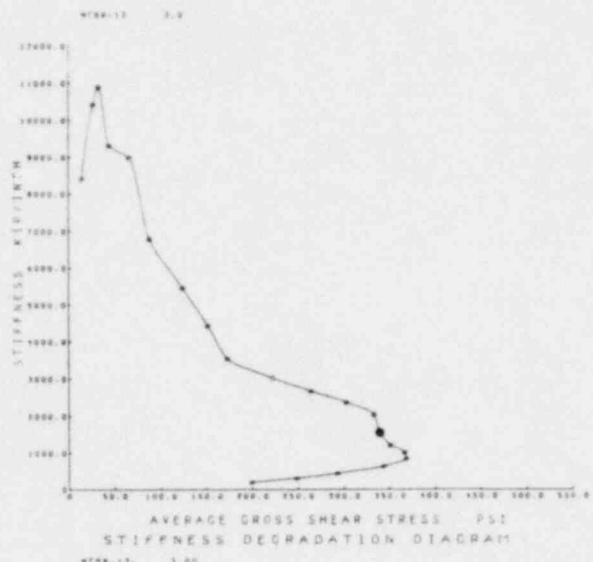
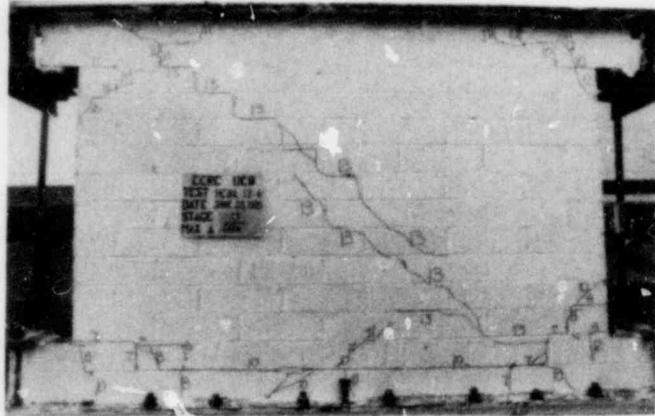
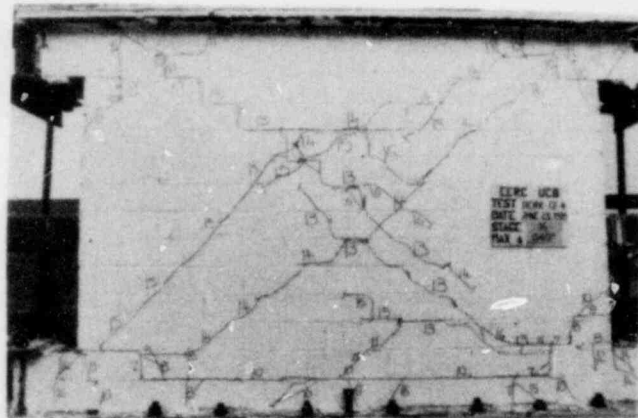
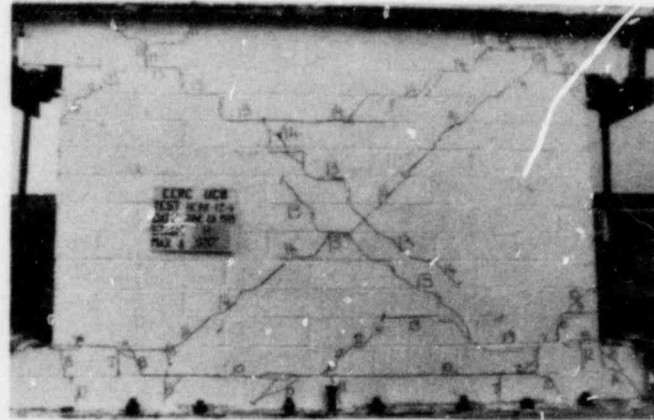


FIG. A.9 CONTINUED HCBR-12-3



●
Stage Stage
13 14



Stage Stage
16 18

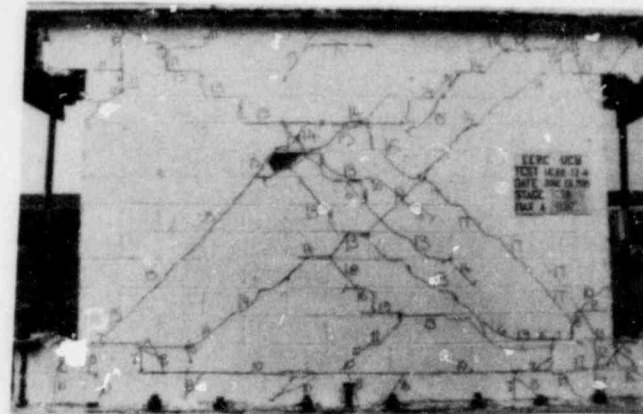


FIG. A.10 SUCCESSIVE CRACK FORMATION AND EXPERIMENTAL RESULTS TEST HCBR-12-4



Stage 20 Stage 21

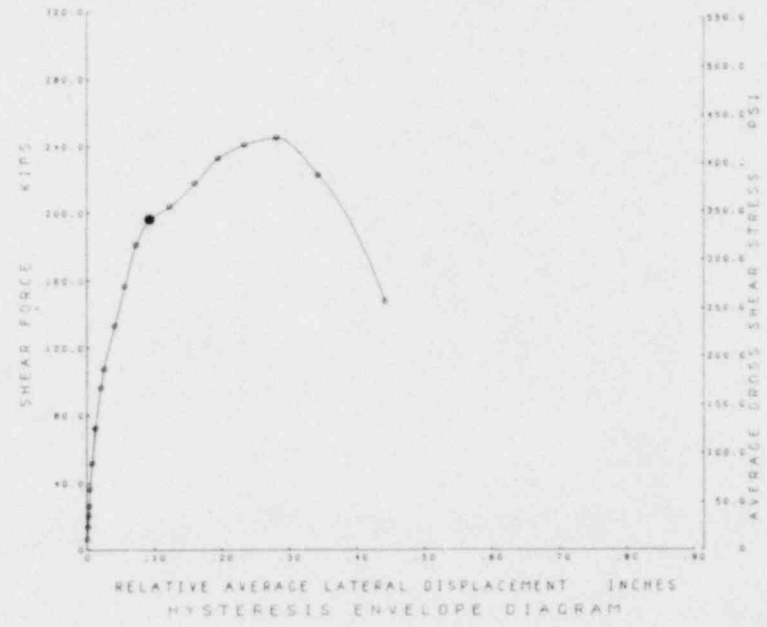
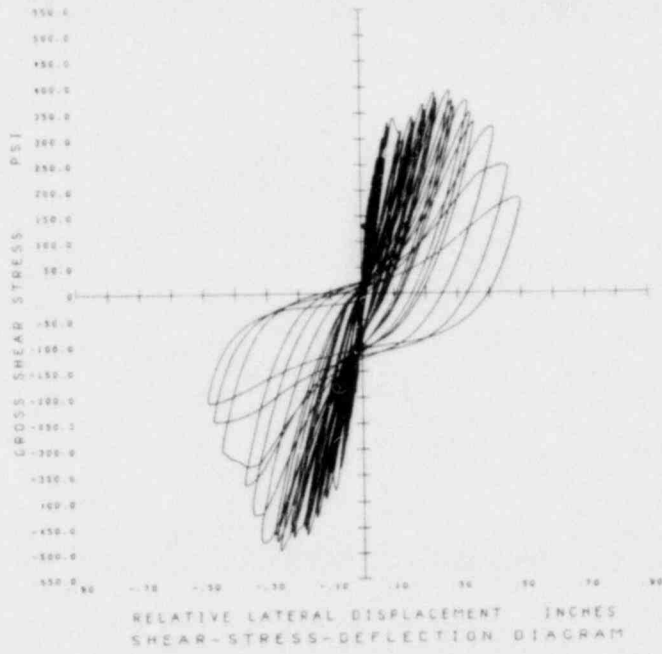
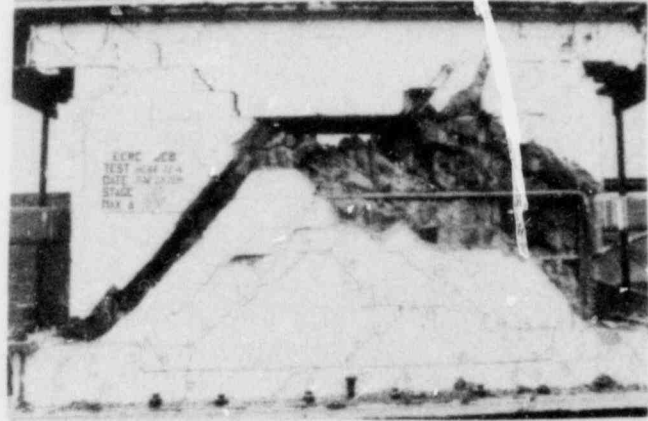


FIG. A.10 CONTINUED HCBR-12-4

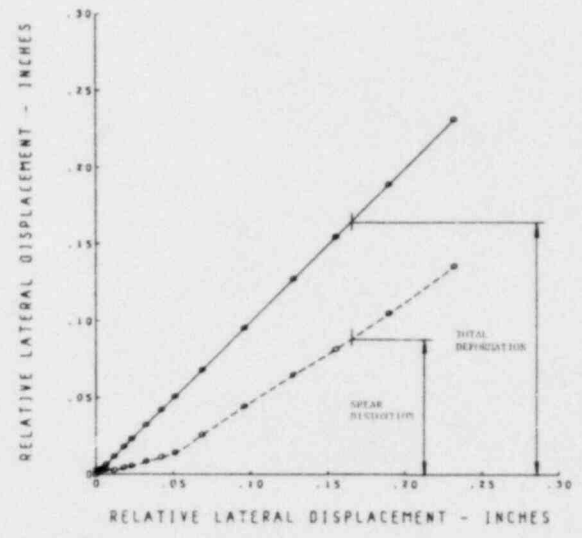
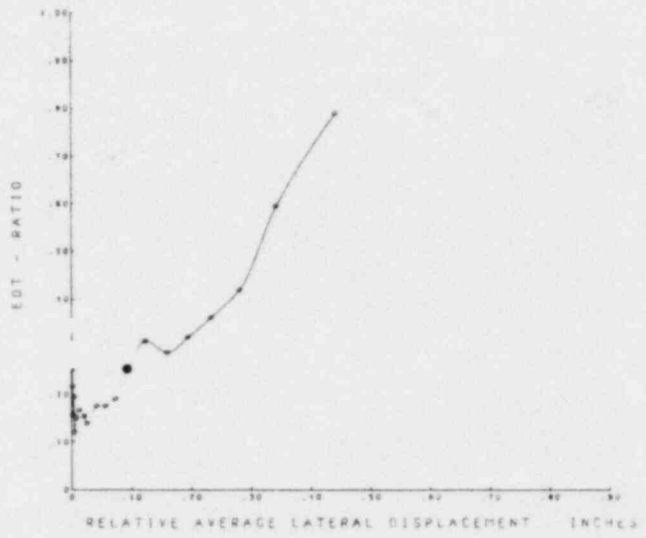
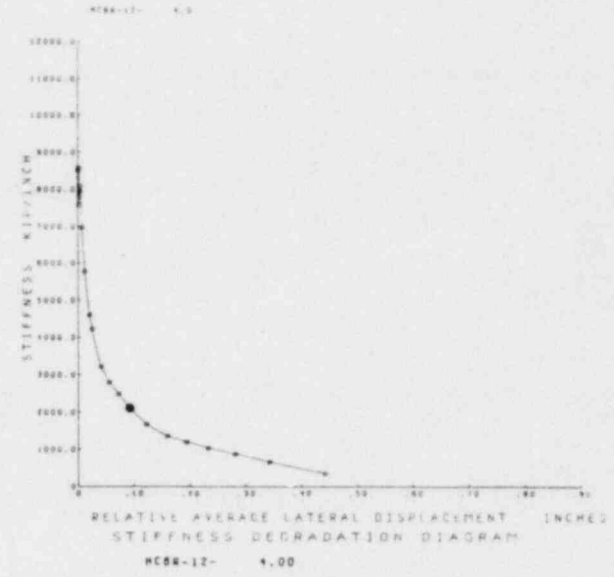
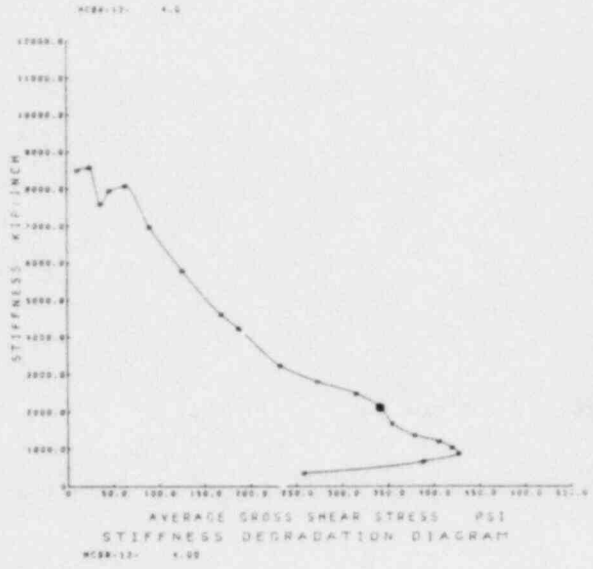
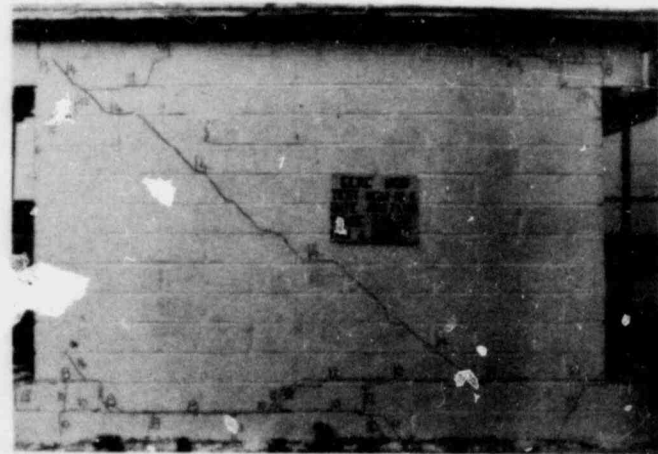


FIG. A.10 CONTINUED HCBR-12-4



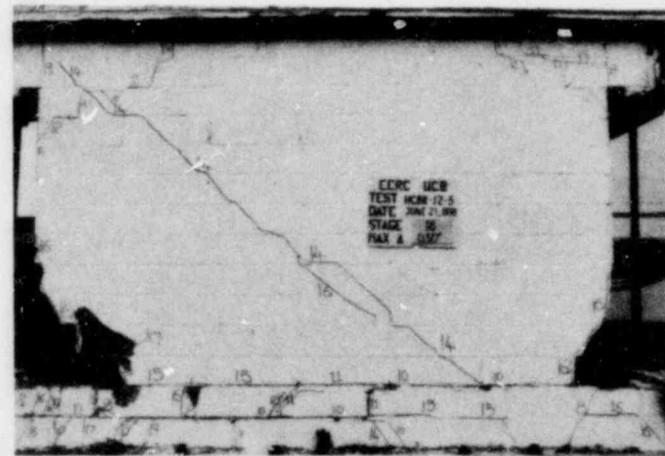
Stage 10



Stage 14

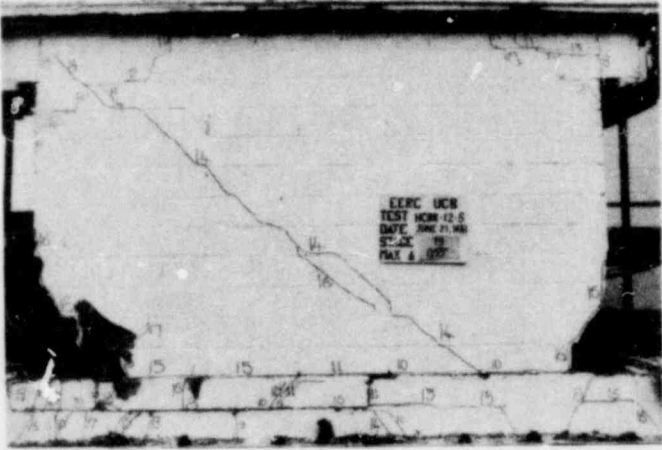


Stage 16



Stage 18

FIG. A.1: SUCCESSIVE CRACK FORMATION AND EXPERIMENTAL RESULTS TEST HCBR-12-5



Stage 19 Stage 20

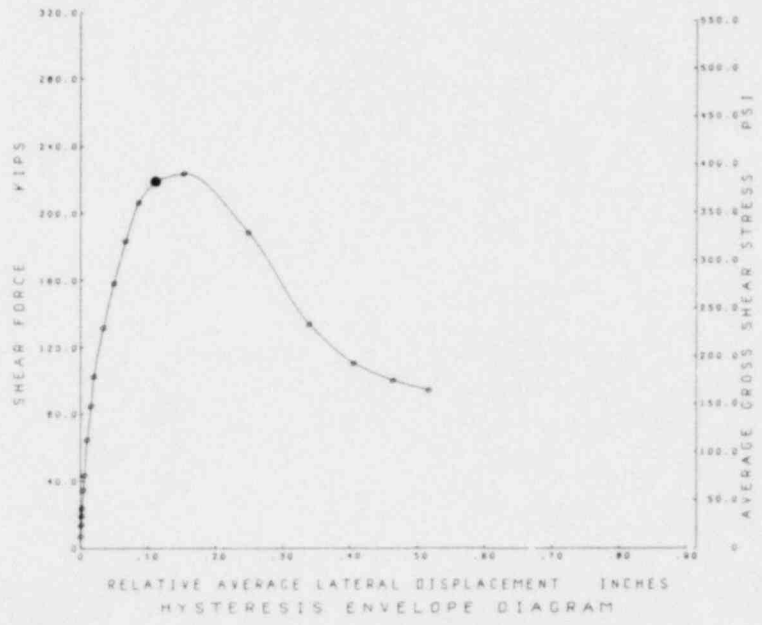
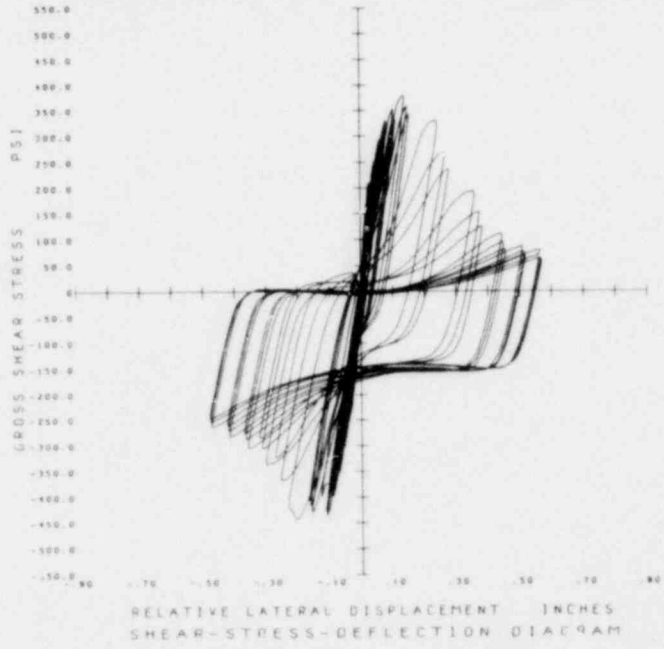


FIG. A.11 CONTINUED HCBR-12-5

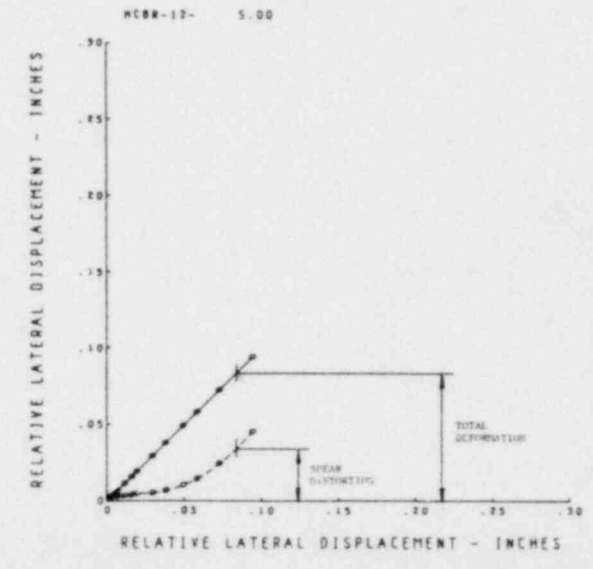
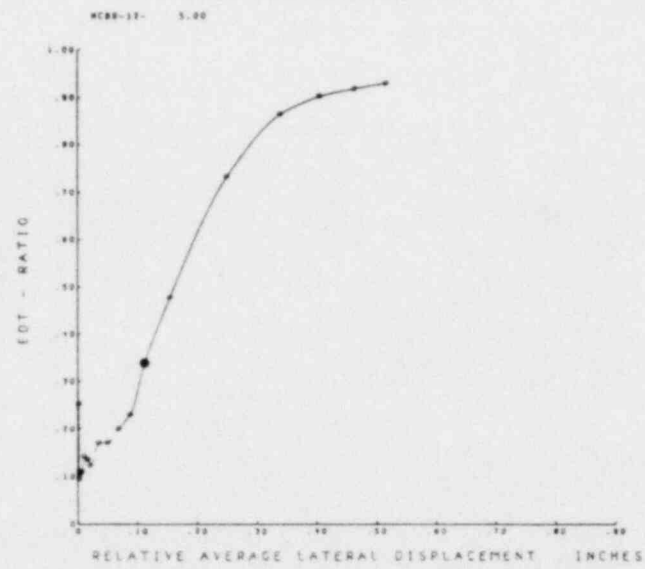
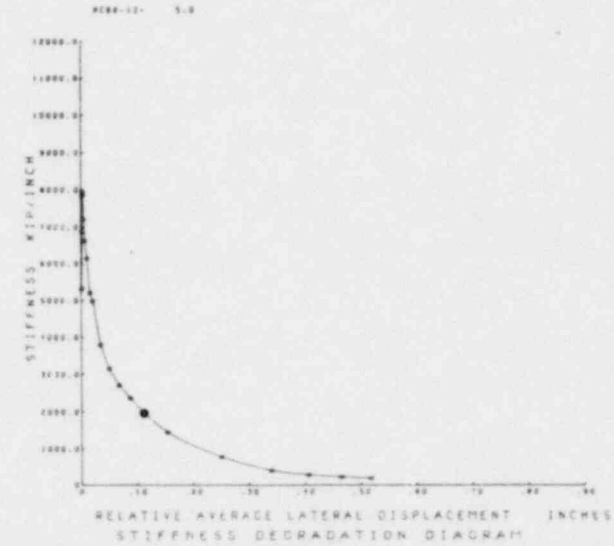
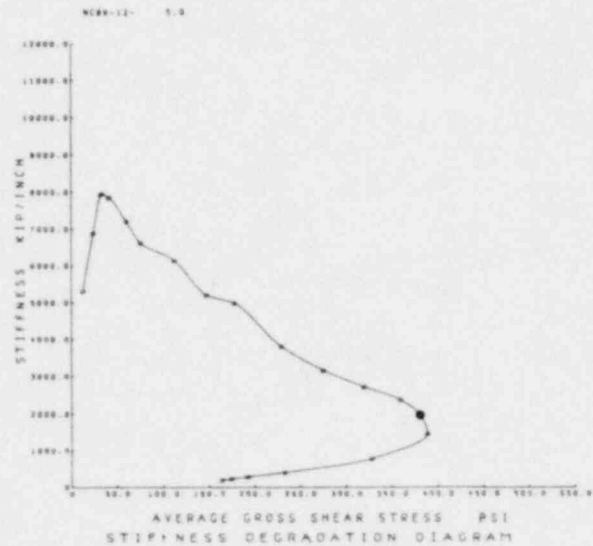
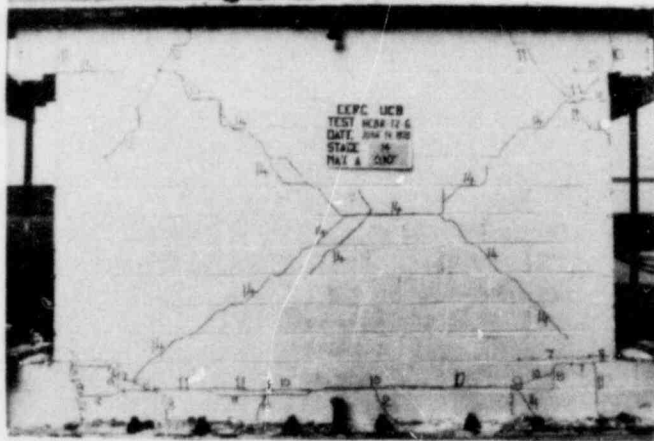
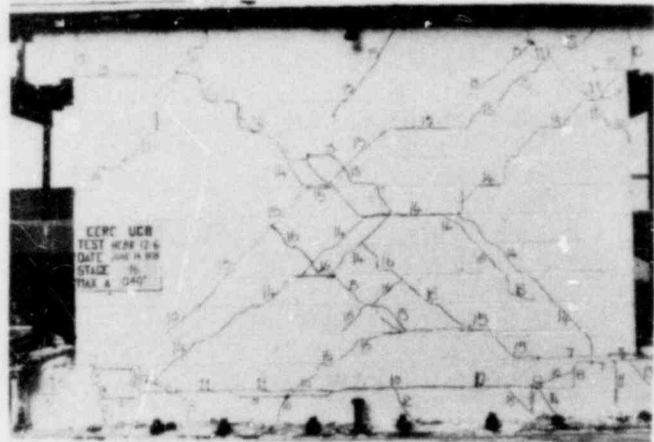


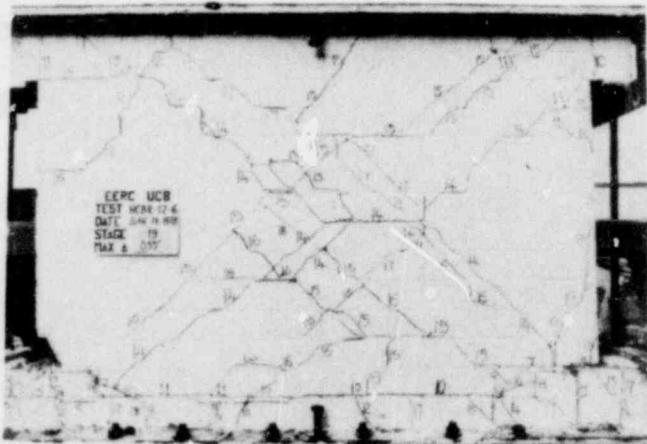
FIG. A.11 CONTINUED HCBR-12-5



Stage 14



Stage 16

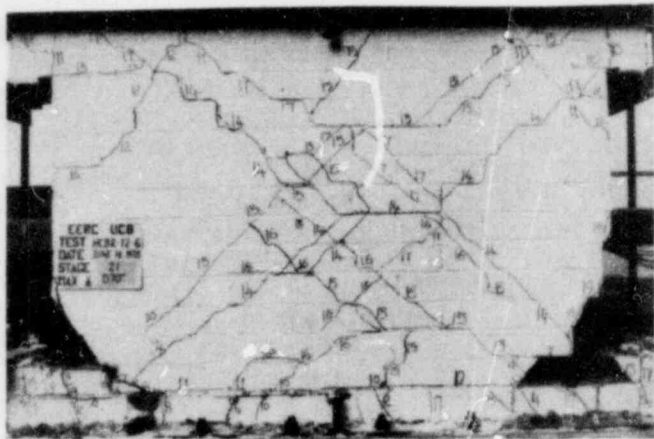


Stage 19



Stage 20

FIG. A.12 SUCCESSIVE CRACK FORMATION AND EXPERIMENTAL RESULTS TEST HCBR-12-6



Stage 21 Stage 22

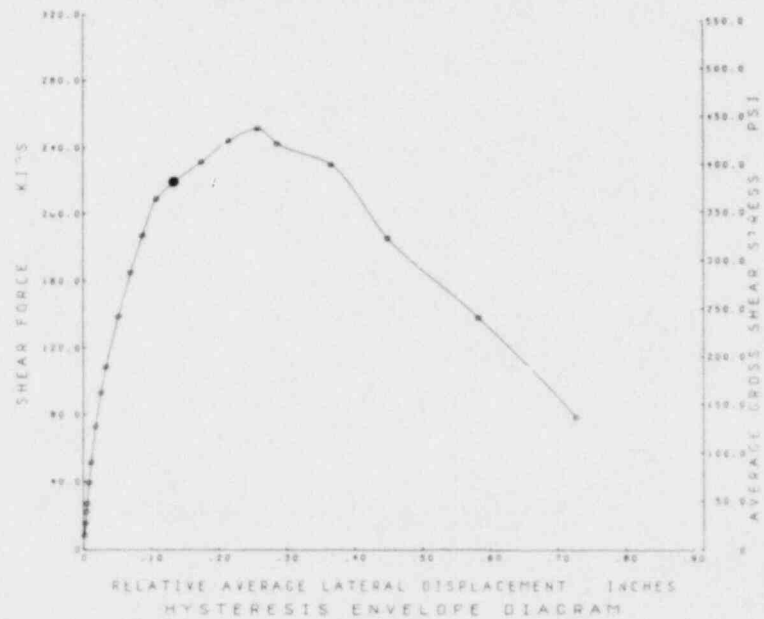
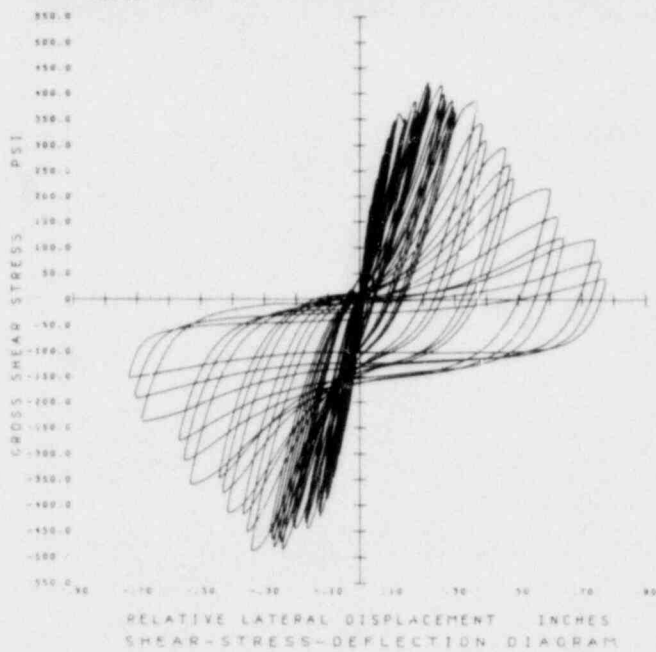
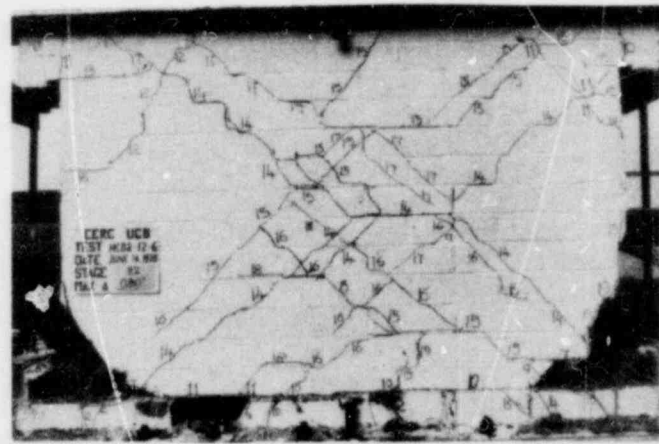


FIG. A.12 CONTINUED HCBR-12-6

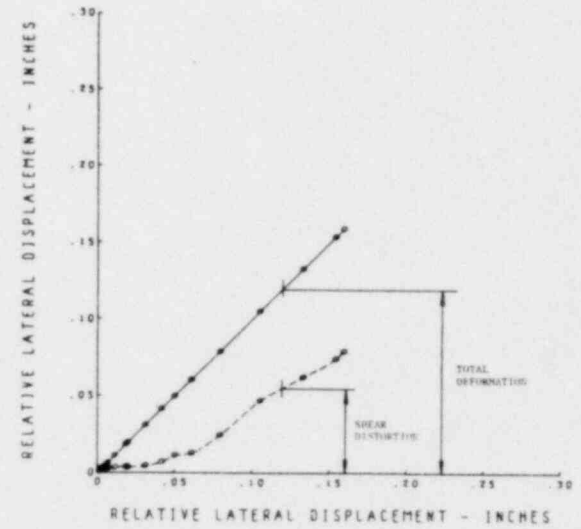
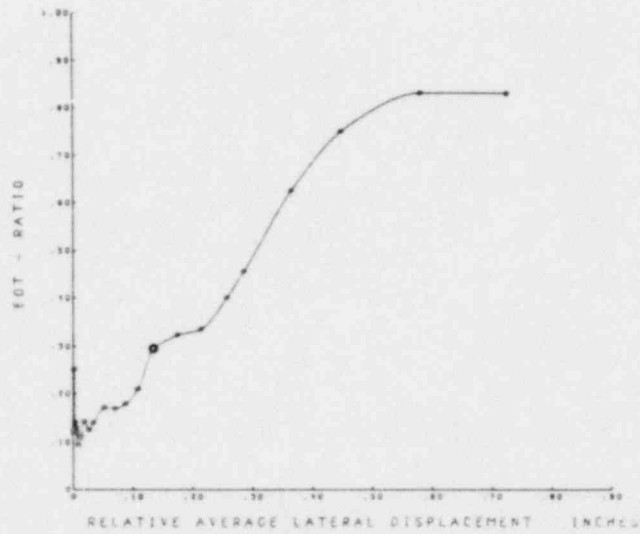
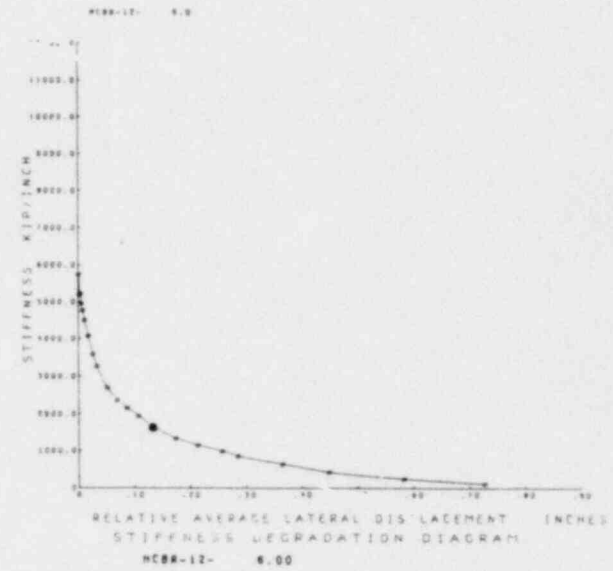
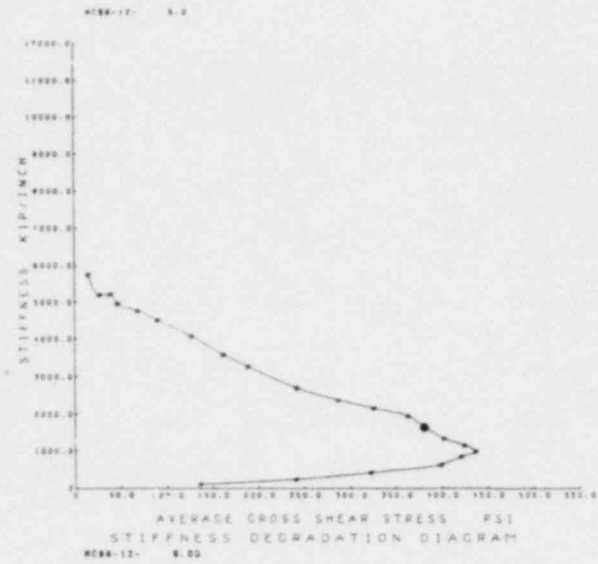
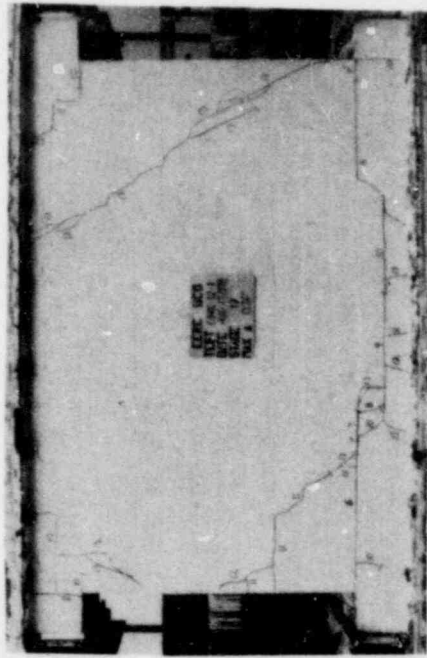
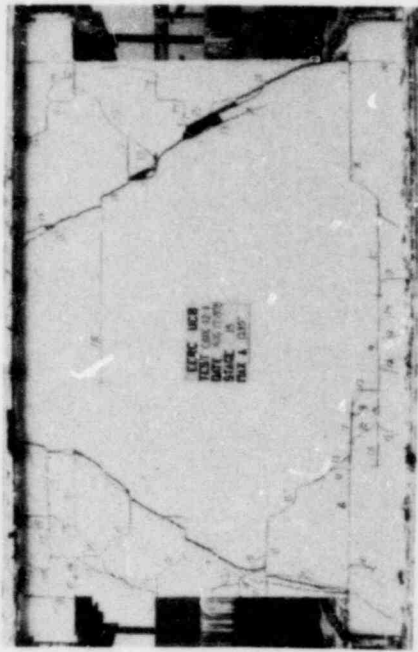


FIG. A.12 CONTINUED HCBR-12-6



●
Stage Stage
11 13



Stage Stage
14 15

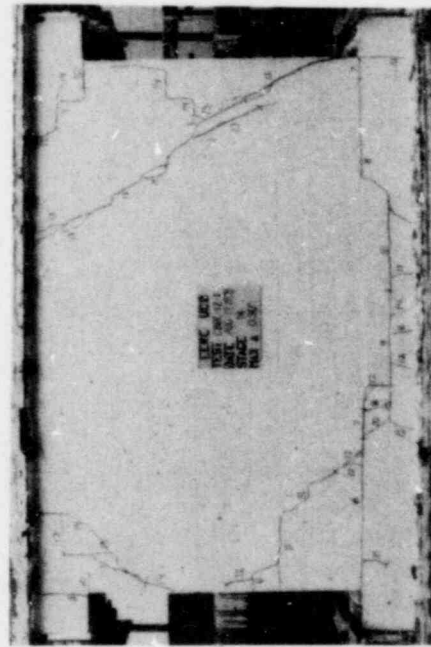
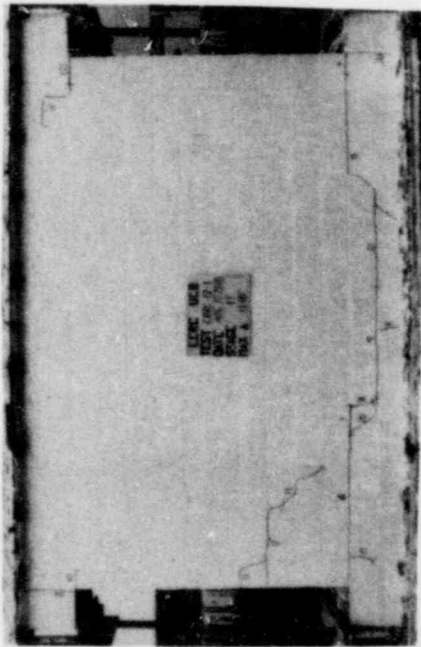


FIG. A.13 SUCCESSIVE CRACK FORMATION AND EXPERIMENTAL RESULTS TEST CBRC-12-1



Stage Stage
16 18

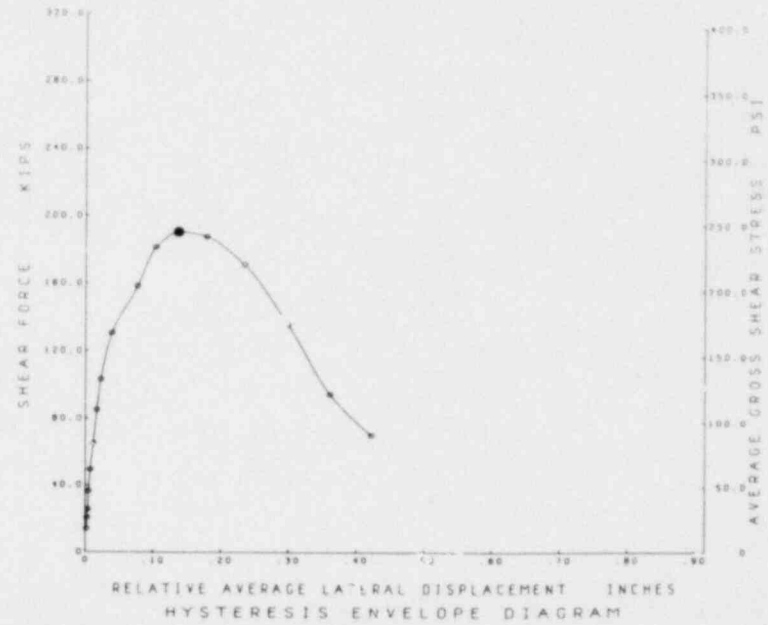
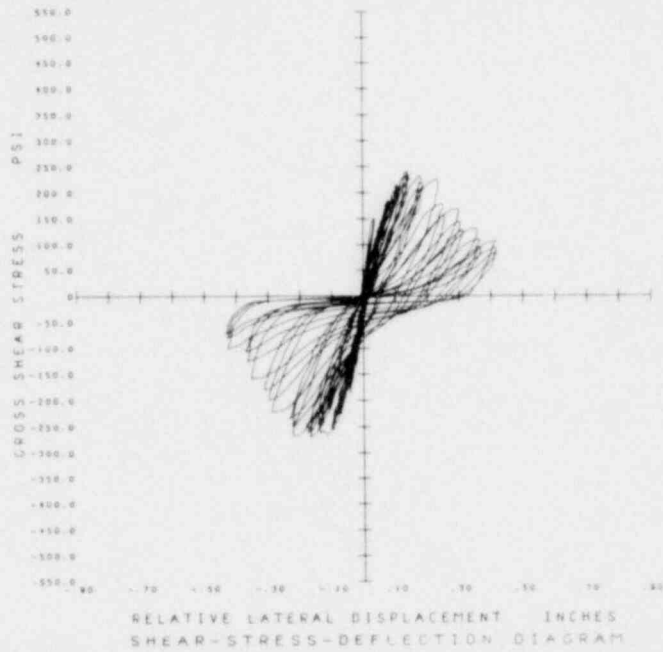


FIG. A.13 CONTINUED CBRC-12-1

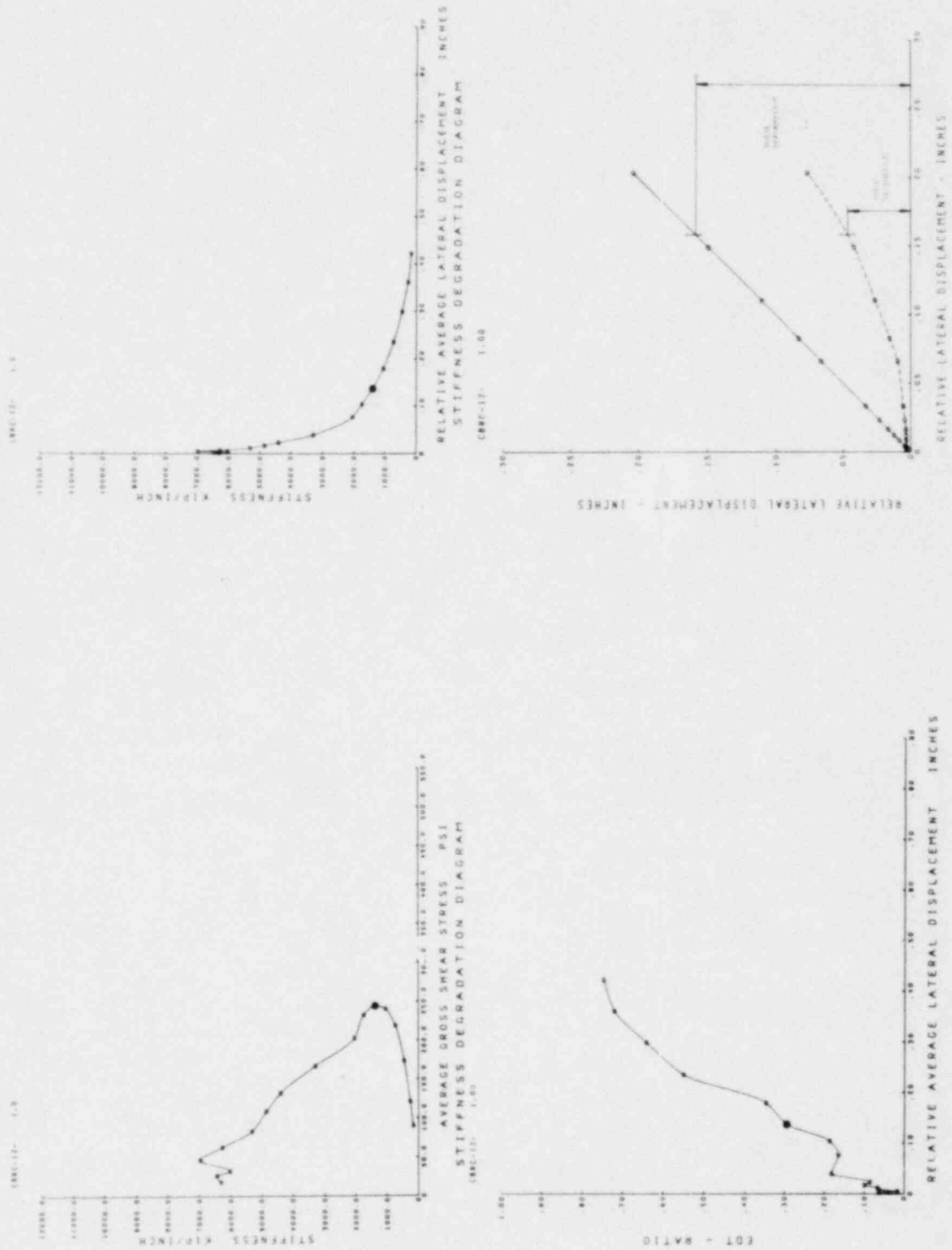
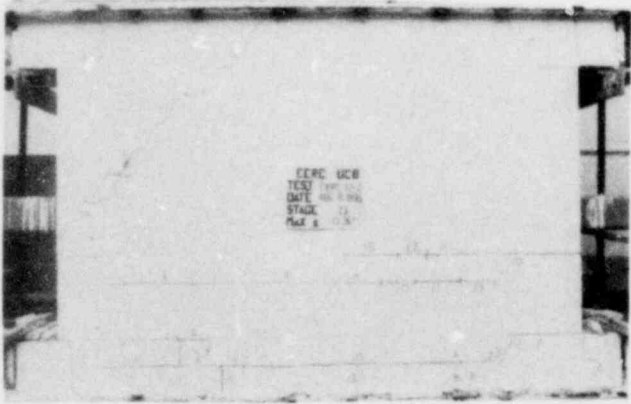
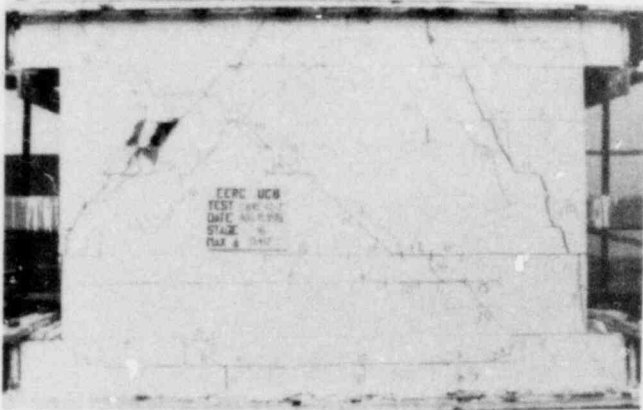
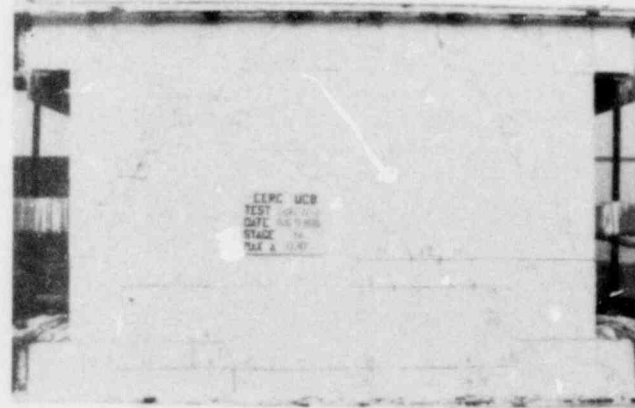


FIG. A.13 CONTINUED CBRF-12-1



Stage Stage
13 14



Stage Stage
16 17



FIG. A.14 SUCCESSIVE CRACK FORMATION AND EXPERIMENTAL RESULTS TEST CBRC-12-2



Stage Stage
18 19

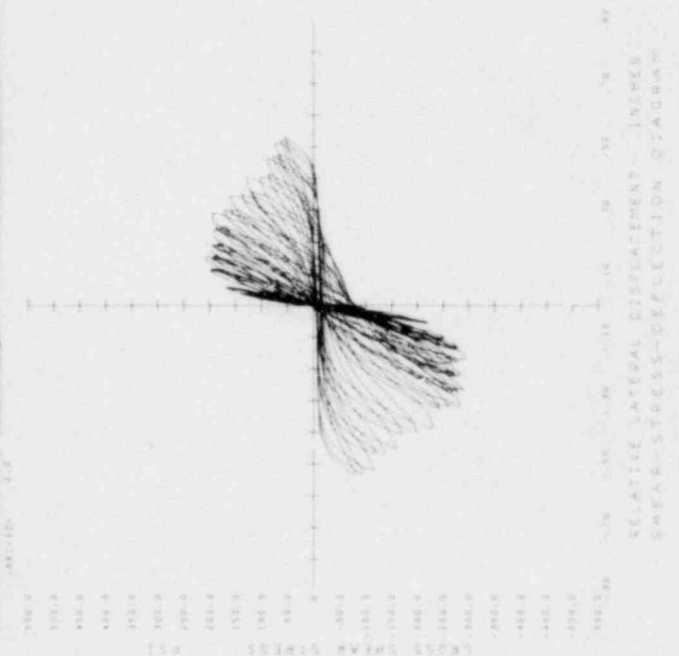
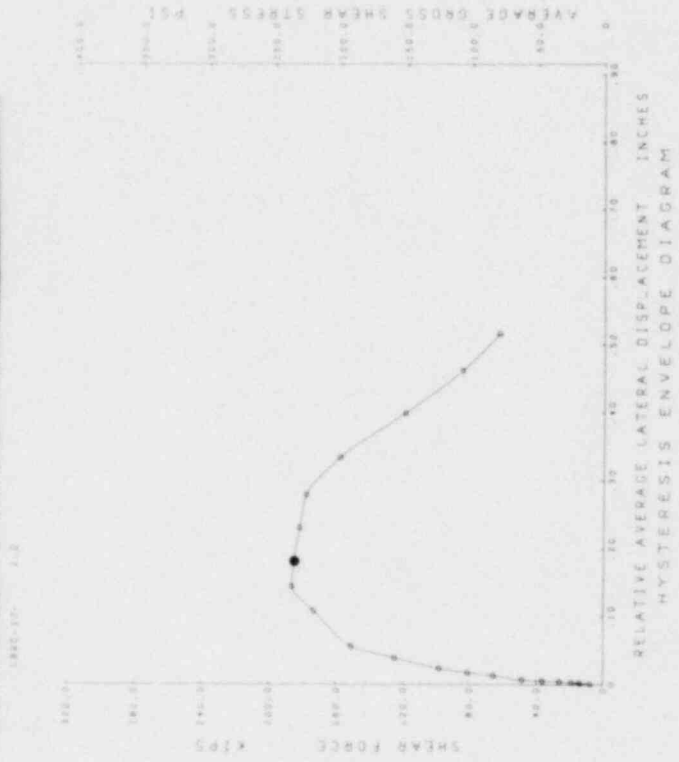


FIG. A.14 CONTINUED CBRC-12-2

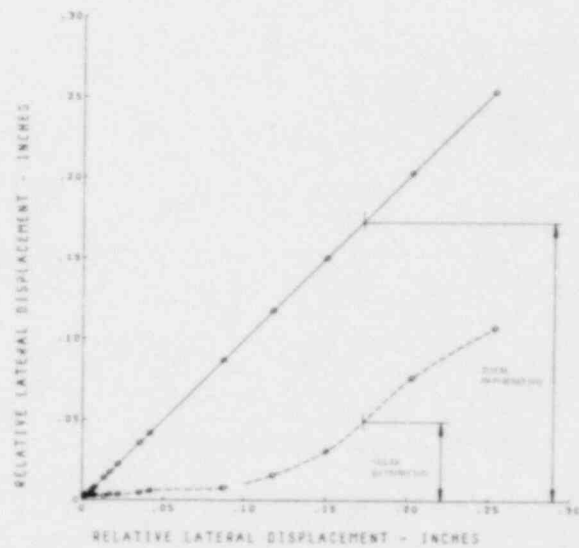
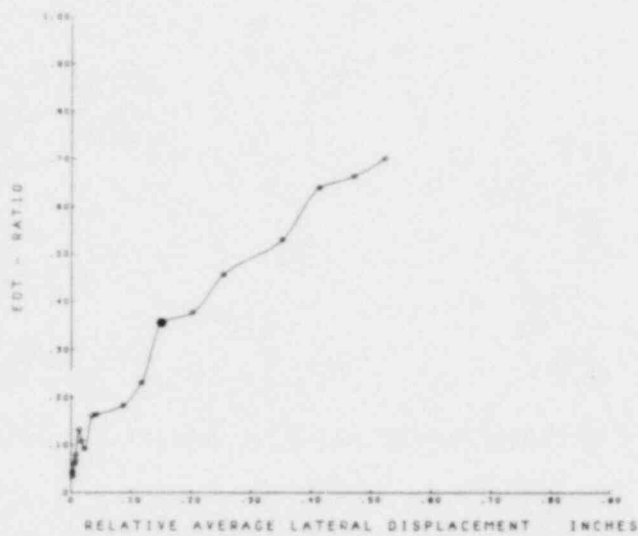
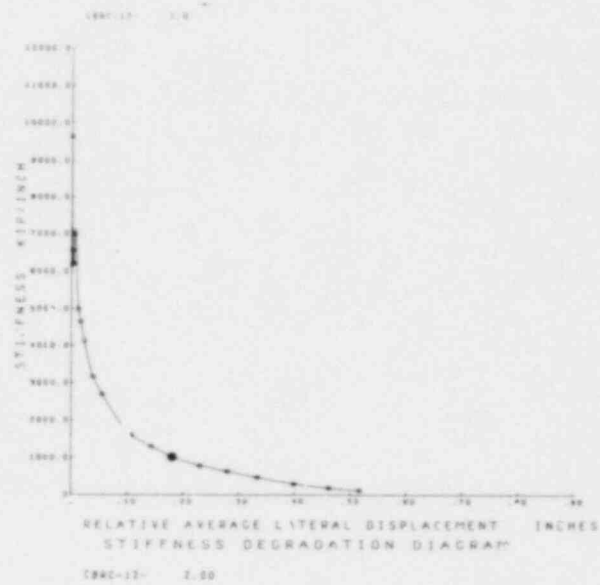
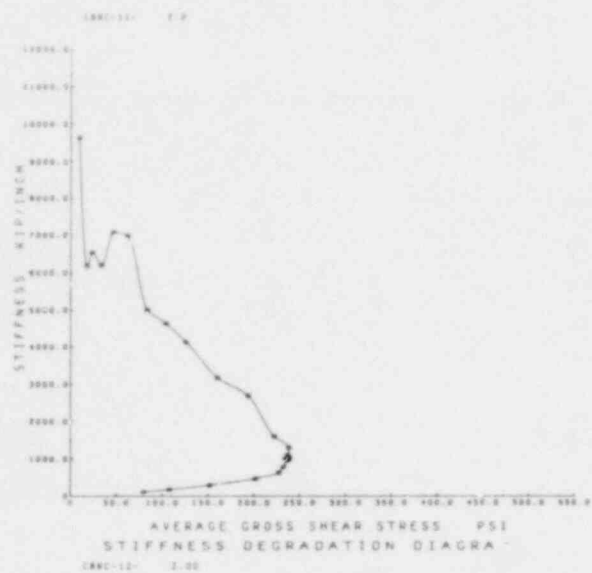
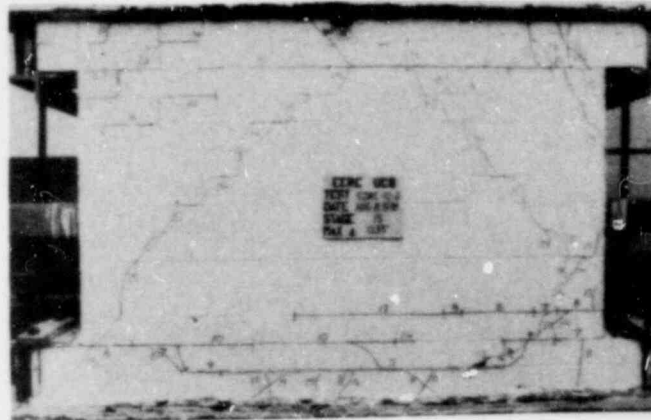


FIG. A.14 CONTINUED CBRC-12-2



Stage Stage
14 15



Stage Stage
17 18

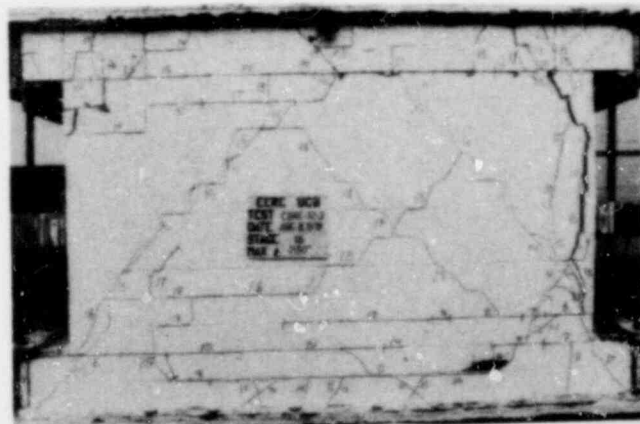
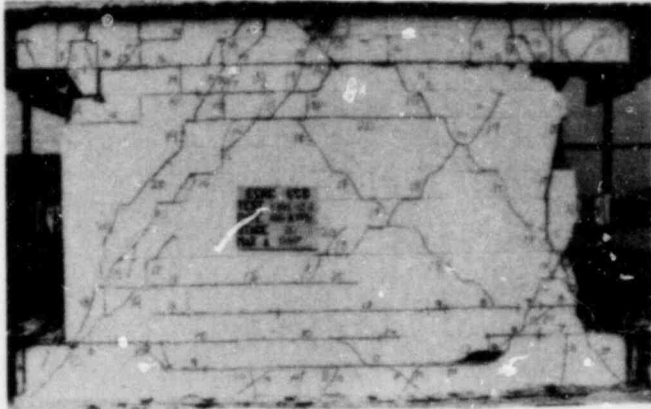


FIG. A.15 SUCCESSIVE CRACK FORMATION AND EXPERIMENTAL RESULTS TEST CBR-12-3



Stage Stage
20 21

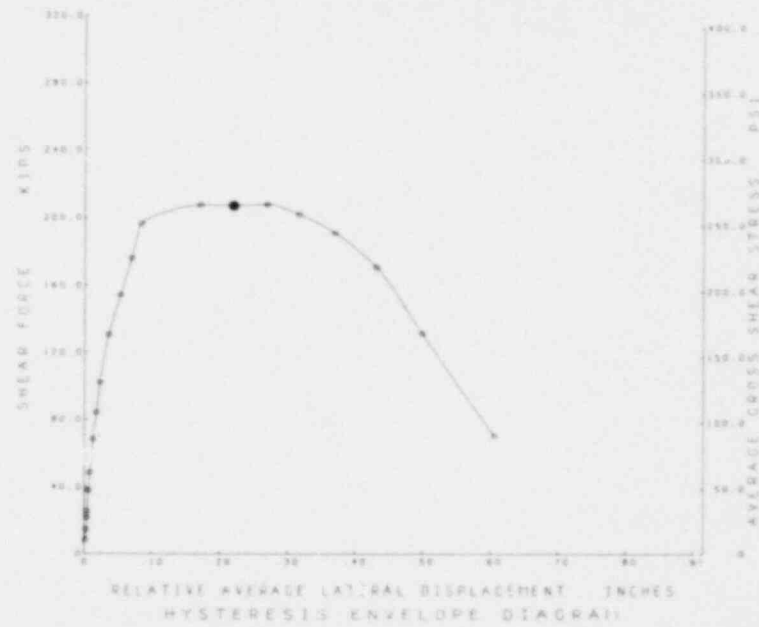
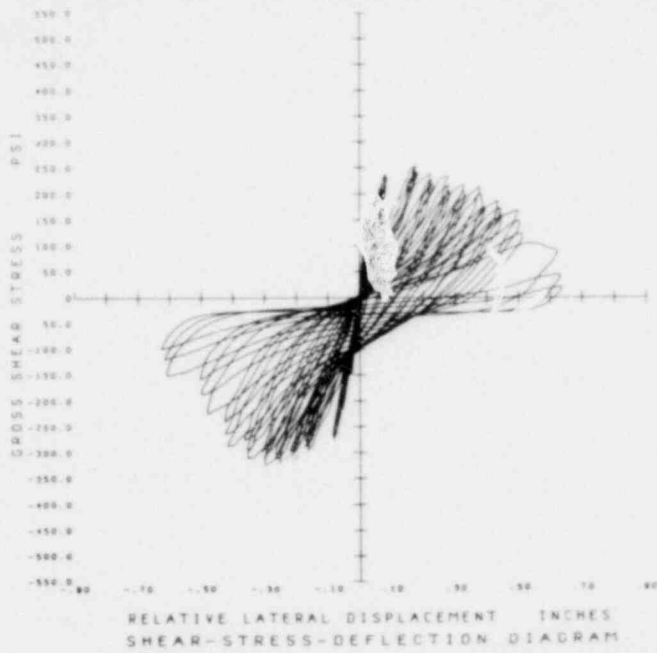
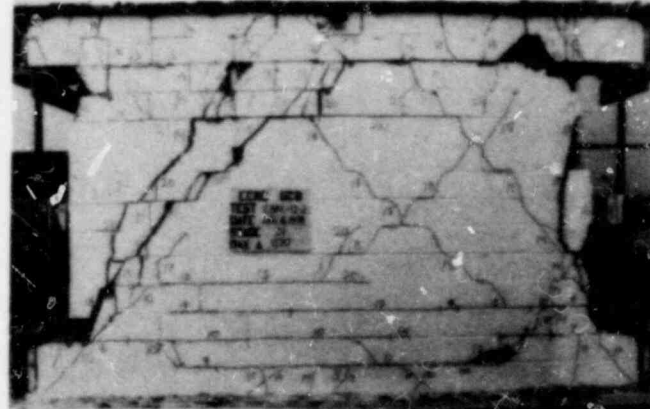


FIG. A.15 CONTINUED CBRC-12-3

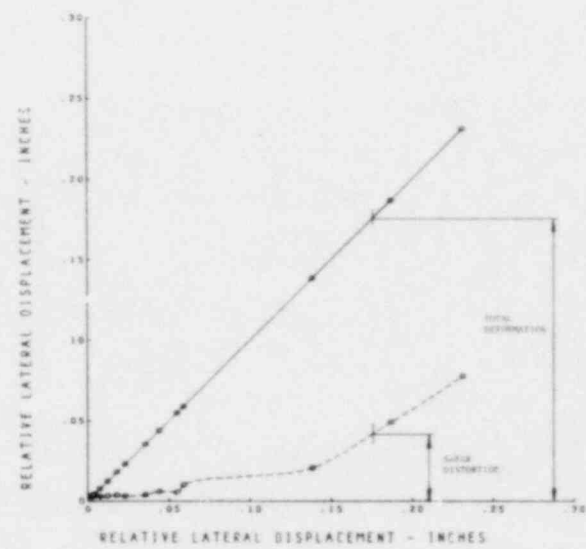
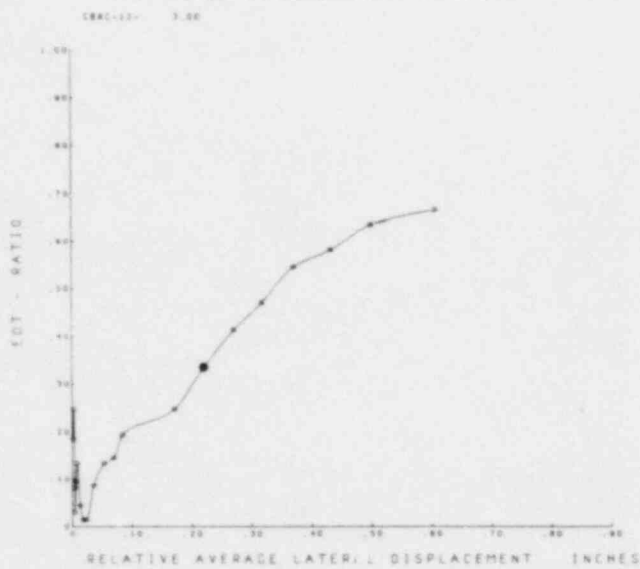
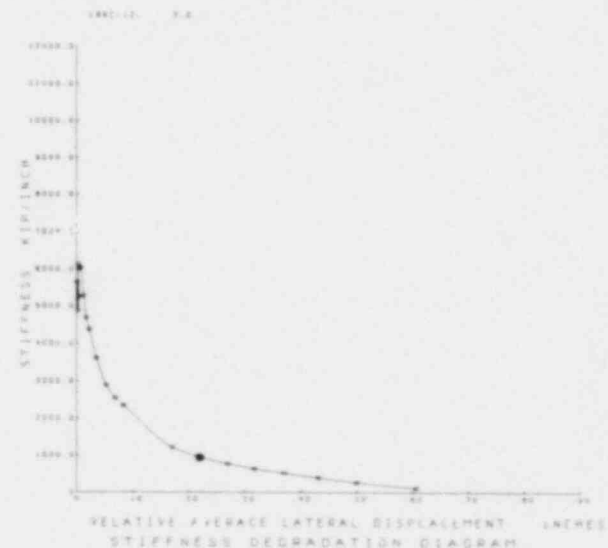
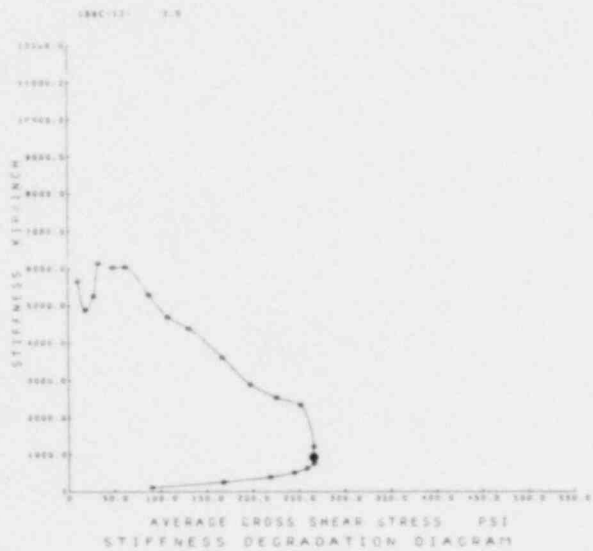
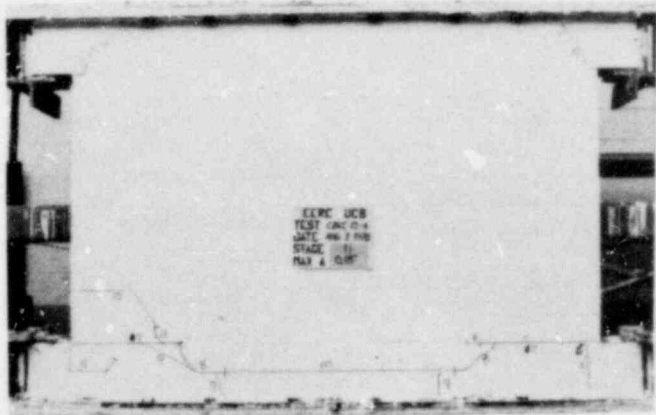
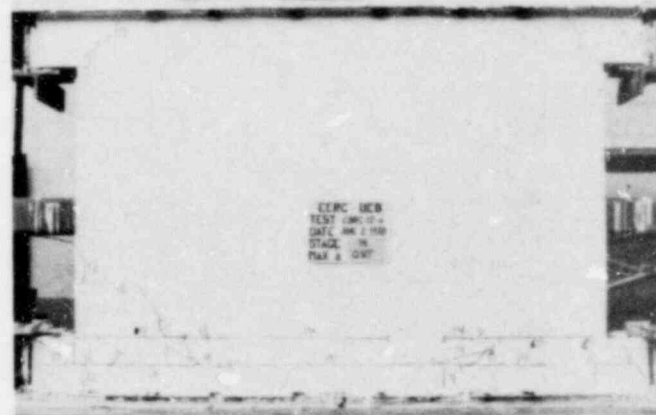


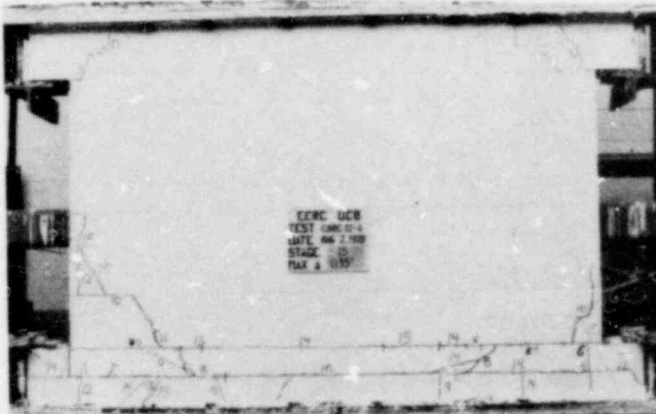
FIG. A.15 CONTINUED CBRC-12-3



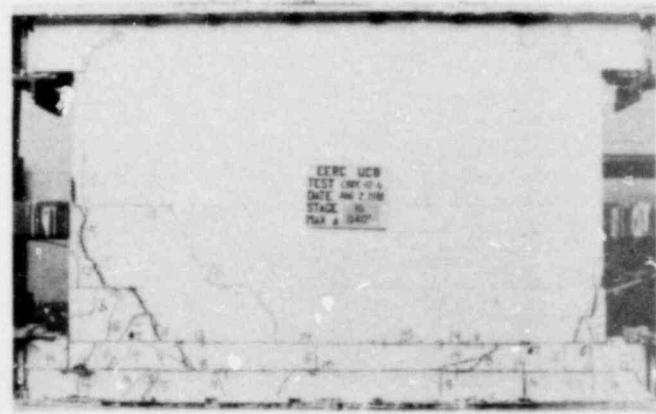
Stage 11



Stage 14

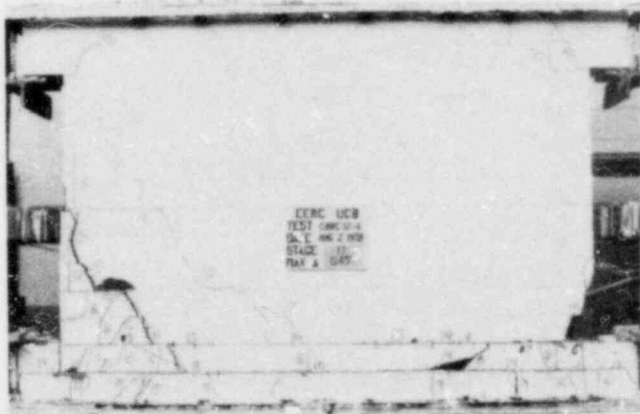


Stage 15



Stage 16

FIG. A.16 SUCCESSIVE CRACK FORMATION AND EXPERIMENTAL RESULTS TEST CBRC-12-4



CBRC-12-4 17



CBRC-12-4 19

Stage Stage
17 19

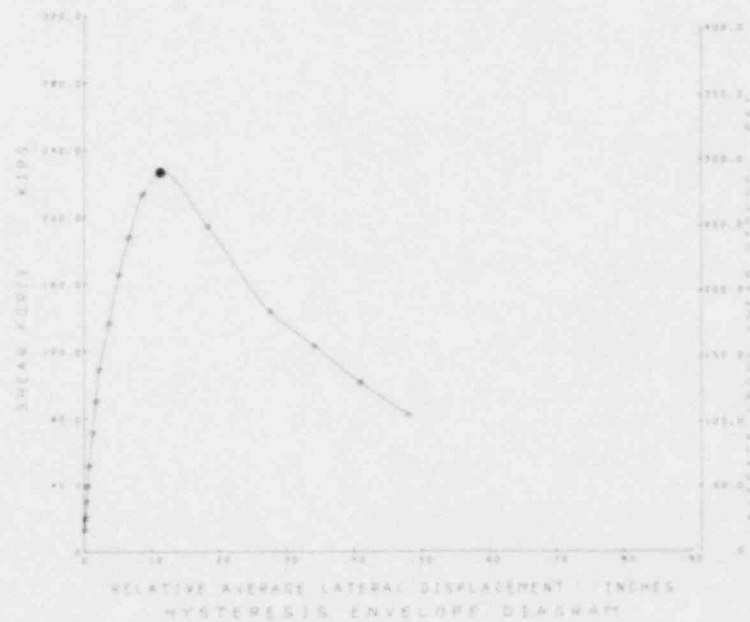
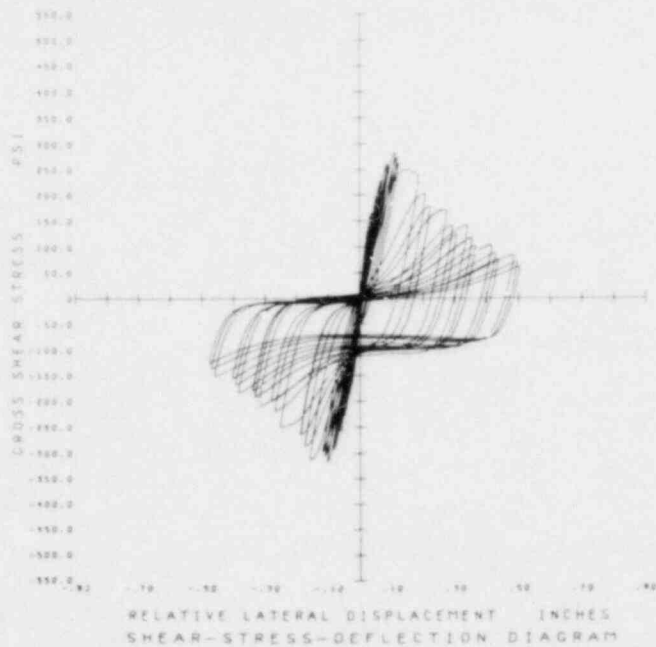
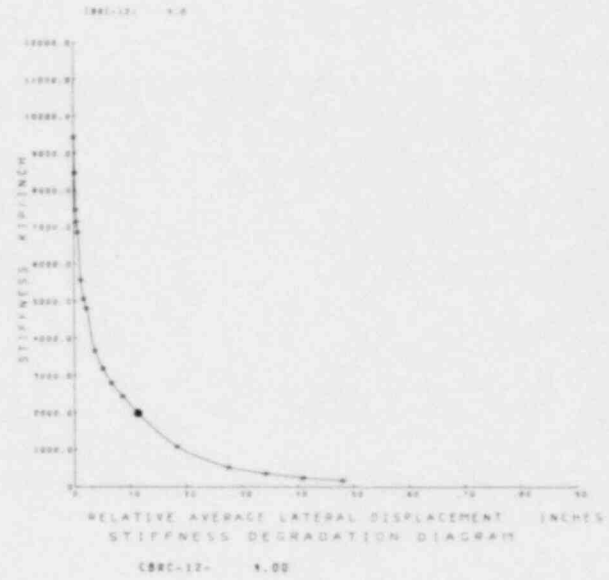
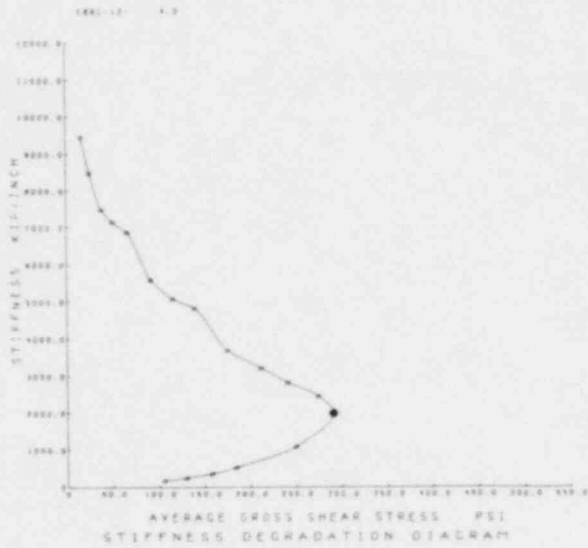
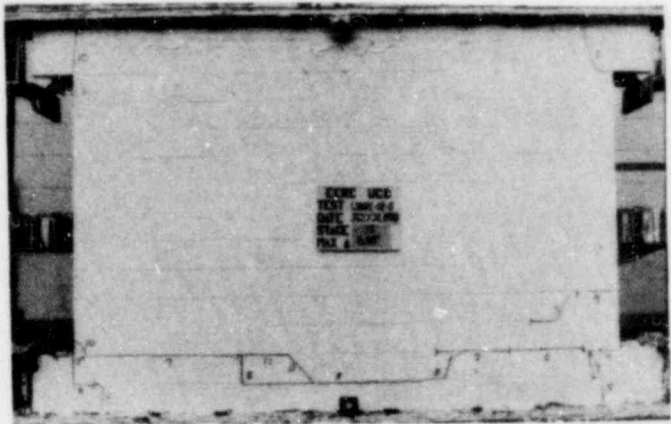


FIG. A.16 CONTINUED CBRC-12-4





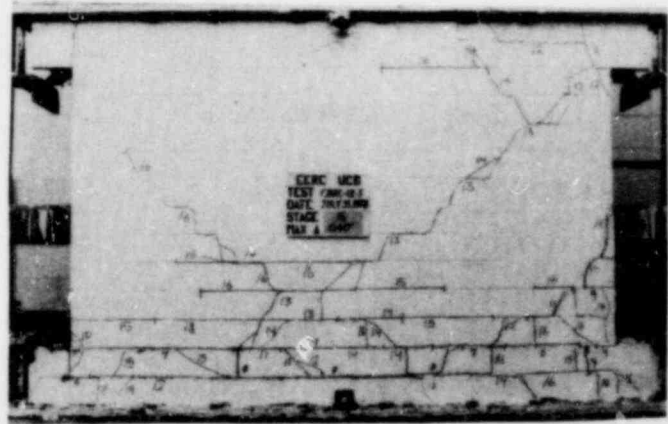
Stage 11



Stage 13

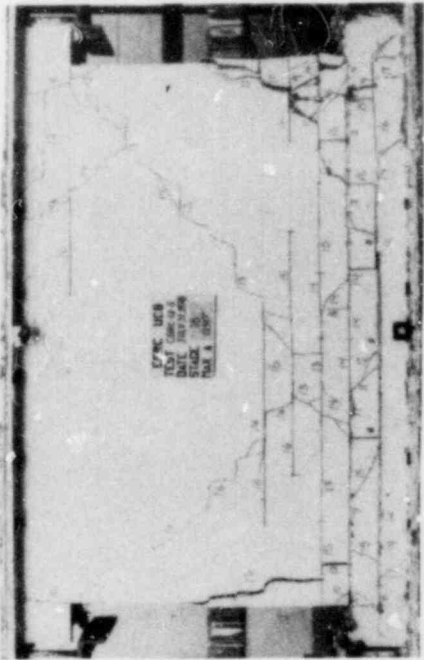


Stage 15

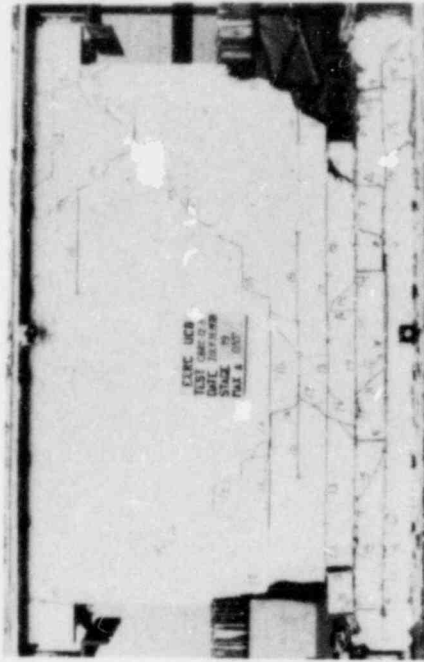


Stage 16

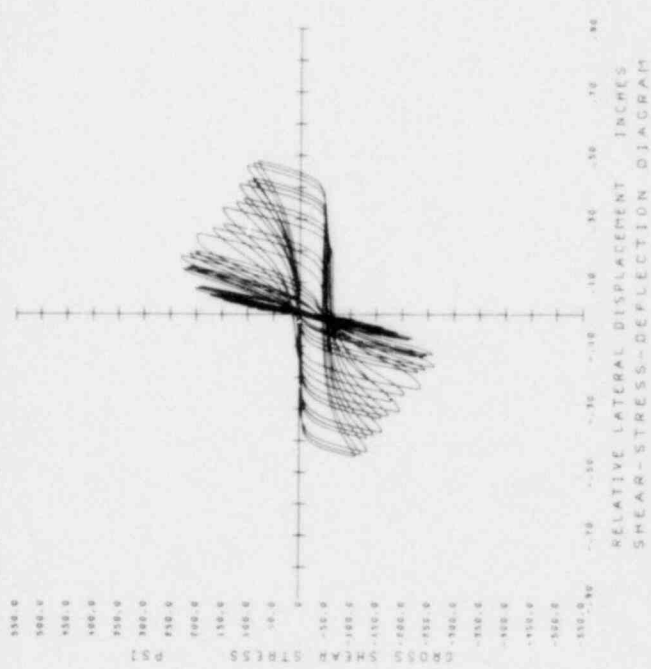
FIG. A.17 SUCCESSIVE CRACK FORMATION AND EXPERIMENTAL RESULTS TEST CBR-12-5



Stage Stage
18 19



CBRC 12-18 S.G.



CBRC 12-19 S.G.

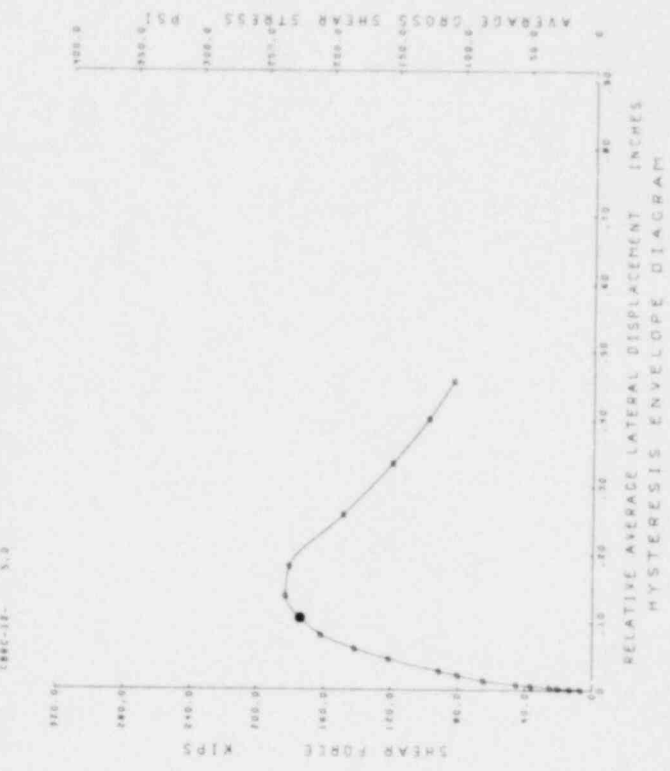


FIG. A.17 CONTINUED CBRC-12-5

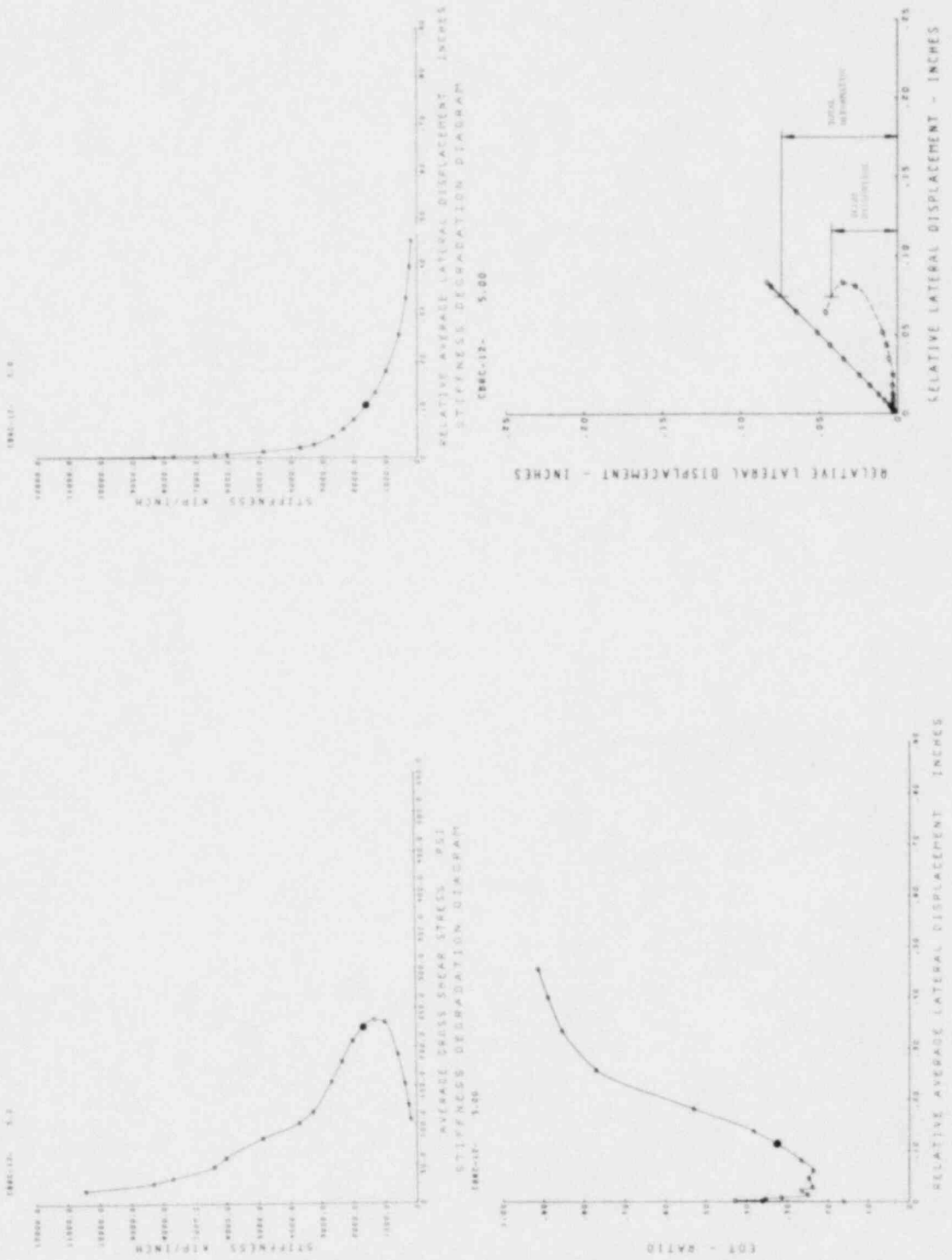
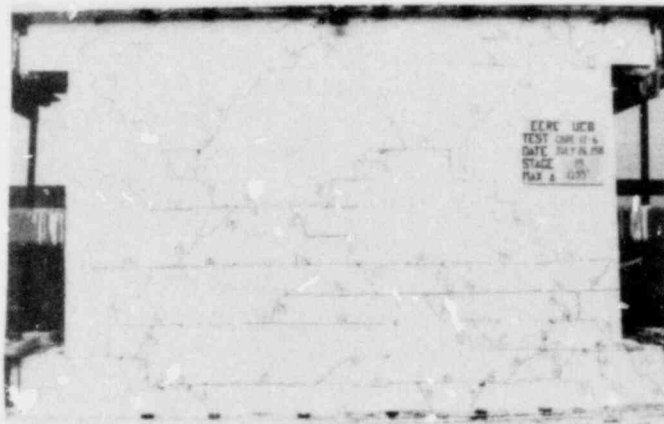
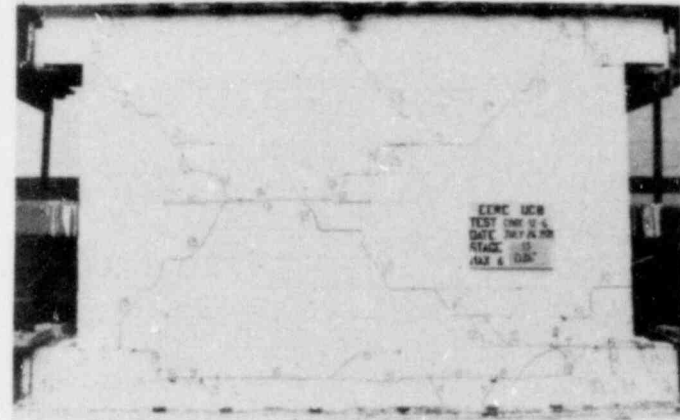


FIG. A.17 CONTINUED CBR-12-5



Stage 12 Stage 13



Stage 15 Stage 16

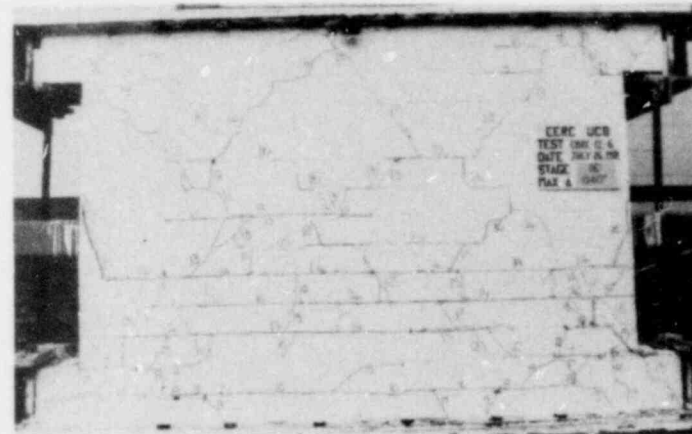


FIG. A.18 SUCCESSIVE CRACK FORMATION AND EXPERIMENTAL RESULTS TEST CBRC-12-6



Stage Stage
17 18

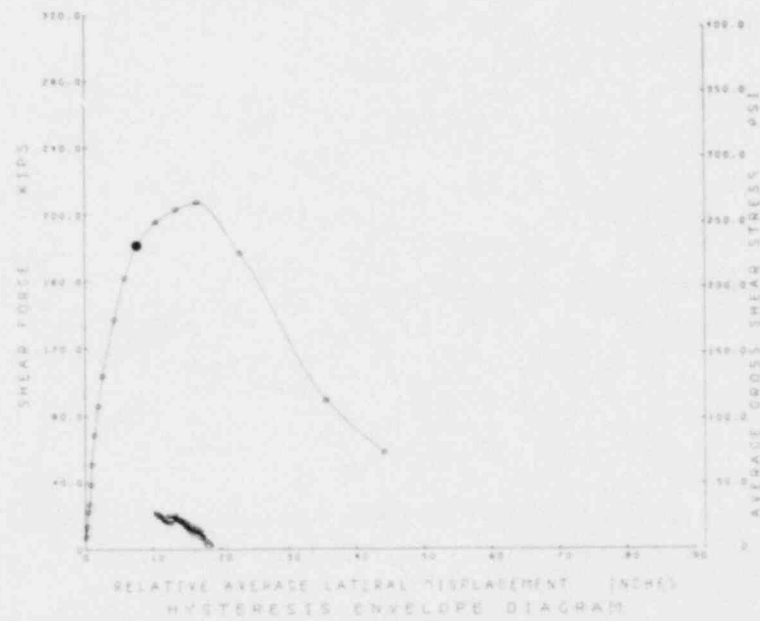
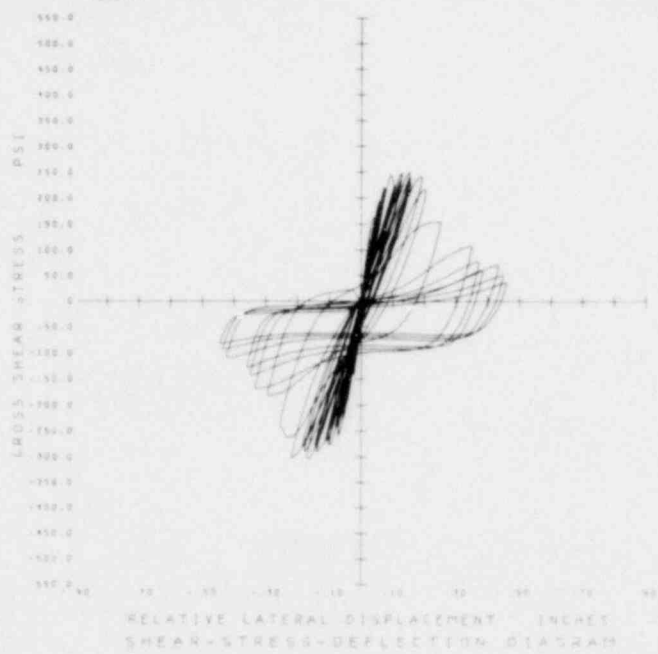
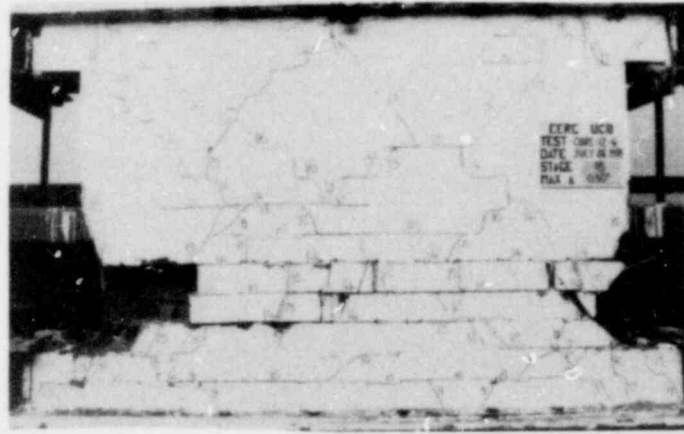


FIG. A.18 CONTINUED CBRC-12-6

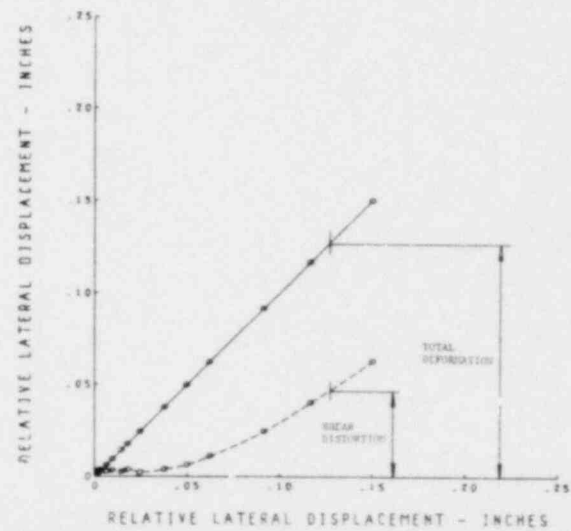
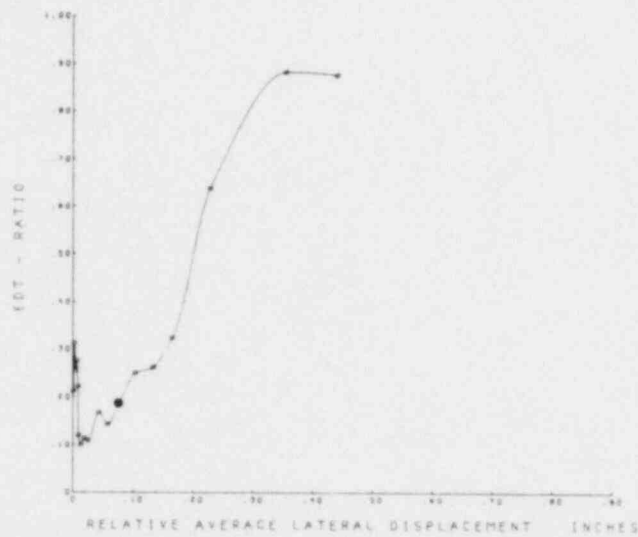
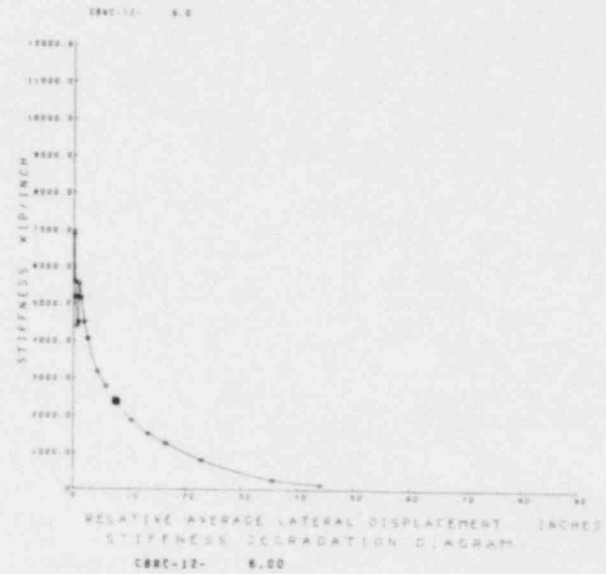
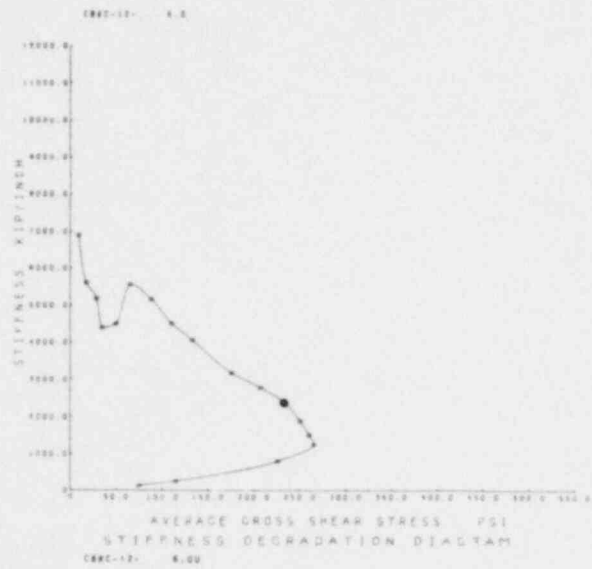


FIG. A.18 CONTINUED CBRC-12-6

EARTHQUAKE ENGINEERING RESEARCH CENTER REPORTS

NOTE: Numbers in parenthesis are Accession Numbers assigned by the National Technical Information Service; these are followed by a price code. Copies of the reports may be ordered from the National Technical Information Service, 5285 Port Royal Road, Springfield, Virginia, 22161. Accession Numbers should be quoted on orders for reports (PB --- ---) and remittance must accompany each order. Reports without this information were not available at time of printing. Upon request, EERC will mail inquirers this information when it becomes available.

- EERC 67-1 "Feasibility Study Large-Scale Earthquake Simulator Facility," by J. Penzien, J.G. Bouwkamp, R.W. Clough and D. Rea - 1967 (PB 187 905)A07
- EERC 68-1 Unassigned
- EERC 68-2 "Inelastic Behavior of Beam-to-Column Subassemblies Under Repeated Loading," by V.V. Bertero - 1968 (PB 184 888)A05
- EERC 68-3 "A Graphical Method for Solving the Wave Reflection-Refraction Problem," by H.D. McNiven and Y. Mengi - 1968 (PB 187 943)A03
- EERC 68-4 "Dynamic Properties of McKinley School Buildings," by D. Rea, J.G. Bouwkamp and R.W. Clough - 1968 (PB 187 902)A07
- EERC 68-5 "Characteristics of Rock Motions During Earthquakes," by H.B. Seed, I.M. Idriss and F.W. Kiefer - 1968 (PB 188 338)A03
- EERC 69-1 "Earthquake Engineering Research at Berkeley," - 1969 (PB 187 906)A11
- EERC 69-2 "Nonlinear Seismic Response of Earth Structures," by M. Dabaj and J. Penzien - 1969 (PB 187 904)A08
- EERC 69-3 "Probabilistic Study of the Behavior of Structures During Earthquakes," by R. Ruiz and J. Penzien - 1969 (PB 187 886)A06
- EERC 69-4 "Numerical Solution of Boundary Value Problems in Structural Mechanics by Reduction to an Initial Value Formulation," by N. Distefano and J. Schujman - 1969 (PB 187 942)A02
- EERC 69-5 "Dynamic Programming and the Solution of the Biharmonic Equation," by N. Distefano - 1969 (PB 187 941)A03
- EERC 69-6 "Stochastic Analysis of Offshore Tower Structures," by A.K. Malhotra and J. Penzien - 1969 (PB 187 903)A09
- EERC 69-7 "Rock Motion Accelerograms for High Magnitude Earthquakes," by H.B. Seed and I.M. Idriss - 1969 (PB 187 940)A02
- EERC 69-8 "Structural Dynamics Testing Facilities at the University of California, Berkeley," by R.M. Stephen, J.G. Bouwkamp, R.W. Clough and J. Penzien - 1969 (PB 189 111)A04
- EERC 69-9 "Seismic Response of Soil Deposits Underlain by Sloping Rock Boundaries," by H. Dezfulian and H.B. Seed - 1969 (PB 189 114)A03
- EERC 69-10 "Dynamic Stress Analysis of Axisymmetric Structures Under Arbitrary Loading," by S. Ghosh and E.L. Wilson - 1969 (PB 189 026)A10
- EERC 69-11 "Seismic Behavior of Multistory Frames Designed by Different Philosophies," by J.C. Anderson and V. V. Bertero - 1969 (PB 190 662)A10
- EERC 69-12 "Stiffness Degradation of Reinforcing Concrete Members Subjected to Cyclic Flexural Moments," by V.V. Bertero, B. Bresler and H. Ming Liao - 1969 (PB 202 942)A07
- EERC 69-13 "Response of Non-Uniform Soil Deposits to Travelling Seismic Waves," by H. Dezfulian and H.B. Seed - 1969 (PB 191 023)A03
- EERC 69-14 "Damping Capacity of a Model Steel Structure," by D. Rea, R.W. Clough and J.G. Bouwkamp - 1969 (PB 190 663)A06
- EERC 69-15 "Influence of Local Soil Conditions on Building Damage Potential during Earthquakes," by H.B. Seed and I.M. Idriss - 1969 (PB 191 036)A03
- EERC 69-16 "The Behavior of Sands Under Seismic Loading Conditions," by M.L. Silver and H.B. Seed - 1969 (AD 714 982)A07
- EERC 70-1 "Earthquake Response of Gravity Dams," by A.K. Chopra - 1970 (AD 709 640)A03
- EERC 70-2 "Relationships between Soil Conditions and Building Damage in the Caracas Earthquake of July 29, 1967," by H.B. Seed, I.M. Idriss and H. Dezfulian - 1970 (PB 195 762)A05
- EERC 70-3 "Cyclic Loading of Full Size Steel Connections," by E.P. Popov and R.M. Stephen - 1970 (PB 213 545)A04
- EERC 70-4 "Seismic Analysis of the Charaima Building, Caraballeda, Venezuela," by Subcommittee of the SEAONC Research Committee: V.V. Bertero, P.F. Fratessa, S.A. Mahin, J.H. Sexton, A.C. Scordelis, E.L. Wilson, L.A. Wyllie, H.B. Seed and J. Penzien, Chairman - 1970 (PB 201 455)A06

- EERC 70-5 "A Computer Program for Earthquake Analysis of Dams," by A.K. Chopra and P. Chakrabarti - 1970 (AD 723 994)A05
- EERC 70-6 "The Propagation of Love Waves Across Non-Horizontally Layered Structures," by J. Lysmer and L.A. Drake 1970 (PB 197 896)A03
- EERC 70-7 "Influence of Base Rock Characteristics on Ground Response," by J. Lysmer, H.B. Seed and P.B. Schnabel 1970 (PB 197 897)A03
- EERC 70-8 "Applicability of Laboratory Test Procedures for Measuring Soil Liquefaction Characteristics under Cyclic Loading," by H.B. Seed and W.H. Peacock - 1970 (PB 198 016)A03
- EERC 70-9 "A Simplified Procedure for Evaluating Soil Liquefaction Potential," by H.B. Seed and I.M. Idriss - 1970 (PB 198 009)A03
- EERC 70-10 "Soil Moduli and Damping Factors for Dynamic Response Analysis," by H.B. Seed and I.M. Idriss - 1970 (PB 197 869)A03
- EERC 71-1 "Koyna Earthquake of December 11, 1967 and the Performance of Koyna Dam," by A.K. Chopra and P. Chakrabarti 1971 (AD 731 496)A06
- EERC 71-2 "Preliminary In-Situ Measurements of Anelastic Absorption in Soils Using a Prototype Earthquake Simulator," by R.D. Borcherdt and P.W. Rodgers - 1971 (PB 201 454)A03
- EERC 71-3 "Static and Dynamic Analysis of Inelastic Frame Structures," by F.L. Porter and G.H. Powell - 1971 (PB 210 135)A06
- EERC 71-4 "Research Needs in Limit Design of Reinforced Concrete Structures," by V.V. Bertero - 1971 (PB 202 943)A04
- EERC 71-5 "Dynamic Behavior of a High-Rise Diagonally Braced Steel Building," by D. Rea, A.A. Shah and J.G. Bouwkamp 1971 (PB 203 584)A06
- EERC 71-6 "Dynamic Stress Analysis of Porous Elastic Solids Saturated with Compressible Fluids," by J. Ghaboussi and E. L. Wilson - 1971 (PB 211 396)A06
- EERC 71-7 "Inelastic Behavior of Steel Beam-to-Column Subassemblies," by H. Krawinkler, V.V. Bertero and E.P. Popov 1971 (PB 211 335)A14
- EERC 71-8 "Modification of Seismograph Records for Effects of Local Soil Conditions," by P. Schnabel, H.B. Seed and J. Lysmer - 1971 (PB 214 450)A03
- EERC 72-1 "Static and Earthquake Analysis of Three Dimensional Frame and Shear Wall Buildings," by E.L. Wilson and H.H. Dovey - 1972 (PB 212 904)A05
- EERC 72-2 "Accelerations in Rock for Earthquakes in the Western United States," by P.B. Schnabel and H.B. Seed - 1972 (PB 213 100)A03
- EERC 72-3 "Elastic-Plastic Earthquake Response of Soil-Building Systems," by T. Minami - 1972 (PB 214 868)A08
- EERC 72-4 "Stochastic Inelastic Response of Offshore Towers to Strong Motion Earthquakes," by M.K. Kaul - 1972 (PB 215 713)A05
- EERC 72-5 "Cyclic Behavior of Three Reinforced Concrete Flexural Members with High Shear," by E.P. Popov, V.V. Bertero and H. Krawinkler - 1972 (PB 214 555)A05
- EERC 72-6 "Earthquake Response of Gravity Dams Including Reservoir Interaction Effects," by P. Chakrabarti and A.K. Chopra - 1972 (AD 762 330)A08
- EERC 72-7 "Dynamic Properties of Pine Flat Dam," by D. Rea, C.Y. Liaw and A.K. Chopra - 1972 (AD 763 928)A05
- EERC 72-8 "Three Dimensional Analysis of Building Systems," by E.L. Wilson and H.H. Dovey - 1972 (PB 222 438)A06
- EERC 72-9 "Rate of Loading Effects on Uncracked and Repaired Reinforced Concrete Members," by S. Mahir, V.V. Bertero, D. Rea and M. Atalay - 1972 (PB 224 520)A08
- EERC 72-10 "Computer Program for Static and Dynamic Analysis of Linear Structural Systems," by E.L. Wilson, K.-J. Bathe, J.E. Peterson and H.H. Dovey - 1972 (PB 220 437)A04
- EERC 72-11 "Literature Survey - Seismic Effects on Highway Bridges," by T. Iwasaki, J. Penzien and R.W. Clough - 1972 (PB 215 613)A19
- EERC 72-12 "SHAKE-A Computer Program for Earthquake Response Analysis of Horizontally Layered Sites," by P.B. Schnabel and J. Lysmer - 1972 (PB 220 207)A06
- EERC 73-1 "Optimal Seismic Design of Multistory Frames," by V.V. Bertero and H. Kamil - 1973
- EERC 73-2 "Analysis of the Slides in the San Fernando Dams During the Earthquake of February 9, 1971," by H.B. Seed, K.L. Lee, I.M. Idriss and F. Makdisi - 1973 (PB 223 402)A14

- EERC 73-3 "Computer Aided Ultimate Load Design of Unbraced Multistory Steel Frames," by M.B. El-Hafez and G.H. Powell 1973 (PB 248 315)A09
- EERC 73-4 "Experimental Investigation into the Seismic Behavior of Critical Regions of Reinforced Concrete Components as Influenced by Moment and Shear," by M. Celebi and J. Penzien - 1973 (PB 215 884)A09
- EERC 73-5 "Hysteretic Behavior of Epoxy-Repaired Reinforced Concrete Beams," by M. Celebi and J. Penzien - 1973 (PB 239 568)A03
- EERC 73-6 "General Purpose Computer Program for Inelastic Dynamic Response of Plane Structures," by A. Kanaan and G.H. Powell - 1973 (PB 221 260)A08
- EERC 73-7 "A Computer Program for Earthquake Analysis of Gravity Dams Including Reservoir Interaction," by P. Chakrabarti and A.K. Chopra - 1973 (AD 766 271)A04
- EERC 73-8 "Behavior of Reinforced Concrete Deep Beam-Column Subassemblages Under Cyclic Loads," by O. Küstü and J.G. Bouwkamp - 1973 (PB 246 117)A12
- EERC 73-9 "Earthquake Analysis of Structure-Foundation Systems," by A.K. Vaish and A.K. Chopra - 1973 (AD 767 272)A07
- EERC 73-10 "Deconvolution of Seismic Response for Linear Systems," by R.B. Reimer - 1973 (PB 227 179)A08
- EERC 73-11 "SAP IV: A Structural Analysis Program for Static and Dynamic Response of Linear Systems," by K.-J. Bathe, E.L. Wilson and F.E. Peterson - 1973 (PB 221 967)A09
- EERC 73-12 "Analytical Investigations of the Seismic Response of Long, Multiple Span Highway Bridges," by W.S. Tseng and J. Penzien - 1973 (PB 227 816)A10
- EERC 73-13 "Earthquake Analysis of Multi-Story Buildings Including Foundation Interaction," by A.K. Chopra and J.A. Gutierrez - 1973 (PB 222 970)A03
- EERC 73-14 "ADAP: A Computer Program for Static and Dynamic Analysis of Arch Dams," by R.W. Clough, J.M. Raphael and S. Mojtahedi - 1973 (PB 223 761)A09
- EERC 73-15 "Cyclic Plastic Analysis of Structural Steel Joints," by R.B. Pinkney and R.W. Clough - 1973 (PB 226 843)A08
- EERC 73-16 "QUAD-4: A Computer Program for Evaluating the Seismic Response of Soil Structures by Variable Damping Finite Element Procedures," by I.M. Idriss, J. Lysmer, R. Hwang and H.B. Seed - 1973 (PB 229 424)A05
- EERC 73-17 "Dynamic Behavior of a Multi-Story Pyramid Shaped Building," by R.M. Stephen, J.P. Hollings and J.G. Bouwkamp - 1973 (PB 240 718)A06
- EERC 73-18 "Effect of Different Types of Reinforcing on Seismic Behavior of Short Concrete Columns," by V.V. Bertero, J. Hollings, O. Küstü, R.M. Stephen and J.G. Bouwkamp - 1973
- EERC 73-19 "Olive View Medical Center Materials Studies, Phase I," by B. Bresler and V.V. Bertero - 1973 (PB 235 986)A06
- EERC 73-20 "Linear and Nonlinear Seismic Analysis Computer Programs for Long Multiple-Span Highway Bridges," by W.S. Tseng and J. Penzien - 1973
- EERC 73-21 "Constitutive Models for Cyclic Plastic Deformation of Engineering Materials," by J.M. Kelly and P.P. Gillis 1973 (PB 226 024)A03
- EERC 73-22 "DRAIN - 2D User's Guide," by G.H. Powell - 1973 (PB 227 016)A05
- EERC 73-23 "Earthquake Engineering at Berkeley - 1973," (PB 226 033)A11
- EERC 73-24 Unassigned
- EERC 73-25 "Earthquake Response of Axisymmetric Tower Structures Surrounded by Water," by C.Y. Liaw and A.K. Chopra 1973 (AD 773 052)A09
- EERC 73-26 "Investigation of the Failures of the Olive View Stairtowers During the San Fernando Earthquake and Their Implications on Seismic Design," by V.V. Bertero and R.C. Collins - 1973 (PB 235 106)A13
- EERC 73-27 "Further Studies on Seismic Behavior of Steel Beam-Column Subassemblages," by V.V. Bertero, H. Krawinkler and E.P. Popov - 1973 (PB 234 172)A06
- EERC 74-1 "Seismic Risk Analysis," by C.S. Oliveira - 1974 (PB 235 920)A06
- EERC 74-2 "Settlement and Liquefaction of Sands Under Multi-Directional Shaking," by R. Pyke, C.K. Chan and H.B. Seed 1974
- EERC 74-3 "Optimum Design of Earthquake Resistant Shear Buildings," by D. Ray, K.S. Pister and A.K. Chopra - 1974 (PB 231 172)A06
- EERC 74-4 "LUSH - A Computer Program for Complex Response Analysis of Soil-Structure Systems," by J. Lysmer, T. Udaka, H.B. Seed and R. Hwang - 1974 (PB 236 796)A05

- EERC 74-5 "Sensitivity Analysis for Hysteretic Dynamic Systems: Applications to Earthquake Engineering," by D. Ray 1974 (PB 233 213)A06
- EERC 74-6 "Soil Structure Interaction Analyses for Evaluating Seismic Response," by H.B. Seed, J. Lysmer and R. Hwang 1974 (PB 236 519)A04
- EERC 74-7 Unassigned
- EERC 74-8 "Shaking Table Tests of a Steel Frame - A Progress Report," by R.W. Clough and D. Tang - 1974 (PB 240 069)A03
- EERC 74-9 "Hysteretic Behavior of Reinforced Concrete Flexural Members with Special Web Reinforcement," by V.V. Bertero, E.P. Popov and T.Y. Wang - 1974 (PB 236 797)A07
- EERC 74-10 "Applications of Reliability-Based, Global Cost Optimization to Design of Earthquake Resistant Structures," by E. Vitiello and K.B. Pister - 1974 (PB 237 231)A06
- EERC 74-11 "Liquefaction of Gravelly Soils Under Cyclic Loading Conditions," by R.T. Wong, H.B. Seed and C.K. Chan 1974 (PB 242 042)A03
- EERC 74-12 "Site-Dependent Spectra for Earthquake-Resistant Design," by H.B. Seed, C. Ugas and J. Lysmer - 1974 (PB 240 953)A03
- EERC 74-13 "Earthquake Simulator Study of a Reinforced Concrete Frame," by F. Hidalgo and R.W. Clough - 1974 (PB 241 974)A13
- EERC 74-14 "Nonlinear Earthquake Response of Concrete Gravity Dams," by N. Pal - 1974 (AD/A 006 583)A06
- EERC 74-15 "Modeling and Identification in Nonlinear Structural Dynamics - I. One Degree of Freedom Models," by N. Distefano and A. Rath - 1974 (PB 241 548)A06
- EERC 75-1 "Determination of Seismic Design Criteria for the Dumbarton Bridge Replacement Structure, Vol. I: Description, Theory and Analytical Modeling of Bridge and Parameters," by F. Baron and S.-H. Pang - 1975 (PB 259 407)A15
- EERC 75-2 "Determination of Seismic Design Criteria for the Dumbarton Bridge Replacement Structure, Vol. II: Numerical Studies and Establishment of Seismic Design Criteria," by F. Baron and S.-H. Pang - 1975 (PB 259 408)A11 (For set of EERC 75-1 and 75-2 (PB 259 406))
- EERC 75-3 "Seismic Risk Analysis for a Site and a Metropolitan Area," by C.S. Oliveira - 1975 (PB 248 134)A09
- EERC 75-4 "Analytical Investigations of Seismic Response of Short, Single or Multiple-Span Highway Bridges," by M.-C. Chen and J. Penzien - 1975 (PB 241 454)A09
- EERC 75-5 "An Evaluation of Some Methods for Predicting Seismic Behavior of Reinforced Concrete Buildings," by S.A. Mahin and V.V. Bertero - 1975 (PB 246 306)A16
- EERC 75-6 "Earthquake Simulator Study of a Steel Frame Structure, Vol. I: Experimental Results," by R.W. Clough and D.T. Tang - 1975 (PB 243 981)A13
- EERC 75-7 "Dynamic Properties of San Bernardino Intake Tower," by D. Rea, C.-Y. Liaw and A.K. Chopra - 1975 (AD/A008 406) A05
- EERC 75-8 "Seismic Studies of the Articulation for the Dumbarton Bridge Replacement Structure, Vol. I: Description, Theory and Analytical Modeling of Bridge Components," by F. Baron and R.E. Hamati - 1975 (PB 251 539)A07
- EERC 75-9 "Seismic Studies of the Articulation for the Dumbarton Bridge Replacement Structure, Vol. 2: Numerical Studies of Steel and Concrete Girder Alternates," by F. Baron and R.E. Hamati - 1975 (PB 251 540)A10
- EERC 75-10 "Static and Dynamic Analysis of Nonlinear Structures," by D.P. Mondkar and G.H. Powell - 1975 (PB 242 434)A08
- EERC 75-11 "Hysteretic Behavior of Steel Columns," by E.P. Popov, V.V. Bertero and S. Chandramouli - 1975 (PB 252 365)A11
- EERC 75-12 "Earthquake Engineering Research Center Library Printed Catalog," - 1975 (PB 243 711)A26
- EERC 75-13 "Three Dimensional Analysis of Building Systems (Extended Version)," by E.L. Wilson, J.P. Hollings and H.H. Dovey - 1975 (PB 243 989)A07
- EERC 75-14 "Determination of Soil Liquefaction Characteristics by Large-Scale Laboratory Tests," by P. De Alba, C.K. Chan and H.B. Seed - 1975 (NUREG 0027)A08
- EERC 75-15 "A Literature Survey - Compressive, Tensile, Bond and Shear Strength of Masonry," by R.L. Mayes and R.W. Clough - 1975 (PB 246 292)A10
- EERC 75-16 "Hysteretic Behavior of Ductile Moment Resisting Reinforced Concrete Frame Components," by V.V. Bertero and E.P. Popov - 1975 (PB 246 388)A05
- EERC 75-17 "Relationships Between Maximum Acceleration, Maximum Velocity, Distance from Source, Local Site Conditions for Moderately Strong Earthquakes," by H.B. Seed, R. Murarka, J. Lysmer and I.M. Idriss - 1975 (PB 248 172)A03
- EERC 75-16 "The Effects of Method of Sample Preparation on the Cyclic Stress-Strain Behavior of Sands," by J. Mullis, C.K. Chan and H.B. Seed - 1975 (Summarized in EERC 75-28)

- EERC 75-19 "The Seismic Behavior of Critical Regions of Reinforced Concrete Components as Influenced by Moment, Shear and Axial Force," by M.B. Atalay and J. Penzien - 1975 (PB 258 842)A11
- EERC 75-20 "Dynamic Properties of an Eleven Story Masonry Building," by R.M. Stephen, J.P. Hollings, J.G. Bouwkamp and D. Jurukovski - 1975 (PB 246 945)A04
- EERC 75-21 "State-of-the-Art in Seismic Strength of Masonry - An Evaluation and Review," by R.L. Mayes and R.W. Clough - 1975 (PB 249 040)A07
- EERC 75-22 "Frequency Dependent Stiffness Matrices for Viscoelastic Half-Plane Foundations," by A.K. Chopra, P. Chakrabarti and G. Dasgupta - 1975 (PB 248 121)A07
- EERC 75-23 "Hysteretic Behavior of Reinforced Concrete Framed Walls," by T.Y. Wong, V.V. Bertero and E.P. Popov - 1975
- EERC 75-24 "Testing Facility for Subassemblages of Frame-Wall Structural Systems," by V.V. Bertero, E.P. Popov and T. Endo - 1975
- EERC 75-25 "Influence of Seismic History on the Liquefaction Characteristics of Sands," by H.B. Seed, K. Mori and C.F. Chan - 1975 (Summarized in EERC 75-28)
- EERC 75-26 "The Generation and Dissipation of Pore Water Pressures during Soil Liquefaction," by H.B. Seed, P.F. Martin and J. ... - 1975 (PB 252 648)A03
- EERC 75-27 "Identification of Research Needs for Improving Aseismic Design of Building Structures," by V.V. Bertero - 1975 (PB 243 136)A05
- EERC 75-28 "Evaluation of Soil Liquefaction Potential during Earthquakes," by H.B. Seed, I. Arango and C.K. Chan - 1975 (NUREG 0026)A13
- EERC 75-29 "Representation of Irregular Stress Time Histories by Equivalent Uniform Stress Series in Liquefaction Analyses," by H.B. Seed, I.M. Idriss, F. Makdisi and N. Banerjee - 1975 (PB 252 115)A03
- EERC 75-30 "FLUSH - A Computer Program for Approximate 3-D Analysis of Soil-Structure Interaction Problems," by J. Lysmer, T. Udaka, C.-F. Tsai and H.B. Seed - 1975 (PB 259 332)A07
- EERC 75-31 "ALUSH - A Computer Program for Seismic Response Analysis of Axisymmetric Soil-Structure Systems," by E. Berger, J. Lysmer and H.B. Seed - 1975
- EERC 75-32 "TRIP and TRAVEL - Computer Programs for Soil-Structure Interaction Analysis with Horizontally Travelling Waves," by T. Udaka, J. Lysmer and H.B. Seed - 1975
- EERC 75-33 "Predicting the Performance of Structures in Regions of High Seismicity," by J. Penzien - 1975 (PB 248 130)A03
- EERC 75-34 "Efficient Finite Element Analysis of Seismic Structure - Soil - Direction," by J. Lysmer, H.B. Seed, T. Udaka, R.N. Hwang and C.-F. Tsai - 1975 (PB 253 570)A03
- EERC 75-35 "The Dynamic Behavior of a First Story Girder of a Three-Story Steel Frame Subjected to Earthquake Loading," by R.W. Clough and L.-Y. Li - 1975 (PB 248 841)A05
- EERC 75-36 "Earthquake Simulator Study of a Steel Frame Structure, Volume II - Analytical Results," by D.T. Tang - 1975 (PB 252 926)A10
- EERC 75-37 "ANSR-I General Purpose Computer Program for Analysis of Non-Linear Structural Response," by D.P. Mondkar and G.H. Powell - 1975 (PB 252 386)A08
- EERC 75-38 "Nonlinear Response Spectra for Probabilistic Seismic Design and Damage Assessment of Reinforced Concrete Structures," by M. Murakami and J. Penzien - 1975 (PB 259 530)A05
- EERC 75-39 "Study of a Method of Feasible Directions for Optimal Elastic Design of Frame Structures Subjected to Earthquake Loading," by N.D. Walker and K.S. Pister - 1975 (PB 257 781)A06
- EERC 75-40 "An Alternative Representation of the Elastic-Viscoelastic Analogy," by G. Dasgupta and J.L. Sackman - 1975 (PB 252 173)A03
- EERC 75-41 "Effect of Multi-Directional Shaking on Liquefaction of Sands," by H.B. Seed, R. Pyke and G.R. Martin - 1975 (PB 258 781)A03
- EERC 76-1 "Strength and Ductility Evaluation of Existing Low-Rise Reinforced Concrete Buildings - Screening Method," by T. Okada and B. Bresler - 1976 (PB 257 906)A11
- EERC 76-2 "Experimental and Analytical Studies on the Hysteretic Behavior of Reinforced Concrete Rectangular and T-Beams," by S.-Y.M. Na, E.P. Popov and V.V. Bertero - 1976 (PB 260 843)A12
- EERC 76-3 "Dynamic Behavior of a Multistory Triangular-Shaped Building," by J. Petrovski, R.M. Stephen, E. Gartenbaum and J.G. Bouwkamp - 1976 (PB 273 279)A07
- EERC 76-4 "Earthquake Induced Deformations of Earth Dams," by N. Seiff, H.B. Seed, F.I. Makdisi & C.-Y. Chang - 1976 (PB 292 065)A08

- EERC 76-5 "Analysis and Design of Tube-Type Tall Building Structures," by H. de Clercq and G.H. Powell - 1976 (PB 252 220) A10
- EERC 76-6 "Time and Frequency Domain Analysis of Three-Dimensional Ground Motions, San Fernando Earthquake," by T. Kubo and J. Penzien (PB 260 556)A11
- EERC 76-7 "Expected Performance of Uniform Building Code Design Masonry Structures," by R.L. Mayes, Y. Omote, S.W. Chen and R.W. Clough - 1976 (PB 270 098)A05
- EERC 76-8 "Cyclic Shear Tests of Masonry Piers, Volume 1 - Test Results," by R.L. Mayes, Y. Omote, R.W. Clough - 1976 (PB 264 424)A06
- EERC 76-9 "A Substructure Method for Earthquake Analysis of Structure - Soil Interaction," by J.A. Gutierrez and A.K. Chopra - 1976 (PB 257 783)A08
- EERC 76-10 "Stabilization of Potentially Liquefiable Sand Deposits using Gravel Drain Systems," by H.B. Seed and R. Booker - 1976 (PB 258 820)A04
- EERC 76-11 "Influence of Design and Analysis Assumptions on Computed Inelastic Response of Moderately Tall Frames," by G.H. Powell and D.G. Row - 1976 (PB 271 409)A06
- EERC 76-12 "Sensitivity Analysis for Hysteretic Dynamic Systems: Theory and Applications," by D. Ray, K.S. Pister and E. Polak - 1976 (PB 262 859)A04
- EERC 76-13 "Coupled Lateral Torsional Response of Buildings to Ground Shaking," by C.L. Kan and A.K. Chopra - 1976 (PB 257 907)A09
- EERC 76-14 "Seismic Analyses of the Banco de America," by V.V. Bertero, S.A. Mahin and J.A. Hollings - 1976
- EERC 76-15 "Reinforced Concrete Frame 2: Seismic Testing and Analytical Correlation," by R.W. Clough and J. Gidwani - 1976 (PB 261 323)A08
- EERC 76-16 "Cyclic Shear Tests of Masonry Piers, Volume 2 - Analysis of Test Results," by R.L. Mayes, Y. Omote and R.W. Clough - 1976
- EERC 76-17 "Structural Steel Bracing Systems: Behavior Under Cyclic Loading," by E.P. Popov, K. Takanashi and C.W. Roeder - 1976 (PB 260 715)A05
- EERC 76-18 "Experimental Model Studies on Seismic Response of High Curved Overcrossings," by D. Williams and W.G. Godden - 1976 (PB 269 548)A08
- EERC 76-19 "Effects of Non-Uniform Seismic Disturbances on the Dumbarton Bridge Replacement Structure," by F. Baron and R.E. Hamati - 1976 (PB 282 981)A16
- EERC 76-20 "Investigation of the Inelastic Characteristics of a Single Story Steel Structure Using System Identification and Shaking Table Experiments," by V.C. Matzen and H.D. McNiven - 1976 (PB 258 453)A07
- EERC 76-21 "Capacity of Columns with Splice Imperfections," by E.P. Popov, R.M. Stephen and R. Philbrick - 1976 (PB 260 378)A04
- EERC 76-22 "Response of the Olive View Hospital Main Building during the San Fernando Earthquake," by S. A. Mahin, V.V. Bertero, A.K. Chopra and R. Collins - 1976 (PB 271 425)A14
- EERC 76-23 "A Study on the Major Factors Influencing the Strength of Masonry Prisms," by N.M. Mostaghel, R.L. Mayes, R. W. Clough and S.W. Chen - 1976 (Not published)
- EERC 76-24 "GADPLEA - A Computer Program for the Analysis of Pore Pressure Generation and Dissipation during Cyclic or Earthquake Loading," by J.R. Booker, M.S. Rahman and H.B. Seed - 1976 (PB 263 947)A04
- EERC 76-25 "Seismic Safety Evaluation of a R/C School Building," by B. Bresler and J. Axley - 1976
- EERC 76-26 "Correlative Investigations on Theoretical and Experimental Dynamic Behavior of a Model Bridge Structure," by K. Kawashima and J. Penzien - 1976 (PB 263 388)A11
- EERC 76-27 "Earthquake Response of Coupled Shear Wall Buildings," by T. Srichatrapimuk - 1976 (PB 265 157)A07
- EERC 76-28 "Tensile Capacity of Partial Penetration Welds," by E.P. Popov and R.M. Stephen - 1976 (PB 262 899)A03
- EERC 76-29 "Analysis and Design of Numerical Integration Methods in Structural Dynamics," by H.M. Hilber - 1976 (PB 264 410)A06
- EERC 76-30 "Contribution of a Floor System to the Dynamic Characteristics of Reinforced Concrete Buildings," by L.E. Malik and V.V. Bertero - 1976 (PB 272 247)A05
- EERC 76-31 "The Effects of Seismic Disturbances on the Golden Gate Bridge," by F. Baron, M. Arikan and R.E. Hamati - 1976 (PB 272 279)A09
- EERC 76-32 "Infilled Frames in Earthquake Resistant Construction," by R.E. Klingner and V.V. Bertero - 1976 (PB 265 892)A13

- UCB/EERC-77/01 "PLUSH - A Computer Program for Probabilistic Finite Element Analysis of Seismic Soil-Structure Interaction," by M.P. Romo Organista, J. Lysmer and H.B. Seed - 1977
- UCB/EERC-77/02 "Soil-Structure Interaction Effects at the Humboldt Bay Power Plant in the Ferndale Earthquake of June 7, 1975," by J.E. Valera, H.B. Seed, C.F. Tsai and J. Lysmer - 1977 (PB 265 795)A04
- UCB/EERC-77/03 "Influence of Sample Disturbance on Sand Response to Cyclic Loading," by K. Mori, H.B. Seed and C.K. Chan - 1977 (PB 267 352)A04
- UCB/EERC-77/04 "Seismological Studies of Strong Motion Records," by J. Shoja-Taheri - 1977 (PB 269 655)A10
- UCB/EERC-77/05 "Testing Facility for Coupled-Shear Walls," by L. Li-Hyung, V.V. Bertero and E.P. Popov - 1977
- UCB/EERC-77/06 "Developing Methodologies for Evaluating the Earthquake Safety of Existing Buildings," by No. 1 - B. Bresler; No. 2 - B. Bresler, T. Okada and D. Zisling; No. 3 - T. Okada and B. Bresler; No. 4 - V.V. Bertero and B. Bresler - 1977 (PB 267 354)A08
- UCB/EERC-77/07 "A Literature Survey - Transverse Strength of Masonry Walls," by Y. Omote, R.L. Mayes, S.W. Chen and R.W. Clough - 1977 (PB 277 933)A07
- UCB/EERC-77/08 "DRAIN-TABS: A Computer Program for Inelastic Earthquake Response of Three Dimensional Buildings," by R. Guendelman-Israel and G.H. Powell - 1977 (PB 270 693)A07
- UCB/EERC-77/09 "SUBWALL: A Special Purpose Finite Element Computer Program for Practical Elastic Analysis and Design of Structural Walls with Substructure Optio: " by D.Q. Le, H. Peterson and E.P. Popov - 1977 (PB 270 567)A05
- UCB/EERC-77/10 "Experimental Evaluation of Seismic Design Methods for Broad Cylindrical Tanks," by D.P. Clough (PB 272 280)A13
- UCB/EERC-77/11 "Earthquake Engineering Research at Berkeley - 1976," - 1977 (PB 273 507)A09
- UCB/EERC-77/12 "Automated Design of Earthquake Resistant Multistory Steel Building Frames," by N.D. Walker, Jr. - 1977 (PB 276 526)A09
- UCB/EERC-77/13 "Concrete Confined by Rectangular Hoops Subjected to Axial Loads," by J. Vallenat, V.V. Bertero and E.P. Popov - 1977 (PB 275 165)A06
- UCB/EERC-77/14 "Seismic Strain Induced in the Ground During Earthquakes," by Y. Sugimura - 1977 (PB 284 201)A04
- UCB/EERC-77/15 "Bond Deterioration under Generalized Loading," by V.V. Bertero, E.P. Popov and S. Viathanatepa - 1977
- UCB/EERC-77/16 "Computer Aided Optimum Design of Ductile Reinforced Concrete Moment Resisting Frames," by S.W. Zagajeski and V.V. Bertero - 1977 (PB 280 137)A07
- UCB/EERC-77/17 "Earthquake Simulation Testing of a Stepping Frame with Energy-Absorbing Devices," by J.M. Kelly and D.F. Tsztoo - 1977 (PB 273 506)A04
- UCB/EERC-77/18 "Inelastic Behavior of Eccentrically Braced Steel Frames under Cyclic Loadings," by C.W. Roeder and E.P. Popov - 1977 (PB 275 526)A15
- UCB/EERC-77/19 "A Simplified Procedure for Estimating Earthquake-Induced Deformations in Dams and Embankments," by F.I. Makdisi and H.B. Seed - 1977 (PB 276 820)A04
- UCB/EERC-77/20 "The Performance of Earth Dams during Earthquakes," by H.B. Seed, F.I. Makdisi and P. de Alba - 1977 (PB 276 821)A04
- UCB/EERC-77/21 "Dynamic Plastic Analysis Using Stress Resultant Finite Element Formulation," by P. Lukkunapvasit and J.M. Kelly - 1977 (PB 275 453)A04
- UCB/EERC-77/22 "Preliminary Experimental Study of Seismic Uplift of a Steel Frame," by R.W. Clough and A.A. Huckelbridge 1977 (PB 278 769)A08
- UCB/EERC-77/23 "Earthquake Simulator Tests of a Nine-Story Steel Frame with Columns Allowed to Uplift," by A.A. Huckelbridge - 1977 (PB 277 944)A09
- UCB/EERC-77/24 "Nonlinear Soil-Structure Interaction of Skew Highway Bridges," by M.-C. Chen and J. Penzien - 1977 (PB 276 176)A07
- UCB/EERC-77/25 "Seismic Analysis of an Offshore Structure Supported on Pile Foundations," by D.D.-N. Liou and J. Penzien 1977 (PB 283 180)A06
- UCB/EERC-77/26 "Dynamic Stiffness Matrices for Homogeneous Viscoelastic Half-Planes," by G. Dasgupta and A.K. Chopra - 1977 (PB 279 654)A06
- UCB/EERC-77/27 "A Practical Soft Story Earthquake Isolation System," by J.M. Kelly, J.M. Eidinger and C.J. Derham - 1977 (PB 276 814)A07
- UCB/EERC-77/28 "Seismic Safety of Existing Buildings and Incentives for Hazard Mitigation in San Francisco: An Exploratory Study," by A.J. Meltsner - 1977 (PB 281 970)A05
- UCB/EERC-77/29 "Dynamic Analysis of Electrohydraulic Shaking Tables," by D. Rea, S. Abedi-Hayati and Y. Takahashi 1977 (PB 282 569)A04
- UCB/EERC-77/30 "An Approach for Improving Seismic - Resistant Behavior of Reinforced Concrete Interior Joints," by B. Galunic, V.V. Bertero and E.P. Popov - 1977 (PB 290 870)A06

- UCB/EERC-78/01 "The Development of Energy-Absorbing Devices for Aseismic Base Isolation Systems," by J.M. Kelly and D.F. Tsatoo - 1978 (PB 284 978)A04
- UCB/EERC-78/02 "Effect of Tensile Prestrain on the Cyclic Response of Structural Steel Connections, by J.G. Bouwkamp and A. Mukhopadhyay - 1978
- UCB/EERC-78/03 "Experimental Results of an Earthquake Isolation System using Natural Rubber Bearings," by J.M. Eidinger and J.M. Kelly - 1978 (PB 281 686)A04
- UCB/EERC-78/04 "Seismic Behavior of Tall Liquid Storage Tanks," by A. Niwa - 1978 (PB 284 017)A14
- UCB/EERC-78/05 "Hysteretic Behavior of Reinforced Concrete Columns Subjected to High Axial and Cyclic Shear Forces," by S.W. Zagajeski, V.V. Bertero and J.G. Bouwkamp - 1978 (PB 283 858)A13
- UCB/EERC-78/06 "Inelastic Beam-Column Elements for the ANSR-I Program," by A. Riahi, D.G. Row and G.H. Powell - 1978
- UCB/EERC-78/07 "Studies of Structural Response to Earthquake Ground Motion," by O.A. Lopez and A.K. Chopra - 1978 (PB 282 790)A05
- UCB/EERC-78/08 "A Laboratory Study of the Fluid-Structure Interaction of Submerged Tanks and Caissons in Earthquakes," by R.C. Byrd - 1978 (PB 284 957)A08
- UCB/EERC-78/09 "Model for Evaluating Damageability of Structures," by I. Sakamoto and B. Bresler - 1978
- UCB/EERC-78/10 "Seismic Performance of Nonstructural and Secondary Structural Elements," by I. Sakamoto - 1978
- UCB/EERC-78/11 "Mathematical Modelling of Hysteresis Loops for Reinforced Concrete Columns," by S. Nakata, T. Sproul and J. Penzien - 1978
- UCB/EERC-78/12 "Damageability in Existing Buildings," by T. Blejwas and B. Bresler - 1978
- UCB/EERC-78/13 "Dynamic Behavior of a Pedestal Base Multistory Building," by R.M. Stephen, E.L. Wilson, J.G. Bouwkamp and M. Butten - 1978 (PB 286 650)A08
- UCB/EERC-78/14 "Seismic Response of Bridges - Case Studies," by R.A. Imbsen, V. Nutt and J. Penzien - 1978 (PB 286 503)A10
- UCB/EERC-78/15 "A Substructure Technique for Nonlinear Static and Dynamic Analysis," by D.G. Row and G.H. Powell - 1978 (PB 288 071)A10
- UCB/EERC-78/16 "Seismic Risk Studies for San Francisco and for the Greater San Francisco Bay Area," by C.S. Oliveira - 1978
- UCB/EERC-78/17 "Strength of Timber Roof Connections Subjected to Cyclic Loads," by P. Gülkan, R.L. Mayes and R.W. Clough - 1978
- UCB/EERC-78/18 "Response of X-Braced Steel Frame Models to Lateral Loads," by J.G. Bouwkamp, R.M. Stephen and E.P. Popov - 1978
- UCB/EERC-78/19 "Rational Design Methods for Light Equipment in Structures Subjected to Ground Motion," by J.L. Sackman and J.M. Kelly - 1978 (PB 292 357)A04
- UCB/EERC-78/20 "Testing of a Wind Restraint for Aseismic Base Isolation," by J.M. Kelly and D.E. Chitty - 1978 (PB 292 833)A03
- UCB/EERC-78/21 "APOLLO - A Computer Program for the Analysis of Pore Pressure Generation and Dissipation in Horizontal Sand Layers During Cyclic or Earthquake Loading," by P.P. Martin and H.B. Seed - 1978 (PB 292 835)A04
- UCB/EERC-78/22 "Optimal Design of an Earthquake Isolation System," by M.A. Bhatti, K.S. Pister and E. Polak - 1978 (PB 294 735)A06
- UCB/EERC-78/23 "MASH - A Computer Program for the Non-Linear Analysis of Vertically Propagating Shear Waves in Horizontally Layered Deposits," by P.P. Martin and H.B. Seed - 1978 (PB 293 101)A05
- UCB/EERC-78/24 "Investigation of the Elastic Characteristics of a Three Story Steel Frame Using System Identification," by I. Kaya and H.D. McNiven - 1978
- UCB/EERC-78/25 "Investigation of the Nonlinear Characteristics of a Three-Story Steel Frame Using System Identification," by I. Kaya and H.D. McNiven - 1978
- UCB/EERC-78/26 "Studies of Strong Ground Motion in Taiwan," by Y.M. Hsiung, B.A. Bolt and J. Penzien - 1978
- UCB/EERC-78/27 "Cyclic Loading Tests of Masonry Single Piers: Volume 1 - Height to Width Ratio of 2," by P.A. Hidalgo, R.L. Mayes, H.D. McNiven and R.W. Clough - 1978
- UCB/EERC-78/28 "Cyclic Loading Tests of Masonry Single Piers: Volume 2 - Height to Width Ratio of .," by S.-W.J. Chen, P.A. Hidalgo, R.L. Mayes, R.W. Clough and H.D. McNiven - 1978
- UCB/EERC-78/29 "Analytical Procedures in Soil Dynamics," by J. Lysmer - 1978

- UCB/EERC-79/01 "Hysteretic Behavior of Lightweight Reinforced Concrete Beam-Column Subassemblages," by B. Forzani, E.P. Popov, and V.V. Bertero - 1979
- UCB/EERC-79/02 "The Development of a Mathematical Model to Predict the Flexural Response of Reinforced Concrete Beams to Cyclic Loads, Using System Identification," by J.F. Stanton and H.D. McNiven - 1979
- UCB/EERC-79/03 "Linear and Nonlinear Earthquake Response of Simple Torsionally Coupled Systems," by C.L. Kan and A.K. Chopra - 1979
- UCB/EERC-79/04 "A Mathematical Model of Masonry for Predicting Its Linear Seismic Response Characteristics," by Y. Mengi and H.D. McNiven - 1979
- UCB/EERC-79/05 "Mechanical Behavior of Light Weight Concrete Confined with Different Types of Lateral Reinforcement," by M.A. Manrique and V.V. Bertero - 1979
- UCB/EERC-79/06 "Static Tilt Tests of a Tall Cylindrical Liquid Storage Tank," by R.W. Clough and A. Niwa - 1979
- UCB/EERC-79/07 "The Design of Steel Energy Absorbing Restrainers and Their Incorporation Into Nuclear Power Plants for Enhanced Safety: Volume 1 - Summary Report," by P.N. Spencer, V.F. Zackay, and E.R. Parker - 1979
- UCB/EERC-79/08 "The Design of Steel Energy Absorbing Restrainers and Their Incorporation Into Nuclear Power Plants for Enhanced Safety: Volume 2 - The Development of Analyses for Reactor System Piping," "Simple Systems" by M.C. Lee, J. Penzien, A.K. Chopra, and K. Suzuki "Complex Systems" by G.H. Powell, E.L. Wilson R.W. Clough and D.G. Row - 1979
- UCB/EERC-79/09 "The Design of Steel Energy Absorbing Restrainers and Their Incorporation Into Nuclear Power Plants for Enhanced Safety: Volume 3 - Evaluation of Commercial Steels," by W.S. Owen, R.M.N. Pelloux, R.O. Ritchie, M. Faral, T. Ohhashi, J. Toplosky, S.J. Hartman, V.F. Zackay, and E.R. Parker - 1979
- UCB/EERC-79/10 "The Design of Steel Energy Absorbing Restrainers and Their Incorporation Into Nuclear Power Plants for Enhanced Safety: Volume 4 - A Review of Energy-Absorbing Devices," by J.M. Kelly and M.S. Skinner - 1979
- UCB/EERC-79/11 "Conservatism In Summation Rules for Closely Spaced Modes," by J.M. Kelly and J.L. Sackman - 1979

UCB/EERC-79/12 "Cyclic Loading Tests of Masonry Single Piers
Volume 3 - Height to Width Ratio of 0.5," by P.A.
Hidalgo, R.L. Mayes, H.D. McNiven and R.W. Clough - 1979

For sale by the National Technical Information Service, U. S. Department of Commerce, Springfield, Virginia 22161.

See back of report for up to date listing of EERC reports.